AGARD-LS-180

AGARD-LS-180

AGARD

ADVISORY GROUP FOR AEROSPACE RESEARCH & DEVELOPMENT
7 RUE ANCELLE 92200 NEUILLY SUR SEINE FRANCE

LECTURE SERIES 180

Combustion of Solid Propellants

(La Combustion des Propergols Solides)

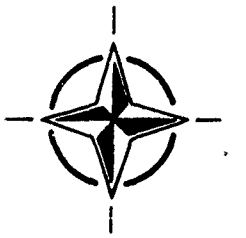

NORTH ATLANTIC TREATY ORGANIZATION

AGARD-LS-180

AGARD
ADVISORY GROUP FOR AEROSPACE RESEARCH & DEVELOPMENT
7 RUE ANCELLE 92200 NEUILLY SUR SEINE FRANCE

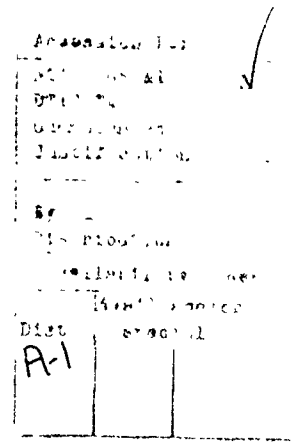

LECTURE SERIES 180

Combustion of Solid Propellants

(La Combustion des Propergols Solides)

This material in this publication was assembled to support a Lecture Series under the sponsorship of the Propulsion and Energetics Panel of AGARD and the Consultant and Exchange Programme of AGARD presented on 4th—5th September 1991 in Quebec City, Canada, 16th—17th September 1991 in Saint-Médard-en-Jalles (near Bordeaux), France and 19th—20th September 1991 in Ankara, Turkey.

North Atlantic Treaty Organization
Organisation du Traité de l'Atlantique Nord

The Mission of AGARD

According to its Charter, the mission of AGARD is to bring together the leading personalities of the NATO nations in the fields of science and technology relating to aerospace for the following purposes

- Recommending effective ways for the member nations to use their research and development capabilities for the common benefit of the NATO community,
- Providing scientific and technical advice and assistance to the Military Committee in the field of aerospace research and development (with particular regard to its military application),
- Continuously stimulating advances in the aerospace sciences relevant to strengthening the common defence posture
- Improving the co-operation among member nations in aerospace research and development,
- Exchange of scientific and technical information,
- Providing assistance to member nations for the purpose of increasing their scientific and technical potential,
- Rendering scientific and technical assistance, as requested, to other NATO bodies and to member nations in connection with research and development problems in the aerospace field

The highest authority within AGARD is the National Delegates Board consisting of officially appointed senior representatives from each member nation The mission of AGARD is carried out through the Panels which are composed of experts appointed by the National Delegates, the Consultant and Exchange Programme and the Aerospace Applications Studies Programme The results of AGARD work are reported to the member nations and the NATO Authorities through the AGARD series of publications of which this is one

Participation in AGARD activities is by invitation only and is normally limited to citizens of the NATO nations

Published July 1991

ISBN 92-835-0630-8

Printed by Specialised Printing Services Limited
40 Chigwell Lane, Loughton, Essex IG10 3TZ

Contents

* Not available at time of printing — Abstract only

Abstract

The history of solid propellants has dramatically changed since the end of the 19th century when Paul Vieille and Nobel discovered the phenomenon of gelatinization of nitrocellulose (either by solvent or by nitroglycerin). The products thus obtained exhibited a new combustion behaviour, combustion in parallel layers. This is the basis of modern gun and rocket solid propulsion.

Extruded double base propellant grains were used for propulsion of rockets before world war II. Composite propellants (a binder, a fuel and an oxidizer) were discovered during the 1940s. They also burn in parallel layers, although microscopically the process is more complex. Since that time, these families of propellants have been improved and are now widely used for the propulsion of tactical rockets, strategic missiles, as well as space launchers. During the operation of rocket motors, many complex combustion phenomena occur. It is the object of Lecture Series 180 to present, and analyse all these combustion phenomena, both theoretically and experimentally:

- Overview on solid propellant combustion within a rocket motor
- Solid propellant steady combustion
- Erosive burning
- Special effects in solid propellant combustion
- Combustion instabilities
- Ignition and unsteady combustion
- Combustion and safety of solid propellant rocket motors.

This Lecture Series, sponsored by the Propulsion and Energetics Panel of AGARD, has been implemented by the Consultant and Exchange Programme

Abrégé

L'histoire des propergols solides a connu un bouleversement profond avec la découverte par Paul Vieille et Nobel, à la fin du dix-neuvième siècle, du phénomène de la gélatinisation de la nitrocellulose (soit par solvant soit par la nitroglycérine). Les produits ainsi obtenus présentaient un nouveau comportement à la combustion: la combustion par couches parallèles. Ce phénomène est à la base de la propulsion par propergols solides des obus et fusées modernes.

Avant la deuxième guerre mondiale des blocs à propergols sans dissolvant furent utilisés pour la propulsion des fusées. Les poudres composites (un liant, un ergol et un comburant) ont été découvertes lors des années 1940: la combustion se fait également par couches parallèles, bien que le procédé soit plus complexe sur le plan micromoléculaire. Depuis lors, ces familles d'ergols ont été améliorées et elles sont désormais très largement employées pour la propulsion des fusées tactiques, des missiles stratégiques et des lanceurs spatiaux. Un grand nombre de phénomènes complexes de combustion se produisent pendant le fonctionnement d'un moteur-fusée et l'objet du cycle de conférences No 180 est de les présenter et de les analyser, tant au plan théorique qu'expérimental:

- panorama de la combustion des propergols solides dans les moteurs-fusées
- la combustion stationnaire des propergols solides
- la combustion érosive
- les effets particuliers de la combustion des propergols solides
- les instabilités de combustion
- l'allumage et la combustion stationnaire
- la combustion et la sécurité des moteurs-fusées à propergols solides.

Ce cycle de conférences est présenté dans le cadre du programme des Consultants et des Echanges, sous l'égide du Panel AGARD de Propulsion et d'Energétique.

List of Authors/Speakers

Lecture Series Director: Dr B. Zeller
Directeur Stratégie et Marketing
Division Défense Espace
SNPE
12, Quai Henri IV
75181 Paris Cedex 04
France

AUTHORS/SPEAKERS

Mr T. Boggs
Naval Weapons Center
Research Dept. Code 38
China Lake, CA 93555
United States

I.G.A. A. Davenas
Directeur de la Technologie et de la Recherche
Division Défense Espace
SNPE
12, Quai Henri IV
75181 Paris Cedex 04
France

Mr J.-R. Duterque
Direction de l'Energétique
ONERA
29, Avenue de la Division Leclerc
92320 Châtillon/Bagneux
France

Mr J.-C. Godon
Direction de l'Energétique
ONERA
29, Avenue de la Division Leclerc
92320 Châtillon/Bagneux
France

Dr Merrill K. King
Program Director, Thermal Systems
Chemical and Thermal Systems Division
National Science Foundation
1800 G Street NW, Room 1110
Washington, DC 20550
United States

Dr P. Kuentzmann
Directeur Scientifique de l'Energétique
ONERA
29, Avenue de la Division Leclerc
92322 Châtillon/Bagneux
France

Prof. K. Kuo
Director of the High Pressure Combustion Lab.
Dept. of Mechanical Eng.
312 Mechanical Eng. Bldg
University Park
Pennsylvania 16802
United States

Mr G. Lengellé
Direction de l'Energétique
ONERA
29, Avenue de la Division Leclerc
92320 Châtillon/Bagneux
France

Mr J.-F. Trubert
Direction de l'Energétique
ONERA
29, Avenue de la Division Leclerc
92320 Châtillon/Bagneux
France

Introduction to the Lecture Series 180

Bernard ZELLER
Directeur de la Stratégie et du Marketing
(Director, Business Development and Planning)
S.N.P.E.
12, Quai Henri IV, 75004 PARIS FRANCE

1. FOREWORD (How LS 180 was initiated)

In 1988 and 1989, AGARD organized a double series of lectures (LS 150) on the subject of Design Methods in Solid Rocket Motors. The Lecture Series Director was Daniel REYDELLET. This Lecture Series was so successful that it was presented in 1988 in Netherlands, Greece, Turkey and United States of America, then, in 1989, in United Kingdom, France, Germany and Italy. A substantial part of this Lecture Series was, of course, dedicated to solid propellant grain design. The question of propellant combustion, which is essential in the principles of rocket motor propulsion, was addressed, but could not thoroughly be detailed. Various aspects were mentioned such as : normal steady combustion, ignition, unsteady combustion, erosive burning, combustion instabilites,.. Numerous attendees of LS 150 asked for more information on these subjects, so that AGARD Propulsion and Energetics Panel proposed that a whole Lecture Series be dedicated to these questions of solid propellant combustion. This proposal was approved by the National Delegates Board of AGARD, then organized by Plans and Programmes of AGARD in connection with the Propulsion and Energetic Panel.

This is the origin of Lecture Series 180 which is a useful follow up of LS 150 in the field of solid propellant behavior (one may also imagine another specialized Lecture Series in the field of solid propellant mechanical properties and grain structural analysis or in the field of rocket motor plume technology).

2. ROLE OF COMBUSTION IN SOLID ROCKET MOTOR OPERATION

Combustion is the central phenomenon of solid rocket motor operation. It is the stage where condensed matter is transformed into gaseous high temperature products. The "potential" energy contained into the propellant is changed into the thermal and kinetic energy of gaseous mixture thanks to a nozzle. The higher temperature and the lower the molecular weight of the mixture, the more impulsive the propellant : specific impulse of a propellant (impulse delivered by the propellant mass unit in given conditions) is proportional to the square root of gas temperature over gas average molecular weight :

$$Is = k\sqrt{\frac{T_c}{M}}$$

However, it is not sufficient to "deliver impulse". This impulse is the integral of thrust versus time and thrust must be controlled during the operation of the rocket motor. Thrust is related to pressure in the rocket motor :

$$F = C_F . P . A_T$$

F : thrust
C_F : nozzle thrust coefficient
P : internal pressure (in the rocket motor)
A_T : nozzle throat cross section area

The internal pressure in the motor is the result of balanced flow rates :

- an input flow rate due to the combustion of the propellant,
- an output flow rate due to the ejection of propellant high temperature combustion products through the nozzle.

This may be written as :

$$\rho S V_c = P . C_D . A_T$$

ρ : propellant density
S : propellant grain burning area
V_c : propellant burning rate
P : internal pressure
C_D : nozzle discharge coefficient
A_T : nozzle throat cross section area

This equation may be written and corresponds to a steady operation only if one assumes that :

- the propellant burns in "parallel layers", that is to say that the burning front recedes at a speed whose vector is perpendicular to the front (normal combustion);
- the propellant burning rate increases proportionally less than the pressure, when the latter increases.

These are the main questions that are discussed in this Lecture Series :

SOLID PROPELLANT MUST BURN IN PARALLEL LAYERS

RELATIVE CHANGE OF BURNING RATE VERSUS PRESSURE MUST BE LOWER THAN RELATIVE PRESSURE CHANGE

Besides these basic requirements, many other phenomena have to be under control. Rocket motors have to be efficient, safe and reliable. Accurate predictive methods must be available (in order to minimize the cost of the rocket motor development programmes). All these requirements demand a detailed knowledge of the phenomena related to ignition, unsteady combustion, erosive burning, combustion instabilities, deflagration to detonation transition,...

3. COMBUSTION IN PARALLEL LAYERS

In 1991, it seems obvious that solid propellant burns in parallel layers. It has not been always like that, and one has to remember that, even nowadays, a failure in that way of burning may induce catastrophic effects such as transition to detonation. Until 1884, solid propellant was mainly

black powder. This propellant, even strongly compacted, could not sustain a full combustion in parallel layers in a gun. In addition, it was smoky and its impulse was limited. In the middle of the nineteenth century, nitrocellulose was recognized as a potentially very interesting propellant. Many attemps were made to use it for gun propulsion. Its force was around three times that of black powder and it was smokeless. Even compacted, this product did not burn regularly and many guns exploded as a result of this unpredictable behaviour.

In 1884, Paul Vieille discovered how to "gelatinize" nitrocellulose using a mixture of ether and ethyl alcohol and removing this solvent. Instead of having a fibrous structure, the nitrocellulose thus obtained was a compact not porous material which burned in parallel layers. This was the birth of single base propellants.

At the same period, Nobel discovered that nitrocellulose, mechanically processed with nitroglycerin at temperatures above normal temperature, was also changed into a compact, non porous material. This was the birth of double base solventless propellant whose thickness may reach several centimeters.

During the twentieth century, new families of solid propellants appeared, such as cast double base propellants and, during World War II, composite propellants.

Composite propellants, made of a polymeric matrix, an oxidiser and a metallic fuel, macroscopically burn in parallel layers, although, microscopically, as the material is not homogeneous, the flame front is not plane. The web thickness of propellant grains based on these propellants has no theoretical limit. Grains of 4 meters diameter have been manufactured.

As mentioned above, burning in parallel layers is not sufficient for designing a satisfactory propellant grain. The propellant grain designer must be provided with propellants having controlable burning rate. The need for high performance rocket motors involves to master erosive burning, combustion instabilities.

4. ORGANIZATION OF THE LECTURE SERIES SESSION

During the session, six speakers will present eight lectures. These speakers are among the western world best specialists in the field of combustion. All of them are leaders in their countries. They have gathered experience all along the years and all of them are now very well known in the field of propellant combustion. Because of their expertise they have important responsabilities and very busy schedules. Despite that, they have devoted an important part of their time to prepare their lectures. We are proud to have them for this lecture series and we acknowledge their common participation, which is a rare event.

4.1 Combustion Phenomena Associated with solid propellant rocket motor operation

Alain DAVENAS will give an overview, from an engineering point of view, of all the phenomena related to combustion which have to be considered for designing a sound solid propellant grain. This lecture is intended to make a link between the engineer and the scientist, between practical issues and basic scientific investigations. Each of the following lectures will be, at least partially, connected with this first lecture.

4.2 Solid propellant steady combustion (two lectures)

Guy LENGELLE and Professor Kenneth K. KUO will adddress this essential point on both physical and theoretical aspects. It is the objective of these lectures to give a comprehensive understanding of the physics of the combustion process of various types of solid propellants and also of their ingredients. Another objective is to provide the attendees of LS 180 with the description of the various up to date models of combustion behaviour of double base and composite propellants.

4.3 Erosive burning of solid propellants

This phenomenon is given more and more consideration because of the permanent trend towards high performance rocket motors, which induces high propellant loading density. Erosive burning have to be controlled, so that it can be used instead of being merely a constraint.

Merrill KING will present a review of experimental and modelling work concerning erosive burning of solid propellants.

Here again, double base and composite propellant behaviour will be analysed and the most up to date models will be discussed.

4.4 Effect of wires on solid propellant ballistics

Several rocket motor grains involve the use of metallic wires. One can mention STINGER and SAM 7 Surface to Air missiles as using that type of rocket motors. Metallic wires are used to amplify solid propellant burning rate and thus to make possible the use of grain geometries which, otherwise, would not be acceptable. Merrill KING will review the phenomenon and the various models available. Some of them are related to the "pure" phenomenon (for propellant strands), other are coupled with the rocket motor chamber ballistics analysis so as to provide prediction of pressure (and thrust) versus time history.

4.5 Combustion instabilities

Combustion instabilities may have, in some rocket motors, catastrophic effects such as overpressure. They are difficult to predict accurately. Basic physical phenomena will be analysed by Paul KUENTZMANN. State of the art of available predictive methods of rocket motor stability will be presented. Some examples will be given in order to illustrate this lecture.

4.6 Ignition and unsteady combustion

Professor KUO will review the literature available in the field of solid propellant ignition so as to present a comprehensive

description and evaluation of the state of the art in ignition to date.

Professor KUO will also present the phenomena and the models related to transient burning. One has to be aware that instantaneous burning rate under transient conditions may differ significantly from the steady state corresponding value.

4.7 Combustion and safety of solid propellant rocket motors

Tom BOGGS will discuss these important topics. The content of his lecture will be partially based on the work presented in Agardograph 316 "Hazard studies for Solid Propellant Rocket Motors" which will be distributed to the Lecture Series attendees. Some updated information will also be presented so that these materials will represent the state of the art in this critical field.

5. CONCLUSION

We shall conclude this Lecture Series by an attempt to make a synthesis on this wide topic of solid propellant combustion and by a round table discussion.

During the synthesis, we shall try to unformally address the topics which were not addressed during the Lecture Series, because although of interest, they were not selected when preparing these sessions. One can mention, rocket motor plume technology, thermodynamical properties (and calculation) of solid propellant, combustion of solid fuel and fuel rich propellants in ducted rockets, computer codes for calculation of propellant grain recession during combustion, comparison between gun propellant combustion and rocket propellant combustion...

During the round table discussion, the lecturers will address, in more details, the points presented during the Lecture Series, that the attendees would like to go deeply into. Together, we shall also try to point out the topics for which the knowledge is not at a satisfactory level, considering the needs for an accurate prediction of performance, safety and reliability of rocket motors operation.

Introduction à la série de conférences LS 180

Bernard ZELLER
Directeur de la Stratégie et du Marketing
SNPE
12, quai Henri IV, 75004 PARIS FRANCE

1. PREAMBULE (Comment est née la Série de conférences LS 180)

En 1988 et 1989, L'AGARD a organisé une double série de conférences (LS 150) sur les méthodes de conception des moteurs à propergol solide. Le directeur de cette série de conférences était l'Ingénieur en Chef de l'Armement REYDELLET du Service Technique des Engins à la Délégation Générale à l'Armement (FRANCE). Cette série de conférences a remporté un tel succès qu'elle a été présentée une première fois, en 1988, aux Pays-Bas, en Grèce, en Turquie et aux Etats-Unis d'Amérique puis une deuxième fois, en 1989, au Royaume Uni, en France, en Allemagne et en Italie. Une part conséquente de cette série de conférences était, bien entendu, consacrée à la conception des chargements de propergol solide. La question de la combustion des propergols, qui est au coeur du principe de la propulsion par moteur à propergol solide, y était traitée, mais pas en détail. Divers points étaient abordés tels que : la combustion normale stationnaire, l'allumage, la combustion instationnaire, la combustion érosive, les instabilités de combustion, etc... De nombreux auditeurs de la Série de conférences LS 150 ayant souhaité obtenir des compléments d'information sur ces sujets, le Comité Energétique et Propulsion (PEP) de l'AGARD a proposé de consacrer une série entière de conférences à cette question de la combustion des propergols solides. Cette proposition a été approuvée par le Conseil des Délégués Nationaux (NDB) de l'AGARD, puis organisée par Plans et Programmes de l'AGARD en relation avec le Comité Energétique et Propulsion.

C'est là l'origine de la série de conférences LS 180 qui est une suite utile de la série de conférences LS 150 (on pourrait aussi envisager, dans le même esprit, d'autres séries de conférences spécialisées, par exemple sur les propriétés mécaniques et le dimensionnement mécanique des chargements de propergol solide, ou encore sur la technologie des jets de propulseur).

2. ROLE DE LA COMBUSTION DANS LE FONCTIONNEMENT DES MOTEURS A PROPERGOL SOLIDE

La combustion est le phénomène central du fonctionnement des moteurs à propergol solide. C'est l'étape où la matière condensée (solide) est transformée en produits gazeux à haute température. L'énergie "potentielle" contenue dans le propergol se change en énergie thermique puis, grâce à une tuyère, en énergie cinétique du mélange des gaz de combustion. Plus la température de ce mélange est élevée et plus la masse moléculaire moyenne de ce mélange est faible, plus le propergol a une impulsion spécifique élevée. L'impulsion spécifique d'un propergol (impulsion fournie par l'unité de masse de propergol dans des conditions données) est proportionnelle à la racine carrée de la température des gaz de combustion divisée par la masse moléculaire moyenne de ces gaz:

$$Is = k\sqrt{\frac{Tc}{M}}$$

Cependant, il n'est pas suffisant de "fournir de l'impulsion". Cette impulsion est l'intégrale de la poussée au cours du temps et la poussée doit être contrôlée (avoir un profil donné) pendant le fonctionnement du moteur. La poussée est liée à la pression dans le moteur par la relation :

$$F = C_F . P . A_T$$

F : poussée
C_F : coefficient de poussée de la tuyère
P : pression à l'intérieur du moteur
A_T : aire de la section droite du col de tuyère

La pression instantanée dans le moteur est le résultat de l'équilibre de flux gazeux entrant et sortant :

- un flux entrant dû à la combustion du chargement de propergol,
- un flux sortant dû à l'éjection des produits de combustion à haute température au travers de la tuyère.

Ceci peut s'écrire ainsi :

$$\rho S/c = P . C_D . A_T$$

ρ : masse volumique du propergol
S : aire de la surface de propergol en combustion
Vc : vitesse de combustion linéaire du propergol
P : pression interne
C_D : coefficient de débit de la tuyère
A_T : aire de la section droite du col de tuyère

Cette équation ne peut être écrite et ne correspond à un régime stable que si l'on fait l'hypothèse que :

- le propergol brûle en "couche parallèle", ce qui signifie que le front de combustion régresse parallèlement à lui-même à une vitesse dont le vecteur est normal au front (combustion normale);
- l'augmentation relative de la vitesse de combustion avec la pression est moindre que l'augmentation relative de cette dernière.

Ces questions sont au coeur de celles qui sont traitées au cours de cette série de conférences.

LES PROPERGOLS SOLIDES DOIVENT BRULER EN COUCHES PARALLELES.

LA VARIATION RELATIVE DE LA VITESSE DE COMBUSTION DOIT ETRE PLUS FAIBLE QUE LA VARIATION CORRESPONDANTE DE LA PRESSION

Au-delà de ces spécifications de base, de nombreux autres phénomènes doivent être connus, maîtrisés et contrôlés. Les moteurs à propergol solide doivent être performants, sûrs et fiables. Il faut disposer de méthodes de prédiction du fonctionnement des moteurs sûres et précises. Ces besoins nécessitent une connaissance approfondie des phénomènes liés à l'allumage, à la combustion instationnaire, à la combustion érosive, aux instabilités de combustion, à la transition de la déflagration vers la détonation...

3. COMBUSTION EN COUCHES PARALLELES

En 1991, il semble évident que les propergols solides brûlent en couches parallèles. Cela n'a pas été toujours le cas, et il faut bien avoir à l'esprit que, même de nos jours, un mode de combustion dégradé par rapport au mode nominal peut induire des effets extrêmement néfastes, tels que la transition déflagration détonation.

Jusqu'en 1884, le propergol solide unique était la poudre noire. Ce propergol, même fortement compacté, ne peut brûler complètement en couches parallèles dans un canon. De plus, il crée beaucoup de fumée et sa force est limitée. Au milieu du 19ème siècle, il est apparu que la nitrocellulose pouvait être un propergol (une poudre) très intéressant: de nombreux programmes d'essai ont été menés à cette époque afin de l'utiliser pour propulser les projectiles dans les canons. Sa force est trois fois supérieure à celle de la poudre noire et elle est sans fumée. Mais, même compacté, ce produit ne brûlait pas régulièrement et ce comportement irrégulier entraînait l'explosion de nombreux canons.

En 1884, Paul VIEILLE a découvert comment gélatiniser la nitrocellulose en la mélangeant intimement avec un mélange éther-alcool puis en éliminant ce solvant, après malaxage et mise en forme de grains ou de bandes. Au lieu d'un matériau à structure fibreuse, la nitrocellulose traitée ainsi avait une structure compacte et non poreuse qui conduisait à une combustion en couches parallèles. C'était la naissance des poudres à simple base.

A peu près à la même époque, Alfred NOBEL découvrait que la nitrocellulose, travaillée mécaniquement avec de la nitroglycérine à des températures supérieures à la normale, se transformait aussi en un matériau compact et non poreux. C'était la naissance des propergols à double base sans solvant dont l'épaisseur peut atteindre plusieurs centimètres.

Au cours du 20ème siècle, de nouvelles familles de propergol solide sont apparues, telles que les propergols à double base moulés et, durant la 2ème guerre mondiale, les propergols composites.

Les propergols composites, à matrice polymérique chargée par un oxydant et un combustible métallique (aluminium) brûlent, d'un point de vue macroscopique, en couches parallèles. Microscopiquement, étant donné que le matériau n'est pas homogène, le front de flamme n'est pas plan et, strictement parlant, la combustion ne s'effectue pas en couches parallèles.

L'épaisseur à brûler de ces chargements de propergol n'a pas théoriquement de limite supérieure. Des chargements de quatre mètres de diamètre ont déjà été fabriqués.

Comme il a été dit plus haut, une combustion en couches parallèles n'est pas suffisante pour qu'un chargement de propergol fonctionne correctement. Le concepteur de chargement doit disposer de propergols dont il doit pouvoir régler la vitesse de combustion. La recherche de performances toujours améliorées implique également une connaissance et une maîtrise de la combustion érosive et des instabilités de combustion.

4. ORGANISATION ET DEROULEMENT DE LA SERIE DE CONFERENCES

Pendant cette session six orateurs présenteront huit conférences. Ces orateurs sont parmi les meilleurs spécialistes mondiaux de la combustion des propergols solides. Tous sont reconnus comme les meilleurs dans leurs pays. Ils ont accumulé des connaissances et de l'expérience au cours des années et, de plus, ils possèdent tous la passion de faire savoir, de transmettre ces connaissances. A cause de cette compétence même, ils ont d'importantes responsabilités et des emplois du temps très chargés. En dépit de cela, ils ont consacré une part importante de leur temps à préparer leur(s) conférence(s). Nous sommes fiers de leur participation à cette série de conférences et nous saluons cette réunion de spécialistes qui est un événement rare.

4.1 Phénomènes de combustion liés au fonctionnement des moteurs à propergol solide

Alain Davenas passera en revue et analysera, du point de vue de l'ingénieur, l'ensemble des phénomènes liés à la combustion dont il faut tenir compte pour pouvoir concevoir et réaliser un chargement de propergol solide de bonne qualité. Le but de cette conférence est d'établir un lien entre l'ingénieur et le scientifique, entre les problèmes pratiques et les recherches scientifiques de base. Chacune des conférences suivantes sera, au moins partiellement, liée à cette première conférence.

4.2 Combustion stationnaire des propergols solides (deux conférences).

Guy LENGELLE et le professeur KUO traiteront cette question essentielle sous ses deux aspects : physique et théorique. C'est le but de ces deux conférences de présenter une description détaillée de la physique des phénomènes liés à la combustion stationnaire de diverses familles de propergol solide (et aussi de leurs constituants). Un autre objectif est de fournir aux auditeurs de cette série de conférences une description tout à fait à jour des différents modèles de combustion des propergols double base et des propergols composites.

4.3 Combustion érosive des propergols solides

Le phénomène de la combustion érosive est étudié de plus en plus car la tendance générale à l'augmentation des performances des moteurs à propergol solide induit une augmentation du coefficient de remplissage de ces moteurs et donc l'apparition beaucoup plus fréquente de la combustion érosive. Il faut connaître et maîtriser ce phénomène, de façon à ce qu'il ne soit plus considéré uniquement comme une contrainte mais qu'il soit éventuellement utilisé fonctionnellement.

Merrill KING passera en revue les travaux les plus récents relatifs aussi bien à la connaissance expérimentale, qu'à la connaissance théorique de la combustion érosive.

4.4 Effets de fils métalliques sur la combustion des propergols solides

Plusieurs chargements de moteur à propergol solide de missiles utilisent des fils métalliques : on peut citer le STINGER et le SAM 7 qui sont des missiles Surface Air à courte portée. Les fils métalliques sont utilisés pour augmenter fortement la vitesse de combustion des propergols solides ce qui autorise l'usage de géométries de chargement particulièrement intéressantes. Merrill KING examinera l'ensemble des phénomènes liés à ce mode particulier de combustion et présentera les modélisations correspondantes. Certaines de ces modélisations sont relatives au phénomène élémentaire, d'autres, couplées à la balistique interne des moteurs, conduisent à une prévision de la pression et de la poussée du moteur en fonction du temps.

4.5 Instabilités de combustion

Les instabilités de combustion peuvent avoir dans certains moteurs-fusées des conséquences très graves, par exemple, des surpressions conduisant à l'explosion de la structure. Elles sont difficiles à prévoir avec précision. Les phénomènes physiques de base seront analysés par Paul KUENTZMANN. L'état des connaissances en ce qui concerne les méthodes de prévision de la stabilité du fonctionnement sera présenté. Quelques exemples pratiques seront donnés afin d'illustrer cette conférence

4.6 Allumage et combustion instationnaire

Le professeur KUO passera en revue et synthétisera la littérature disponible dans le domaine de l'allumage des propergols solides afin de présenter une description et une évaluation de l'état de l'art en ce qui concerne l'allumage des propergols solides.

Le professeur KUO présentera aussi les phénomènes physiques et les modèles liés à la combustion instationnaire. Ce point est important car il peut arriver que la vitesse de combustion d'un propergol dans des conditions très instationnaires soit très différente de la vitesse observée à la même pression mais dans des conditions stationnaires.

4.7 Combustion et sécurité des moteurs à propergol solide

Tom BOGGS traitera cette question de grande importance. Le contenu de sa conférence sera fondé en partie sur le travail présenté dans l'AGARDographie 316 "Hazard Studies for Solid Propellant Rocket Motors" qui sera distribuée aux auditeurs de la Série de Conférences. Une mise à jour des informations sera également présentée de sorte que cette conférence représentera l'état des connaissances dans ce domaine capital.

5. CONCLUSION

Nous conclurons cette série de conférences d'une part en essayant de synthétiser les connaissances sur le large sujet de la combustion des propergols solides et, d'autre part, en organisant une table ronde sur le sujet.

Pendant la synthèse, nous tenterons de traiter de manière informelle quelques sujets non abordés pendant la série de conférences et qui seraient d'intérêt pour les auditeurs. Ces sujets pourraient être choisis parmi les suivants :

- technologie des jets de moteurs à propergol solide;
- propriétés thermodynamiques des propergols solides;
- combustion des combustibles solides et des semi-propergols dans les statofusées;
- calcul de l'évolution de surface en combustion d'un chargement de propergol;
- comparaison de la combustion des propergols pour moteurs-fusées et des poudres à canon;
- effets du vieillissement sur les propriétés de combustion, etc...

Pendant la table ronde, les conférenciers traiteront plus en détail les sujets, présentés durant leur(s) conférence(s), que les auditeurs voudraient voir approfondir. Ensemble, nous tenterons également de mettre en évidence les domaines où les connaissances ne sont pas à un niveau suffisant pour satisfaire les besoins de prévision du fonctionnement, des performances, de sécurité et de fiabilité des moteurs à propergols solide.

PHENOMENES DE COMBUSTION RENCONTRES DANS LE FONCTIONNEMENT DES PROPULSEURS A PROPERGOL SOLIDE

Alain Davenas
SNPE - Division Défense Espace
12, quai Henri IV - 75181 PARIS CEDEX 04

RESUME

La conception et la maîtrise du fonctionnement d'un moteur à propergol solide à haute performance implique une connaissance approfondie et l'élaboration de modèles précis de nombreux phénomènes physiques : combustion, interaction de l'écoulement interne avec la combustion, instabilités, formation du jet... dans lesquels les caractéristiques de combustion du propergol jouent un rôle important.

L'amélioration de ces modèles et les connaissances d'origine expérimentale de nombreuses anomalies balistiques permettent aujourd'hui au concepteur d'un nouveau moteur de prédire ses performances avec une précision de l'ordre de quelques pour-cent. Les principales difficultés rencontrées sont toujours liées à la disponibilité d'un propergol ayant de "bonnes caractéristiques" de cinétique de combustion.

L'imprécision des prévisions balistiques et les variabilités balistiques sont principalement liées à l'influence du procédé de fabrication du chargement de propergol sur ses caractéristiques cinétiques.

L'existence et l'importance des instabilités de combustion particulièrement dans la propulsion des missiles tactiques avec des propergols discrets est probablement encore aujourd'hui le plus grand risque rencontré lors du développement d'un nouveau moteur.

Dans l'avenir, l'accent mis sur la réduction de la vulnérabilité et la recherche de propergols discrets à haute énergie induiront de nouveaux efforts de recherche sur les caractéristiques de combustion des propergols et le développement de nouvelles architectures de moteurs : sans tuyère, hypervéloces, à impulsion multiple...nécessitera de nouveaux efforts de modélisation et d'essais.

1. INTRODUCTION

Dans cette conférence, nous avons tenté d'aborder les problèmes de combustion associés au fonctionnement des propulseurs selon le point de vue de l'ingénieur et du praticien. Nos collègues présenteront certainement des approches plus rigoureuses et plus fondamentales de chacun des phénomènes évoqués.

D'autre part, l'état de l'art que nous décrivons est bien entendu largement lié à une expérience personnelle dans l'organisme et le pays dans lequel nous travaillons. Dans ces conditions, et également compte tenu des questions de confidentialité, il est certain que cette description pourra apparaître, sur certains points, incomplète pour certains lecteurs ou auditeurs très informés. Les discussions pourront d'ailleurs être l'occasion d'enrichir le sujet avec la participation de l'auditoire.

Une difficulté consistait à cerner l'étendue exacte du sujet. Nous nous sommes inspirés pour cela du contenu de l'ouvrage de Kuo et Summerfield (1) et retenu essentiellement de traiter les caractéristiques de combustion intrinsèques des propergols, leur modification éventuelle selon l'architecture et le procédé de réalisation du chargement, la combustion érosive mais pas ou peu l'aérodynamique interne qui connaît actuellement d'immenses développements mais ne relève pas directement des phènomènes de combustion, d'instabilité, et complété cette présentation par l'examen des caractéristiques de combustion liées à certaines géométries ou caractéristiques particulières de chargements.

2. FONCTIONNEMENT DES MOTEURS A PROPERGOL SOLIDE

La combustion d'un propergol solide est caractérisée par la façon dont la surface du chargement régresse lorsqu'il brûle. La vitesse de combustion est la distance parcourue par le front de flamme par unité de temps, mesurée dans une direction normale à la surface de combustion. Il est admis que ce front est régulier et qu'il progresse dans la plupart des cas dans une direction normale à lui-même (combustion par couches parallèles). Ceci a été vérifié expérimentalement, par exemple en procédant à des extinctions à différentes phases d'un tir et en examinant la surface obtenue.

Le fonctionnement d'un moteur typique (fig.1) correspond à l'égalité des débits gazeux issus de la combustion du propergol d'une part et du débit éjecté par la tuyère d'autre part. La vitesse de combustion et la pression interne ou pression de chambre p_c sont alors reliés par :

$$P_c = \frac{\rho S v}{C_D A_t}$$

où S est l'aire de la surface en combustion, A_T l'aire du col de la tuyère et C_D le coefficient de débit de la tuyère.

Le paramètre $K = S/A_T$ appelé serrage est un paramètre important pour caractériser le fonctionnement interne du moteur.

La vitesse de combustion du propergol est une fonction de la pression

$$v = f(p)$$

Dans un intervalle de pression, elle peut souvent être représentée par une loi (loi de Saint-Robert) du type :

$$v = a p^n$$

de sorte que :

$$p^{n-1} = \rho \frac{S a}{C_D A_T}$$

ce qui montre que dès que l'évolution de surface est connue l'évolution de la pression est déterminée. Des codes bi et tridimensionnels ont été développés pour calculer cette évolution géométrique.

Certains codes peuvent prendre en compte une vitesse de combustion variable en fonction du temps et de l'espace, ce qui permet de tenir compte d'anomalies balistiques qui seront décrites ultérieurement (2).

L'effet de la température sur la vitesse de combustion et donc sur les lois de pression et de poussée est caractérisé par deux coefficients :

$$\pi_K = \frac{1}{v}\left(\frac{\partial v}{\partial \theta}\right)_K$$ caractérise la sensibilité du moteur (K constant)

$$\pi_P = \frac{1}{v}\left(\frac{\partial v}{\partial \theta}\right)_P$$ caractérise la sensibilité du propergol (p constant)

Il est facile de démontrer la relation :

$$\pi_K = \frac{\pi_P}{1-n}$$

entre les coefficients de température. On constate qu'un exposant élevé a des conséquences néfastes car les spécifications de propulsion imposent généralement des variations réduites de la durée de combustion du moteur.

Nous verrons ultérieurement que des exposants élevés conduisent également à des valeurs élevées de la réponse acoustique du propergol qui aggraveront la sensibilité du moteur l'utilisant aux instabilités de combustion.

Il n'est donc pas étonnant que l'ingénieur chargé de la conception du moteur souhaite disposer d'exposants de pression les plus faibles possibles et que le formulateur demande aux chercheurs sur les mécanismes de combustion de l'aider dans cette tâche.

3. LES FAMILLES DE PROPERGOLS SOLIDES ET LEUR CARACTERISTIQUES DE COMBUSTION

3.1 Les propergols

Six familles de propergols sont aujourd'hui principalement utilisées industriellement. Elles sont décrites en détail dans des ouvrages spécialisés (3) :

- Les propergols double base extrudés ou SD (sans dissolvant) en français dont les principaux ingrédients sont la nitrocellulose et la nitroglycérine. Après imprégnation de la nitrocelluloses par la nitroglycérine, généralement dans l'eau, qui conduit à une pâte ou galette, la composition est élaborée par malaxage avec des additifs, laminage et extrusion sous forme de bloc. Les procédés modernes utilisent l'extrusion continue avec des machines bivis.

- Les propergols double base moulés (Epictète en français) ont des compositions analogues mais sont préparés par gélatinisation d'une poudre à mouler à base de nitrocellulose et contenant les additifs préalablement préparés par un mélange riche en nitroglycérine.

  Les propergols SD et Epictète sont souvent appelés homogènes car les espèces oxydantes et réductrices sont contenues dans la même molécule.

- Les propergols double base peuvent être chargés avec des charges énergétiques telles que l'hexogène ou l'octogène (en français Nitramites) ou d'autres charges énergétiques telles que perchlorate d'ammonium (PA) ou aluminium. Ce sont des double base composites.

- Les propergols du type double base moulés peuvent être modifiés par réticulation de la nitrocellulose, éventuellement conjuguée avec un polymère hydroxylé polyester ou polycaprolactone.

  Ces quatre familles peuvent être chargées avec des solides énergétiques; aujourd'hui pratiquement seulement des charges de type CHON sont utilisées ce qui leur confère des caractéristiques de discrétion, ou de "fumée minimum" du fait que les espèces condensées dans les produits éjectés sont en concentration faible dans la plupart des conditions atmosphériques rencontrées.

- Les propergols composites sont basés sur un liant non énergétique, généralement hydrocarboné (typiquement de type polybutadiène) et sur le perchlorate d'ammonium auquels sont éventuellement ajoutés une poudre d'aluminium et éventuellement des ingrédients énergétiques tels que l'hexogène ou l'octogène. Ils sont fabriqués par malaxage des charges avec les ingrédients liquides du liant, coulée ou injection et cuisson. Les propergols sans aluminium sont à "fumée réduite" : il n'y a formation de fumée que dans certaines conditions d'humidité et de température ambiante qui permettent la condensation de l'eau avec le gaz chlorhydrique résultant de la combustion du perchlorate.

- Les propergols à haute énergie sont des composites basés sur un liant énergétique généralement plastifié par un ester nitrique ou un mélange d'esters nitriques. Les charges sont en général tout ou partie des suivantes : hexogène, octogène, PA, aluminium conférant suivant le cas des caractéristiques d'indiscrétion totale, de fumées réduites ou de fumées minimales.

A côté de ces principaux composants, les compositions de ces propergols peuvent contenir divers ingrédients à faible taux tels que : stabilisants, catalyseurs balistiques, additifs anti instabilités, suppresseur de post-combustion, etc...

Les termes de "fumée réduite" ou de "fumée minimale" employés précédemment ne sont évidemment pas suffisants pour permettre de classer ou de comparer des propergols entre eux et vis-à-vis des applications. Un groupe de travail de l'AGARD (4) a élaboré une méthode afin de permettre des comparaisons entre des propergols élaborés dans différents organismes et différents pays. L'idée de base de la méthode est de caractériser le niveau de fumée primaire et secondaire de tout propergol. Pour ne pas dépendre des moyens de mesure de la transmission optique dans le jet et des résultats absolus, la classification proposée repose sur la comparaison à deux propergols de référence et le classement sera basé sur des sanctions du type "plus que" ou "moins que".

3.2 Caractéristiques de combustion

La limitation des vitesses de combustion disponibles pour un projet donné est l'une des grandes frustrations des concepteurs de moteurs.

En pratique ces vitesses sont déterminées à diverses températures avec des petits moteurs standard d'évaluation balistique. Ils utilisent, autant que possible, des chargements conduisant à des courbes de pression plates et des fins de combustion sans résiduel pour permettre des mesures précises.

Des méthodes plus efficaces économiquement sont de plus en plus utilisées. Elles permettent d'obtenir v = f(P) sur tout un domaine de pression à l'aide de dispositifs à serrage variable au cours du tir. La vitesse de régression du propergol peut même être mesurée directement par ultrasons à partir d'une mesure instantanée de l'épaisseur du propergol inbrulée (5).

PROPERGOLS SD

La figure 2 montre des courbes vitesse-pression typiques d'un propergol double base SD. Outre l'utilisation de modificateurs balistiques, des noirs de carbone sont souvent incorporés car ils ont une efficacité importante pour régler la vitesse de base de la composition s'ils sont associés aux modificateurs balistiques (seuls ils sont sans effet). Le taux de noir de carbone est souvent utilisé industriellement comme paramètre de réglage pour réajuster la vitesse de combustion lors de changements de lots de matières premières.

Les autres paramètres influents de la composition sont bien entendu le taux et la granulométrie des catalyseurs balistiques. Même si des spécifications étroites relatives à la granulométrie et la surface spécifique des catalyseurs existent, il est souvent nécessaire lors d'un changement de lot de ces ingrédients critiques de procéder à une nouvelle qualification de l'asortiment de matières premières à utiliser en production par des fabrications et des tirs de blocs standard en faisant varier un paramètre de réglage. Lorsque les spécifications balistiques sont particulièrement pointues, il peut être nécessaire d'aller jusqu'au tir de vérification d'un moteur témoin avant de lancer la production.

Les paramètres du procédé ont également une influence importante sur le niveau de vitesse et sur le coefficient de température, dans la mesure où ils agissent sur l'homogénéité de la dispersion des catalyseurs et sur l'état de gélatinisation des propergols. On peut ainsi observer une nette influence du temps et de la température de laminage sur la diminution de l'exposant de pression et l'apparition du plateau.

Propergols double base moulés

Les moficateurs balistiques utilisés sont analogues, par contre l'influence du procédé passe par un mécanisme différent : le paramètre le plus influent est celui de la gélatinisation de la poudre à mouler lors de son élaboration en fonction du taux et de la nature du solvant utilisé. Le solvant de moulage utilisé pour l'élaboration du propergol aura plus ou moins de facilité à dissoudre le grain de poudre à mouler selon la façon dont il a été préparé et cela a de grandes conséquences sur les caractéristiques du propergol obtenu à composition finale identique.

Le réglage industriel passe donc généralement par la réalisation de lots témoins ou partiels de poudre à mouler à partir desquels sont réalisés des blocs standard qui sont ensuite tirés. A partir de mélanges de ces partiels, on pourra alors réaliser un lot de poudre à mouler qui sera à nouveau testé. Un lot de base pour la production industrielle pourra alors être constitué. On conçoit que ceci entraine des cycles extrêmement longs pour le réglage et la production de ces propergols et des coûts élevés. Il n'a malheureusement pas été possible d'établir des abaques permettant à coup sûr d'obtenir les bonnes caractéristiques balistiques à partir de partiels de caractéristiques connues.

Une autre particularité de ces propergols est la possibilité de mélanger des poudres à mouler de caractéristiques volontairement différentes ce qui permet une adaptation des caractéristiques cinétiques et balistiques. Ceci est en particulier réalisé pour l'incorporation d'additifs antilueurs (suppresseurs de la post combustion). Ceux-ci, généralement des sels de potassium, s'ils sont incorporés directement, interfèrent avec les mécanismes de platonisation par les modificateurs balistiques. Par contre, un mélange de certaines proportions de poudres à mouler, l'une contenant seulement les additifs balistiques, l'autre seulement l'agent antilueur, permet de conserver les caractéristiques cinétiques initiales. Il est même possible d'aller plus loin et d'incorporer une troisième poudre à mouler ne comportant ni additif balistique, ni additif antilueur, sans que les bonnes caractéristiques cinétiques soient modifiées alors que bien entendu la discrétion et l'énergie disponible sont augmentées. Ses proportions peuvent même être utilisées comme paramètre de réglage du second ordre pour ajuster industriellement la vitesse de combustion.

Propergols composites

La vitesse de combustion des propergols composites au perchlorate d'ammonium est essentiellement contrôlée par la granulométrie de celui-ci, les plus fines conduisant aux vitesses les plus élevées. Elle croit aussi avec le taux de PA. Un grand nombre de variétés granulométriques sont donc utilisées industriellement pour ajuster la vitesse : des variétés de granulométrie moyenne 400, 200, 100, 10, 3 et 1 micron sont généralement utilisées.

La vitesse peut être également modifiée à l'aide de catalyseurs de combustion. Le chromite de cuivre et l'oxyde ferrique sont utilisés depuis longtemps. Pour accéder à des vitesses plus élevées, il est nécessaire de pouvoir introduire l'élément actif en concentration plus élevée et sous une forme plus active. Des dérivés liquides du fer ont donc été mis au point (dérivés

ferrocéniques). Ils sont incorporés au liant. L'utilisation simultanée de perchlorates ultrafins conduit aux formulations aux vitesses les plus élevées dans la pratique industrielle. Le fait que les plastifiants ferrocéniques peuvent migrer pendant le vieillissement du propergol a conduit à la mise au point de prépolymères ferrocéniques qui participent au réseau réticulé du liant (6) Les catalyseurs les plus efficaces sont probablement les dérivés organiques du bore (décaborane et dérivés) mais il ne semble pas qu'il y ait eu de développement industriel conséquent de ces composés à la synthèse difficile et onéreuse. De nouveaux oxydes de fer ultrafins sont aujourd'hui développs pour concurrencer les dérivés ferrocéniques mais ceux-ci gardent a priori deux avantages : ils modifient peu la viscosité des pâtes de propergols et les variations de vitesse de lot à lot sont plus faciles à maîtriser qu'avec un catalyseur solide pour lequel la surface spécifique est un paramètre important.

Les exposants de pression sont généralement dégradés par l'utilisation de perchlorates fins, en particulier au-dessus de 200 bars. Les catalyseurs de combustion permettent souvent une amélioration.

L'influence de la présence d'aluminium dans la composition est généralement due deuxième ordre, sauf dans le cas où le propergol est soumis à des accélérations élevées.

Industriellement, il est souvent nécessaire de procéder à un nouveau réglage de la vitesse de combusiton lorsqu'il y a changement de lot des ingrédients les plus actifs (particulièremeit PA et catalyseur). Il est possible d'agir sur la proportion des diverses granulométries et sur le taux de catalyseur, s'il y en a (cette dernière méthode est généralement recommandée). Même avec les mêmes matières premières des variations du procédé de fabrication peuvent influencer la vitesse, par exemple le temps d malaxage (broyage du PA de granulométire élevée). Nous verrons plus loin que le procédé de coulée peut également la modifier.

La figure 3 résume les plages de vitesse de combustion des principales familles de propergols industriels.

Coefficient de température

Grâce aux effets plateau ou mésa, les propergols double base peuvent conduire à des coefficients de température très faibles. Ceci est généralement d'autant plus difficile à obtenir que l'énergie (le potentiel) du propergol est élevée.

Les valeurs de π_p, pour les composites du PA sont généralement de l'ordre de 0,2% C^{-1}.

Autres propergols : nous nous bornerons à quelques indications.

L'introduction d'une nitramine dans les propergols double base conduit généralement à une réduction du niveau de vitesse. Pour des taux de charges limités (quelques dizaines de pour-cent) la cinétique de combustion du propergol est cependant modifiée (fig. 4). Pour des taux élevés (propergols à heute énergie), elle est fortement modifiée, le mécanisme de décomposition de la nitramine l'emportant. Ceci est également vrai pour les composites à base de nitramines (7).

4. INFLUENCE DES ECOULEMENTS INTERNES SUR LA VITESSE DE COMBUSTION

Les produits de combustion du propergol interagissent avec sa combustion et peuvent modifier la loi de combustion.

Dans les tout premiers calculs balistiques des performances d'un moteur, il est souvent supposé que la vitese des gaz de combustion est négligeable et que l'écoulement ne s'accélère qu'à l'entrée du convergent de la tuyère pour atteindre la vitesse du son locale au col. Selon la géométrie du chargement on peut cependant calculer des vitesses de l'ordre de 100 à 150m/s dans le plan de sortie du canal central après allumage et pressurisation du moteur. Deux types de phénomènes caractéristiques sont rencontrés :

- une perte de charge et un gradient de pression entre l'avant et l'arrière du canal central,
- une augmentation locale de la vitesse de combustion due à la combustion érosive.

Le moment le plus critique dans le fonctionnement d'un propulseur intervient donc juste après l'allumage, alors que l'ensemble est pressurisé et que les sections de passage par lesquelles les gaz doivent s'écouler sont minimales (fig. 5). Dans certains cas des différences de pression avant-arrière de plusieurs MPa ont été rencontrées.

Au stade de l'avant-projet, il est nécessaire de quantifier de façon rapide et simple l'intensité probable des effets d'écoulement Le tableau I ésume les ordres de grandeur des principaux paramètres influents : Kp et J et es effets correspondants observés :

$$J = \frac{K_p}{K} \qquad \text{où Kp est le serrage}$$

local dans une section considérée du canal: rapport de cette section à l'aire de la surface de combustion en amont de celle-ci.

K_p est lié au débit masse unitaire G :

$$G = \rho \, v \, K_p$$

J donne une idée de la vitesse maximale des gaz (on a approximativement J=M, nombre de Mach, dans la section de sortie du canal) et des difficultés de balistique intérieure susceptibles d'être rencontrées.

Des valeurs élevées de J et même J=1 (moteur sans tuyère) peuvent être utilisées si la géométrie du bloc est adaptée à :

- des gradients de pression élevés;
- une combustion érosive élevée;
- une phase d'allumage délicate.

Combustion érosive : l'augmentation locale de la vitesse de combustion due à l'écoulement tangent à la surface du propergol par rapport à la vitesse mesurée sans écoulement important est appelée combustion érosive. La valeur de Kp du

chargement donne une idée du risque de combustion érosive. Ce phénomène est dû à un accroissement des transferts de chaleur de la zone de flamme à la surface de propergol. De nombreux modèles physiques ont été élaborés pour représenter et quantifier le phénomène (8) (9).

Les modèles monodimensionnels sont généralement assez bien adaptés pour le calcul de la balistique interne de chargements tactiques ayant des L/D élevés avec une section de canal central peu ou lentement variable suivant l'axe. La précision de ces modèles (environ 5% sur la pointe de pression à l'allumage) permet de définir des chargements avec des J élevés et une combustion érosive importante dans la partie arrière du canal. Les modèles bi et surtout tridimensionnels incluant la combustion érosive sont beaucoup moins au point et d'une utilisation difficile.

Des modèles prédictifs satisfaisants existent aujourd'hui pour les propergols composites mais ils manquent encore relativement pour les propergols contenant des nitramines qui paraissent nettement moins sensibles à la combustion érosive.

La combustion érosive est souvent rencontrée dans les moteurs tactiques en raison de leur élancement et de coefficients de remplissage élevés. Elle est souvent considérée comme un problème ou une contrainte du dimensionnement. Réciproquement, il y a de plus en plus de cas où la combustion érosive est utilisée dans le dimensionnement pour mieux satisfaire les spécifictions de propulsion. En général de fortes poussées initiales sont recherchées et la combustion érosive peut fournir le supplément de poussée que la surface initiale ne peut fournir à elle seule.

5. PREVISION DES CARACTERISTIQUES BALISTIQUES, ANOMALIES ET DISPERSIONS BALISTIQUES

Les caractéristiques cinétiques mesurées lors de tirs de petits propulseurs standard doivent souvent être corrigées de quelques pour-cent lors d'un changement d'échelle du moteur. Le procédé de fabrication et ses variations peuvent également avoir une certaine influence sur les caractéristiques de combustion du propergol. Ces facteurs doivent être pris en compte pour une bonne prévision des caractéristiques balistiques d'un moteur.

L'erreur possible sur la loi de vitesse de combustion réelle du propergol dans le calcul balistique d'un nouveau chargement est probablement le facteur qui a le plus d'influence sur la prévision de la loi de pression ou de poussée du moteur qui l'utilise. L'expérience préalable accumulée lors du développement de moteurs de configurations variées est importante pour recaler les prévisions si bien que les données correspondantes sont souvent gardées confidentielles par les sociétés qui développent de nouveaux moteurs.

Nous examinerons à présent trois types d'anomalies balistiques susceptibles de modifier la prévision issue d'un calcul "naïf" et souvent rencontrées dans la pratique.

Effet de bord - Celui-ci peut être particulièrment mis en évidence lors du tir de blocs pleins en combustion frontale dans lesquels apparaît une progressivité inattendue de la pression au cours du tir. Des extinctions en cours de tir font apparaître une augmentation de la surface de combustion qui s'explique très bien par un accroissement de la vitesse de combustion au voisinage de l'inhibiteur entraînant une formation progressive de cône.

Cette modification locale de la vitesse peut avoir de très nombreuses causes, certaines spécifiques aux blocs brulant en combustion frontale, d'autres qui peuvent se retrouver dans tous les types de chargements.

Les principales causes peuvent être les suivantes :

- plus forte concentration de particules fines au voisinage de l'interface (perchlorate fin, catalyseurs balistiques, etc...);
- migration d'ingrédients liquides du propergol dans la protection thermique et modification locale de la composition : augmentation locale du taux de charges solides dans les composites, migration de l'ester nitrique dans les propergols à double base;
- échauffement du propergol par conduction des matériaux au voisinage de l'interface lorsqu'il existe des interstices alimentés par les gaz de combustion.

Effet Hump ou bosse - L'analyse des courbes de pression et de poussée en fonction du temps de tirs de chargements en propergol composite montre que le procédé de fabrication a une influence sur la cinétique de combustion de propergols composites. On observe par exemple que les courbes de pression de blocs standards du contrôle balistique coulés à partir du même propergol et mis en forme avec noyau en place ou par noyautage après coulée présentent des différences caractéristiques. On observe sur la figure 6 que la courbe relative au premier type de bloc présente une bosse caractéristique à mi-épaisseur brulée. on observe en outre que :

- à mi-épaisseur la vitesse de combustion est toujours supérieure de 3 à 7% pour les blocs mis en forme avec noyau en place.
- l'amplitude de la bosse de pression n'est pas fonction de la vitesse de combustion de la composition. Des extinctions ont par ailleurs montré que la surface de combustion est dans les deux cas très proche de la surface théorique : il faut donc attribuer cet effet à une variation de la vitesse de combustion en fonction de l'épaisseur à bruler.

Certaines explications ont été avancées (10). A la coulée des zones enrichies en liant se créeraient par strates au contact du noyau et de la structure dans le cas de la mise en forme noyau en place. Les zones enrichies en liant brûlent moins vite, ce qui expliquerait que la vitesse de combustion soit fonction de l'épaisseur

combustion soit fonction de l'épaisseur brûlée, alors que ces strates sont détruites au noyautage.

Une loi de type $V_2/V_0=f(e)$ où e est l'épaisseur à brûler peut être établie expérimentalement et utilisée dans les avant-projets.

Influence des sollicitations mécaniques - Des sollicitations mécaniques apparaissent dans les chargements moulés-collés lors des cycles thermiques auxquels est soumis le missile et lors de la mise sous pression du tir. Dans certaines zones de chargements en propergol composite soumises à des contraintes internes importantes, une décohésion entre les charges et le liant peut apparaître. Le propergol acquiert alors une porosité interne et devient compressible et la vitesse de combustion est modifiée. La figure 7 illustre cet effet sur un brin de propergol étiré puis inhibé avec un matériau de raideur suffisante pour maintenir l'allongement.

Dans ces condtions, si l'on veut dresser un bilan de nos capacités prédictives lors de la mise au point d'un nouveau moteur, nous sommes tentés, compte tenu de notre expérience, de faire la synthèse suivante : si l'on caractérise par exemple l'erreur possible sur la prévision a priori de la courbe de pression d'un nouveau moteur, il y a deux cas extrêmes en l'absence de combustion érosive :

- Soit il s'agit d'un propergol déjà bien connu et d'architecture de chargement ainsi que d'associations de matériaux d'aménagement interne également bien connues et testées dans des dimensions analogues. Dans ce cas, l'écart entre pévision et tir peut ne pas dépasser 2%.

- Soit il s'agit d'une architecture très nouvelle et d'assemblages de matériaux également nouveaux. Dans ce cas, l'erreur de prévision peut atteindre, voir dépasser 5%.

S'il y a de la combustion érosive, il peut s'y ajouter une erreur de prévision qui peut atteindre 10 à 15% de la valeur de la pointe de surpression érosive.

Il faut cependant noter que d'autres causes d'erreurs ou de dispersions balistiques que nous allons examiner à présent peuvent intervenir. Une présentation récente (11) analyse les causes et l'ampleur des dispersions balistiques, en examinant l'influence de divers paramètres sur la variabilite des durées de combustion. Les coefficients de variation relatifs à la masse de propergol, à sa densité, au coefficient de débit, à l'aire de col de tuyère sont relativement faibles. Les facteurs prépondérants sont :

- la variabilité de la surface de combustion (variations de géométrie liées au procédé de fabrication : désaxage du noyau par exemple) qui peut s'exprimer lors de la prévision d'un premier tir par la méconnaissance de la surface de combustion exacte (compte tenu des refroidissements, déformations, etc...) après cuisson du chargement;

- les variabilités sur la vitesse de combustion réelle du propergol qui trouvent leur source dans les variations des matières premières et du procédé de abrication.

6. INSTABILITES DE COMBUSTION

Le phénomène d'instabilité de combustion peut se produire lorsque des perturbations excitent les modes acoustiques de la chambre de combustion. Des facteurs d'amplification ou d'amortissement vont intervenir : écoulement, particules condensées dans les gaz, tuyère, etc...qui peuvent conduire à une aggravation ou une atténuation du phénomène. Ce phénomène peut se traduire par des vibrations de pression et une augmentation de pression moyenne qui, dans certains cas, peuvent atteindre un niveau inacceptable.

Pour établir un bilan sur le risque d'apparition d'instabilités, une procédure en deux étapes est généralement employée (théorie linéaire).

La pression acoustique dans la chambre est représentée par :

$$\frac{p'}{p_c} = \sum_i \epsilon^{\alpha_i t} e^{j\omega_i t} \psi_i(M) \qquad (j^2 = -1)$$

Po = pression moyenne
P' = pression instantanée au point M
ω_i = pulsation du mode de rang i et de fréquence fi
ψ_i = forme du mode spatial de rang i
α_i = coefficient d'amortissement ($\alpha_i < 0$) ou d'amplification ($\alpha_i > 0$) du mode de rang i

La première étape consiste à calculer les modes acoustiques spécifiques de la cavité en utilisant généralement des méthodes d'éléments finis.

La deuxième étape consiste à calculer . Ces calculs doivent utiliser des éléments décrivant la réponse acoustique du propergol, l'effet des particules condensées, etc...

Selon la valeur de , somme algébrique des coefficients de gain ou d'amortissement, il est possible d'apprécier le risque d'instabilité. Pour un mode de fréquence fi, une valeur de α_i supérieure à 0,1 fi indique une tendance significative à une instabilité de combustion, la géométrie du chargement ou le propergol doivent être alors modifiés.

Réponse acoustique du propergol - Le facteur de gain lié à la réponse acoustique du propergol est souvent calculé à partir de mesures au propulseur en T. D'autres techniques utilisent la modulation périodique forcée d'un moteur standard. Ces dispositifs sont très limités en fréquence. Des modèles de la réponse ont été élaborés, basés sur la description de la zone de combustion. Culick (12) a proposé l'expression suivante :

$$R = \frac{n\,AB}{\lambda + A/\lambda - (1+A) + AB}$$

où :

est une fonction complexe de la fréquence
est l'exposant de pression de la loi $v = ap^n$
A et B sont des constantes issues d'une

analyse physico chimique (énergies d'activation, température de surface...)

Problèmes pratiques d'instabilités de combustion et remèdes possibles

Les instabilités acoustiques sont généralement classées en deux grandes catégories : transverses (radiales et tangentielles) et longitudinales.

- Les instabilités transverses des moteurs tactiques en raison de leurs dimensions ont des fréquences élevées (10000-50000 Hz) et la réponse du propergol est alors très difficile à mesurer. Ces instabilités sont souvent observées avec des propergols non alumin·sés car ces modes sont souvent bien amortis lorsqu'il y a des particules condensées dans les gaz. Le risque d'apparition de ces instabilités est difficile à estimer a priori et des critères semi-empiriques doivent être appliqués.

  Généralement un domaine stable pour un propergol donné peut être caractérisé par une pression de chambre et le rapport de la longueur à un diamètre équivalent du canal central.

  Les principales "recettes" pour agir sur les instabilités transverses consistent à jouer sur :

  - des changements de géométrie qui modifient la fréquence des modes propres de la cavité;
  - un changement de la pression moyenne pour se rapprocher du domaine stable;
  - l'utilisation de structures amortissantes dans la cavité : tige de résonance, barrières, etc...;
  - addition d'une faible quantité de particules réfractaires (carbure de silicium, de zirconium, alumine...) choisies pour fournir l'amortissement maximal à la fréquence considérée. C'est probablement de nos jours le procédé le plus couramment utilisé car il a généralement peu d'influence sur la loi de vitesse et le dimensionnement du chargement.

Nous examinerons à présent des exemples de chacun de ces procédés.

Géométrie

Nugeyre et al (13) ont présenté un cas de couplage acousto-structural dans un chargement libre en propergol double base chargée en hexogène. Ce couplage provoquait l'explosion du moteur à l'allumage à -40° après rupture de l'opercule. Au préalable, des essais très satisfaisants avaient lieu à toutes températures sur un moteur à peu près identique : la seule différence était un accroissement de 1,4mm du diamètre de la structure et du bloc. Aucune des hypothèses habituelles ne pouvait expliquer le phénomène. Un calcul des modes propres de la cavité montra que la fréquence du premier mode transverse était extrêmememnt proche d'un mode propre longitudinal du solide (860 contre 856 Hz) alors que le même calcul sur la première définition conduisait à une différence nettement plus importante. Il fut conjecturé que le phénomène résultait de la rupture mécanique du propergol vitreux à cette température par résonance due au couplage du solide avec les vibrations du gaz dans la cavité; phénomène amorcé par l'ébranlement dû à la rupture de l'opercule.

Un essai montra qu'un changement dans les conditions d'allumage permettait d'éviter l'incident. D'autres essais montrèrent qu'un changement léger de la géopétrie de la section étoilée du canal central aboutisant à un changement des fréquences des modes propres permettait également de résoudre le problème. Les deux remèdes furent finalement appliqués.

Dans un autre cas où, compte tenu de l'échelle, des essais sur moteur réel étaient également possibles, il a été montré que parmi tous les paramètres influents possibles, la variation de ceux relatifs à la géométrie du bloc avait le plus d'effet. En particulier une section étoilée ayant un nombre de branches impair était plus favorable pour la réduction des instabilités que la géométrie en ayant un nombre pair (14).

Influence de la pression

L'influence de la pression de fonctionnement a été systématiquement étudiée de façon empirique dans le cas de chargements de propergol double base, particulièrement sensibles aux instabilités transverses. Les fréquences sont liées à la géométrie du canal central. A serrage constant, pour un chargement de diamètre donné D, il existe généralement une longueur L au-dessus de laquelle apparaissent des instabilités (figure 8). On peut établir un domaine D, L/D d'instabilité que l'on caractérise par la dérive de pression nominale: P/P. On montre également que les pressions jouent un rôle important : absentes à pression élevée, elles appaaissent en revanche vers les basses pressions qui correspondent généralement à la limite inférieure de l'effet plateau. Il et possible de définir une pression seuil ou un serrage seuil au-delà duquel il n'y a plus d'instabilité.

Structures amortissantes (Résonateur d'Helmoltz, tige de résonance). La tige de résonance est le dispositif le plus utilisé. Il est constitué par une tige encastrée à l'avant du propulseur qui occupe tout ou partie de la longueur du canal. Les sections rectangulaires ou cruciformes de ces tiges sont les plus efficaces : elles empêchent la rotation des gaz et suppriment les pics de pression, surtout au début du tir. Ce type de remède a été appliqué de façon souvent très empirique à de nombreux chargements de propergol double base. Une combinaison de cette technique avec l'amortissement par particules solides a été décrite (15) : la tige est enrobée de sulfate de potassium qui joue le double rôle de fournisseur de potassium susceptible d'empêcher la post-combustion dans l'atmosphère des gaz de combustion et de générateur de particules solides dans la chambre de combustion.

Amortissement par particules - La figure 9 montre l'évolution des instabilités de combustion pour un chargement en propergol SD dans lequel on incorpore un taux croissant d'un additif réfractaire dont la

granulométrie a été choisie, compte tenu de sa densité pour avoir l'effet d'amortissement maximal sur le mode acoustique responsable des instabilités.

7. NOUVELLES COMPOSITIONS, NOUVELLES ARCHITECTURES, NOUVEAUX PROBLEMES

Dans les trente dernières années, l'évolution des propergols a été essentiellement caractérisée par la recherche d'une augmentation des performances énergétiques et d'une adaptation des caractéristiques cinétiques aux spécifications des missions envisagées: augmentation des domaines de température, extension des domaines de durées de combustion, etc...

Au plan des applications militaires depuis quelques années, est apparu le besoin d'accroitre la sureté de fonctionnement et la survivabilité des plateformes de combat (bateaux, avions, chars...) dans l'ambiance du champs de bataille ou dans des circonstances accidentelles, ce qui entraîne en particulier au niveau des ensembles propulsifs la nécessité d'augmenter leur discrétion pour diminuer la détectabilité et leur sensibilité aux agressions telles que: incendie, impact par fragments ou par balles, détonation par sympathie.

Au plan de la vulnérabilité, des améliorations progressives peuvent être apportées par des dispositions compensatoires : systèmes de déconfinement rapide ou structures en matériaux adaptés, action sur les propergols pour modifier leurs caractéristiques de combustion : réduction des vitesses de combustion à basse pression après déconfinement, etc...mais pour respecter toutes les spécifications et obtenir des propergols réellement insensibles il est nécessaire d'agir plus profondément sur la composition des matériaux énergétiques.

Ceci est particulièrement vrai pour les propergols détonables lorsqu'ils sont amorcés par onde de choc que sont les propergols à fumée minimale du type double base, nitramites, EMCDB. Il faut alors avoir recours à de nouveaux ingrédients énergétiques qui peuvent soit être utilisés pour augmenter l'énergie des compositions actuelles, soit être utilisés au même niveau d'énergie ou à un niveau inférieur en améliorant les caractéristiques de vulnérabilité. Ainsi le PAG, polyazide de glycidyle, nouveau polymère énergétique peut être utilisé en conjonction avec des nitramines : hexogène ou octogène ou bien être couplé avec des oxydants beaucoup moins énergétiques tels que le nitrate d'ammonium pour augmenter le diamètre critique des compositions discrètes. D'autres recherches sont en cours conduisant à envisager d'autres charges solides nitrées que l'hexogène ou l'octogène. Les caractéristiques de combustion de ces produits sont très nouvelles et les premiers essais montrent de grandes difficultés à maîtriser les exposants de pression et les coefficients de température. Ces nouveaux produits devraient donc relancer les études de mécanismes de combustion. Par ailleurs, s'agissant de propergols discrets générant peu d'espèces condensées dans la chambre, les problèmes d'instabilité de combustion risquent de se poser à nouveau.

Parallèlement, de nouveaux concepts et de nouvelles architectures de chargement émergent dans les applications.

Ces systèmes requièrent des propergols présentant des caractéristiques de combustion particulières et doivent éventuellement présenter en plus les caractéristiques de vulnérabilité réduite et de discrétion. Il s'agit en particulier des propulseurs sans tuyère, des propulseurs pour systèmes hypervéloces et des moteurs à impulsions multiples ("pulse motors").

Propulseurs sans tuyère - Le principe de fonctionnement de ces moteurs conduit à une courbe de pression chambre fortement dégressive (associée à une poussée fortement progressive). L'optimum du fonctionnement conduit à rechercher un compromis sur l'exposant de pression : pas trop élevé à haute pression au début du tir, pas trop faible à base pression pour ne pas avoir une impulsion spécifique trop faible en fin de tir. D'autres complications peuvent apparaître avec la combustion érosive ainsi que par suite la déformation du chargement sous pression qui modifie le serrage.

Propulseurs pour systèmes hypervéloces - Dans ces propulseurs, une impulsion maximale en un temps court est souvent recherchée. L'optimisation du moteur conduit à le faire fonctionner à une pression moyenne élevée typiquement comprise entre 150 et 250 bars, domaine dans lequel la maîtrise des exposants de pression est moins bien assurée.

Moteurs à impulsions multiples - Dans ces moteurs de missiles qui présentent souvent, après une propulsion classique, une phase de vol aérodynamique suivie d'une impulsion en phase terminale, il serait souhaitable de pouvoir disposer de très grandes vitesses de combustion dans la phase finale afin de réaliser une combustion frontale, ces vitesses ne pouvant pas toujours être obtenues avec les propergols classiques même avec l'utilisation de la combustion pilotée par fils.

On voit qu'il y a encore bien du travail pour les chercheurs et les techniciens en matière de combustion.

Bibliographie

1. Kuo K.K. et Summerfield M., Fundamentals of Solid Propellant Combustion, Progress in Astronautics and Aeronautics, Volume 90 AIAA, New-York, 1984.

2. Saintoux, E. et al, ELEA tool for 3D Surface, Regression Analysis in Propellant Grains, AIAA 89 2782, AIAA/ASME/SAE 25th Joint Propulsion Conference, 1989.

3. Davenas, A., Technologie des Propergols Solides, Masson, Paris, 1989.

4. Terminology and Assesment Methods of Solid Propellant Rocket Exhaust Signature, AGARD Advisory Report AR 287 (to be published 1991).

5. Kuentzmann P. et al, Mesure de la vitese de combustion des propergols solides par ultrasons, La Recherche Aérospatiale, 1979-1, pp 55-72) janvier-février 1979.

6. Raynal S. et Doriath G., New Functional Prepolymers for High Burning Rate Solid Propellants, AIAA 86-1594, AIAA/ASAE/ ASME, 22nd Propulsion Conference, 1986.

7. Davenas A., Amélioration des propriétés balistiques et des propriétés mécaniques tous temps des propergols sans fumée, AGARD CP 259, Solid Rocket Motor Technology, OSLO, 1979.

8. Razdan, M.L. and KUO K.K., Erosive Burning of Solid Propellants. Progress in Astronautics and Aeronautics, vol 90, PP 515-598 984.

9. King, M.J., A Model of the Effects of Pressure and Cross Flow Velocity on Composite Propellant Burning Rate, AIAA 79-1171, AIAA/SAE/ASME 15th Propulsion Conference, 1979.

10. Friedlander, M. and Jordan, F.W. Radial Variation of Burning Rate in Center Perforated Grains, AIAA 84-1442, AIAA/SAE/ASME 20th Propulsion Conference, 1984.

11. Eister S.D. and Davis R.J., Predicting Burn Time Variations in Solid Rocket Motors, AIAA 90 2736, 26th AIAA/SAE/ASME/ASEE Joint Propulsion Conference, 1990.

12. Culick, F.E.C., Stability of high frequence pressure oscillations in rocket combustion chambers. AIAA Journal, 1e, 5, 1097-1104, 1963.

13. Nugeyre J.C. et al, An Example of Failure by Acoustic Coupling of a Free Standing Double Base Grain, AIAA 81 1525, AIAA/SAE/ASME 17th Joint Propulsion Conference, 1981.

14. Kaczmarek R.E. et al, Tangential Mode Instability in Double-Base Solid Rocket Motors, A Case Study, AIAA 82-1063, AIAA/SAE/ASME 18th Joint Propulsion Conference, 1982.

15. Brownlee N.G. and Marble P.B., An experimental investigation in Solid Propellant Rocket Motors, Solid Propellant Rocket Research Conference, ARS paper 1067, 1960.

Tableau 1

Effet du rapport d'autoserrage sur la nature et l'intensité des phénomènes dus aux écoulements dans un chargement

J	K	Présence de combustion érosive	Valeur de l'écart de pression Δp
$<0,2$	<50	non	Faible dans tous les cas en général inférieure à 5% de $p_{J,}$
	50 à 100	oui pour $v < 10$ mm/s	
	100 à 150	oui pour $v < 20$ mm/s	
	>150	oui pour toutes les compositions Très importante pour $v < 10$ mm/s	
0,2 à 0,35	<50	non	Environ 10% de $p_{J,}$ pour J = 0,3
	50 à 100	oui pour $v < 10$ mm/s	
	100 à 150	oui pour $v < 20$ mm/s	
	>150	oui pour toutes les compositions Très importante pour $v < 10$ mm/s	
0,35 à 0,5	<50	oui pour $v < 10$ mm/s	Environ 15% de p_{av} pour J = 0,4
	50 à 150	oui pour $v < 20$ mm/s	
	>150	oui pour toutes les compositions Très importante pour $v < 10$ mm/s	
0,5 à ,8	<50 et de 50 à 150	Oui importante pour $v < 20$ mm/s	Peut atteindre 40% de p.
	>150	oui pour toutes les compositions Très importante pour $v < 10$ mm/s	
1	Pour toute valeur	oui Intense pour $v < 10$ mm/s - Importante pour $v < 20$ mm/s Faible pour $v < 30$ mm/s	La pression dans la section sonique est telle que : $p \simeq 0,56\ p_{av}$

P_{av} : pression de fonctionnement mesurée à l'avant du chargement.

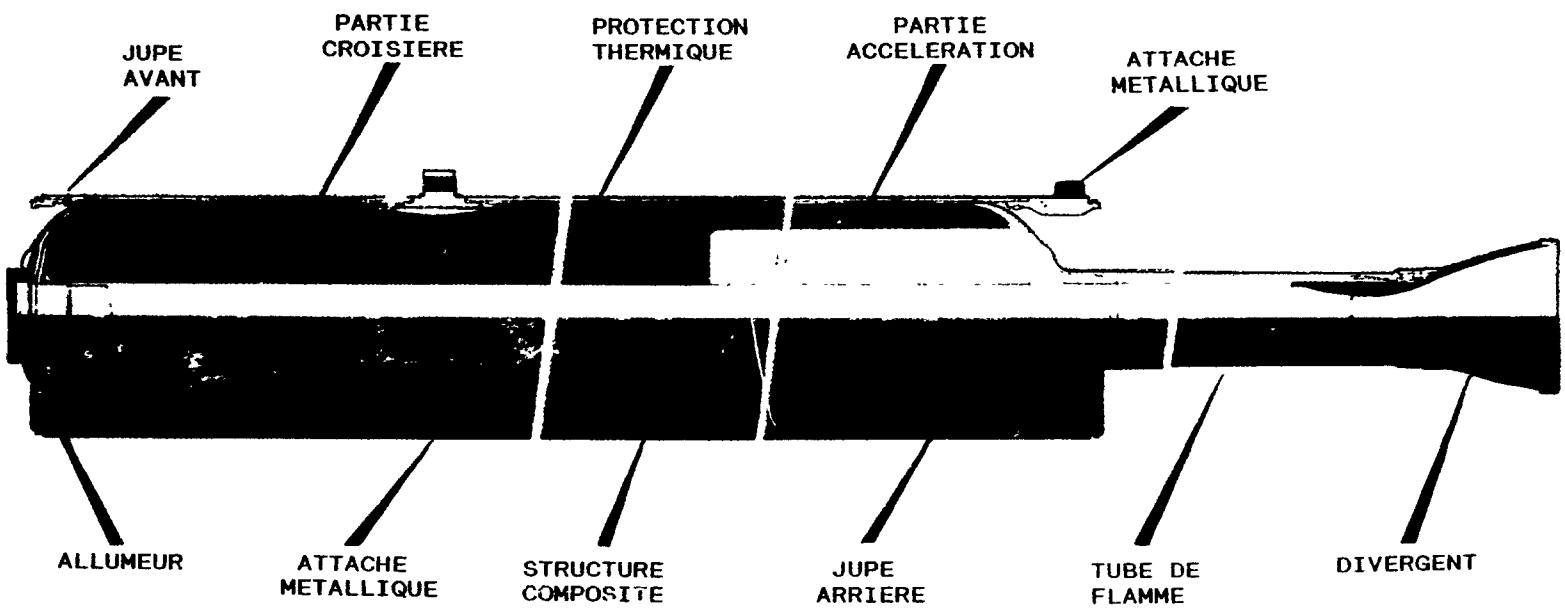

Figure 1: Propulseur typique (missile tactique)

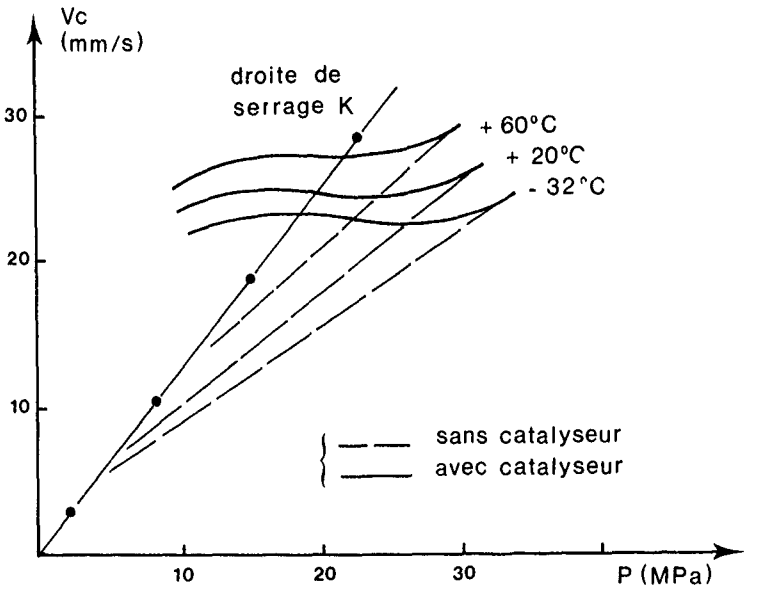

Figure 2: Courbes vitesse-pression typiques d'un propergol double-base

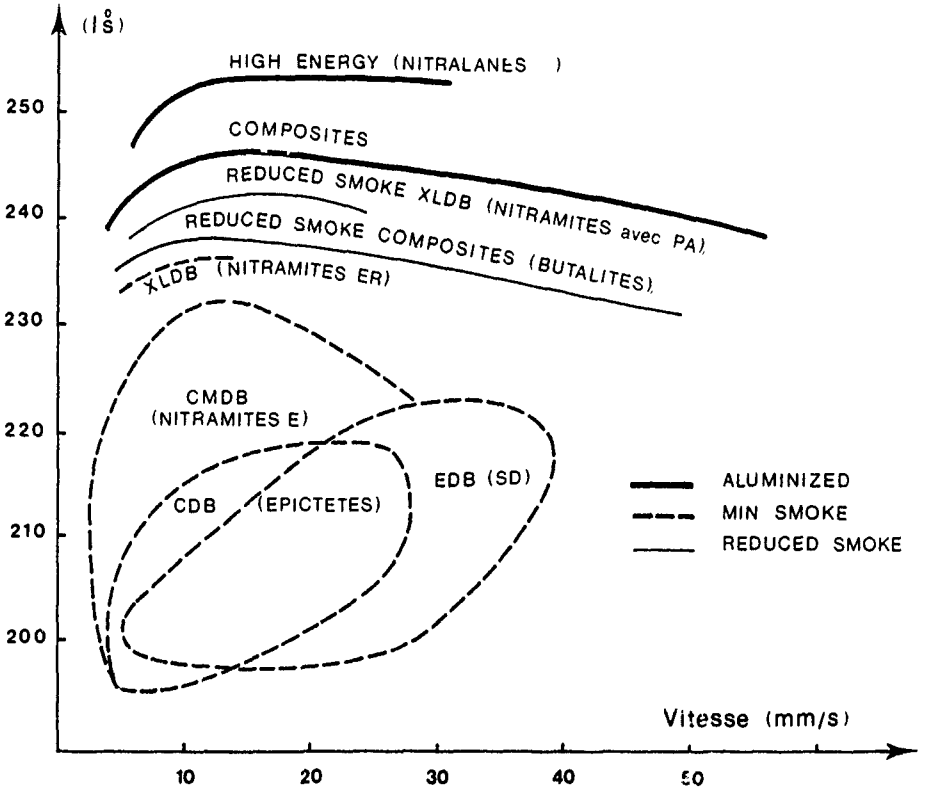

Figure 3: Impulsion spécifique pratique standard et plages de vitesse de combustion des principales familles de propergols

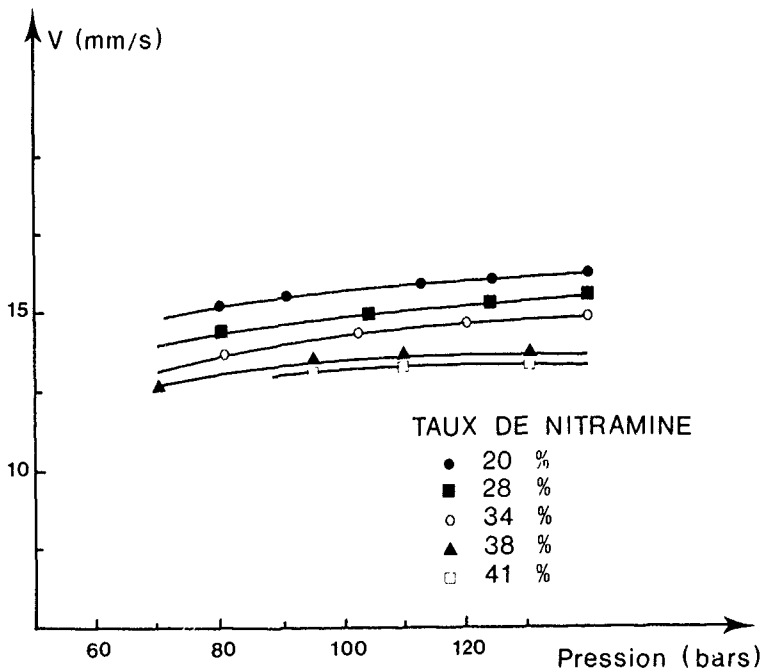

Figure 4: Influence sur la combustion d'une double base de l'incorporation d'hexogène

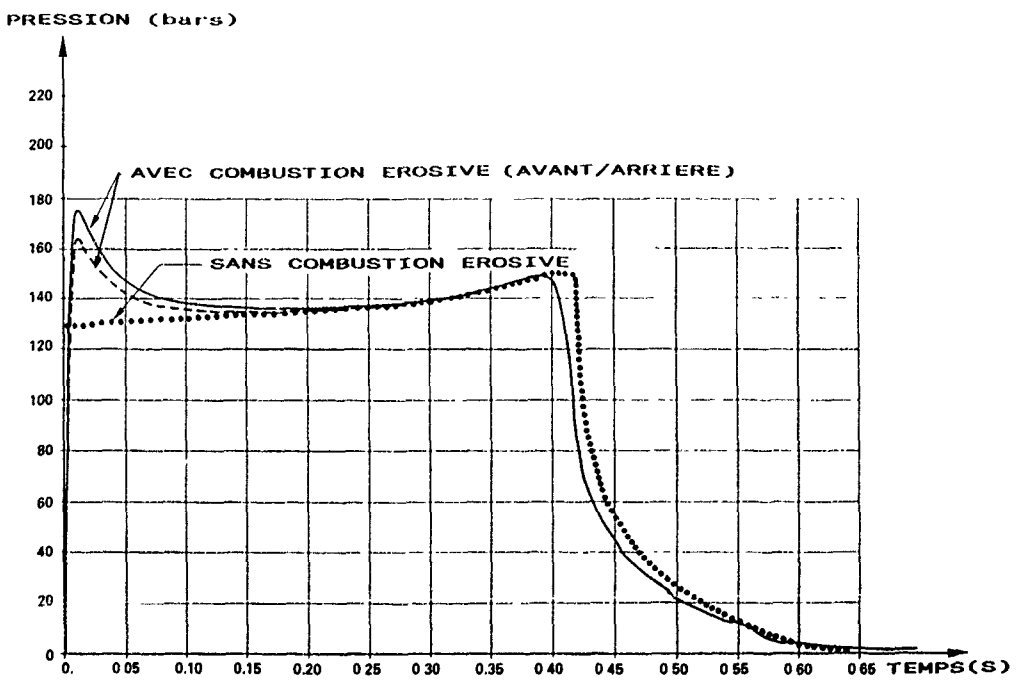

Figure 5: Courbe de pression avec et sans prise en compte de la combustion érosive

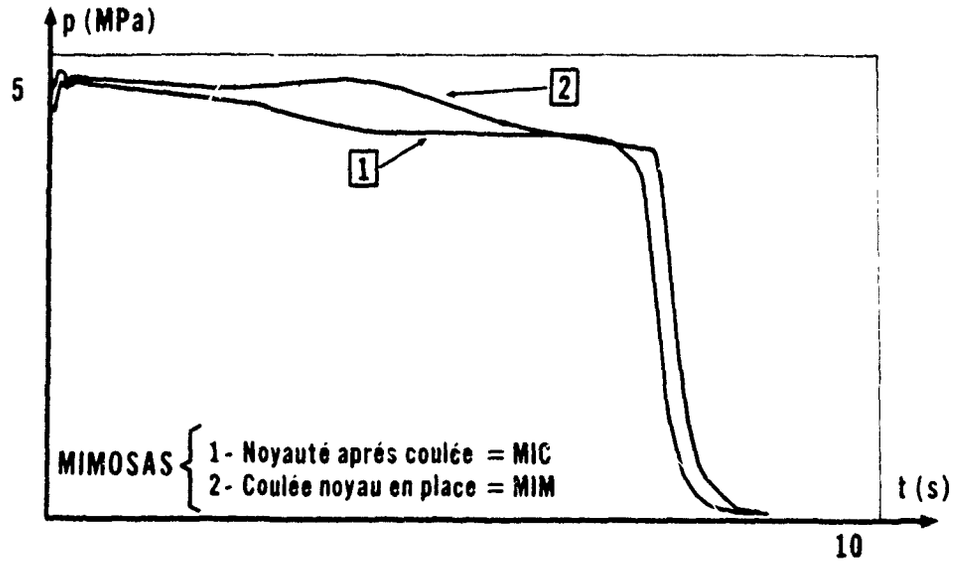

Figure 6: Courbe de pression d'un chargement réalisé par noyautage avant ou après coulée

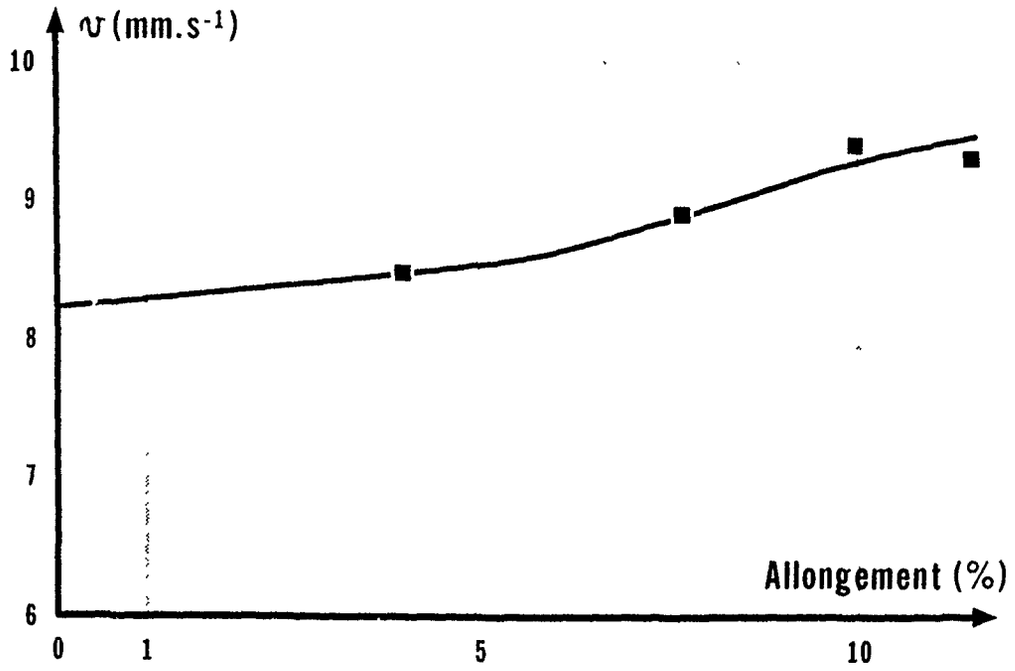

Figure 7: Influence de l'allongement sur la loi de vitesse

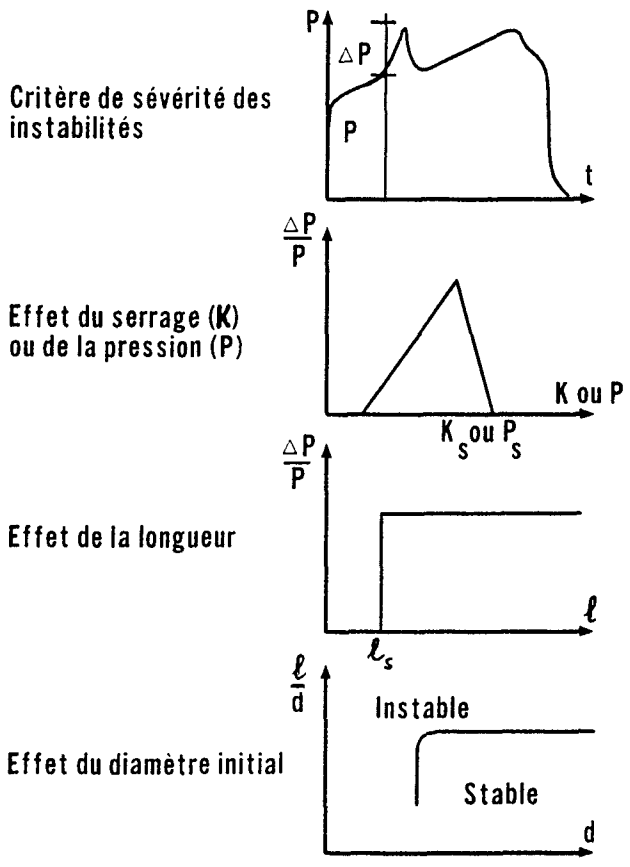

Figure 8: Domaine de fonctionnement stable

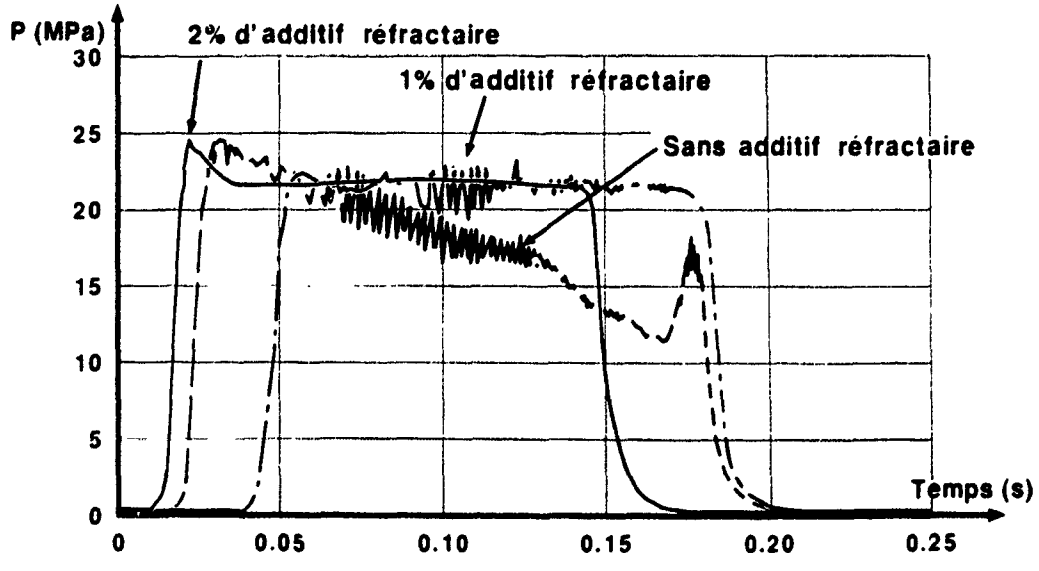

Figure 9: Influence de l'incorporation d'un additif antiinstabilités

SOLID PROPELLANT STEADY COMBUSTION--PHYSICAL ASPECTS

Guy LENGELLÉ, Jean-Robert DUTERQUE, Jean-Claude GODON, Jean-François TRUBERT
Research Scientists, Energetics Department

Office **N**ational d'**E**tudes et de **R**echerches **A**érospatiales
29, Avenue de la Division Leclerc

92320 CHATILLON (FRANCE)

ABSTRACT

A review of the understanding of the combustion mechanisms of solid propellants is presented. Such an understanding is an important part of the process carried out to master the behavior of solid propellants and to obtain desired characteristics (with respect to energetic level, burning rate level, sensitivity to pressure and initial temperature, nature of emitted combustion products, vulnerability to various aggressions...).

The propellants and propellant components considered are :

- double-base propellants, based on nitrocellulose and nitroglycerin,
- active binder, based on an inert polymer and a liquid nitrate ester,
- inert binders, such as polybutadiene,
- ammonium perchlorate,
- nitramines, such as HMX,
- composite ammonium perchlorate-inert binder propellants,
- composite propellants based on a nitramine and an active binder,
- aluminum, with respect to the two previous types of propellants,
- additives, when appropriate.

The features of the combustion zone described are :

- in the condensed phase, the thickness of the temperature profile and of the decomposition zone, the kinetics of the decomposition, the energy released, the nature of the gases evolved, the surface temperature,

- in the gas phase, the type of flame structure (diffusion or kinetically controlled), the possibility of staging (such as in double-base propellants), the kinetics of the reaction(s), the energy released, the flame temperature (primary and final, when applicable).

It is concluded that a fairly proper knowledge of the combustion of the various components and propellants has been acquired (to be now extended to new ingredients, oxidizers or binders). Furthermore, based on this knowledge, a first approach modeling description can be achieved, which should be improved progressively in the next few years. Such a description can be useful in accompanying the elaboration of new propellants and in preparing the investigation of more complicated regimes such as those of erosive burning and of non-stationary response.

INTRODUCTION

Much work has been devoted in various countries to investigating the combustion mechanisms of solid propellants. It is timely to bring together the information on the combustion of the individual components as well as of their combination into propellants. This review is about the existing components and propellants : double-base propellants and active binders, inert binders, ammonium perchlorate, HMX and the corresponding composite propellants, ammonium perchlorate - inert binder (plus possibly aluminum), HMX (or RDX) - active binder.

The viewpoint adopted here is that of the understanding of the combustion behavior of propellants. Therefore as much information as possible is presented about the fundamentals of the processes (thermal properties, kinetics in the condensed phase and in the gas phase...), whereas no attempt is made to establish a complete catalog of practical results on various propellants with different particle sizes, catalysts, variations on the percentage of ingredients.

Some space is taken up by physico-chemical modeling. The aim is not so much to give the elements of mathematical descriptions which could be used for a priori computations of burning characteristics of propellants (to the extent that such computations are possible). The point is more to put to test the hypotheses made on the mechanisms of combustion by incorporating them in reasonable models and confronting the results thus obtained to experimental data.

These descriptions can also be viewed, alongside with the data given for each component or propellant, as useful for coping with the regimes of combustion which go beyong stationary combustion : that is erosive burning and unsteady (under pressure excursions or pressure oscillations) combustion responses.
The table below gives information about the various types of propellants of actual use.

Double-base propellants (made by the extrusion or powder casting techniques) are used in anti-tank rockets or missiles and in some tactical missiles. Their main advantage is that they produce a minimum amount of smoke (only from a small amount of additives).

Composite propellants based on ammonium perchlorate (AP) without aluminum generate reduced smoke, HCl and H_2O vapor will precipitate into droplets in the plume under given temperature and humidity conditions. They are used for various tactical missiles. With aluminum, they are widely used in missiles and space launchers. They produce alumina smoke, which, in the case of space

Performances / characteristics of various propellants

PROPELLANT	COMPOSITION (main ingredients)	ρ_p g/cm³	I_s(70/1) theor. (pract.)	APPLICATIONS/CHARACTERISTICS
Extruded DB	Nitrocellulose Nitroglycerin	≤ 1.66	≤ 230 s (≃ - 10 s)	- Anti-tank rockets and missiles - AS rockets - Some tactical missiles (SA) Minimum smoke
Powder cast DB	Nitrocellulose Nitroglycerin	≤ 1.66	≤ 225 (≃ - 10 s)	- Anti-tank missiles - Some tactical missiles (AS) Minimum smoke
AP composite	Ex : 88% AP - 12% HTPB	1.72	≃ 250 (≃ - 10s)	- Some AS rockets - Some tactical missiles Reduced smoke ($HCl-H_2O$)
AP composite with aliminum	Ex : 68 AP - 20 al. - 12 CTPB	≃ 1.82	265 (≃ - 20 s)	- AA tactical missiles - Anti-ship missiles (booster) - Tactical ballistic missiles - Strategic ballistic missiles - Apogee motors - Boosters for space launchers (Titan III, IV, Space Shuttle, Ariane V...) Smoky (Al_2O_3)
HMX (RDX) composite	HMX or RDX - XLDB binder	< 1.75	< 255 (≃ - 15 s)	- Anti-ship missiles (cruise) - SA missiles Minimum smoke (without AP)
HMX composite with aluminum	XLDB binder	1.87	273	- Strategic ballistic missiles (upper stages) (Trident, MX...) Smoky (Al_2O_3)

Sources : Air et Cosmos n° 1000, may 1984. Annales des Mines, jan-feb. 1986. Aéronautique et Astronautique, n° 138, 1989.

launchers, could be considered in the future to be undesirable (along with HCl).

Composite propellants based on nitramines and an "active" binder (cross linked polymer with nitroglycerin or other liquid nitrate esters) are used more and more. Without aluminum, they are in the minimum smoke category and they replace DB propellants. With aluminum, they reach the highest specific impulse and density and are used so far for upper stages of strategic missiles.

The combustion of the components and then of the various propellants will be seen in the next chapters.

A few general references about chemical propulsion, solid propellants and combustion can be found at the end of the main text, ahead of more specialized references introduced progressively in the following chapters.

COMBUSTION OF DOUBLE-BASE PROPELLANTS AND ACTIVE BINDERS

1. Introduction

It seems appropriate to consider double-base propellant combustion mechanisms in the first place because they correspond to relatively simpler premixed processes which lend themselves to a better understanding and because they have been investigated for a long time (starting in the 1950's) in the US, USSR, UK, Japan and France in particular.

As will be seen, the mechanisms involved in the combustion of double-base propellants will apply as well to the active binders (≃ 1/3 polymer, ≃ 2/3 nitroglycerin, or another liquid nitrate ester).

General background on the combustion of double-base propellants can be found in references [1-6].

Double-base propellants are made in a number of ways. When they are rolled or extruded, the components are nitrocellulose and nitroglycerin, to which some stabilizers such as centralite and plasticizers are added. When they are cast, a casting powder (made of nitrocellulose, some nitroglycerin, and the various additives) is swelled within the mold by a liquid mixture of nitroglycerin and triacetin. The grain thus obtained is then inhibited and used free standing in the motor. The propellant ingredients can also be mixed, cast, cross-linked, and the grain case bonded.

Depending on the relative amounts of nitrocellulose and nitroglycerin, the energetic level of the propellant can be increased or, in the usual terminology, its "heat of explosion" or "calorimetric value", that is, the heat evolved in a calorimetric bomb by combustion under an inert atmosphere. One can then talk about "cool" and "hot" compositions.

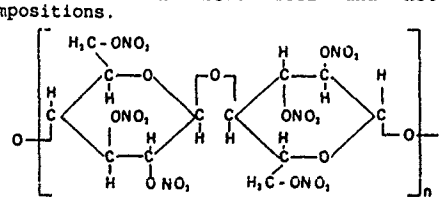

Nitrocellulose

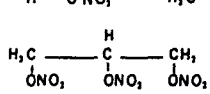

Nitroglycerin

Example of composition : 1100 cal/g propellant, 52.25% NC, 42.75% NG, 5% others.

Double-base propellants are used in small and medium sized rockets and thus exposed to varying ambient temperatures. The sensitivity of the motor operation to temperature depends upon the propellant burning rate sensitivity to both the temperature and the pressure. As can be seen on Fig. 1, the pressure exponent, in the usual empirical law $v_b = p^n$, is around 0.7 and increases to nearly 1 at high pressure. Super-rate effects (Fig. 2) are created by the use of additives, most often lead and copper salts combined with carbon black. At the end of the super-rate zone, the burning rate falls back to that of the control propellant, with the occurence of a nearly zero pressure exponent zone, a "plateau" effect, or a negative exponent zone, a "mesa" effect. These terms are used by analogy with topographical features. A fairly complete set of results can be found in reference [6]. It is only in these reduced pressure exponent zones that the propellant is used to minimize the motor operation sensitivity to ambient temperature. Due to this fact, the study of the combustion of propellants without additives should be conceived only as a first step leading to an understanding of modified (that is, with additives) propellants.

2. Flame Structure

From the works mentioned previously it is possible to describe the combustion wave structure of double-base propellants, in particular its chemical processes, see Fig. 3. The various data will be discussed and justified later. Gas analysis results are from reference [7]; they refer to mass fractions.

The propellant components pass unaffected through a preheated zone of a few tens of micrometers in a few milliseconds and reach a superficial degradation zone (or "foam" zone in the early literature) where the temperature becomes high enough for the molecular degradation to take place, initiated by the rupture of the C-O-//-NO_2 bond. Simultaneous recombination occurs so that a mixture of NO_2, aldehydes, but also NO emerges from the surface and the net energy balance of the degradation is exothermic. At pressures under about 100 atm, a clearly separated primary flame ("fizz" zone) and a secondary flame ("luminous" flame) are observed, the first involving NO_2-aldehydes reactions and the second probably NO-CO reactions. In this pressure range the secondary flame is too far away to have any effect on the surface or even to induce a temperature gradient into the primary flame. The burning rate is then entirely under the influence of the latter. This corresponds to a burning rate/pressure law with a 0.7 pressure exponent (Fig. 1). As the pressure increases, the secondary flame enhances and then merges into the primary flame and a transition is observed to a zone with a pressure exponent close to 1. When the secondary flame is fully developed, even at pressures for which it does not yet influence the burning rate, the final products (N_2, CO, CO_2, H_2O and H_2) and the final temperature (2100-3100 K, depending on the heat of explosion) are attained.

The following table gives data relative to the various zones of the combustion wave.

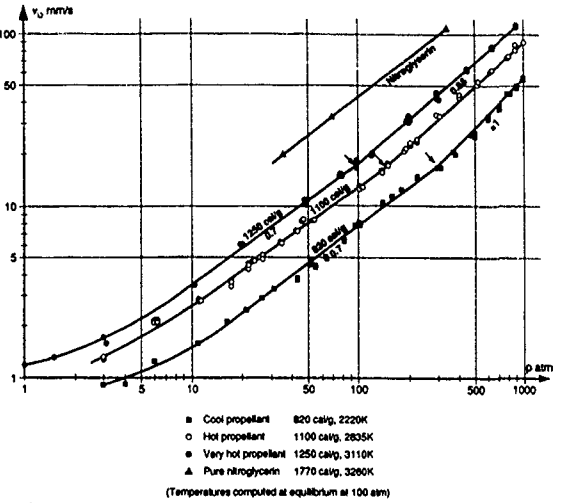

Fig. 1 BURNING RATE VS PRESSURE LAWS DOUBLE - BASE PROPELLANTS

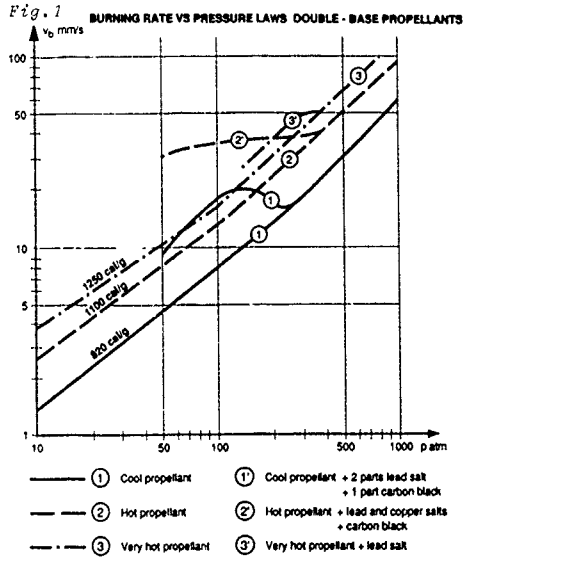

Fig. 2 SUPER - RATE EFFECTS - DOUBLE-BASE PROPELLANTS

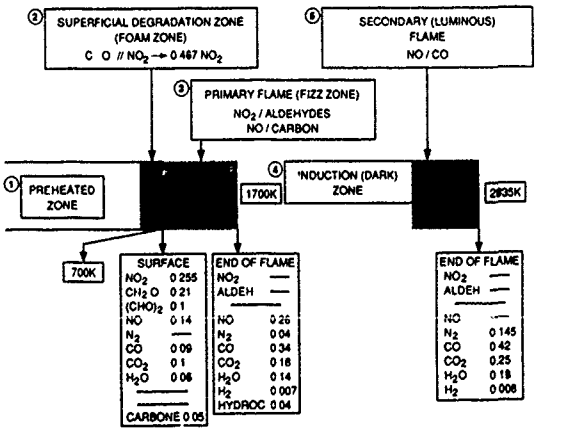

Figures for an 1100 cal/g propellant. Surface and primary flame (at 11 atm) mass fractions from gas analysis

Fig. 3 VARIOUS ZONES IN THE COMBUSTION OF A DOUBLE BASE - PROPELLANT

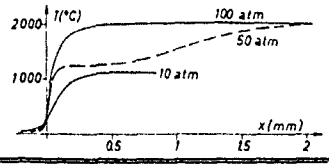

Pressure atm.	10	50	100
v_b mm/s	1.9	6.7	10.6
T_s, K	610	662	685
Preheated zone, µm (measured/ computed)	140/ 194	50/55	45/35
Residence time in preheated zone, ms	100	8	3
Superficial degradation zone µm	11	3	2
Residence time in superficial zone, ms	6	0,5	0,2
Flame thickness, µm (measured)	200	75	110 (secondary flame)

Measured results from Zenin

Characteristics of the combustion zones.

3. Condensed phase processes

The preheated zone of a regressing propellant is described by the conservation of energy in a coordinate (x > 0 in the gas phase) regressing with the surface :

$$\rho_p v_b c_p dT/dx = d(\lambda_p dT/dx)/dx \qquad (1)$$

in such a way that a temperature profile

$$(T-T_o)/(T_s-T_o) = \exp(x\ v_b/d_p),$$
$$d_p \equiv \lambda_p/\rho_p c_p \qquad (2)$$

will progress with the surface into the propellant. From measurements up to 100°C and from ignition experiments, representative average values are taken as :

ρ_p = 1.6 g/cm^3, c_p = 0.4 cal/g K,
λ_p = 5.1 10^{-4} cal/s cm K
d_p = 0.8 10^{-3} cm^2/s

Values of the condensed phase properties. Double-base propellants.

The thickness $e_{cond.}$ of the conduction zone can be taken conventionally as

$$T(\text{end of cond. zone}) - T_o = 10^{-2}\ (T_s - T_o)$$

$$e_{cond.} = (d_p/v_b)\ \ln 10^2 \qquad (3)$$

As an example, for v_b = 10 mm/s $e_{cond.}$ = 37µm, a thickness through which the temperature rises from 293 K to about 700K.

The residence time through this conduction zone is :

$$\tau_{cond.} = (d_p/v^2_b)\ \ln 10^2 \qquad (4)$$

about 4 ms in this example; a very short time for a temperature increase of 400K.

The superficial degradation zone has its thickness ruled by the conservation of the non degraded propellant mass fraction Y_p :

$$\rho_p v_b dY_p/dx = -\rho_p A_c \exp(-E_c/RT), \qquad (5)$$

with the decomposition represented by an Arrhenius law. Numerous investigations by thermogravimetry, differential scanning calorimetry, on nitrocellulose, nitroglycerin and other nitrate esters, as well as on double base propellants , and ignition studies [5] result in ·

Decomposition order 0, A_c = 1 $10^{17} s^{-1}$,
E_c = 40 kcal/mole

Values for the condensed phase degradation kinetics. Double-base propellants.

The thickness of the degradation layer is related to the fast drop in the degradation rate When this rate is 10^{-2} that at the surface temperature the lower limit of the reaction layer is reached

$$\exp[-\mathcal{E}_c\ (1 - \Delta T/T_s)] = 10^{-2} \exp(-\mathcal{E}_c),$$

$$\mathcal{E}_c \equiv E_c/RT_s,$$

the temperature drop is then

$$\Delta T/T_s = 1/(1 + \mathcal{E}_c / \ln 10^2) \qquad (6)$$

ΔT = 100 K for T_s = 700 K. Such a temperature drop inserted in eq. (2) gives an estimation of the reaction layer thickness

$$e_{reaction} = (d_p/v_b)\ \ln[1 - \Delta T/(T_s - T_o)]$$

or taking into account the magnitude of the reduced activation energy ($\mathcal{E}_c$ = 30).

$$e_{reaction} = e_{cond.}\ T_s/\mathcal{E}_c\ (T_s - T_o) \qquad (7)$$

For the values taken above, at v_b = 10 mm/s e_{react} = 2 µm, with an associated residence time τ_{react} of 0.2 ms.

The summation of Eq. (5) through the degradation layer results in :

$$\rho_p v_b(Y_{p,s} - Y_{p,o}) = -\int \rho_p A_c \exp(-E_c/RT)\ dx \qquad (8)$$

$$v_b = A_c \exp(-E_c/RT_s)\ e_{reaction}$$

$$= A_c \exp(-\mathcal{E}_c)(d_p/v_b)\ \ln 10^2 (1/\mathcal{E}_c)[T_s/(T_s - T_o)]$$

A more rigorous approach [8] (which is almost identical to a numerical computation [9]) gives :

$$v_b^2 = (d_p/\mathcal{E}_c)\ A_c \exp(-\mathcal{E}_c)/$$

$$(1 - T_o/T_s - Q_s / 2\ c_p T_s) \qquad (9)$$

This equation indicates a relation between surface temperature and burning rate : the mass flow rate $\rho_p v_b$ emitted from the surface is the result of the decomposition of the propellant into gases throughout the superficial degradation layer, Eq.(8). The

higher the burning rate v_b, the smaller the residence time $\tau_{react.} \sim 1/v_b^2$, and the higher is the surface temperature reached to allow for the complete degradation of the propellant.

Traverses with micro-thermocouples (as seen previously the thickness of the combustion wave is of the order of tens of μm) allow to obtain measurements of the surface temperature [2,3,4,5]. One example is given on Fig. 4. The results from various sources are collected (see [5] for references), as burning rate versus $1/T_s$, on Fig. 5. Also indicated is the correlation obtained from Eq.(9). Having in mind the inevitable scatter in measurements due to the thinness of the combustion wave, some conclusions can be reached (see also Refs. [3,10]). The initial degradation of the propellant components is controlled by the breaking of the $-C-O-//-NO_2$ bond (characterized by the 40 kcal/mole activation energy). This is considered to be a temperature sensitive only process, irreversible (therefore not influenced by the pressure level). It is noteworthy that the kinetics of the degradation is the same from thermal decomposition (by TG and DSC) at about 400 K, to ignition from 400 to 500 K [5] and combustion at temperatures up to 700K. Also important is the conclusion, if one looks at the details of Fig. 5, that the presence of super rate producing additives does not affect the condensed phase kinetics.

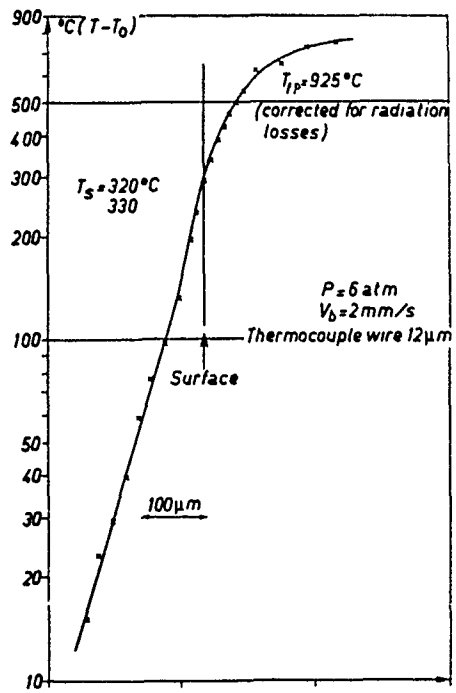

Fig. 4 **TEMPERATURE PROFILE IN THE CONDENSED PHASE**

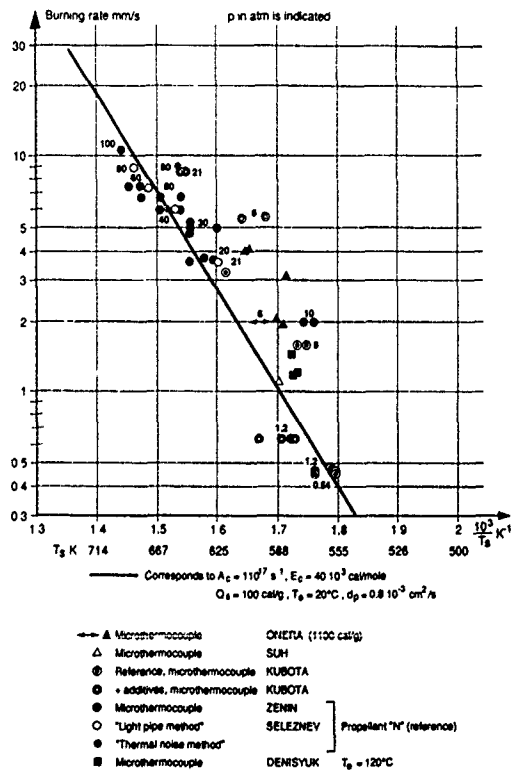

Fig. 5 **PYROLYSIS LAW FOR DOUBLE - BASE PROPELLANTS**

The energetics of the reaction layer is now to be considered. The initial degradation of the propellant, taking into account the assumed decomposition of nitroglycerin into $3NO_2$, 2 CH_2O and 0.5 $(CHO)_2$, is thought to give (for the example of the 1100 cal/g propellant) the mass balance

1 propellant → 0.467 NO_2 + 0.364 CH_2O + 0.1 $(CHO)_2$ + 0.06 hydrocarbons (10)

with a corresponding endothermic heat of degradation

Q_d = - 135 cal/g of propellant.

It is thought [5,9,10] that within the superficial layer the exothermic reaction between NO_2 and aldehydes can start. A plausible mole balance (in order to match various results, in particular the analysis [7] of the gases emitted from the surface of regressing propellants) is

$NO_2 + CH_2O \rightarrow NO + 1/2\ CO + 1/2\ CO_2 + 1/2\ H_2O + 1/2\ H_2$ (11)

with a corresponding exothermic heat of reaction

Q_{NO2} = 1040 cal/g of NO_2.

Conservation of the species NO_2 (in terms of mass faction Y) is written (no diffusion is taken into account)

$$\rho_p v_b \frac{dY_{NO2}}{dx} = Y_{NO2,i}\ \rho_p\ A_c \exp\left(-E_c/RT\right) - A_{NO2}\ (p^n/RT)\ Y_{NO2} \exp(-E_{NO2}/RT) \quad (12)$$

if a first order with respect to the molar concentration of NO_2 is assumed (it will be seen that this is probably the case).

Conservation of energy is written

$$\rho_p v_b \, cdT/dx - d(\lambda dT/dx)/dx = - Q_d \dot{\omega}_p - Q_{NO2} \dot{\omega}_{NO2} \qquad (13)$$

with $\dot{\omega}_p$ the rate of reaction of the propellant, as in Eq. (5), and $\dot{\omega}_{NO2}$ that of NO_2 as in the second term of Eq.(12). The summation of Eqs. (5,12,13) through the condensed phase to the surface leads to

$$\lambda \, dT/dx \mid_s = \rho_p v_b \, (c_g T_s - c_p T_o - Q_s) \qquad (14)$$

$$\equiv \rho_p v_b \, Q_c$$

$$Q_s \equiv Q_d + Q_{NO2} \, (Y_{NO2,i} - Y_{NO2,s}) \qquad (15)$$

The first equation is the heat balance at the surface, the heat flux from the flame in the gas phase allows the heating and pyrolysis of the propellant. The net heat of decomposition of the propellant Q_s is exothermic to the extent that some NO_2 reacts exothermically already in the condensed phase.

From thermocouple traverses such as that of Fig. 4 and the balance of Eq. (14) the net heat Q_s can be estimated (again scatter should be expected) The results from various sources are given on Fig. 6. The net heat of decomposition is seen to be exothermic and increasing with burning rate (due to an increase in pressure). Summation of Eq. (12) yields (with Eq. (5) taken into account)

$$\rho_p v_b (Y_{NO2,i} - Y_{NO2,s}) = A_{NO2} \int (p\mathcal{M}/RT) \, Y_{NO2} \exp(-E_{NO2}/RT) \, dx$$

$$= A_{NO2} \, (p\mathcal{M}/RT_s) \, Y_{NO2} \exp(-E_{NO2}/RT_s) e_{react.}$$

and with Eq. (8)

$$Y_{NO2,i} - Y_{NO2,s} \sim (p\mathcal{M}/RT_s) \exp(-E_{NO2}/RT_s)/\exp(-E_c/RT_s)$$

This relation indicates that the amount of NO_2 reacting in the condensed phase will increase with pressure, and thus Q_s will increase, if the reacting rate for NO_2 catches up with the decreasing residence time in the degradation layer,

$$\tau_{react.} \sim 1/v_b^2 \sim 1/\exp(-E_c/RT_s)$$

(due to Eq.(9)). A plausible law is obtained for a first order NO_2 reaction with an activation energy E_{NO2} between 5 and 10 kcal/mole.

One important feature of Fig. 6 is that the heat evolved in the condensed phase is not affected by the presence of additives.

4. Flame zone

As seen above, the reaction between NO_2 and aldehyde starts in the condensed phase in such a way that the surface gas composition [7] indicated on Fig. 3 is obtained, with NO_2 being significantly less (0.255) as compared to what results from the initial degradation of the propellant (0.467, in the case of an 1100 cal/g propellant) and with NO already present (0.14). The mole balance of Eq. (11) allows to match as well the gas analysis at the end of the primary flame ([7], measurements at 11 atm)

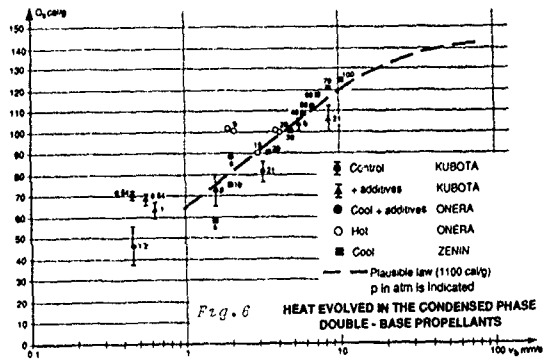

Fig. 6 HEAT EVOLVED IN THE CONDENSED PHASE DOUBLE - BASE PROPELLANTS

$$NO_2 + CH_2O \rightarrow NO + 1/2 \, CO + 1/2 \, CO_2 + 1/2 \, H_2O + 1/2 \, H_2 \qquad (11)$$

Q_{NO2} = 1040 cal/g of NO_2.

It is likely that aldehyde-aldehyde reactions also occur following (again to match the gas analysis results) :

$$CH_2O + CH_2O \rightarrow CO + 1/2 \, C_2H_6 + H_2O \,, \quad Q_{ald.1} = 389 \text{ cal/g of } CH_2O \qquad (16)$$

$$(CHO)_2 + (CHO)_2 \rightarrow 4 \, CO + 2 \, H_2 \,, \quad Q_{ald.2} = - 533 \text{ cal/g of } (CHO)_2 \qquad (17)$$

At low pressure when probably only the reaction of (11) can take place, an energy balance between initial temperature and end of the primary flame yield :

$$c_g \, T_{fp} - c_p \, T_o = Q_d + Q_{NO2} \, Y_{NO2,i}, \quad p \leq 1 \text{ atm} \qquad (18)$$

since the initial NO_2 is totally consumed in the condensed phase and the primary flame. An evaluation of T_{fp} = 1340 K results. It is seen on Fig. 7 that measurements with small thermocouples indicate a large increase with pressure in the primary flame temperature from this value. The aldehyde reactions of Eqs. (16,17) do not produce energy in significant amount. It has ther been assumed [5] that the NO already present at the surface as well as that produced from the NO_2-aldehyde reaction react with the layer of

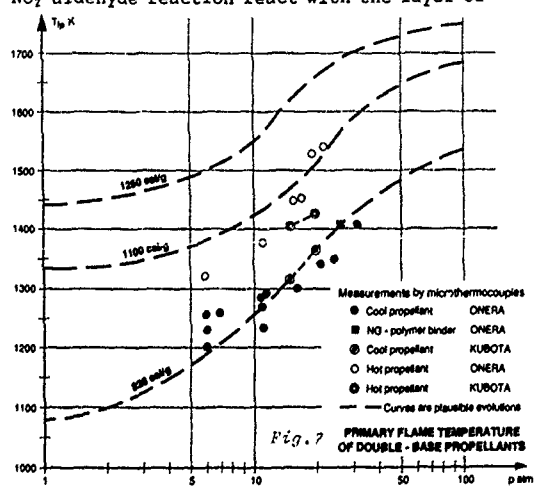

Fig. 7 PRIMARY FLAME TEMPERATURE OF DOUBLE - BASE PROPELLANTS

carbon residue attached to the surface which is observed by direct visualisation under combustion and after extinction by scanning electron microscopy.

The NO/ carbon reaction had been investigated in [11]. If one makes use of the results obtained, the conservation of the species carbon can be written as (the carbon layer regressing with the surface)

$$v_b d\rho_c/dx = (\mathcal{M}_c/\mathcal{M}_{NO})\ \dot{\omega}_{NO} \qquad (19)$$

$$\dot{\omega}_{NO} = -A_{NO/c} \exp(-E_{NO/c}/RT)\rho_c S_{s,c} Y_{NO}\ p\mathcal{M},$$

in g/cm³s

(this form resulting from the way the data of [11] is cast), the reaction balance being assumed to be :

$$NO + C \rightarrow 1/2\ N_2 + CO,$$

$$Q_{NO/c} = 1600 \text{ cal/g of NO} \qquad (20)$$

and $S_{s,c}$ being the specific surface area of the carbon (at most 10^6 cm²/g). Reference [11] produces (after rounding $E_{NO/c}$)

$$A_{NO/c} = 2\ 10^{-3} \text{ mole/s cm}^2 \text{ atm},$$

$$E_{NO/c} = 30 \text{ kcal/mole}$$

A rough estimate of the amount of N_2 produced by reaction (20) through the primary flame is given by (with $\dot{m} \equiv \rho_p v_b$ the mass flow rate)

$$\dot{m} Y_{N2,fp} = -(1/2)\ (\mathcal{M}_c/\mathcal{M}_{NO})\ \bar{\dot{\omega}}_{NO}\ x_f$$

$\bar{\dot{\omega}}_{NO}$ being evaluated at average values through the flame. With p = 11 atm, v_b = 0.28 cm/s, Y_{NO} = 0.2, ρ_c = 0.5 g/cm³, T_f = 1400K and x_f = 400 µm (from thermocouple measurements) it is obtained.

$$Y_{N2,fp} = 0.06$$

a reasonable value (with respect to the result of Fig. 3). This tends to indicate that the NO/carbon reaction has a kinetics indeed fast enough with respect to the residence time allowed in the primary flame.

An energy balance taking into account the NO/carbon reaction is written :

$$c_g T_{fp} - c_p T_o = Q_d + Q_{NO2} Y_{NO2,i} + Y_{NO,cons.}\ Q_{NO/c} + Q_{ald}\ Y_{ald,cons.} \qquad (21)$$

(the taking into account of the aldehyde reaction cools the flame by about 80 K). In this balance $Y_{NO,cons.}$ is the amount of NO consumed in the primary flame :

$$Y_{NO,cons.} = Y_{NO2,i}\ (\mathcal{M}_{NO}/\mathcal{M}_{NO2}) - Y_{NO,fp}$$

in the case of the example of Fig. 3 and taking into account the uncertainty on the measurements : $Y_{NO,cons.}$ = 0.035 to 0.047 and Eq. (21) results in T_{fp} = 1420 to 1475 K, an admissible value when compared to the results of Fig. 7.

The temperature profile in the primary flame is controlled by the conservation of energy ($\dot{m} \equiv \rho_p/v_b$) [5].

$$\dot{m} c_g\ dT/dx - d(\lambda_g/dT/dx) = -Q_{NO2}\ \dot{\omega}_{NO2} - Q_{NO/c}\ \dot{\omega}_{NO} - Q_{ald.}\ \dot{\omega}_{ald.} \qquad (22)$$

c_g = 0.35 cal/g K,

$\lambda_g = 1.25\ 10^{-4}(T/700)^{0.7}$ cal/cm s K

$\mathcal{M}$ = 30 g/mole

Values considered as representative for the gas phase. Double-base propellants.

The evaluation of the heat flux received at the surface, which will then control the burning rate according to Eq. (14), results from the summation of Eq. (22) through the flame zone. Only a true numerical evaluation of the temperature and species profiles will give the proper heat flux. However conclusions can be drawn from approximate relations. The activation energies of the reactions of Eq. (22) being moderate, the flame is distributed and an approximation of the temperature profile is given by :

$$(T_f - T)\ /\ (T_f - T_s) = \exp(-x/x_f) \qquad (23)$$

which will produce a shape such as that of Fig. 4.

With Eq. (14)

$$\lambda_{g,s}\ dT/dx|_s \equiv q_s = \dot{m} Q_c \equiv \rho_p v_b\ (c_g T_s - c_p T_o - Q_s) \qquad (14)$$

Eq. (23) yields

$$q_s = \lambda_{g,s}\ (T_f - T_s)/x_f$$

$$x_f = \lambda_{g,s}\ (T_f - T_s)/\dot{m} Q_c \qquad (24)$$

The summation of Eq. (22) through the flame results in

$$\dot{m} c_g\ (T_f - T_s) + q_s = Q_g \bar{\dot{\omega}}_g x_f \quad (\bar{\dot{\omega}}_g > 0, \text{ average rate})$$

or with Eqs. (14,24), and taking into account an overall equation for conservation of energy

$$c_g\ (T_f - T_s) = Q_g - Q_c,$$

$$\dot{m} = [\bar{\dot{\omega}}_g\ \lambda_{g,s}\ (T_f - T_s)\ /\ Q_c]^{1/2} \qquad (25)$$

At very low pressure, ~ 1 atm, when only the NO_2 reaction probably takes place, the burning rate follows pressure according to, see Eq. (12),

$$\dot{m} \equiv \rho_p v_b \sim (\bar{\dot{\omega}}_{NO2})^{1/2} \sim p^{1/2} \exp(-E_{NO2}/2\ RT_{fp}) \qquad (26)$$

a pressure exponent which is indeed observed, see Fig. 1. As the pressure increases the NO/carbon reaction takes on more importance and, Eq. (19),

$$\dot{m} \equiv \rho_p v_b \sim [p \exp(-E_{NO2}/RT_{fp}) + \sim p \exp(-E_{NO/c}\ /\ RT_{fp})]^{1/2}, \qquad (27)$$

which, with the increase of the flame temperature with pressure, see Fig. 7, accounts for the pressure exponent of 0.7.

At higher pressures, above about 150 atm for the 1100 cal/g propellant for example, a change in the pressure sensitivity, Fig. 1, is observed. This tends to indicate that the secondary flame, probably characterized by a

second order, with respect to pressure, reaction for NO, comes into the primary flame and progressively dominates it, with a pressure exponent, according to Eq (25), increasing to close to 1.

Results on Fig. 8 for the 1250 cal/g propellant indicate the temperature sensitivity of the burning rate defined as

$$\sigma_p = (d \ln v_b / dT_o) \text{ at } p \text{ given} \qquad (28)$$

According to Eq. (27) the burning rate is under the influence of a premixed flame heat flux and therefore very sensitive to changes in the primary flame temperature, in the pressure domain when the two flames are separated. From Eq. (21) any change in initial temperature will affect the primary flame temperature and therefore induce a change in burning rate. As the pressure rises the primary flame temperature increases (up to 1800 K) and then for higher pressures the burning rate comes under the influence of the final flame (with a temperature reaching 3110 K for the 1250 cal/g propellant). It is seen from Eq. (27) that a given change in T_o and therefore in T_f has a smaller impact on the burning rate for higher flame temperatures, that is for higher pressures, a tendency observed on Fig. 8.

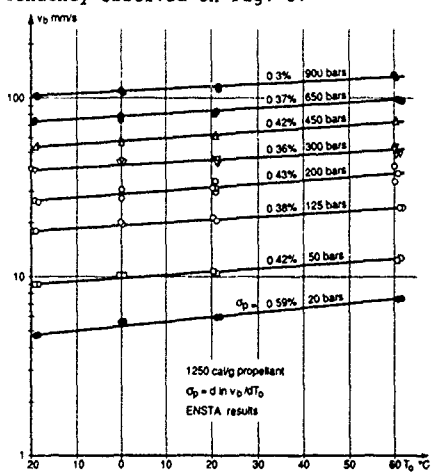

Fig. 8 **TEMPERATURE SENSITIVITY OF DOUBLE - BASE PROPELLANTS**

5. Active binders

Various types of active binders, based on nitrocellulose or an inert binder and nitroglycerin or less energetic liquid nitrates, can be used, see reference [10] for a complete description. The cross-linked double-base binders (XLDB) will be considered here, in which the polymer is cured with an isocyanate after mixing with NG.

Composition : ≈ 1/3 NG, 2/3 polyethylene glycol. Heat of explosion : 850 cal/g.

T_{ff} = 2000 K. ρ_p = 1.42 g/cm³.

c_p = 0.46 cal/g K.

λ_p = 3.9 10^{-4} cal/cm s K. d_p = 0.6 10^{-3} cm²/s

$Y_{NO2,i}$ = 0.421. Q_d = - 150 cal/g

Values for a XLDB binder.

Although the burning rates of the different active binders can be, for a given heat of explosion, somewhat different at low pressures [10], above 10 atm the differences become small , see Fig. 9. In the case of a double-base propellant and of a XLDB binder (that of the above table), with nearly the same heat of explosion, the burning rates for a large range of pressure are very close, Fig. 10.

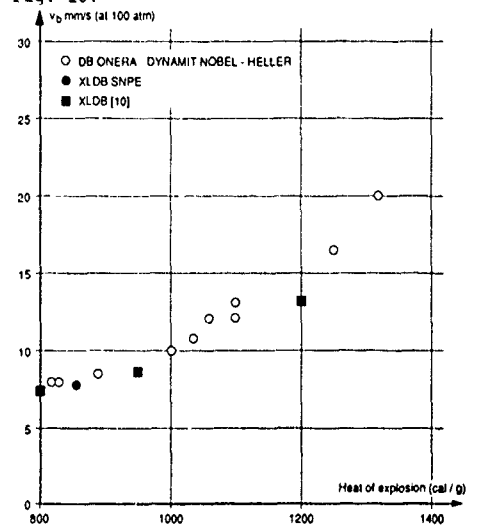

Fig. 9 **BURNING RATE VS HEAT OF EXPLOSION.DOUBLE-BASE PROPELLANTS AND XLDB BINDERS**

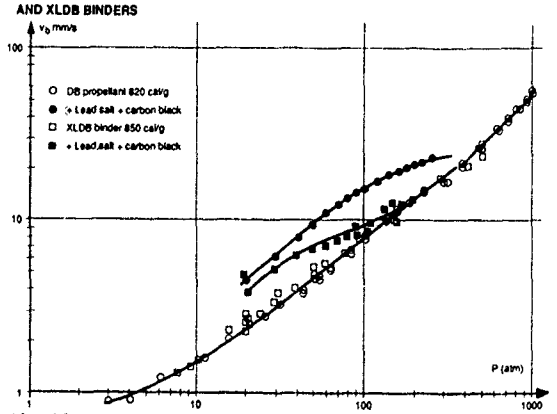

Fig. 10 **DOUBLE - BASE PROPELLANT AND ACTIVE BINDER BURNING RATES**

Measurements for XLDB binders of the degradation kinetics, of the surface temperature, of the heat evolved in the condensed phase, as in Fig. 6. and of the primary flame temperature, Fig .7, show that these characteristics are very close to those of DB propellants.

NO_2	CH_2O	$(CHO)_2$	NO	CO	CO_2	H_2O	HC
0.31	0.37	0.08	0.07	0.03	0.04	0.02	0.08

Gases evolved from the surface, mass fractions. XLDB binder [7].

Gas analysis at the surface gives results which are qualitatively comparable to those of DB propellants, Fig. 3.

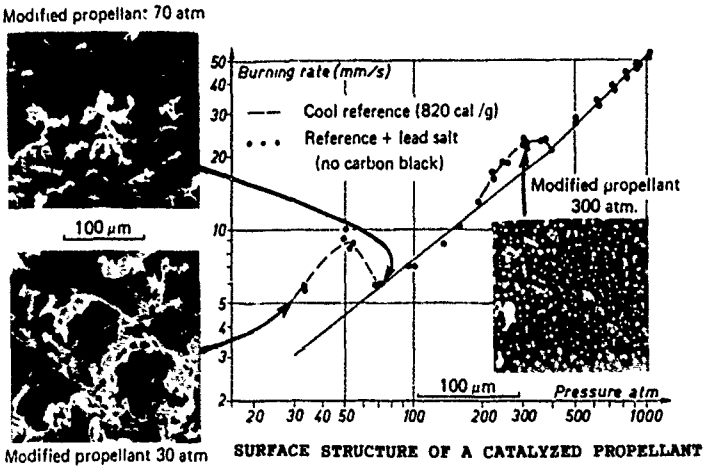

Fig. 11

SURFACE STRUCTURE OF A CATALYZED PROPELLANT

6. Mechanisms of action of additives

The incorporation of a few per-cents of lead (and copper) salts and carbon black enables to obtain super-rate effects followed by mesa or plateau effects in the burning rate versus pressure laws of double-base propellants, Fig. 2, as well as of active binders, Fig.10, although in the latter case these effects are much less pronounced.

What is thought to be the mechanism of action of the additives has been presented in references [5,6] by ONERA and recently in reference [12].

It has been found that the active part of the lead salt is the oxide of lead which accumulates above the propellant surface, after the salt has been trapped in the carbon residue layer which can be observed immersed in the primary flame (the decomposition kinetics of the salt is slower than that of the propellant components and it thus emerges from the surface unchanged). If the propellant (when its heat of explosion increases) or the active binder naturally produces less carbon residue, then the lead salt particles are in large part ejected from the surface and cannot act. This is the case probably when the amount of nitrocellulose is reduced (hot double-base propellants) or almost absent (XLDB binders). In the latter case however the inert polymer leaves some carbonaceous residue. Addition of carbon black is probably favorable because it accumulates on the surface in the naturally produced carbon layer.

It has been found that PbO reacts preferentially with aldehydes to form carbon and CO_2. It has been observed systematically [6] that there is a relation between the amount of carbon residue and the importance of the super-rate observed (for example, depending on the fabrication process : solventless extrusion, powder casting, mixing). It was seen that the primary flame is due to an NO_2-aldehyde reaction. But NO starts to react with carbon as well close to the surface leading to the increase in primary flame temperature of Fig. 7. It is believed that the extra carbon produced in the presence of additives enhances the NO/C reaction (see ref. [12] for more results on this reaction), depositing extra energy in the primary flame (an increase in primary flame temperature is observed in the presence of additives [5]) and resulting in a higher heat flux to the surface, and thus a higher burning rate.

Figure 11 shows surface structures of a cool propellant with a strong super-rate and a corresponding thick carbon residue. In this case, visualisation shows that a physical effect occurs in which the secondary luminous flame attaches in streaks to the carbon layer and deposits its high temperature (~ 2200 K as compared to the ~ 1400 K of the primary flame) closer to the surface. The abrupt end of the super-rate, the mesa effect, is believed to be due to the too thick carbon residue being expelled from the surface. At the end of the mesa effect the surface is almost clean of carbon.

In the case of hot propellants, Fig. 2, the super-rate is probably due only to the chemical effect of the enhanced NO/C reaction. As the pressure increases the secondary flame, where NO will react anyway, merges into the primary flame and progressively the modified propellant is caught up by the reference propellant, a plateau effect thus resulting.

In the high pressure domain when the flame system has reduced to one overall flame, a second super-rate occurs (when only lead salt or oxide is added), see Fig. 11 for the cold propellant and Fig. 2 for a 1250 cal/g propellant. This effect seems to be purely physical, related to the presence of lead oxide particles accumulating and imbedding into the surface, Fig. 11, with for example an enhancement of the thermal conductivity of the flame zone or a flame holder effect (the protruding particles perturbs the flow from the surface). At higher pressures and burning rates the thickness of the condensed phase heated zone and reaction layer and flame zone becomes so small that the particles will not attach to the surface or will be too large to perturb the combustion process.

PYROLYSIS OF INERT BINDERS

A number of books and works has been devoted to the behavior of polymers, whether or not usable as binders, under thermal loads, references [13-17]. Much work has been carried out with thermogravimetric analysis (TGA) or differential scanning calorimetry (DSC) with heating rates at most of the order of 1°C/s. Under linear pyrolysis (for a binder within a solid propellant) the rate of temperature increase is of the order of 10^5 °C/s. It is far from obvious a priori that the degradation kinetics will remain the same. In Ref. [8] it was attempted to establish that this is indeed the case for a number of polymers.

Although it is hardly a propellant binder Teflon is an interesting reference polymer. Its degradation kinetics (obtained by TGA) and thermal properties [8] (λ_p = 6.34 10^{-4} cal / cm K s, ρ_p = 2.1 g/cm^3, c_p = 0.25 cal/g K) are indicated on Fig. 12. In order to extrapolate these characteristics to the regime of linear pyrolysis (obtained experimentally by pressing the sample on a hot plate) the procedure of reference [8], also explained in the condensed phase paragraph of the double-base propellants chapter, is applied. In the case of a first order (with respect to the non degraded polymer) reaction the relation between regression rate and surface temperature is (again, numerical computation shows this relation to be accurate to about 1%)

$$v^2_r = (d_p/\mathscr{E}_c)\, A_c \exp(-\mathscr{E}_c) / [(-\ln Y_{p,s})(1 - T_o/T_s - Q_s/c_pT_s) + Q_s/c_pT_s] \quad (1)$$

$$\mathscr{E}_c \equiv E_c/RT_s$$

Q_s being the heat evolved in the condensed phase, in this case endothermic and about -340 cal/g ($Y_{p,s}$ mass fraction of the remaining polymer at the surface can be set at 0.01). It is seen on Fig. 12 that there is a good match between extrapolated law and measurements. These measurements are obtained under various atmospheres, showing no influence of this factor. The conclusion is then reached that the pyrolysis of such a polymer is an irreversible thermal mechanism.

In the case of an actual, widely used, propellant binder such as carboxyl terminated polybutadiene (CTPB) the same extrapolation can be made, Fig. 13 (the thermal properties used : λ_p = 3.6 10^{-4} cal/cm K s, ρ_p = 0.91 g/cm^3, c_p = 0.39 cal/g K), and compared to the results of Ref. [15], where the linear pyrolysis of various binders is achieved by the heat flux from an arc-image furnace, the surface temperature being obtained by infra-red pyrometry. It is interesting to note that in these experiments no effect of pressure was found, strengthening the idea that the limiting pyrolysis mechanism is the irreversible thermal degradation of the polymer bonds. In this case the match is unfortunately not as clear as in the case of Teflon. The agreement, considering the extent of the extrapolation, is satisfactory for regression rates up to 1 mm/s. Above, it might be assumed that radiating carbon residues stagnating on the surface cause the I.R. pyrometer to overestimate the surface temperature, a point seen in ONERA

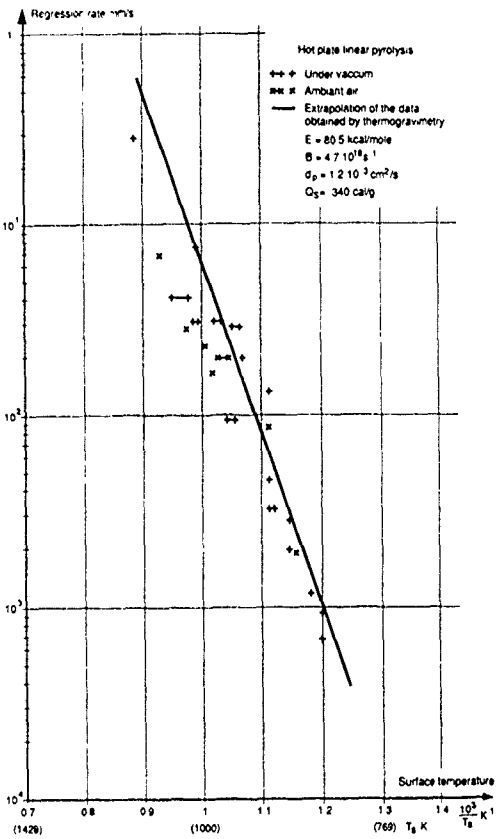

LINEAR PYROLYSIS AND EXTRAPOLATION OF THERMOGRAVIMETRIC RESULTS EXAMPLE OF TEFLON

Fig. 12

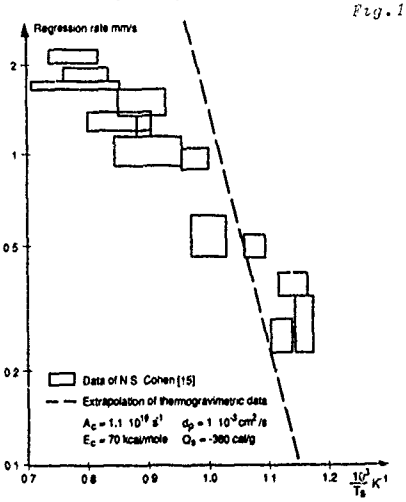

Fig. 13

LINEAR PYROLYSIS OF CARBOXYL TERMINATED POLYBUTADIENE

experiments. In further considerations, the pyrolysis law based on the TGA kinetics will be considered to apply.

Equation (1) and Fig. 13 indicate how the surface temperature adjusts itself to allow the polymer to degrade into gases when the regression rate changes. Further

considerations to better know the binder behavior are the nature of the gases resulting from the pyrolysis and the corresponding heat of degradation. From the results of [13] a mole balance is roughly (for 100 g of polymer) :

$$C_7 H_{11.24} O_{0.2} \left(\ldots - \underset{H}{\overset{H}{C}} - C = C - \underset{H}{\overset{H}{C}} - \ldots\right)$$

→ 12 % $CH_2 = CH_2$, 15 % $CH_3 - CH_3$, 17 % $CH_3 - CH = CH_2$, 5 % $CH_3 - CH_2 - CH_3$, 28 % $CH_2 = CH - CH = CH_2$, 14 % $CH_2 = CH - CH_2 - CH_3$, 4% $CH_3 - CH_2 - CH_2 - CH_3$ ...

It is shown on Fig. 14 the energetics involved in the degradation of CTPB (in particular the taking into account of the above gas composition is coherent with the measurements of [15]). For a given heat flux q_s, in cal/cm²s, at the surface, the energy balance is

$$q_s = \rho_p v_r \left[c_p (T_s - T_o) - Q_s\right] \qquad (2)$$

with Q_s the endothermic heat of degradation about - 360 cal/g.

COMBUSTION OF AMMONIUM PERCHLORATE

Ammonium perchlorate (AP), $NH_4 ClO_4$, is a widely used oxidizer and as such has been the object of numerous investigations. References [18 to 22] are a sampling, with [22] giving a detailed list. A view of the combustion of AP is presented herein attempting to make use as much as possible of the various experimental data available. Due to the large number of works on AP combustion, somewhat contradictory interpretations and corresponding models have been produced. A simplified model will be presented, which is considered to represent reasonably the combustion mechanism of AP, although it will not be in agreement with all of the above mentioned interpretations.

1. Condensed phase behavior

The considerations presented previously for the condensed phase of a pyrolysing monopropellant apply to AP. The conduction zone has a thickness

$$e_{cond.} = (d_p/v_b) \ln 10^2$$

(with the thermal diffusivity [21] $d_p = 1.2\ 10^{-3}$ cm²/s at an average temperature in the heat wave), thus equal to ≈ 50 µm, for a burning rate of 10 mm/s.

c_p = 0.31 cal/g K (orthorhombic phase < 513 K) = 0.365 cal/g K (cubic phase)

ρ_p = 1.95 g/cm³ , $d_p = 2.5\ 10^{-3} - 4.55\ 10^{-6}$ T(°C) cm²/s

Condensed phase values for AP [19,21]

Based on observations by scanning electron microscopy after extinction, the idea has been advanced that the self-deflagration of AP, possible only above 20 atm, requires that a large amount of exothermic reaction already takes place in the condensed phase in a thin liquid layer (above a melting temperature estimated at 835 K) [19,20,21,22].

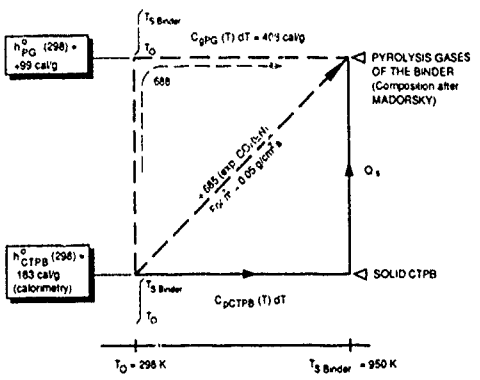

Fig. 14 ENERGETICS OF CARBOXYL TERMINATED POLYBUTADIENE

2. Energetics of the AP combustion

The model of [19] is subscribed to in order to describe the combustion of AP alone. The AP undergoes a phase transition at 513 K, melts around 835 K and, in the thin (a few microns) superficial liquid layer thus created, an exothermic reaction, affecting 70% of the AP, takes place and creates the final combustion gases, O_2 in particular. The remaining 30 % of the AP sublime into NH_3 and $HClO_4$ which react exothermically in a premixed flame very close to the surface (about 1 micron), Fig.15.

From the data collected in [19] the change of enthalpy per gram of AP required to bring the AP to its surface temperature, $T_{s,AP}$, is estimated as

$$\Delta h_{s,AP} = 0.31 (513-293) + 21 + 0.365 (835-513) + 60 + 0.328 (T_{s,AP} - 835),$$

$$= 266 + 0.3..9 (T_{s,AP} - 835) \text{ cal/g} \qquad (1)$$

where the heat of transition and the heat of liquefaction appear. The exothermic condensed phase degradation involves an enthalpy change of [19]

$$\Delta h_{D,AP} = - 380 \text{ cal/gram of reacting AP.} \qquad (2)$$

The heat of sublimation is 58 ± 2 kcal/mole or

$$\Delta h_{s,AP} = 476 \text{ to } 510 \text{ cal/gram of subliming AP} \qquad (3)$$

The adiabatic flame temperature for the combustion of AP alone has been estimated in [16] to be $T_{f,AP}^{ad} = 1205$ K, corresponding to the reaction

$$NH_4 ClO_4 \rightarrow 0.265 N_2 + 0.12 N_2O + 0.23 NO + 1.62 H_2O + 0.76 HCl + 0.12 Cl_2 + 1.015 O_2. \qquad (4)$$

The change of enthalpy, $\Delta h_{c,AP}$, corresponding to the combustion of the sublimed NH_3 and $HClO_4$ (to give the combustion products of (4)) is obtained from the equation expressing the conservation of enthalpy between the unreacted AP at initial temperature and the combustion products dowstream of the flame :

$$0.3\ \Delta h_{c,AP} + c_g (T_{f,AP}^{ad} - T_{s,AP}) + 0.3\ \Delta h_{s,AP} + 0.7\ \Delta h_{D,AP} + \Delta h_{s,AP} = 0. \qquad (5)$$

For c_g = 0.3 value taken in [19] it is found

$$\Delta h_{c,AP} = -850 \text{ to } -885 \text{ cal/gram of reacting AP,} \quad (6)$$

depending on the value adopted for the heat of sublimation, 476 or 510 cal/g, and independently of the value of $T_{s,AP}$ in the range found in [19].

It should be noticed that the value given here for the transformation of the AP into gases (that is NH_3 and $HClO_4$ for the subliming 30% and the combustion gases of (4) for the 70% reacting in the condensed phase), namely

$$-Q_s = 0.3\ (476 \text{ to } 510) + 0.7\ (-380)$$

$$= -123 \text{ to } -113 \text{ cal/g of AP,} \quad (7)$$

is also found in [10], where a model for the combustion of AP similar to that of [19] is adopted. The heat evolved in the condensed phase Q_s (> 0 if exothermic) will be set equal to 120 cal/g.

One last check of consistency can be performed : with the enthalpy of formation of AP at h^0_{AP} = - 602 cal/g and that of the combustion products of (4) h^0_{CP} = - 877 cal/g, an overall energy balance between initial AP and combustion products is

$$c_g\ T_{f,AP}^{ad} + h^0_{CP} = c_{ortho}\ T_0 + h^0_{AP} \quad (8)$$

resulting in $T_{f,AP}^{ad}$ = 1215 K, close enough to the previous value.

3. Surface pyrolysis of the AP

Attempts to measure the surface temperature give values between 670 and 973 K. These results, obtained either using thermocouples imbedded in the AP pellet, or by measuring the radiation emitted by the surface, are always associated with some uncertainty due to the operating methods. In effect, the large size of the thermocouples, in relation to the temperature gradients encountered, favors errors; further, the measurement represents an averaging of surrounding conditions. The temperatures thus obtained are therefore probably somewhat lower than in reality. In the case of experiments using an optical technique, the surface temperature is deduced from measuring the radiation emitted by the latter and transmitted by the gaseous layer. The disturbance caused by the radiation of the gases and the screening action of the flame limits the application of this method to 60 atm. That is why the original technique suggested by Seleznev [23], and carried using a sapphire light guide inserted in the solid substance and reading of the infra-red emission in the direction of the condensed phase, has the considerable advantage of providing a direct measurement of the radiation emitted by the surface, without any hot gases and the reaction of the flame being interposed. Its application can therefore be extended to high pressures and the measurements appear to be more convincing. These results enable to determine the AP pyrolysis law.

Further, estimates of the AP melting temperature are put forward by a number of authors; the values suggested vary from 715 to 865 ± 20 K and are useful in interpreting the extinction phenomenon at low pressure.

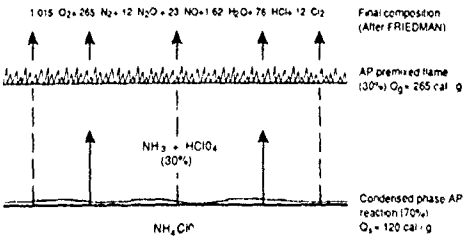

Fig. 16 AUTONOMOUS COMBUSTION OF AMMONIUM PERCHLORATE

The pyrolysis law of the AP is written as

$$\dot{m}_{AP} = \rho_{AP}\ v_{bAP} = A_{s,AP} \exp\left[-E_{s,AP} / RT_s\right] \quad (9)$$

The parameters characterizing the pyrolysis law are determined so as to obtain a good agreement between the rates and the surface temperatures measured by Seleznev [23] (Fig. 16). The activation energy obtained is 20 kcal/mole, a figure compatible with the various estimates encountered. The measurement of the surface temperature made at 40 atm is the only one which deviates from that computed by the pyrolysis law used. On the other hand, for the critical rate of 0.27 cm/s obtained at 20 atm (AP combustion pressure limit), this law allows for a surface temperature of 830 K, corresponding to the assumed AP melting temperature [19].

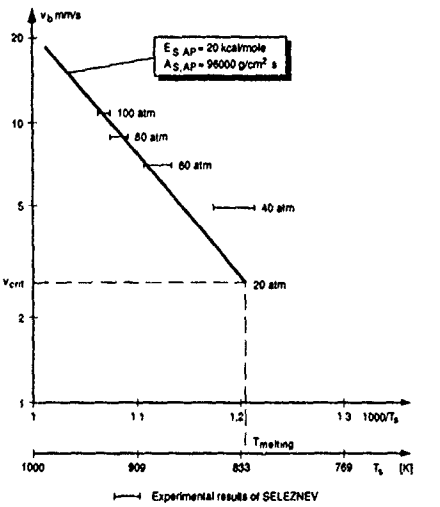

Fig. 16 PYROLYSIS LAW FOR AMMONIUM PERCHLORATE

4. Flame structure of the AP combustion

The approach of [19] considers 14 different reactions to describe the flame zone of the AP, involving 30 % of the material sublimed into NH_3 and $HClO_4$. An overall second order reaction is then obtained

$NH_3 + HClO_4 \rightarrow$ products of Eq. (4)
with an activation energy of $E_{g,AP}$ = 15 kcal/mole.

A simplified model can be constructed if one assumes the flame thickness to be very small

as compared to the stand-off distance from the surface [20,21,22]. The conservation of energy is then ruled by

$$\dot{m}\ c_g\ dT/dx - d(\lambda_g\ dT/dx)/dx = 0 \qquad (10)$$

with boundary conditions

$$T = T_s \text{ at } x = 0\ ,\ \lambda_g\ dT/dx|_s = \dot{m}\ Q_c \qquad (11)$$

with $\dot{m} = \rho_{AP}\ v_{b,AP}$ and Q_c the heat required to bring the AP from T_o to gases from the surface, see Eq. (1) and Eq. (7),

$$Q_c = \Delta h_{H,AP} - Q_s$$

The temperature profile is then

$$T = T_s + (Q_c/c_g)\ [\exp\ (\dot{m} \times c_g/\lambda_g) - 1] \qquad (12)$$

When $T = T_{f,AP}^{ad}$ the flame stand-off distance is reached

$$x_f = (\lambda_g/\dot{m}c_g)\ \ln\ [1 + c_g\ (T_{f,AP}^{ad} - T_s)\ /\ Q_s] \qquad (13)$$

Equation (5) for the overall enthalpy balance can be written

$$c_g\ (T_{f,AP}^{ad} - T_s) + Q_c = Q_g,$$

$$Q_g = - 0.3\ \Delta h_{c,AP} > 0$$

and the relation for x_f becomes

$$x_f = (\ \lambda_g\ /\dot{m}\ c_g)\ \ln(Q_g/Q_c) \qquad (14)$$

The flame, being premixed, is controlled by the chemical kinetics and the time required for the reaction to occur can be expressed as

$$\dot{\omega}\tau_{ch} \sim \rho_g$$

$\dot{\omega}$ being the reaction rate

$$\dot{\omega} \sim p^2\ A_{g,AP}\ \exp\ (\ -\ E_{g,AP}/RT_{f,AP}^{ad}\ ) \qquad (15)$$

The flame stand-off distance is then :

$$x_f \sim v_g\ \ \tau_{ch} \sim (\ \dot{m}/\rho_g)\ \tau_{ch}\ \sim \dot{m}\ /\ \dot{\omega} \qquad (16)$$

This combined with Eq. (14) results in

$$\dot{m} \sim [\ (\ \lambda_g/c_g)\ \dot{\omega}\ \ln\ (Q_g/Q_c)]^{\ 1/2} \qquad (17)$$

and thus for a second order reaction as in (15) a pressure exponent in $\dot{m} \sim p^n$ close to 1.

ρ_{AP}	= 1.95 g/cm^3
$E_{s,AP}$	= 20 kcal/mole
$A_{s,AP}$	= 96000 g/cm^2 s
$E_{g,AP}$	= 650 g/cm^3 s atm^2
γ	= 30 %
c_g	= 0.3 cal/g K
λ_g	= 1.9 10^{-4} cal/cm s K

Values considered as representative for the AP flame zone.

Taking into account the various values given it is obtained for v_b = 10 mm/s ($T_{s,AP}$ = 925 K) the flame stand-off distance, Eq. (14), (Q_g = 265 cal/g , Q_c = 175 cal/g) x_f = 1.3 µm.

The only input data which is not defined from outside considerations is the pre-exponential factor $A_{g,AP}$ used as a floating parameter for the model. Various numerical values associated with the input parameters of the model are brought together in the above table. Just by the choice of the prefactor $A_{g,AP}$ adjusted at 650 g/cm^3 s atm^2, the model satisfactorily reproduces variations in the AP burning rate due to pressure as well as to the change in the initial temperature of the product. Figure 17 provides a comparison of computed rate curves with experimental points [21].

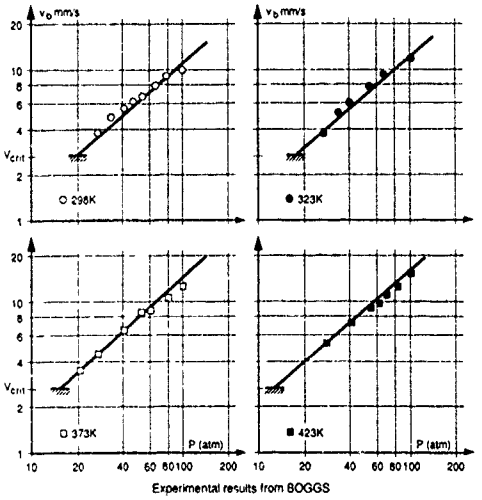

Fig. 17 BURNING RATE OF AMMONIUM PERCHLORATE AT DIFFERENT INITIAL TEMPERATURES

At sufficiently high pressures, the energy transmitted from the flame toward the surface, to which must be added the effect of the superficial exothermic reactions, maintains the surface temperature above the AP melting point. When the pressure falls, the premixed flame moves away and the surface temperature can then fall below the limiting value, thus causing the disappearance of the liquid surface layer which was enabling the exothermic reactions to occur. The energy from the flame is then much too small to maintain a pyrolysis which has become strongly endothermic and AP no longer burns. This minimum pressure, beyond which the combustion cannot propagate itself, sets the pressure limit for AP self-degradation.

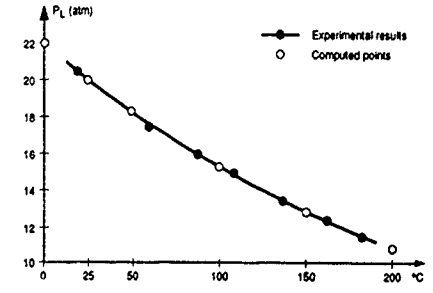

Fig. 18 (Experimental results from ENSTA)

LIMITING PRESSURE FOR COMBUSTION OF AMMONIUM PERCHLORATE

On the basis of this hypothesis, the combustion pressure limit is reached when the surface temperature is equal to the AP melting temperature. It is interesting to use the model in order to follow the variation of the computed limiting pressure with the initial temperature. At atmospheric temperature, the combustion limit is 20 atm,

in agreement with experimental results. The critical rate of 0.27 cm/s and the surface temperature of 830 K, representing the AP melting temperature, corresponds to it. The computation method consists, for the initial temperature varying between 0 and 200° C, in finding for what pressure the surface temperature is equal to 830 K. A comparison between the computed and experimental pressure limits is excellent, Fig. 18, and confirms the soundness of the hypothesis follow ng which AP only burns if the surface temperature exceeds its melting temperature.

One further set of results is presented. Questions have been raised about the combustion of AP at high pressures above about 100 atm, with many conflicting results. Measurements of burning rates on carefully inhibited samples are presented on Fig. 19. It is concluded that no strong change of combustion regime is observed. The model based on the above presented hypothesis seems to follow quite well the results to high pressures.

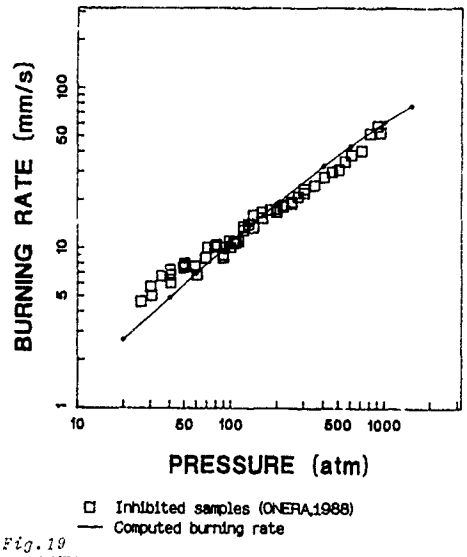

Fig. 19 **BURNING RATE OF AMMONIUM PERCHLORATE**

COMBUSTION OF HMX

The combustion of HMX, which has balanced oxidizing and combustible elements (to reach CO, H_2O and N_2) and a combustion temperature of 3280 K, is controlled by processes in the condensed phase as well as in the flame zone. Information about these processes is to be found in references [24 to 31] (also [21]).

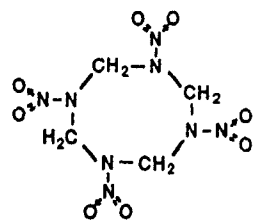

1. Condensed phase processes

The kinetics of the decom osition of HMX can be obtained by differential thermal analysis

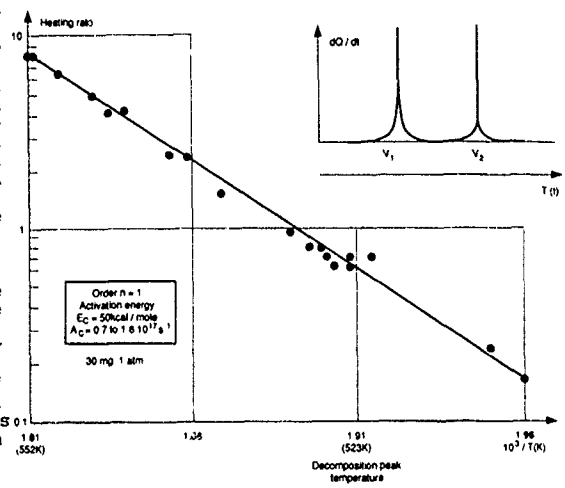

Fig. 20 **DIFFERENTIAL THERMAL ANALYSIS OF HMX DECOMPOSITION**

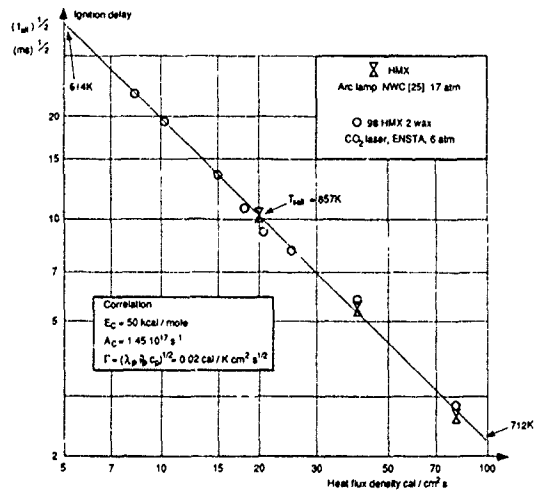

Fig. 21 **IGNITION OF HMX**

[24,29]. A fairly extensive review is given in Ref. [25]. Results obtained around the (assumed) melting temperature are indicated on Fig. 20, with the kinetics extracted for a reaction order of 1.

The condensed phase properties considered to be representative are indicated below

ρ_p = 1.9 g/cm^3, c_p = 0.33 cal/g K
$d_p \equiv \lambda_p/\rho_p\ c_p$ = 1 10^{-3} cm^2/s
(also found from thermocouple traverses)
λ_p = 6.3 10^{-4} cal/cm s K

Condensed phase properties (average in the thermal wave) for HMX [31].

Another technique to obtain the decomposition kinetics, at somewhat higher temperatures, is through ignition tests, by exposing the

sample to a given surface heat flux and detecting the delay for the first exothermic ignition reaction (rapid deviation of the surface temperature from that of an inert material). The results are seen on Fig. 21 and confirm those obtained by DTA (the first method gives a good estimate of the activation energy, whereas the ignition experiments are better for estimating the prefactor). All these results correspond to an irreversible thermal decomposition of the HMX bonds with no influence of the pressure.

Finally, the investigation of the condensed phase processes under combustion is carried out by determining the temperature profile through the combustion wave by use of micro-thermocouples. As was seen on several occasions the thermal wave thickness is :

$$e_{cond.} = \ln 10^2 \, d_p / v_b \qquad (1)$$

that is, in the case of Fig. 22, $e_{cond.} \simeq 220$ µm. The thermocouple junction has to be very small, in the present case 5 µm platinum wires are welded end to end by electric discharge with the junction at about this size. A measurement of the thermal diffusivity is also obtained, close to that indicated in the above table.

The relationship between the surface temperature (obtained from measurements such as that of Fig.22) and the burning rate is displayed on Fig. 23. Scatter of the measurements is hard to avoid (about 50 K). Also indicated are thermocouple results from reference [28]. The pyrolysis law is also established from the decomposition kinetics obtained by DTA and by ignition experiments, making use of the approach mentioned for double-base propellants as well as for inert binders according to which [8], for a first order reaction,

$$v^2_b = (d_p/\mathscr{E}_c)\, A_c \exp(-\mathscr{E}_c)/$$

$$[(-\ln Y_{p,s})\,(1-T_o/T_s - Q_s/c_pT_s) + Q_s/c_pT_s] \qquad (2)$$

$\mathscr{E}_c \equiv E_c / RT_s$ and Q_s is the heat evolved in the superficial reaction layer of the HMX; its value will be seen next. The amount of HMX at the surface $Y_{p,s}$ is set at 0.01. It is seen that there is continuity between the decomposition (thermal breaking of the chemical bonds, with probably no participation of the vaporization of the HMX) under DTA conditions, $\simeq$ 550 K, for ignition, from 600 to 700 K, and under combustion, up to 900 K. This conclusion on such a continuity, which is not a priori guaranted, was also reached for double-base propellants.

From the temperature profiles, as on Fig. 22, the heat evolved in the condensed phase can be evaluated by use of the relation

$$\lambda_g \, dT/dx|_s = \rho_p v_b \, [c_g T_s - c_p T_o - Q_s] \qquad (3)$$

with $Q_s > 0$ if exothermic. The results of Fig.24 show that indeed the transformation of HMX into gases is exothermic. The energy absorbed by the breaking of the HMX bonds is more than compensated by exothermic reactions taking place in the superficial degradation layer probably between NO_2 and HCHO (see further for the identification of these gases). This mechanism was already observed for double-base propellants.

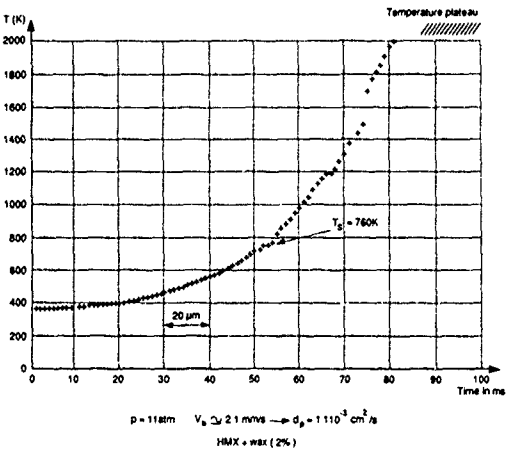

Fig. 22

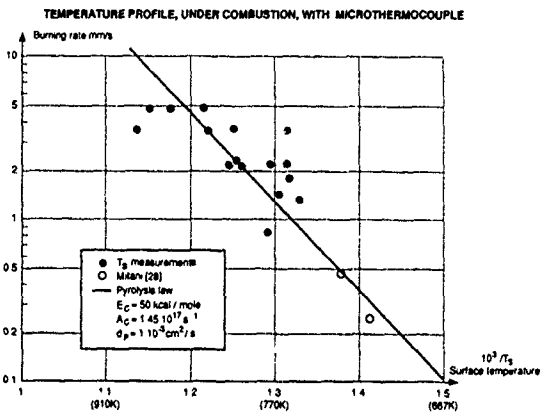

Fig. 23 PYROLYSIS LAW FOR HMX

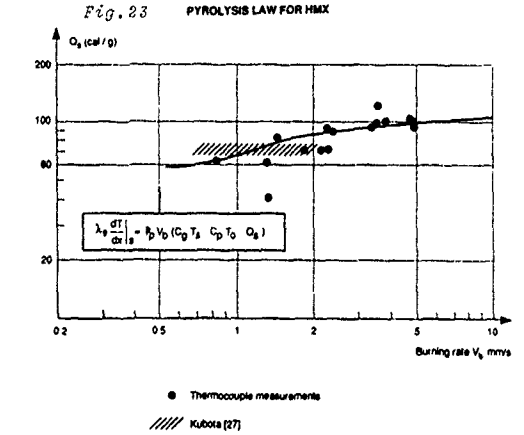

Fig. 24 HEAT EVOLVED IN THE CONDENSED PHASE OF HMX

Experiments have been performed [7] by maintaining the linear regression (at about 1 mm/s) of HMX samples with an external heat flux (radiation or contact with a heated plate) under vacuum so as to avoid any gas flame. The sampled gases are then analyzed by mass spectrometry. The following table indicate the results.

NO_2	NO	N_2O	N_2	CO_2	CO	H_2O	H_2	HCHO	HCN
22.2	17.5	19.1	3	1.4	1.6	3.7	0.1	14.1	16.8
	59 %							31 %	

Gases evolved from the surface of HMX.Mass fractions [7].

It is seen that the initial degradation produces probably NO_2 and N_2O in similar amounts and HCHO and HCN. See also for such conclusions reference [32]. Exothermic reactions involving NO_2 occur in the superficial degradation layer to give a large amount of NO. Results in rough agreement with those of the above table have also been obtained in Ref. [33] with an infra-red analysis technique.

2. Gas phase behavior

The production from the condensed phase of HMX of several oxidizing gases, NO_2, N_2O and NO , can create a two-stage flame. This was seen to be the case for double-base propellants for which NO_2 and NO are created in the condensed phase : the primary flame involves NO_2 and the secondary flame NO; above ~ 200 atm the two flames merge into one. In the case of HMX, observation at pressures around 1 atm reveals the existence of a dark induction zone and a detached luminous flame, similar to those of double-base propellants. Also the micro-thermocouple traverses below about 10 atm, such as in Fig. 22, show a plateau in the temperature profile at about 2000 K, much below the final temperature of 3280 K.

The burning rate of HMX, as single crystals or as pressed samples, obtained in Ref.[25] is shown on Fig. 25. The evolution of this burning rate with pressure shows that around 20 atm a pressure exponent of about 1 is attained, revealing that the staged flame has collapsed into one (as in the case of double-base propellants above about 200 atm).

It was seen in the chapter on double-base propellants that in the case of a distributed flame an approximation for the temperature profile is

$$(T_f - T)/ (T_f - T_s) = \exp (- x/x_f) \qquad (4)$$

with

$$x_f = \lambda_{g,s} (T_f - T_s) / \dot{m} Q_c,$$

$$Q_c = c_g T_s - C_p T_o - Q_s \qquad (5)$$

(at v_b = 10 mm/s this will give x_f = 15 µm)

and the burning rate becomes

$$\dot{m} = \rho_p v_b = [\bar{\omega}_g \lambda_{g,s} (T_f - T_s)/ Q_c] \qquad (6)$$

With $\bar{\omega}_g$ the summed reaction rate through the flame zone. More complete descriptions of the flame zone can be found in references [29,30], the conclusions of which are essentially those which can be extracted from the above simplified approach.

c_g = 0.35 cal/g K,

$\lambda_g = 1.25\ 10^{-4}\ (T/700)^{0.7}$ cal/cm s K

Values considered to be representative of the gas phase of HMX.

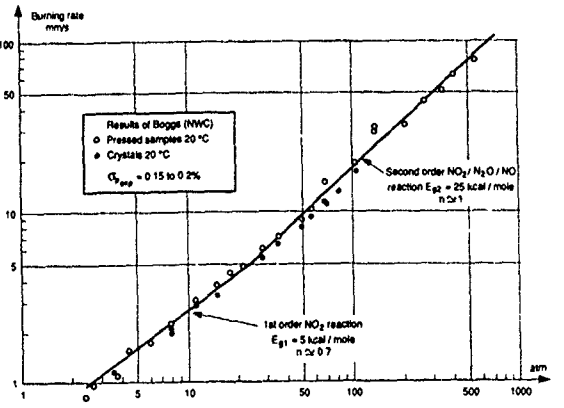

Fig. 25 VITESSE DE COMBUSTION DE L OCTOGENE

At low pressures the primary flame, involving NO_2 in a first order reaction, controls the burning rate, with, according to Eq. (6), a pressure exponent around 0.5. At higher pressures the collapsed flame is probably dominated by a second order reaction involving NO and N_2O, with a pressure exponent close to 1.

COMBUSTION OF COMPOSITE PROPELLANTS

This chapter is devoted to the description of propellants made of an oxidizer, ammonium perchlorate or HMX, and a binder, inert such as polybutadiene or active, a mixture of a liquid nitrate and a polymer. For the sake of

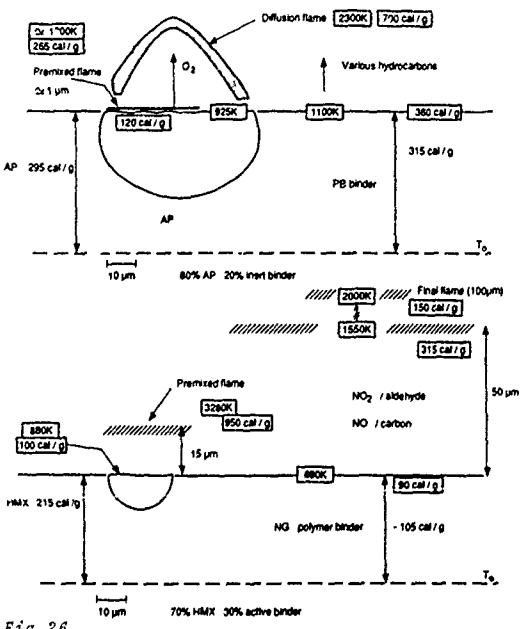

Fig. 26

Figures for a burning rate of 10 mm / s Positive heats are exothermic.
COMPARATIVE PICTURE OF AP-INERT BINDER AND HMX-ACTIVE BINDER COMBUSTION

clarity only these two categories will be considered, the main point being, as was said in the introduction, to attempt to improve the understanding of the combustion of propellants rather than to present an extensive catalog of results.

1. Comparative picture of composite propellants combustion

Drawing from the results presented previously for the various components the comparative picture of AP-inert binder and HMX-active binder is found on Fig. 26.

The combustion of AP results in a premixed flame at about 1 μm from the surface at ~ 1200 K or higher . From this flame 1 mole of O_2 comes out for each initial AP mole. From the binder surface at nearly the same temperature combustible gases are ejected, which, after diffusion, react with O_2. As will be seen further on, the diffusion flame height is related to the AP particle size. The smaller the particle size the closer is the flame and the higher the heat flux to the surface and therefore the burning rate of the propellant. The pyrolysis of the inert binder is purely endothermic (heat required to bring the temperature to 1100 K and heat to decompose it into gases). In the case of particles of a few tens of μm, the burning of the AP being close to adiabatic (its flame receives some heat flux from the final flame, but computation results show that there is only a moderate deviation from adiabatic conditions), the heat flux from the final flame serves primarely to keep the binder regressing.

The combustion of HMX is also through a premixed flame, about 15 μm from the surface, reaching the final stage of 3280 K. The gases emitted from this flame cannot sustain any further combustion. The active binder goes through its own combustion, with a primary flame reaching ~ 1550 K some 50 μm from the surface. The final flame somewhat further away reaches about 2000K. There is no direct interaction between the two components of the propellant. The burning of the propellant is then an average of the individual burning rates. There exist however an indirect interaction of the active binder on the HMX particles. As was seen, the thermal properties of HMX and the active binder are close and the HMX particles are immersed in the temperature profile of the binder. Upon reaching the surface the top of the particle is at about 700 K, the surface temperature of the binder. This so happens to be very much the temperature for first ignition of HMX (see Fig. 21). There will be however a transition delay of the HMX particle to full combustion for which its surface temperature is about 900 K. This will be dealt with in more details further on.

In the case of AP, the ignition temperature is around 650 K and the surface temperature for full combustion is around 900 K. Immersed in the inert binder with a surface temperature of ~ 1100 K the AP should reach combustion as soon as it is uncovered with no transition delay.

2. Propellant burning rate resulting from components rates.

Various approaches have been presented in the the literature to build the propellant burning rate from the components' own burning rates. One of the first comprehensive models for composite propellant combustion modeling, Ref. [34], had a picture of AP and binder burning in parallel with a partitioning of the surface between the two ingredients and a surface averaged propellant burning rate. This view is also found in Refs. [35,36], with Ref.[37] being a complete review for AP-inert binder propellants, including references preceding the work of [34]. A view of sequential burning, in which a given path goes through oxidizer particles separated by layers of binder, with as a consequence a time averaged propellant burning rate, was first presented in Ref. [39]. This view was subscribed to in [40], although the details have since then evolved into the option presented herein (which seems to be coherent with the latest view of M. Beckstead [42]).

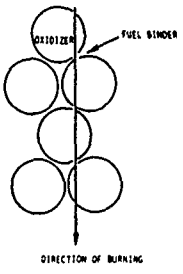

Time-averaged propellant burning Averaging of the components' burning rates, HMX and active binder, in Ref. [38] into the propellant burning rate is obtained by assuming that the components melt and mix at the surface and then form an average premixed gas flame. Due to the very small thickness of the melt (to the extent that melting occurs) layers (of the order of μm) and very short residence times in these layers (tenths of ms) it is believed that such premixing of the components should not take place. This is also the conclusion of [42].

Finally, in the recent work of Ref. [41] a surface average is operated for AP-binder interactions whereas a time average HMX-binder approach is adopted within the same mixed oxidizers propellant.

In a randomly packed arrangement of oxidizer spheres of diameter D_{ox}, with the average height through the sphere from a given direction (perpendicular to the surface) $\bar{h}_{ox}$, and for a volume of 1 cm^2 on the surface by 1 cm in depth, the number of particles intercepted along 1 cm of length being N, one has :

$$N\bar{h}_{ox}\ 1\ cm^2/N\bar{h}_b\ 1\ cm^2 = \xi_{ox}/(1-\xi_{ox}) \qquad (1)$$

with $\bar{h}_b$ the average binder height between particles and ξ_{ox} the volume fraction loading in oxidizer. Then it comes :

$$\bar{h}_b = \bar{h}_{ox}\ (1-\xi_{ox})\ /\ \xi_{ox} \qquad (2)$$

and due to

$$N(\bar{h}_{ox} + \bar{h}_b) = 1\ cm$$

$$N = \xi_{ox}/\bar{h}_{ox} \qquad (3)$$

For a propellant burning rate $v_{b,p}$, the time to run through 1 cm of depth is

$$t = 1/v_{b,p} = t_{ox} + t_b = N\,\bar{h}_{ox}/v_{b,ox}$$

$$+ N\Delta t_{ox} + N\bar{h}_b/\ v_{b,b}\ \Delta t_{ox} \qquad (4)$$

Δt_{ox} being the (possible) transition delay to full combustion after the top of the oxidizer particle has reached the surface. Then the

propellant burning rate, as expressed with the component burning rates, is, with Eq. (3) taken into account,

$$1/v_{b,p} = \xi_{ox}/v_{b,ox} + \xi_{ox}\Delta t_{ox}/N\bar{h}_{ox} + (1 - \xi_{ox})/v_{b,b} \quad (5)$$

Consideration of a sphere being traversed randomly along a given direction leads after some computation to $h_{ox} = D_{ox}(\Pi/4)^2$.

In the case of AP- inert binder propellants with no transition delay the propellant burning rate is

$$1/v_{b,p} = \xi_{ox}/v_{b,AP} + (1 - \xi_{ox})/v_{b,b} \quad (6)$$

The relationship between volume fraction loading ξ and mass fraction loading α being

$$\alpha_i = \xi_i \rho_i/\rho_p \quad (7)$$

$$\Sigma\xi_i = 1 \ , \ 1/\rho_p = \alpha_{ox}/\rho_{AP} + (1 - \alpha_{ox})/\rho_b \quad (8)$$

that is for example for an 88% AP - 12 % PB binder $\rho_p = 1.72$ g/cm^3.

The mass burning rate of the propellant is

$$\dot{m}_p = \rho_p v_{b,p}$$

and Eq. (6) yields

$$1/\dot{m}_p = \alpha_{ox}/\dot{m}_{AP} + (1 - \alpha_{ox})/\dot{m}_b \quad (9)$$

In the case of a propellant loaded with aluminum, it is known that the aluminum particles are ejected from the surface [43,44] (Ref. [44] being an extensive review of the processes of aluminum combustion) and burn at several hundreds of µm from the surface. The view of the combustion of aluminum is summarized here.

The volume fractions being

$$\xi_{ox}, \ \xi_b, \ \xi_{al}$$

Eq. (8) becomes

$$1/\rho_p = \alpha_{ox}/\rho_{ox} + \alpha_b/\rho_b + \alpha_{al}/\rho_{al} \quad (10)$$

that is, for example, for a 70% AP, 20% aluminum ($\rho_{al} = 2.7$ g/cm^3), 10% PB binder ($\rho_b = 0.91$/cm^3), $\rho_p = 1.84$ g/cm^3.

With respect to the burning rate of the propellant loaded with aluminum it is obtained :

$$1/v_{b,p} = \xi_{ox}/v_{b,ox} + N_{al}\bar{h}_{al}/v_{b,al} + N_{al}\Delta t_{al} + \xi_b/v_{b,b} \quad (11)$$

The "burning" rate of aluminum can be considered as infinite since it is ejected from the surface, whereas its "transition delay" is the time for the binder to regress through the particle height

$$\Delta t_{al} = \bar{h}_{al}/v_{b,b}$$

Also, for each component $N\bar{h} = \xi$ its volume fraction loading. The propellant burning rate becomes

$$1/v_{b,p} = \xi_{ox}/v_{b,ox} + \xi_b/v_{b,b} + \xi_{al}/v_{b,b} = \xi_{ox}/v_{b,ox} + (1 - \xi_{ox})/v_{b,b} \quad (12)$$

that is the relation which would be obtained for a corresponding propellant with no aluminum, with the binder filling in for it.

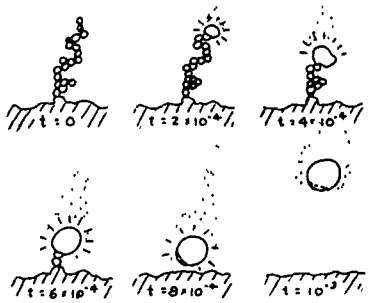

Sketches of selected frames of a high speed motion picture illustrate a protracted ignition-agglomeration event in which the hottest portion of the accumulate inflames and precipitates the complete inflamation-agglomeration of the (already hot) accumulate.

- Aluminum melts at 930 K (inert binder at 1100 K) (active binder at 700K)

- Al_2O_3 protective coating melts at 2300 K collapses into cap, leading to inflamation of Al agglomerate (several 10's of µm)

- Aluminum vaporizes at ~ 3300 K and reacts in semi-spherical flame with CO_2 from AP-binder flame

- Caps gives Al_2O_3 particles of a few µm, spherical flame gives Al_2O_3 smoke of ~ 1µm.

DESCRIPTION OF ALUMINUM COMBUSTION

From an energetics point of view the modeling of the combustion of aluminized propellants should include at the surface the heat of fusion of aluminum ~ 100 cal/g of Al. One can see Ref. [45] for such an approach.

3 HMX-active binder propellants

Both HMX and the active binder have independant burning rates. The resulting propellant burning rates is given by Eq. (5), where the transition delay has to be evaluated.

The emerging HMX particle offers to the external heat flux the surface area of the sphere cap which has been exposed by the binder regressing at $v_{b,b}$ after the time t from first appearance has evolved

$$S = \Pi D_{ox}(v_{b,b} t)$$

With α being the part of the sphere which is heated by the superficial flux ϕ , the temperature rise is

$$\alpha(\rho_p c_p)_{ox} dT/dt \ (4\Pi/3)(D_{ox}/2)^3 = \phi \Pi D_{ox} v_{b,b} t \quad (13)$$

The heat flux received is that of the binder flame when the particle first emerges and it transitions to that of the HMX flame when the particle has reached full combustion, a transition formula being assumed to be

$$\phi = \phi_b + [(T_s(t) - T_{s,b})/(T_{s,ox} - T_{s,b})](\phi_{ox} - \phi_b)$$

with

$$\phi_{ox,b} = \rho_p v_b \, (c_g T_s - c_p T_o - Q_s)|_{ox,b}$$

The fraction of the sphere heated by the flux is taken to be, with K finally adjusted at 0.1,

$$\alpha = \exp\left(- K \, D_{ox}/e_p^* \right)$$

e_p^* is the thermal wave thickness for which the temperature is at 90% of its surface value, that is, sufficiently close to it,

$$(T - T_o)/(T_s - T_o) = 0.9$$

$$= \exp(-e_p^* \, v_{b,b}/d_p) \qquad (14)$$

When $D_{ox}/e_p^* \to 0$ the particle is vanishingly small with respect to the thickness of the layer at about the surface temperature, $\alpha \to 1$ and the particle is heated in its entirety by the heat flux. If $D_{ox}/e_p^* \to \infty$ the particle is very large compared to the surface layer, $\alpha \to 0$, it is heated on a vanishingly small part. When $D_{ox} = e_p^*$, $\alpha = 0.9$, the particle is immersed in the binder layer at $T = T_{s,b}$ and it is almost totally heated by the external flux. The transition delay from Eq. (13) is then

$$\Delta t_{ox}^2 = \alpha(\rho_p c_p)_{ox}(D_{ox}^2/ 3 \, v_{b,b})$$

$$[T_{s,ox} - T_{s,b}]/(\phi_{ox} - \phi_b)] \ln (\phi_{ox} / \phi_b) \qquad (15)$$

One noteworthy feature of this relation is that the transition delay is proportional to the particle size D_{ox}, in such a way that inserted in Eq. (5) it renders the burning rate insensitive to D_{ox}, a fact which is observed experimentally for HMX-energetic binder propellants [40].

Figures 27 and 28 show two examples of propellant burning rate laws with the corresponding components rates. It is seen that the propellant burning rate is intermediate between those of HMX and of the binder (its being close to that of the binder at pressures under 100 atm is coincidental). The model presented above, and, what is important, the mechanisms it takes into account (that is the absence of diffusional interaction between the components and the importance of a transition delay for the HMX particles), is quite representative of the experimental results. Some of the details of the making of the burning rate are given in the following table.

PRESSURE	20 atm	100 atm	250 atm
$v_{b,b}$	2,4 mm/s	7,1	14,5
$T_{s,b}$	622K	667	698
$v_{b,ox}$	4,5 mm/s	17	37,5
$T_{s,ox}$	828K	907	962
% of burning time due to delay	32 %	16 %	4 %
$v_{b,p}$	2,3 mm/s	9,4	22,7

Elements for the evaluation of the burning rate. 70% HMX - 30% active binder.

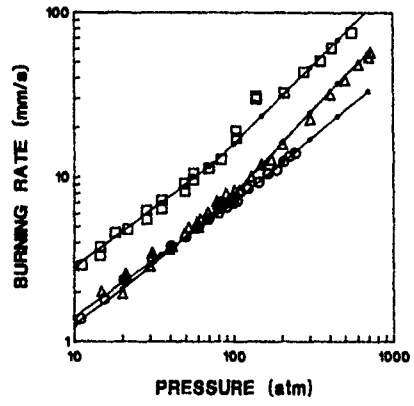

Fig.27 **EXPERIMENTAL AND COMPUTED BURNING RATE OF A NITRAMINE BASED PROPELLANT.**

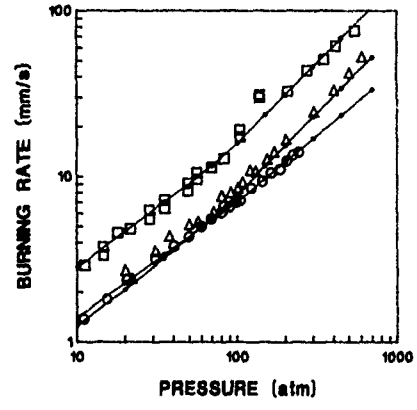

Fig.28 **EXPERIMENTAL AND COMPUTED BURNING RATE OF A NITRAMINE BASED PROPELLANT.**

It is seen that at low pressures the transition delay has a strong impact and the burning rate of the propellant happens to fall close to that of the binder. At high pressure the propellant burning rate is nearly the time average of the components rates (without delay the average at 250 atm is 24 mm/s).

It is observed that, for a given HMX-energetic binder composition, the burning rate law is locked and that there is no way to tailor it (as can be done in AP-inert binder compositions by acting upon the particle size). Furthermore the pressure exponent is too high to be acceptable for the

motor operation. Attempts to act upon the HMX burning rate by the use of additives have not been successful. One possibility of action however is with additives specific to double-base propellants, lead and copper salts and carbon black , incorporated in the active binder. It has been found on Fig. 10 that a moderate super-rate effects can be obtained. It is seen on Fig. 29 that such a modified binder associated with HMX, and after optimization of the amount and of the size of the additives, yields a burning rate law with moderate pressure exponent and initial temperature sensitivity.

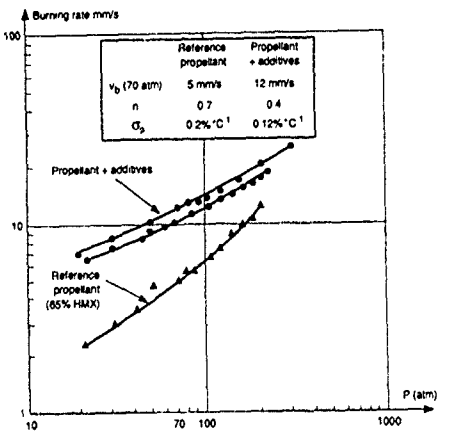

Fig. 29 HMX - ACTIVE BINDER PROPELLANT WITH ADDITIVES

4. AP-inert binder propellants

The burning rate of a propellant based on AP and an inert binder such as CPTB is thought to be described by the averaging rule of Eq. (9) from the burning rates of the components. In this case the binder has of course no autonomous burning rate. Its regression rate will be due to the heat flux from the diffusion flame, as depicted on Fig. 26, between O_2 from the AP flame and the hydrocarbons from the pyrolysis of the binder. A description of such a flame is given here.

A column of O_2 containing gases is ejected from a particle with an efficient diameter D^*_{ox} proportional to D_{ox} at a velocity v_g, such that $\dot{m}_p = \rho_g v_g$. This column is consumed by a lateral diffusion characterized by a diffusion velocity

$$v_{diff} = A_d \mathcal{D} / (D/2) \qquad (16)$$

D being the local diameter of the column, A_d some constant of order 1 and $\mathcal{D}$ the diffusion coefficient in cm^2/s. The variation of the column diameter is then given by

$$dD = - 2 v_{diff} dt \ , \ dx = v_g dt$$

$$D\, dD = 4 A_d \mathcal{D}\, dx / v_g$$

Resulting in

$$D_{ox}^{*2} = 8 A_d \mathcal{D} x_{fd} / v_g$$

$$x_{fd} = D_{ox}^{*2} \dot{m}_p / 8 A_d \rho \mathcal{D} \qquad (17)$$

When the lateral diffusion of O_2 and hydrocarbon gases into each others is purely laminar the diffusion coefficient $\mathcal{D}$ is expressed as :

$$\mathcal{D} = \mathcal{D}_o T^a / p \ , \ \rho \mathcal{D} = \mathcal{D}_o T^{a-1} \mathcal{M} / R$$

(with the equation for perfect gases $p/\rho = RT/\mathcal{M}$ being used) and the flame stand-off distance

$$x_{fd} = D_{ox}^{*2} \dot{m}_p (R/\mathcal{M}) / 8 A_d \mathcal{D}_o T^{a-1} \qquad (18)$$

does not depend explicitely upon the pressure. In this limiting case and due to the fact that
$\dot{m}_p \sim 1/x_f$, it is obtained

$$\dot{m}_p \sim 1/D_{ox}$$

independent of the pressure level and strongly dependent on the particle size

As will be seen later, it has been found that the diffusion flame process might become turbulent at high pressures when large differences exist between the mass flow rates emitted from the AP and from the binder. This conclusion is also mentioned in reference [37]. A general expression for a turbulent transport coefficient is

$$\rho \mathcal{D} \sim \rho u' l$$

with u' the magnitude of the fluctuating gas velocity and l its scale. It is then assumed

$$l \sim D_{ox}/2 \ , \ \rho u' \sim (\dot{m}_{ox} - \dot{m}_b)$$

that is the turbulent enhancement is related to the difference between the mass flow rates within the O_2 containing column and in the surrounding gases. Then Eq. (17) becomes

$$x_{fd} = D_{ox}^{*2} \dot{m}_p / 8 A_d (\rho \mathcal{D})_{eff} \qquad (19)$$

$$(\rho \mathcal{D})_{eff} = \mathcal{D}_o T^{a-1} \mathcal{M} / R$$

$$+ K (D_{ox}/2) (\dot{m}_{ox} - \dot{m}_b) \qquad (20)$$

where K should be of the order of 0.1.

An extra flame thickness related to the chemical time for the completion of the O_2-hydrocarbons reaction should be taken into account. From the chapter on AP, Eq. (16), it is obtained

$$x_{fr} = \dot{m}_p / A_r p^2 A_{g,f} \exp (- E_{g,f} / RT_f) \qquad (21)$$

the characteristics being related to the final O_2-hydrocarbons flame.

The stages of the combustion of an AP propellant are shown on Fig.30, which is to be seen side by side with Eq. 26 for the corresponding values. The usually made description of this flame structure is to assume very thin flames, treated as discontinuities [34,35,36]. The temperature profiles are then ruled by the equation for conservation of energy

$$q - x^* dq/dx = 0$$

$$q \equiv \lambda_g dT/dx \ , \ x^* \equiv \lambda_g / \dot{m}_p c_g$$

with the solution between two positions x and x_f given by :

$$q = q_f \exp [(x - x_f) / x^*]$$

The final flame being a discontinuity where the energy Q_f is deposited, the heat flux from this flame toward the surface is (no flux goes to the outside of the flame)

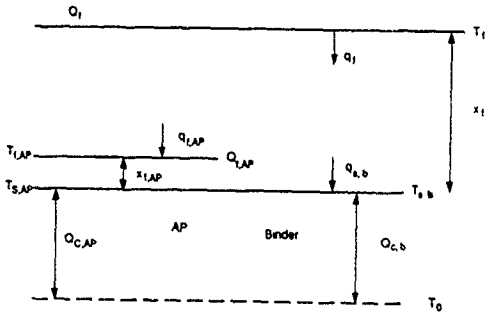

Fig. 30 STAGES OF AN AP-INERT BINDER PROPELLANT

$$q_f = \dot{m}_p Q_f,$$

thus

$$q(x) = \dot{m}_p Q_f \exp [(x - x_f) / x^*] \qquad (22)$$

The mass regression rate of the binder is then given by

$$\dot{m}_b Q_{c,b} = q_s = \dot{m}_p Q_f \exp (- x_f/x^*] \qquad (23)$$

where the constituting elements of this relation have been seen in the chapter on inert binders. It should be noticed that to simplify the description a uniform mass flow rate $\dot{m}_p$ is taken in the gas phase above the binder and the AP flame.

The mass burning rate of the AP, referring to Eqs. (13 and 17) of the corresponding chapter, is

$$\dot{m}_{AP} = \{(\lambda_g/c_g)\ \Phi_{AP} \ln [1 + c_g (T_{f,AP} - T_{s,AP}) / Q_{c,AP}]\}^b \qquad (24)$$

with

$$\Phi_{AP} = p^2 A_{g,AP} \exp [- E_{g,AP}/RT_{f,AP}]$$

Now, due to the fact that the AP flame receives a heat flux from the final flame, the flame temperature is no longer the adiabatic temperature ($T_{f,AP}{}^{ad}$ = 1205 K). It is given by

$$\dot{m}_{AP} c_g (T_{f,AP} - T_{s,AP}) + \dot{m}_{AP} Q_{c,AP} = \dot{m}_{AP} Q_{g,AP} + q_{f,AP} \qquad (25)$$

with, from Eq. (22), the heat flux from the main flame into the AP flame

$$q_{f,AP} = \dot{m}_p Q_f \exp [(x_{f,AP} - x_f)/x^*]$$

Results for the burning rate of AP-CTPB propellants are indicated on Fig. 31, where it is seen a strong influence of the AP particle size. The model described above, and what is important the mechanisms it contains, gives a satisfactory account of these results.

For the very small AP particle sizes the final flame is mostly dominated by the chemical process, very sensitive to pressure, as is the AP flame. This results in a variation of the burning with a pressure exponent close to 1.

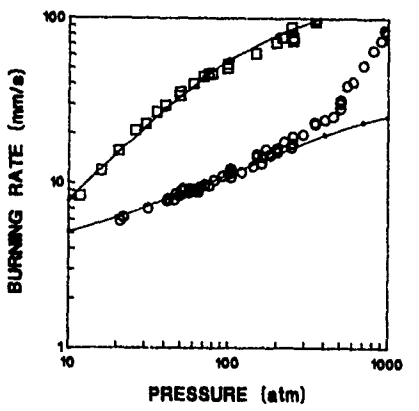

Fig. 31 AP-INERT BINDER PROPELLANTS.

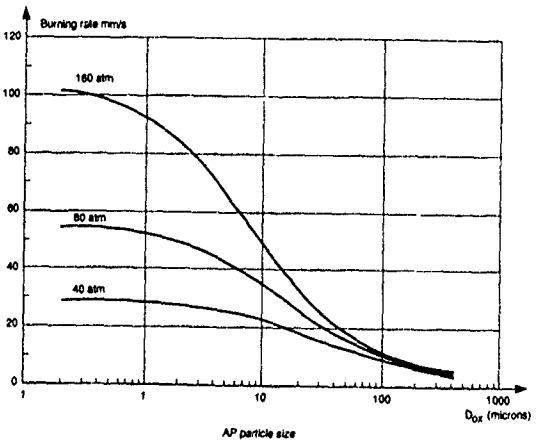

Fig. 32

80% AP - 20% CTPB
BURNING RATE (COMPUTED RESULTS) VS AP PARTICLE SIZE

For large particle sizes the final flame is dominated by the diffusion process, which is insensitive to pressure. This, combined with the pressure dependant flame of the AP, see Fig. 26, gives rise to a propellant burning rate which is moderately sensitive to pressure. It is found in the modeling that the contribution of the turbulent diffusion, see Eq. (20), becomes important above about 1.[illegible] atm. However above 300 to 400 atm the burning rate of the propellant undergoes a sharp exponent break that the model cannot follow. In some references this exponent break has been assumed to be due to the burning rate of the AP which would also increase sharply. It has been seen on Fig. 19 that, when the samples are carefully inhibited, this is not the case.
The strong influence of the AP particle size upon the propellant burning rate, as expressed by the modeling, is also shown on

Fig. 32. It is seen that at about 1 µm there is no further gain in the burning rate. This is due to the fact that there will always exist a non vanishing flame stand-off distance related to the chemical time for the O_2-hydrocarbons reaction.

On Fig. 33 the burning rate computed from the mechanisms modeled as described above is compared to results from the literature [35,36] for mixed AP particle sizes. The agreement is adequate for the larger particle sizes and qualitative for the small ones (Now, how representative are the particle sizes indicated ?). This reveals that the physico-chemical features incorporated in the model of the AP-inert binder propellant are probably sound. However, once a model has been "tuned" to represent a set of experimental results, as on Fig. 31, it cannot be expected that it will "predict" accurately other results for different values of the parameters.

It has been seen that by acting upon the AP particle size it is possible to tailor the burning rate of the propellant, but that there exist a limiting size below which the effect will be non existent, Fig. 32. It is possible to gain further by incorporating metallic additives, Fig. 34, such as the ferrocenic type (which during processing will dissolve into the not yet cross-linked binder for a proper mixing). Various results, and in particular the similarity of action of a silicon binder which produces on the propellant surface a fine structure of S_iO_2 residue, indicate that the mode of action is physical (rather than catalytic, in the sense of enhancing some chemical reactions). The layer of residue deposited on the surface has probably a flame-holding effect, the gases flowing in tortuous paths through this residue will react closer to the surface in such a way that an enhanced heat flux will act on the surface.

CONCLUSIONS

A review has been presented of the combustion mechanisms of components and of solid propellants. Some noteworthy points are stressed here.

Double-base propellants and active binders : a fairly good knowledge of the processes in the condensed and gas phases has been acquired. The main point is the presence of a two-flame system, involving $NO_2 \rightarrow NO \rightarrow N_2$, collapsing into one flame above 200 to 300 atm. Specific additives (lead and copper salts and carbon black) have a true chemical interaction, the enhancement of the NO-carbon reaction, bringing some of the energy normally evolved in the second flame closer to the surface. This knowledge carries over to the active binders, which are however less prone to super-rate effects because they produce less structured carbon residue.

Inert binders : not so many reliable pyrolysis measurements have been performed on actual binders. It has been shown (from comparisons for a number of materials) that the pyrolysis characteristics obtained at low heating rate (by thermogravimetric analysis or differential scanning calorimetry) should extrapolate and apply under combustion conditions. The pyrolysis is a thermal breaking of the cross-links and of the polymer, not affected by additives.

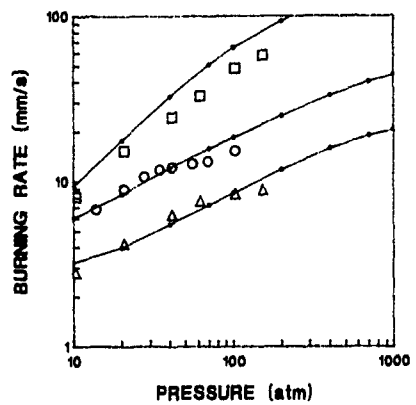

Fig. 33 **AP-INERT BINDER PROPELLANTS.**

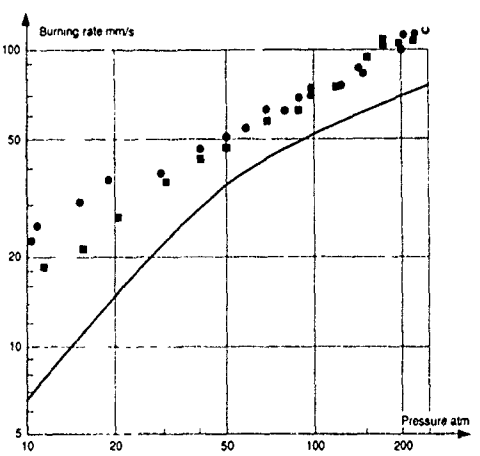

Fig. 34

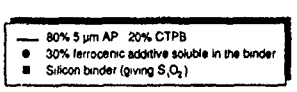

AP - INERT BINDER PROPELLANTS WITH ADDITIVES

Ammonium perchlorate : it is believed that the mechanism of combustion is properly known. A large amount, about 70%, of the AP exothermically decomposes in a thin (~ 1 µm) condensed phase superficial layer, the remaining 30% sublimes into NH_3 and $HClO_4$ which react in a flame very close (~ 1 µm) to the surface. Due to the thickness, and the very short residence time associated, of these zones, additives have no true catalytic (i.e. chemical) action.

HMX : the combustion of HMX (or RDX) is qualitatively comparable to that of a DB propellant, with the occurence of two flames,

involving NO_2 and N_2O/NO. However above 20 atm these flames collapse into one and therefore it is not possible to induce super-rate effects with specific additives, as was the case for DB propellants Also, additives which were hoped to accelerate the melting-decomposition of HMX fail to act under combustion conditions.

AP or HMX (RDX)-inert or active binder (aluminum) propellants :
the approach believed to describe adequately the combustion of composite propellants is a sequential one. When following a path through the propellant, it meets successively the combustion of the oxidizer particles and of the binder layers.
In the case of AP-inert binder propellants, the propellant burning rate is an average of the components' rates. However an interaction flame between O_2 from AP and hydrocarbons from the binder enhances the rate of AP and allows the pyrolysis of the binder. The burning rate of the propellant can be quite widely tailored by reducing the AP particle size and further by adding metallic compounds which leave an oxyde residue layer, the action of which is likely to be a flame holding effect, i.e. a physical action. Aluminum incorporated in such propellants of course increases the final temperature by as much as 1000K, but its combustion is so far from the surface that it does not influence the regression rate of the propellant.

In the case of HMX-active binder propellants both components have autonomous burning rates. The resulting propellant burning rate is the average of the two rates, with a further slowing down due to the fact that the HMX particles upon reaching the surface have to undergo a transition to full combustion. This delay is of importance up to roughly 150 atm; above it tends to become negligible. No additives have been found to act on HMX and additives of the DB type act only moderately on the active binder. The tailorability of HMX-active binder propellants is therefore more limited than for AP propellants.
Further trends on new ingredients are related in the first place to the need to reduce the vulnerability of missile motors employing solid propellants to various aggressions : "cook off" due to fires, bullet or fragment impact, "sympathetic detonation". Another emerging concern is that of the pollution caused by the large boosters of space launchers, using AP-inert binder-aluminum propellants, with production of HCl and Al_2O_3 smoke.

These considerations have led to reconsidering ingredients suc as ammonium nitrate, NH_4NO_3, discarded previously as being insufficiently energetic, and to introducing energetic binders such as GAP, glycidil azide polymer (containing the N_3 group, inducing an exothermic decomposition), or oxidizers containing the NO_2 group while being less sensitive than HMX or RDX.
It is hoped that the large amount of information gathered and the understanding acquired about the already used propellants ingredients will allow an efficient approach to the mastering of the behavior of the new ingredients and the corresponding propellants.

ACKNOWLEDGEMENTS

The work of ONERA has been carried out in large part under contracts from the Direction des Recherches, Etudes et Techniques, Délégation Générale à l'Armement and in cooperation with the Société Nationale des Poudres et Explosifs (B. Gossant, R. Couturier and their colleagues) and with the Ecole Nationale Supérieure des Techniques Avancées (E. Cohen-Nir).

J.C. Amiot and J. Hommel have actively participated in the experimental work.

Much information was exchanged, in particular through the AGARD consultant program, with M.W. Beckstead, Brigham Young University, and N.S. Cohen, consultant. Had time permitted, this chapter could have been written with them.

REFERENCES

General references (chemical propulsion, solid propellants, combustion)

- Timnat Y.M., Advanced Chemical Rocket Propulsion, Academic Press, London, 1987.

- Williams F.A., Barrère M. and Huang N.C., Fundamental Aspects of Solid Propellant Rockets, AGARDograph 116, 1969.

- Kuo K.K. and Summerfield M. (Eds), Fundamentals of Solid Propellant Combustion, Volume 90 of Progress in Astronautics and Aereonautics, 1984.

- Williams F.A , Combustion Theory (Second Edition), Benjamin/Cummings Publising Co, Menlo Park, 1985.

- Kuo K.K., Principles of Combustion, John Wiley and Sons, New York, 1986.

Double-base propellants and active binders references

1. Heller C.A. and Gordon A.S., "Structure of the Gas Phase Combustion Region of a Solid Double-Base Propellant", The Journal of Physical Chemistry, Vol.59, n°8, pp773-777, 1955.

2. Zenin A.A., "Structure of Temperature Distribution in Steady-State Burning of a Ballistite Powder", Combustion, Explosion and Shock Waves, Vol.2, n°3, pp.67-76, 1966.

3. Kubota N., Ohlemiller J.J., Caveny L.H. and Summerfield M., "The Mechanism of Super-Rate Burning of Catalyzed Double-Base Propellants", 15th Symposium (International) on Combustion, pp. 529-537, The Combustion Institute, 1975.

4. Kubota N. and Ishihara A., "Analysis of the Temperature Sensitivity of Double-Base Propellants", 20th Symposium (Internaitonal) on Combustion, pp. 2035-2041, The Combustion Institute, 1984.

5. Lengellé G., Bizot A., Duterque J. and Trubert J.F., "Steady-State Burning of Homogeneous Propellants", in Fundamentals of Solid-Propellant Combustion (Ed. K.K. Kuo and M. Summerfield), Vol.90 of Progress in Astronautics and Aeronautics, 1984.

6. Duterque J., Hommel J. and Lengellé G., "Experimental Study of Double-Base Propellants Combustion Mechanisms", Propellants, Explosives, Pyrotechnics, Vol. 10, pp. 18-25, 1985.

7. Trubert J.F., "Analysis of the Condensed Phase Degradation Gases of Energetic Binders", La Recherche Aérospatiale, 1989, n°2 (march-april), pp. 69-79; AGARD/PEP Specialists' Meeting on Smokeless Propellants, Florence, September 1985, AGARD C.P. n° 391.

8. Lengellé G., "Thermal Degradation Kinetics and Surface Pyrolysis of Polymers", AIAA Journal, Vol.8, n° 11, pp. 1989-1996, 1970.

9. Bizot A. and Beckstead M.W., "A Model for Double-Base Propellant Combustion", 22nd Symposium (International) on Combustion, pp. 1827-1834, The Combusiton Institute, 1988.

10. Cohen N.S. and Lo G.A., "Combustion Chemistry of Nitrate Ester-Based Propellants", AIAA paper 83-1198, june 1983; 20th JANNAF Combustion Meeting, october 1983.

11. Song Y.H., Beer J.M and Sarofim A.F. "Reduction of Nitric Oxide by Coal Char at Temperatures of 1250-1750 K", Combustion Science and Technology, Vol. 25, pp. 237-240, 1981.

12. Youfang C., "Combustion Mechanism of Double-Base Propellants with Lead Burning Rate Catalysts", Propellants, Explosives, Pyrotechnics, Vol. 12, pp. 209-214, 1987

Inert binders references

13. Madorsky S.L., Thermal Degradation of Organic Polymers, Interscience Publishers, New York, 1964

14. Jellinek H.H.G., Aspect of Degradation and Stabilization of Polymers, Elsevier Scientific Publishing Co, New York, 1978.

15. Cohen N.S. Fleming R.W. and Derr R.L., "Role of Binders in Solid Propellant Combustion", AIAA Journal, Vol. 12, n° 2, pp. 212-218, 1974.

16. Blazowski W.S., Cole R.B. and Mc Alevy R.F., "An Investigation of the Combustion Characteristics of Some Polymers Using the Diffusion Flame Technique", Stevens Institute of Technology, TR ME-RT 71004, 1971.

17. Beck W.H., "Pyrolysis Studies of Polymeric Materials Used as Binders in Composite Propellants : A Review", Combustion and Flame, Vol. 70, pp. 171-190, 1987.

Ammonium perchlorate references

18. Levy J.B., and Friedman R., "Further Studies of Pure Ammonium Perchlorate Deflagration", 8th Symposium (International) on Combustion, pp. 663-672, The Combuston Institute, 1962.

19. Guirao C. and Williams F.A., "A Model for Ammonium Perchlorate Deflagration between 20 and 100 atm", AIAA Journal, Vol. 9, n°7, pp. 1345-1356, 1971.

20. Beckstead M.W., Derr R.L. and Price C.F., "The Combustion of Solid Monopropellants and Composite Propellants", 13th Symposium (International) on Combustion, pp. 1047-1056, The Combustion Institute, 1971.

21.Price C.F., Boggs T.L. and Derr R.L., "The Steady State Combustion Behavior of Ammonium Perchlorate and HMX", AIAA paper n° 79-0164, 17th Aerospace Sciences Meeting, 1979.

22. Godon J.C., "Model of Ammonium Perchlorate Self-Deflagration", La Recherche Aérospatiale, 1982- 2, pp. 43-50.

23. Seleznev V.A., "An Optical Method of Measuring the Burning Surface Temperature of Condensed Systems", Combustion and Flame, Vol. 13, n°2, 1969.

HMX references

24. Rogers R.N., "DSC Determination of the Kinetics Constants of Systems that Melt with Decomposition", Thermochemica Acta, Vol. 3, pp. 437-447, 1972.

25. Boggs T.L., "The Thermal Behavior of RDX and HMX", in Fundamentals of Solid-Propellant Combustion (Ed. K.K. Kuo and M. Summerfield), Vol. 90 of Progress in Astronautics and Aeronautics, 1984.

26. Cohen N.S., Lo G.A. and Crowley J.C., "Model and Chemistry of HMX Combustion", AIAA Journal, Vol. 23, n°2, p. 276, 1985.

27. Kubota N. and Sakamoto S., "Combustion Mechanism of HMX", 19th International Annual Conference of ICT, Karlsruhe, june 1988.

28. Mitani T. and Williams F.A., "A Model for the Deflagration of Nitramines", 21st Symposium (International) on Combustion, pp. 1965-1974, The Combustion Institute, 1986. Also, Sandia Report 86-8230, december 1986.

29. Lengellé G. and Duterque J., "Combustion of Propellants Based on HMX", AGARD/PEP Specialists' Meeting on smokeless Propellants, AGARD CP n° 391, Florence, septembre 1985.

30. Bizot A. and Beckstead M.W., "A Model for HMX Combustion", International Seminar on Flame Structure, Alma-Ata (USSR), september 1989.

31. Shoemaker R.L. et al, "Thermophysical Properties of Propellants", Thermal Conductivity, Vol. 18, pp. 199-211, 1985.

32. Hatch R.L., "Chemical Kinetics of HMX Combustion", 24th JANNAF Combustion Meeting, Monterey, Cal , october 1987.

33. Brill T.B., "Heat Flow / Chemistry Interface in the Condensed phase (HMX)", ONR Worskshop on Energetic Material Initiation Fundamentals, Livermore, Cal., december 1988.

Composite propellants references

34. Beckstead M.W., Derr R.L., and Price C.F., "A Model of Composite Solid-Propellant Combustion Based on Multiple Flames", AIAA Journal, Vol.8, n°12, pp 2200-2207, 1970.

35. Cohen N.S., "Review of Composite Propellant Burn Rate Modeling", AIAA Journal Vol.18, n°3, pp 277-293, 1980.

36. Cohen N.S. and Strand L.D., "An Improved Model for the Combustion of AP Composite Propellants", AIAA paper n°81-1553, 17th Propulsion Conference, 1981.

37. Ramohalli K.N.R., "Steady State Burning of Composite Propellants", in Fundamentals of Solid-Propellant Combustion (Ed.K.K. Kuo and M. Summerfield), Vol.90 of Progress in Astronautics and Aeronautics, 1984.

38. Cohen N.S., Crowley J.C. and Lo G.A., "Effects of HMX Addition on the Combustion of Energetic Binders", 21st JANNAF Combustion Meeting, october 1984.

39. Beckstead M.W. and Mc Carty K.P., "Modeling Calculations for HMX Composite Propellants", AIAA Journal, Vol.20, n°1, pp.106-115, 1982.

40. Duterque J. and Lengellé G., "Combustion Mechanisms of Nitramine Based Propellants with Additives", AIAA paper n°88-3253, 24th Propulsion Conference, 1988. Journal of Propulsion and Power, Vol.6, n°6, pp. 718-726, december 1990

41. Blomshield F. and Osborn J., "Nitramine Composite Solid Propellant Modeling", AIAA paper n°90-2311, 26th Propulsion Conference, 1990.

42. Beckstead M.W., "A Model for Composite Modified Double-Base Propellant Combustion", 26th JANNAF Combustion Meeting, October 1989.

43. Cohen N.S., "A Pocket Model for Aluminum Agglomeration in Composite Propellants", AIAA Journal, Vol.21, n°5, pp.720-725, 1983.

44. Price E.W., "Combustion of Metalized Propellants", in Fundamentals of Solid-Propellants Combustion (Ed. K.K. Kuo and M. Summerfield), Vol.90 of Progress in Astronautics and Aeronautics, 1984.

45. Renie J.P. and Osborn J.R., "Combustion Modeling of Aluminized Propellants", AIAA paper n° 79-1131, 15th Propulsion Conference, 1979.

Modelling Aspects of Solid Propellant Steady-State Combustion

by

Kenneth K. Kuo, Ph.D.
Director of the High Pressure Combustion Laboratory
Dept. of Mechanical Engineering
312 Mechanical Engineering Building
University Park
Pennsylvania 16802
United States

ABSTRACT

In the modelling of steady-state burning of composite propellants under zero cross-flow situations, a comprehensive review was made by Prof. K.N.R. Ramohalli of the University of Arizona, as Chapter 8 of a recent AIAA Progress Series volume entitled, *Fundamentals of Solid Propellant Combustion*, edited by Profs K.K. Kuo and M. Summerfield Also, an excellent chapter on "Steady-State Burning of Homogeneous Propellants", was contributed by Dr G. Lengellé and co-workers in the same book volume. The contents of their chapters will be used as the key material for presentation in the first lecture topic. For the combustion of composite propellants, certain basic aspects related to solids loading, particle size and shape, binder type, processing influences, and the vapor phase mechanics will be briefly mentioned in an effort to develop a feeling for the composite propellant system. Typical burn-rate influences of ingredient and processing variations will be mentioned. The majority of the discussion focuses on the most widely used type of composite propellant, Ammonium perchlorate (AP) as an oxidizer with inert hydrocarbon binder systems. The thorough analysis of AP combustion by Glurao and Williams, the granular diffusion flame model of Summerfield, the Hermance model, the Beckstead-Derr-Price model, and the petite ensemble model will be described. More recent statistical analyses of polydisperse heterogeneous systems will also be presented

For homogeneous propellants, the key process which control the burning rate will be discussed. The theoretical formulation, which includes governing equations for both solid and gas phases, the chemical kinetic considerations, boundary conditions, etc., will be described. Some comparisons of calculated results with experimental data will also be presented.

All of the presentation materials are available in the open literature.

EROSIVE BURNING OF SOLID PROPELLANTS

Merrill K. King
4634 Tara Drive
Fairfax, Virginia 22032
USA

SUMMARY

This paper presents a review of experimental and modeling work concerning erosive burning of solid propellants (augmentation of burning rate by flow of product gases across a burning surface), with particular emphasis on studies by this author. A brief introduction describes motor design problems caused by this phenomenon, particularly for low port/throat area ratio motors and, in the limit, nozzleless motors. Various experimental techniques for measuring crossflow sensitivity of solid propellant burning rates are described, with a conclusion that accurate simulation of the flow, including upstream flow development, in actual motors is important since the degree of erosive burning depends not only on local mean crossflow velocity and propellant nature, but also on this upstream development. In the modeling area, a brief review of "simplified" models and correlating equations is presented, followed by description of more complex numerical analysis models. Both composite [ammonium perchlorate (AP)] and double-base propellant models are reviewed, with emphasis on this author's models. A "second generation" composite model developed by this author is shown to give good agreement with data obtained in a series of tests in which composite propellant composition and heterogeneity (particle size distribution) were systematically varied. Finally, use of the numerical models for development of erosive burning correlations (of much more practical use to the ballistician) is described, and brief discussion of scaling (particularly of minimum velocity required for initiation of erosive burning) is presented.

1.0 INTRODUCTION/BACKGROUND

The flow of combustion product gases at high velocity across a burning solid propellant surface is often found to lead to a significant increase in burning rate over that obtained at the same pressure in the absence of cross-flow - this phenomenon is referred to as erosive burning and the increase in burning rate is known as the erosive burning rate. An example of this effect is shown in Figure 1, where data of Marklund and Lake (1) are presented in the form of burning rate versus pressure curves for an AP/polyester propellant at several crossflow velocities. With most (but not all) propellants, there is a minimum crossflow velocity below which erosive burning is not observed - this is referred to as the threshold velocity and can be as high as several hundreds of meters/second, particularly for high-burning-rate formulations.

In recent years, requirements for ever higher propellant mass fractions in solid propellant rocket motors and for higher thrust-to-weight ratios have led to development of centrally-perforated grain

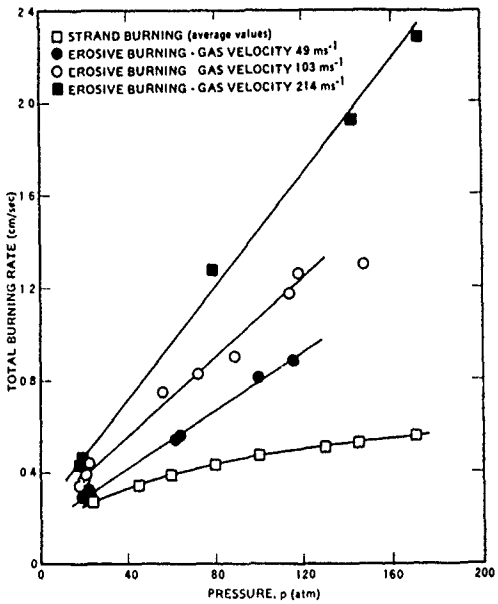

Figure 1. Erosive Burning of an AP/Polyester Propellant as a Function of Pressure At Several Gas Velocities (1)

configurations with relatively low port-to-throat ratios. As a result, during the early portion of operation of such motors, there are high velocities across burning propellant surfaces in the aft portion of the grain, with these velocities rapidly decreasing with time as the grain port opens up. The erosive burning accompanying these high velocities, even though partly offset by burning rate decreases accompanying resultant pressure decrease down the bore (see Reference 2 for sample calculations) leads to an initial overpressure relative to mean operating pressure during the early portion of the motor operation, in turn leading to requirement for a heavier case for a given mean operating pressure (undesirable). In addition, if the designer does not somehow compensate for the unequal initial burning rates along the grain (for instance by using a thicker web in the aft regions) the propellant will burn out unevenly, leading to a long pressure and thrust tailoff (often also undesirable).

Use of grain configurations with slots, stars, or "wagon-wheels" at various locations along the port is common practice: in many cases, velocities of gas flow in these regions can become quite high relative to mean flow through the central port, again leading to local erosive burning which must be compensated for in the motor design. Little attention has

been given to this problem in published literature - a recent effort by Ayris and Petrovic (3) does address erosive burning in a star-configuration centrally-perforated motor.

A series of studies has demonstrated that the nozzleless motor concept (mass flow choking at the end of a cylindrical bore) offers significant economic and operational advantages over a more conventional rocket system when considered for some tactical weapon systems (notably air-launched integral-rocket-ramjet systems where ejection of a throat pack during transition from boost to sustain operation is highly undesirable). This concept requires that the flow within the bore or central perforation of a grain accelerate to the point that sonic conditions are achieved at the aft end. In this situation, the high-velocity environment results in substantial erosive burning, with burning rates significantly higher than those measured in a conventional strand bomb being encountered.

Nozzleless rockets present a unique challenge to analytical understanding because the gas velocity reaches sonic and supersonic velocities on the grain surfaces, leading to a realm of erosive burning never before considered. The effects are critical in that the erosive burn rate contributions strongly influence performance level, performance repeatability and thrust misalignment. More than in any conventional motor, the exact erosive burn rate behavior must be held constant from batch to batch if reproducibility is not to be a problem. The performance sensitivity of a nozzleless motor to erosion is due to the fact that the maximum erosion occurs at the choke point in the bore. Since this point is the effective throat area, and the throat area versus time is thus a function of regression rate, the result is a chamber pressure history which varies strongly with erosion.

With nozzleless motors, the effects of erosive burning are further magnified due to higher crossflow velocities (in the Mach 1 range) and due to the fact that the aft end port/throat area ratio does not decrease with time since the aft end is the throat (in most cases). Assuming that an erosive burning rate correlation of the form $r/r_o = 1 + k_2 M$ (M being the crossflow Mach Number) is applicable and allowing for the fact that static pressure decrease down the bore accompanying the velocity increase tends to decrease burning rate for propellants with a positive pressure exponent (usual), countering the erosive effects to some extent, it may be shown (Reference 2) that for a nozzleless motor with a uniform bore radius

$$\frac{r_{aft}}{r_{fore}} = \frac{(k_2 + 1)}{(\gamma + 1)^n} \qquad (1)$$

where r is the local burning rate (function of pressure and crossflow velocity), γ is the product specific heat ratio, and n is the propellant burning rate-pressure exponent. Values of $(r_{aft}/r_{fore})_{initial}$ as a function of the erosivity constant (k_2) and the burning rate exponent (n) are presented in Table I. As may be seen, for the case of no erosion ($k_2 = 0$) the aft end will recede more slowly than the fore end, due to lower pressure at the aft end. As

Table I. Simplified Ballistic Analysis of a Nozzleless Motor With Uniform Port Area.

$r/r_o = 1 + k_2 M$, $r_o = bp^n$

n	k_2	r_{aft}/r_{fore}
0.4	0.0	0.72
	0.5	1.08
	1.0	1.45
	1.5	1.80
0.6	0.0	0.61
	0.5	0.92
	1.0	1.23
	1.5	1.54
0.8	0.0	0.52
	0.5	0.78
	1.0	1.05
	1.5	1.31

k_2 increases, the r_{aft}/r_{fore} ratio also increases, going through unity (generally desirable) at a value of k_2 which depends on the burning rate exponent. The results of Table I give some indication of the sensitivity of nozzleless motor design to the erosive burning characteristics of the propellant and thus further point out the importance of information regarding the propellant's erosive burning characteristics to the designer.

Since there is such a strong interaction between the local flow environment and the propellant burning rate, it is necessary to be able to predict this interaction in order to design and calculate the performance of a low port/throat area ratio rocket (particularly a nozzleless rocket with a port/throat area ratio of unity). With such a predictive capability, the motor designer can either design his grains to compensate for mean erosive burning effects on grain burn pattern, or, knowing how propellant formulation parameters affect erosion sensitivity, vary propellant parameters in such a way as to minimize these effects. Accordingly, considerable effort, experimental and analytical, has been carried out over the past few decades with the goals of understanding, being able to predict, and being able to control erosive burning characteristics of solid propellants. An excellent review of much of this work is presented in Reference 4.

2.0 EXPERIMENTAL STUDIES OF EROSIVE BURNING

In the experimental characterization of erosive burning of solid propellants, the investigator is faced with a conflict between a desire to perform inexpensive tests with relatively easy direct measurement of burning rate in the presence of crossflow (as exemplified by tests in which a hot product gas stream generated by a "driver" motor is passed over strips or pellets of the propellant of interest, with relatively easy optical access for measurement of burning rate as a function of pressure and crossflow velocity) and a desire to more accurately simulate the development of the flow field upstream of the point of interest seen in an actual motor (which in the limit can only be done by performing actual motor tests). This latter method has the disadvantage that while the erosive burning process is being studied under actual motor conditions, these conditions

are difficult to determine accurately. Pressure and velocity vary through the chamber and also change with time. Such burn rate measurement techniques as interrupted burning must use time-averaged values, and the time periods must be relatively long. Continuous measurement of burning rates within a rocket by x-ray requires special elaborate equipment. The use of probes to measure burning rates and pressures is difficult because many probes are required, and also runs the risk of interfering with the chamber flow and disturbing normal burning.

The major drawback of former method lies in the fact that, as pointed out by several authors (5-10), the level of burning rate augmentation depends not only on the mean crossflow velocity at the point of interest, pressure, and the propellant itself, but also on the influence of the upstream nature of the product gas flow on the local turbulence structure. In actual cylindrically perforated motor grain ports, the flow is highly two-dimensional in the forward part of the of the motor, where inertial terms in the momentum equations describing the flow dominate the viscous terms, leading to the classic "inviscid no-slip" velocity profiles, described by Culick (11) and measured in cold-flow simulations of cylindrically-perforated motors by Yamada and Goto (12) and Dunlap, et al (13). Beddini (8,9) has performed extensive analysis of the development of such flows, obtaining good agreement with the cold-flow experimental work - from his studies, he concludes that turbulence first develops in the center of the grain port and eventually works out to the walls (propellant surface) with subsequent development of more nearly classical one-dimensional boundary layer profiles as the blowing ratio (ratio of radial velocity of products leaving the propellant surface to crossflow velocity) decreases down the motor port. Kutataladze and Leont'ev (14) have developed empirical relationships for the skin friction coefficient in such transpired flows in which, for blowing ratios above a critical value (which depends on several parameters) the boundary layer is considered to be totally blown off the surface (analogous to Beddini's conclusion that a turbulent boundary layer does not exist in the high-blowing-ratio upstream regions of the motor). In Kutataladze's formulation, as in other correlations of blowing effects, as the blowing ratio decreases further below this critical value, the ratio of skin friction to zero-blowing skin friction (for a given crossflow Reynolds' Number) increases continuously until it approaches a value of unity at very low blowing rates (classic fully-developed boundary layer). Obviously, in experiments where product gases are blown across tablets or other small specimens of propellant without the upstream boundary layer attachment and development phenomena seen in cylindrically-perforated motors (or, even worse, in slots or other complex central port configurations, which to this author's knowledge have received no attention to date as regards boundary layer development) the turbulence profiles will be different at a given crossflow velocity than in such CP grains. Whether the resultant effects on erosive burning rate at a given pressure and crossflow velocity are first or second order is not clear to this author at this time, but it seems highly unlikely that they are totally negligible.

The measurement of erosive burning by use of propellant specimens located outside of a rocket chamber has been investigated by Viles (15), Zucrow (16), Vilyunov, et al (17), Saderholm (18), and Marklund and Lake (1), the last authors using two experimental configurations, one with tablets and the other with strips of solid propellant, both positioned inside a tube connected to the exhaust stream of a test rocket. As discussed above, there is considerable question about the nature of the flow across the specimen, but the parameters of mean flow rate, pressure, regression rate, and even temperature are relatively easily measured quite accurately in such a device. Both Viles (15) and Saderholm (18) tested the validity of their data as pertains to actual motor conditions by calculations of a number of pressure-time curves for motor firings under erosive conditions using the data obtained from their measurements with externally-located samples. Agreement between these calculations and measured pressure-time traces were excellent, leading them to conclude that their experimental procedures for obtaining erosive burning rates were valid.

As indicated above, the use of actual motor tests to determine erosive burning characteristics of propellants has the advantage that the erosion process is being studied under the exact conditions that prevail in a rocket chamber. The disadvantage is that these conditions are difficult to determine accurately. Green (14), Kreidler (20), and Peretz (21) have all utilized interrupted-burning techniques in studying erosive burning. Ayris and Petrovic (3) have utilized real-time X-ray techniques to study erosive burning in a star-configuration motor, with limited success to date. Strand, et al (22,23) have utilized plasma capacitance gages to measure erosive burning in CP grain motors, while Traineau and Kuentzman (7) have used ultrasonic burning-rate measurement techniques to study erosive burning in nozzleless motors. Finally, Waesche and O'Brien (24) have evaluated (on paper) various possible techniques, including microwave-doppler measurements, for continuous measurement of burning rates at various locations along a cylindrically-perforated-grain motor.

In addition to experimental studies involving external flow of propellant exhaust gases across tablets or other small propellant specimens (one extreme, yielding relatively inexpensive tests and ease of data analysis, but with major doubts as regards direct relevance to motors as discussed above) and those involving actual use of motors (other extreme, expensive, with difficulty in obtaining accurate measurements) three additional experimental approaches for study of erosive burning, offering compromises between these limits have been employed by investigators at Princeton University (25), Pennsylvania State University (26), and Atlantic Research Corporation (27): these are briefly described below.

The Princeton study employed a 50 cm long slab motor (depicted in Figure 2) which could be quenched during the early stages of motor operation. This slab motor had a

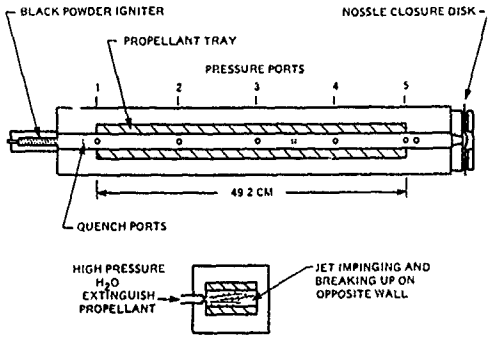

Figure 2. Princeton University Slab Motor Used To Obtain Erosive Burning Data (25)

rectangular port with two opposing flat propellant slabs cast into trays, each slab being 2.54 cm wide by 49.2 cm long with an initial gap between slabs of (typically) 0.7 cm. Rectangular nozzles were sized to give initial port-to-throat area ratios of 1.50, 1.20, and 1.06, corresponding to Mach Numbers at the end of the slabs of 0.4 to 0.7. A liquid quench system was used to extinguish the propellant at 0.05 to 0.07 seconds after ignition. Static pressure versus time and total distance burned were measured at five axial locations. A desired form of erosive burning rate expression and one-dimensional compressible flow equations were integrated with various choices of adjustable parameters in the erosive burning rate expression until optimal agreement of measured and calculated pressure-time variation at all measurement locations was obtained. (Lack of instantaneous burning rate data necessitated specification of an erosive burning rate expression form, though the form is not restricted as to type) with the measured (post-test) erosion data being used to evaluate unknown constants in the expression for a given propellant and operating pressure.

In the experimental study at Pennsylvania State University, two-dimensional slabs of propellant were utilized in a windowed test chamber with hot combustion products from a "driving motor" flowing over the sample at various velocities (subsonic and supersonic) and chamber pressures. (See Figure 3.) The test chamber was 39 cm long with a rectangular cross-section of 7 cm by 2.54 cm. This chamber was equipped with a transparent plexiglas window assembly composed of an inner sacrificial window, a middle window, and a top window, with the inner window being replaced after each test. The test-propellant sample was clearly visible through this assembly. An interchangeable wedge-shaped steel leading edge was used, with the test propellant sample being glued to the top flat surface of the leading edge, whose length (10.8 cm) allowed development of a turbulent boundary layer over most of the propellant sample (though likely somewhat different in structure from the turbulent boundary layer encountered in an actual motor). The spillage channel depicted in Figure 3 was used to enable the boundary layer to develop from the beginning of the leading edge. An interchangeable top plate was used to vary channel height and thus gas velocity across the sample. (Pressure gradient could also be varied by use of a tapered top plate.) An interchangeable exit nozzle was used to control pressure (and, in combination with the top plate, velocity in the test chamber). The instantaneous regression rate of the propellant was recorded by a high-speed (1000-1500 frames per second) camera and deduced via a motion analyzer. Details of the experimental device, test procedures and data analysis procedures (notably used for calculation of burning rate and free-stream gas velocity in the test section, not directly measurable) are given in Reference 26.

The experimental test apparatus and procedures employed in the Atlantic Research study of erosive burning are described in detail in Reference 27. A schematic of the basic test apparatus is presented as Figure 4. A cylindrically-perforated 6C4 driver grain (15.2 cm outside diameter, 10.2 cm inside diameter) whose length was chosen to give the desired operating pressure for a given test, produced a high velocity gas flow through a transition section into a rectangular test section which contained the test grain (generally the same formulation as the driver grain). The contoured transition section

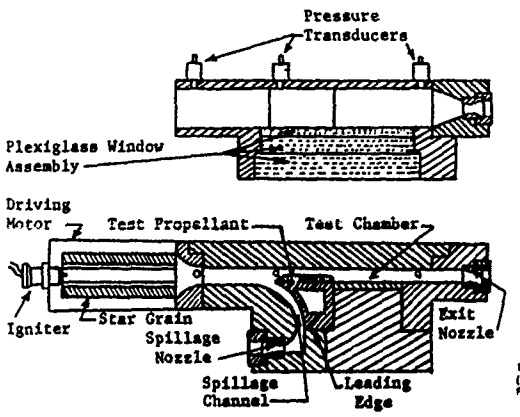

Figure 3. Schematic Diagram of the Erosive-Burning Test Apparatus Employed At Pennsylvania State University (26)

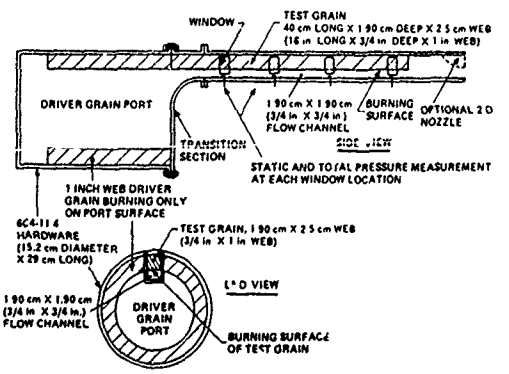

Figure 4. Schematic of Atlantic Research Erosive Burning Test Apparatus (27)

was approximately 10 cm long. The test grain extended from the test section back through the transition section to butt against the driver grain in order to eliminate leading edge effects which would be associated with a test grain standing alone. The test grain was approximately 30 cm long (plus the 10 cm extending through the transition section) by 1.90 x 2.50 cm web and burned only on the 1.90 cm face. The flow channel of the test section was initially 1.90 cm x 1.90 cm, opening up to 1.90 cm x 4.45 cm as the test propellant burned back through its 2.54 cm web. For high Mach number tests, the apparatus was operated in a nozzleless mode with the gases choking at or near the end of the test grain, while for lower Mach Number tests, a two-dimensional nozzle was installed at the end of the test channel.

During each test, pressure and crossflow velocity varied with time and location along the test grain. (For the nozzleless tests, pressure varied significantly with time and location, while crossflow velocity varied considerably with location but not significantly with time. For tests using a nozzle with an initial port to throat area ratio of 1.5 or higher, on the other hand, pressure did not vary strongly with location but did rise with time due to the progressivity of the driver grain, while crossflow velocity varied strongly with time and slightly with location.) These variations permitted design of tests to yield considerable burning rate-pressure-crossflow velocity data in relatively few tests, provided that these parameters could be measured continuously at several locations along the test grain. These parameters were measured in the following manner.

The burning rate was directly measured by photographing the ablating grain with a high-speed motion picture camera through a series of four quartz windows located along the length of the test section. Frame by frame analysis of the films permitted determination of instantaneous burning rate as a function of time at each of the four window locations.

For nozzled cases, the measured location of the burning propellant surface at each window as a function of time, together with the known constant throat area, permitted straightforward calculation of the crossflow velocity as a function of time. However, the very sensitive dependence of Mach Number on area ratio for M > 0.5 made calculation of crossflow velocity from area ratio measurement quite poor for nozzleless cases. Accordingly, for these tests, stagnation pressure was determined at the aft end of the test section and used in combination with the driver chamber pressure for calculation of the stagnation pressure in the test section as a function of time and position. Static pressure wall taps at each window location were used for measurement of static pressure as a function of time for both nozzled and nozzleless cases. From the static and stagnation pressure values determined as a function of time and position down the test section, crossflow Mach Number and velocity were calculated as a function of time at each window location in the test section for the nozzleless cases.

In general, studies of the erosive burning of solid propellants have involved use of only one, or at most, two to four different propellants, without study of the effects of systematic variation of propellant compositional and heterogeneity characteristics on sensitivity of burning rate to crossflow velocity. General observations from these studies (1,15-20,28-30) include:

1. Plots of burning rate versus gas velocity or mass flux at constant pressure are usually not fitted best by a straight line.
2. Threshold velocities are often (but not always) observed.
3. Occasionally, "negative" erosion rates are observed. (There is some controversy as to the cause, with a preponderance of opinion learning toward it being stifling of the propellant combustion by flow of melted binder across o dizer crystals.)
4. Slower burning propellants are more strongly affected by crossflows than higher burning-rate formulations.
5. At high pressure, the burning rate under erosive conditions tends to approach the same value for all propellants (at the same flow velocity) regardless of the burning rate of the propellants at zero crossflow.
6. Erosive burning rates do not depend upon core gas temperature of the crossflow (determined from tests in which various "driver propellant's" products are flowed across a given test propellant).

One exception to the statement that in most studies to date, examination of the effects of systematic variation of propellant parameters (composition, oxidizer particle distribution, etc.) on sensitivity of the propellant to crossflow was not carried out

Table II. Propellant Matrix (AP Composite Propellants) Tested by King (31-33).

Formulation	Composition	Rationale
4525	73/27 AP/HTPB, 20μ AP	Baseline Formulation, Flame Temperature = 1667K
5051	73/27 AP/HTPB, 200μ AP	Compare with 4525 for AP Size Effect and Base Burning Rate Effect
4685	73/27 AP/HTPB, 5μ AP	Compare with 4525 and 5051 for AP Size Effect and Base Burning Rate Effect
4869	72/26/2 AP/HTPB/Fe_2O_3, 20μ AP	Compare with 4525 for Base Burning Rate Effect at Constant AP Size
5542	77/23 AP/HTPB, 20μ AP	Compare with 4525 for Mixture Ratio and Flame Temperature Effect at Constant AP Size. T = 2065K
5565	82/18 AP/HTPB, 13.65% 90μ AP, 68.35% 200μ AP	AP Sizes Chosen to Match Base Burning Rate of 4525. Compare With 4525 for Mixture Ratio and Flame Temperature Effect T = 2575K
5555	82/18 AP/HTPB, 41% 1μ AP, 41% 7μ AP	Compare with 5565 for Effect of Base Burning Rate
7993	82/18 AP/HTPB, 41% 7μ AP, 41% 90μ AP	Further Study of AP Size and Base Burning Rate Effects
7996	82/18 AP/HTPB, 41% 90μ AP, 41% 200μ AP	Further Study of AP Size and Base Burning Rate Effects
8019	82/18 AP/HTPB, 27.3% 1μ AP, 27.3% 20μ AP, 27.4% 200μ AP	Further Study of AP Size and Base Burning Rate Effects
6626	74/21/5 AP/HTPB/Al, 70% 90μ AP, 4% 200μ AP	Same Flame Temperature and Base Burning Rate as 5565. Compare with 5565 for Al Effect.
7523	70/28/2 AP/Polyester/Fe_2O_3 (20μ AP)	Baseline Polyester Formulation, T = 2250K, AP Size Chosen to Match BR of 4869 - Compare with 4869 for Binder Effect
7605	78/20/2 AP/Polyester/Fe_2O_3 Bimodal AP (23.4% 20μ, 54.6% 200μ)	Medium Temperature (2800K) Polyester Formulation. Compare with 7523. Also compare with 5542 for Binder Effect at Nearly Constant Base Burning Rate

is the work of King (31-33) who systematically varied parameters with a series of eleven AP composite propellant formulations, listed in Table II (along with rationale for their selection). Detailed results of this test series (carried out in the Atlantic research test apparatus described above) will be given in a later section where measured erosive burning rates are compared with predictions of a composite propellant erosive burning model by King. A summary of the observed effects of various parameters on ε (the ratio of burning rate with crossflow to that without it) at constant pressure and crossflow velocity is presented here as Table III. As observed by previous studies (summarized above), base (no-crossflow) burning rate is seen to have a major effect on crossflow sensitivity, erosive burning ratio increasing with decreasing base rate at fixed pressure.

Table III. Effects of Various Formulation Parameters on Sensitivity of AP-Composite Propellants to Crossflow as Observed by King (31-33).

Comparison	Parameters Studied	Effect on Erosive Burning
4525, 5051, 4685	Varied d_p, r_o at Fixed Binder Type, Fixed Flame Temperature	d_p ↑ = r_o ↑ = ε ↓
4525, 4869	Varied r_o at Fixed AP Size, Binder Type, and Flame Temperature	r_o ↑ = ε ↓
4685, 4869	Varied d_p at Fixed r_o, Binder Type, and Flame Temperature	d_p ↑ = ε ↓ Slightly
4525, 5542	Varied O/F Ratio (and Thus Flame Temperature) and r_o at Fixed Binder Type and Fixed AP Size	T_f ↑ = r_o ↑ = ε ↓
5565, 4525	Varied O/F Ratio (and Thus Flame Temperature) at Fixed Binder Type and Fixed r_o	T_f ↑ = ε Unchanged
5565, 5555, 7993, 7996, 8019	Varied d_p, r_o at Fixed Binder Type, Fixed Flame Temperature	d_p ↑ = r_o ↑ = ε ↓
5565, 6626	Aluminum Versus Non-Aluminum at Fixed r_o, Binder Type, and Flame Temperature	Al = ε Unchanged
4869, 7523	Different Binder Type; r_o, d_p Held Constant, Differing Flame Temperature (Polyester Hotter)	At Low P, ε Unchanged At High P, ε Higher for Polyester
5542, 7605	Different Binder Type, r_o Held Constant, Differing Flame Temperature (Polyester Hotter) and d_p	At Low P, ε Unchanged At High P, ε Higher for Polyester

Conclusions from Above Comparisons

1. The augmentation factor is strongly dependent on base burning rate.
2. There is a small residual effect of oxidizer particle size, at fixed burning rate.
3. O/F (flame temperature) effects ε for HTPB systems only through effect on base burning rate.
4. At fixed base burning rate, aluminum has no effect on ε.
5. Polyester binder formulations are slightly more sensitive to crossflow than HTPB formulations at fixed base burning rate.

d_p - Oxidizer Particle Diameter
r_o - Base (No Crossflow) Burning Rate
T_f - Flame Temperature
ε - r/r_o (Ratio of Burning Rate With a Given Crossflow to the Base Rate)
O/F - Oxidizer/Fuel Ratio

3.0 EMPIRICAL EXPRESSIONS AND RELATIVELY SIMPLE MODELS FOR CALCULATION OF EROSIVE BURNING RATES

Several empirical expressions for calculation of the ratio of total burning rate (expressed as the sum of zero-crossflow rate plus erosive contribution) of a propellant to the zero-crossflow rate at the same pressure appear in the literature - these generally take one of the following forms:

$$\varepsilon = r/r_o = 1 + K_1 (V - V_t)^m, \; m \leq 1 \qquad (2)$$

$$\varepsilon = r/r_o = 1 + K_2 (M - M_t)^m, \; m \leq 1 \qquad (3)$$

$$\varepsilon = r/r_o = 1 + K_3 (G - G_t)^m, \; m \leq 1 \qquad (4)$$

ε = Erosion ratio
r = Total burning rate
r_o = Normal burning rate (no crossflow) at the same pressure
K_1, K_2, K_3 = Empirical constants
V = Crossflow velocity
M = Crossflow Mach number
G = Crossflow mass flux
m = Empirical constant

where the subscript "t" refers to threshold crossflow conditions below which erosion does not occur. (Some propellants have been correlated with non-zero threshold values, while others have been correlated with threshold values set equal to zero.) Effective implementation of such expressions to describe the response of solid propellant burning rates to crossflow of course requires a fairly extensive data base for each propellant of interest over the range of pressure and crossflow velocity range of interest (extrapolation being quite risky).

Since characterization of a given formulation's burning rate dependency on crossflow at various pressure levels tends to be fairly expensive, a model which permits the designer to predict this dependency without erosive burning testing of various candidate formulations for a given application is highly desirable. In addition, an accurate model which properly accounts for the mechanisms involved in erosive burning can be used by a propellant formulator in developing a formulation which will have desired ballistic properties in a given motor design with a minimum of trial-and-error searching. As a minimum, a model which will permit prediction of erosive burning over a wide range of conditions for a given formulation, given only relatively inexpensive strand-burning data is highly desirable. Even better would be the ultimate development of a model which would permit prediction of burning rate as a function of pressure and crossflow velocity given only composition and ingredient size data. Such a model should provide explanation of the observed burning rate characteristics in the presence of crossflow in terms of the hydrodynamic conditions induced near the propellant surface by the crossflow coupled with the chemical and physical processes which constitute the propellant deflagration mechanism. In the latter area, it appears obvious that different models are required for homogeneous (double-base) and heterogeneous (composite) propellants.

Over the years, a large number of erosive burning models of varying degrees of sophistication have been developed; a list of models examined by this author (with the exception of several complex models utilizing extensive numerical analysis procedures, which are described in the next section) is presented as Table IV. These models mostly fall into one of three categories, as indicated.

Table IV. General Categories of Models of Erosive Burning Briefly Discussed in This Section (Section 3.0).

1. Models Based on Augmented Heat Transfer From the "Core Gas" in the Presence of Crossflow.

   e.g., Lenoir and Robillard (34)
   Zucrow, Osborn, and Murphy (35)
   Saderholm (18)
   Markland and Lake (1)

2. Models Based on Alteration of Transport Properties in the Region Between Flame Zone(s) and the Propellant Surface by Crossflow.

   e.g., Saderholm, Biddle, Caveny, and Summerfield (36)
   Lengelle (37)
   Corner (38)
   Vandenkerchove (39)
   Zeldovich (40)
   Vilyunov (17)
   Geckler (41)
   Parkinson, et. al. (5,6,42)

3. Models Based on Chemically Reacting Boundary Layer Theory

   e.g., Tsuji (43)

4. Miscellaneous

   e.g., Klimov (44)
   Molnar (45)
   Miller (46)

Models in the first category are based on the assumption that the erosive burning is driven by increased heat transfer from the mainstream gas flow resulting from the increased mass flux parallel to the grain surface. The best-known and most widely used model, that of Lenoir and Robillard (34), falls into this category. Since this model is the one most widely used today by motor designers (actually it is a "data-fitting" tool, requiring experimental data for each new formulation, rather than a true predictive model), it will be discussed in more detail than the others. In this model, the authors state that the total burning rate (r) is the sum of two effects: a rate dependent on pressure (r_o, the normal burning rate), and a second erosive rate (r_e) dependent upon the combustion gas flow rate. This equation entails an assumption that the pressure-dependent "base" rate, r_o, is unaffected by an increase in total rate at a given pressure, an assumption which almost certainly cannot be true. This problem has been discussed in detail by King (47), with derivation of a modified Lenoir and Robillard expression allowing for the coupling of flame standoff distance with burning rate. While Lenoir and Robillard assume $r = r_o + r_e$, allowance for the coupling effect results in $r = (r_o^2/r) + r_e$. In physical terms, Lenoir and Robillard have failed to account for the fact that the increased burning rate caused by erosive feedback at constant pressure results in the propellant flame being pushed further from the surface, decreasing its heat feedback rate and, thus, decreasing the propellant burning rate part of the way back toward the base rate.

A more general weakness of models in the first category is that these models predict substantial dependence of erosive burning on the temperature of the core gas; such dependence was found by Markland and Lake (1), in experiments with propellant tablets exposed to crossflow products from motors operating at different flame temperature (1700°K and 2400°K) and later by King (48), in the Atlantic Research apparatus described earlier (with driver propellants with flame temperatures of 1667°K and 2425°K) to be completely absent. (The Lenoir and Robillard model predicts that the erosive contribution should be 50 percent higher with the higher temperature driver in each case, as discussed in detail in References 27 and 48.) This observed lack of dependence of erosive burning rate on core gas temperature tends to indicate that all models in the first category in Table IV are on shaky grounds.

The model of Zucrow, Osborn, and Murphy (35) is worthy of particular attention, since it is the only model known to this writer which permits prediction of negative erosion which has been observed in some cases. However, it may be shown that this prediction results from a physically impossible result of a mathematical extrapolation. The basic burning rate expression employed is:

$$r = r_o + \frac{h\,(T_{Combustion} - T_{surface,\,avg.})}{Q\rho_{prop}} \qquad (5)$$

where Q is basically the heat required to preheat and vaporize unit mass of the propellant (with some corrective adjustments) and h is the heat transfer coefficient from the core gas to the propellant surface. Ancillary expressions used include:

$$h = h_o\,(C_h/C_{ho}) \qquad (6)$$

$$C_h/C_{ho} = 1 - \beta_T B \qquad (7)$$

$$B = \rho_{prop} r_o / C_{ho} G \qquad (8)$$

where β_T is a constant transpiration parameter and C_{ho} and h_o are the Stanton Number and the heat transfer coefficient in the absence of crossflow, all other parameters being as defined earlier.

The difficulty lies in the use of Equation 7 for the ratio of the Stanton Number with crossflow to that without crossflow. This expression should only be used for values of $\beta_T B \ll 1$. As it is, at sufficiently small values of G, B exceeds $1/\beta_T$. When this occurs, Equation 7 yields a negative value for the Stanton

Number (violating the Second Law of Thermodynamics), and thus the heat transfer coefficient h becomes negative, and the second term of of Equation 5 also becomes negative, yielding a predicted burning rate, r, less than the burning rate in the absence of crossflow, r_o. The correct limit for C_h/C_{ho} as $G \to 0$ ($B \to \infty$) is unity, while Equation 7 predicts it to go to minus infinity.

The models of Saderholm (18) and Marklund (1) are not vastly different from that of Lenoir and Robillard, except that Saderholm totally ignores the "base" (no crossflow) burning rate in comparison to the erosive contribution, a treatment that seems a bit drastic, particularly for fairly low crossflow velocities.

The second category of models listed in Table IV includes models based on the alteration of transport properties in the region between the gas flame and the propellant surface by the crossflow, generally due to turbulence effects. Included in this category are models in which the thermal conductivity in this region is raised by turbulence and models in which the time for consumption of fuel gas pockets leaving the surface is reduced by the effects of turbulence on diffusivity. Four of these models were developed for double-base propellants. In three of these, the models of Corner (38), Zeldovich (40), and Vilyunov (17), the basic approach is to calculate, using various boundary layer hydrodynamic models, an effective ratio of turbulent thermal conductivity (or diffusivity) to laminar conductivity and relate this to increased flux to the propellant surface from the gas flame and, thus, to increased rate of ablation of the propellant surface. The Vanderkerchove (39) model, however, is somewhat different. In this model, he assumes that the key heat transfer driving temperature is achieved at the inner edge of the fizz zone. He then assumes that in cases where, in the absence of crossflow, this fizz zone would begin at a distance from the surface greater than the distance from the surface to the edge of the laminar sublayer (calculated from a universal u^+, y^+ correlation approach) with crossflow, this edge of the fizz zone will be fixed by the edge of the laminar sublayer. Whenever this is the case, the resultant "flame" position will be closer to the surface than without crossflow, the resultant heat flux (calculated as the ratio of the thermal conductivity to the "flame" offset distance) will be higher, the propellant surface temperature will increase, and the propellant ablation rate will become higher. Since the laminar sublayer thickness decreases with increasing crossflow velocity, the burning rate will also increase with this parameter.

The models of Lengelle (37) and Saderholm, Biddle, Caveny, and Summerfield (36) for composite propellant erosive burning are somewhat similar in principle, though the latter model is applied to the special case of very fuel-rich propellants at quite low crossflows. The basic propellant combustion mechanism assumed is the granular diffusion model in which pockets of fuel vapor leave the surface and burn away in an oxidizer continuum at a rate strongly dependent upon the rate of micromixing of the oxidizer vapor into the fuel vapor pocket. The driving mechanism by which the crossflow is assumed to increase the burning rate is through increased turbulence associated with increasing crossflow raising the turbulent diffusivity in the mixing region (thus increasing the rate of mixing and decreasing the effective distance of the diffusion flame from the surface) and raising the effective turbulent thermal conductivity. Both the decrease in distance from heat release zone to surface and the increase in thermal conductivity increase the heat flux to the surface, thus causing the propellant to ablate more quickly. There are several notable weaknesses associated with the Lengelle model: (1) the granular diffusion flame model is not physically realistic; (2) the AP monopropellant flame is ignored; and (3) the boundary layer treatment used to calculate the dependence of the effective turbulent diffusivity and conductivity on the crossflow is unrealistic in its use of one-seventh power velocity law all the way from the freestream to the surface.

In the more recent studies of Parkinson, et. al. (5,6,42), only alteration of the effective thermal conductivity between the propellant gas flame zone and the surface by crossflow-induced turbulence is considered as a driving mechanism for erosive burning. In their first work (42), the authors use blown-boundary layer theory to calculate the Stanton Number (controlling heat feedback) as a function of the skin friction coefficient in the presence of blowing, utilizing expressions based on the work of Kutataladze and Leont'ev (14) for calculation of this coefficient. They then use the calculated Stanton Number for comparison of the heat feedback rate from the gas flame to the surface with that based on pure conduction (no-crossflow case), allowing for the fact that increased burning rate will push the flame zone further away from the surface (under their assumption that the "delay time" of the reaction is not affected by the turbulence) in arriving at an expression for the total burning rate as a function of the no-crossflow rate and the Stanton Number. In their two subsequent papers (5,6), they expand their analysis to include treatment of the laminar sublayer thickness relative to the flame standoff distance and modify their blown-boundary-layer analysis to allow the skin friction factor to only asymptotically approach zero at high blowing rates, rather than being identical to zero at blowing ratios (blowing rate/crossflow rate) greater than a critical value (Kutataladze approach).

Only one model, that of Tsuji (43), is listed in the third category of Table IV; however, further modeling efforts in this category, of considerably greater complexity, are discussed in the next section. The Tsuji study, unfortunately, is not particularly useful due to the assumption of a totally-laminar boundary layer and limitation to a situation where the free-stream velocity is proportional to the distance from the head-end of the grain. Other simplifications include assumption of premixed stoichiometric fuel and oxidizer (rendering the model inapplicable to composite propellant systems) and use of one-step global kinetics.

In the "Miscellaneous" category of Table IV, the Klimov model (44) is mainly aimed at calculation of threshold crossflow velocities (below which the propellant is unaffected by crossflow). Klimov claims that the threshold velocity is the mainstream crossflow velocity above which the "turbulence front" subsides onto the propellant surface (recall earlier mention of Buddini's work (8,9) supporting this hypothesis) and presents boundary-layer analysis procedures for calculating this threshold velocity as a function of the transpiration (blowing) velocity of gases ablating from the propellant surface. In addition, he postulates that negative erosion is due to "stirring up" of cool streams of binder decompositon products over the oxidizer surface, leading to intensification of their cooling effect and to screening of heat feedback from oxidizer/fuel diffusion flames.

Molnar's model (45), developed for homogeneous propellants with a laminar crossflow, is based on an assumption (which does not appear to this author to be realistic) that the lateral velocity gradient at the burning surface governs erosive burning. Miller (46) assumes that the time for a unit of propellant mass to be consumed is a linear sum of a chemical reaction time and "the time required for turbulent transport of heat to the propellant surface"; such an additivity approach seems quite unrealistic.

4.0 COMPLEX NUMERICAL ANALYSIS EROSIVE BURNING MODELS

Modeling efforts in this area include those of Beddini (8-10), with major emphasis on fluid dynamic aspects but a very oversimplified unrealistic treatment of solid propellant combustion itself; composite propellant (49-51) and double-base propellant (52) models by Kuo, et. al., with emphasis on flow dynamic aspects but also with inclusion of treatment of combustion processes; a "first-generation" composite propellant model (27,48,53), "second-generation" composite propellant model (31,32,54), and a double-base propellant model (55,56) by King (with more emphasis on combustion mechanism details coupled with a more empirical treatment of fluid dynamic aspects); and a composite propellant model by Renie, et. al. (57-59), which is similar to and derivative of the King "second-generation" composite model and accordingly will not be discussed further. The Beddini and Kuo models will be briefly described below, while this writer's models will be described in more detail (author's perogative!). It should be noted that even the models emphasizing fluid dynamic aspects of erosive burning are limited to simple configurations and do not deal with slots, stars, or other irregular perforations (often used in practical motors) which generally result in highly three-dimensional flows.

4.1 BEDDINI MODELING EFFORTS

Beddini (8-10) has carried out what is probably the most realistic and thorough analysis of the flow structure (including turbulence) involved in the erosive burning of solid propellants in either two-dimensional slab configurations or in the port of a cylindrically-perforated motor, employing second-order closure turbulence analysis procedures. With his approach, he has been able to predict flow development structures consistent with those measured by Yamada and Goto (12) in cold-flow studies simulating blowing-wall rocket motors ports, structures considerably different from those predicted using more standard k-e developing turbulent boundary layer analyses, such as those employed by Kuo and coworkers (49-52), discussed later. However, his combustion model is highly idealized (not representative of actual flame structures in either composite or double-base propellant combustion) - consequently, it is concluded that his results are mainly of use for trend analysis (e.g., scaling of threshold effects, an important area of interest in itself) rather than for prediction of the erosive burning characteristics of specific propellants.

4.2 MODELING EFFORTS OF KUO AND COWORKERS

In Reference 49, Kuo and coworkers present an analyis of erosive burning of composite propellants in the geometry of their test apparatus (described earlier), a flat-plate with a fixed leading edge. In this work, they perform a parabolic turbulent boundary-layer analysis using a k-e model for closure of their turbulent equations. [In standard fashion, they begin with general unsteady-state conservation equations for mass, momentum, fuel, oxidizer, enthalpy, etc., replace the instantaneous variables with mean plus fluctuating components, and time-average the resulting equations, leading to a number of $\overline{X'Y'}$ crossproducts which must be correlated for closure of the problem.] In the near-wall region, they utilize a modified Van Driest (60) turbulent viscosity formulation, with inclusion of a term based on the work of Cebeci and Chang (61) to account for wall roughness, for calculation of turbulent kinetic energy and dissipation. In their analysis, they assume that the heat release at any point in the gas-phase is controlled by eddy breakup, which is proportional to the square root of local turbulent kinetic energy level and to the radial gradient of unburned fuel concentration. Among other simplifications regarding the combustion processes, they assume infinite kinetics for the oxidizer/fuel flame, neglect molecular diffusion as regards mixing, and neglect the gas-phase ammonium perchlorate monopropellant flame, considered by most modelers of composite propellant combustion to be an important factor. In solving their equations, the authors employ a standard Patankar-Spalding numerical approach, marching along the grain from the leading edge (parabolic problem).

In Reference 50, the previous model is extended to treatment of erosive burning in the port of a cylindrically-perforated propellant grain; in this study, both the developing (inviscid core flow) and fully-developed regions of the flow are considered. The marching analysis is initiated at the point where the boundary layer starts to develop (though it is not clear how the authors decide where this is). In general, the analysis is quite similar to that used for the flat-plate analysis except for addition of treatment of axial pressure gradients associated with

flow acceleration down the bore. In Reference 51, the analysis is further extended to formulations containing HMX and aluminum as well as ammonium perchlorate and binder, with treatment of the species formed by reaction of ammonium perchlorate and binder as an "equivalent oxidizer" and these formed by HMX and aluminum as "equivalent fuel" - this author has considerable difficulty with this concept.

Comparison of theoretical results predicted using the flat-plate analysis with experimental results obtained by the Penn State investigators (26) shows close agreement. From the results of this study, the authors conclude that the mechanism of erosive burning is increased turbulence activity near the regressing propellant surface with increased crossflow velocity. Both experimental and theoretical results indicate that erosive burning is more pronounced at higher pressure; in addition, erosive burning rate in a rocket motor is predicted to decrease with increasing port diameter, in agreement with observations of many investigators in scale-up studies and motor development programs.

This author has major disagreements with the modeling approach described above. It appears that the modelers are discarding mechanisms which determine burning rate in the absence of strong crossflow. Now this author can understand that at very high turbulence levels associated with high crossflows, leading to erosive burning ratios far greater than unity, this neglect might be acceptable. However, at lower levels of crossflow, where the erosive burning ratio is not far from unity (say, less than 2), it seems obvious that both erosive and non-erosive mechanisms must contribute to the total burning rate in that nature in general does not permit discontinuous changes from all one mechanism to all another with small changes in the parameter affecting their relative significance. (That is, it is very difficult for this author to see how mechanisms determining the zero-crossflow rate disappear as soon as the total rate rises several or even tens of percent above this zero-crossflow rate.) Basically, the model appears to have a major deficiency resulting from the assumption that the heat release from an oxidizer/fuel gas flame is totally controlled by eddy breakup, with the result that in the absence of crossflow-induced turbulence no contribution to the propellant ablation is made from O/F gas flame heat feedback. (As turbulent kinetic energy goes to zero in this model, eddy breakup goes to zero and, with neglect of molecular diffusion mixing processes, mixing and reaction also go to zero.) Thus, in the absence of crossflow, this model requires that all heat necessary for preheating and vaporizing the propellant ingredients at the observed zero-crossflow rate must be supplied by surface/subsurface heat release and/or a collapsed ammonium perchlorate monopropellant flame, a scenario considered unrealistic by all modern modelers known to this author. (That is, the O/F flame in modern ammonium perchlorate composite propellant models is calculated to make an important contribution to the surface heat balance at zero crossflow under all reasonable pressure conditions - in fact, the dependence of zero-crossflow burning rate on oxidizer particle size results from the importance of the O/F flame.)

Another area of major difficulty with the motor port grain model lies in the use of a one-dimensional inviscid core flow plus boundary layer approach at and near the head end of the grain port. As has been shown experimentally by Yamada and Goto (12) and by Dunlap, et. al. (13), and analytically by Beddini (8-10), among others (as discussed earlier), the entire flow near the head end of a perforated grain port must be highly two-dimensional, precluding use of such an analysis. Only at a distance a considerable number of diameters downstream of the motor head end, where the ratio of blowing velocity to crossflow velocity has dropped below a critical value (as the crossflow velocity builds up) is such an analysis applicable. In the upstream regions, the highly two-dimensional nature of the flow results in near-wall turbulence intensities being quite small compared to those that would be predicted by the analysis of Kuo and coworkers. As a result, as discussed by Beddini, erosive effects in the upstream regions of perforated grains should be considerably less than predicted by this analyses.

In Reference 51, Kuo and coworkers present a model of erosive burning of double-base propellants; analysis of the flow is similar to that for their composite propellant modeling. In this study, the authors do treat multiple reaction zones, observed in the combustion of double-base propellants. Again, however, in calculation of heat release rates in these zones, the authors assume that these are controlled by eddy breakup, in this case involving the mixing of "lumps" of unburned and fully-burned gases. Accordingly, the heat release rate again goes to zero as turbulent kinetic energy goes to zero since they have once more neglected molecular diffusion mixing processes - thus, this model too is suspect for crossflows not leading to high erosive burning ratios since it cannot give the correct zero-crossflow burning rate limit, in this author's opinion a minimum requirement for a realistic erosive burning model as discussed above.

4.2 MODELING EFFORTS OF KING

4.2.1 FIRST-GENERATION COMPOSITE PROPELLANT MODEL

The "first-generation" composite propellant erosive burning model by King (27,48,53) is based on a hypothesis that augmentation of burning rate by crossflow is caused solely by the bending of columnar diffusion flames (involving reaction of ammonium perchlorate and binder decomposition products) with resultant movement of this O/F flame closer to the surface, causing increased heat feedback flux; affects of crossflow-induced turbulence on transport properties is not considered. Although this model does yield good predictive capability for erosive burning rates, it requires physically unrealistic values of some of the parameters grouped in three constants used to fit zero-crossflow burning rate data (an integral part of the procedure).

Accordingly, this model was eventually discarded by the author in favor of a more fundamental "second-generation" model (presented in the next section) in which both zero-crossflow and erosive burning rates are predicted from first principles and in which both flame-bending and turbulence-augmented transport property mechanisms are included. However, for sake of completeness, a brief description of the "first-generation" model is included here.

A schematic depicting the "first generation" composite propellant erosive burning model is presented in Figure 5. In the

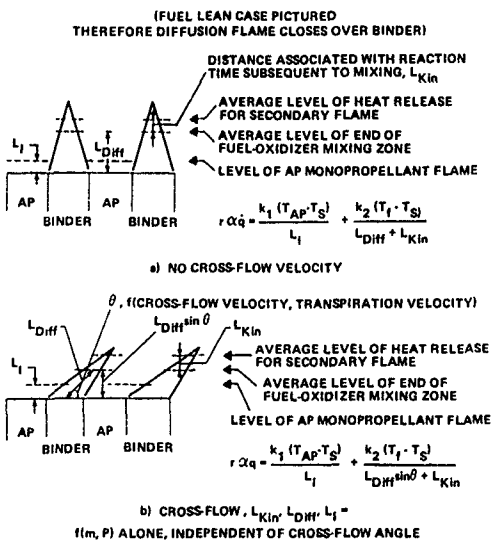

Figure 5. Sketch of King First-Generation Model Postulated Erosive Burning Mechanism

first part of the figure, the flame processes occuring in the absence of crossflow are depicted. There are two flames considered: an ammonium perchlorate deflagrat on monopropellant flame close to the surface; and a columnar diffusion flame resulting from mixing and combustion of the ammonium perchlorate deflagration products and fuel binder pyrolysis products at an average distance somewhat further from the surface. Three important distance parameters considered are the distance from the propellant surface to the "average" location of the kinetically controlled ammonium perchlorate monopropellant heat release (L_I), the distance associated with mixing of the oxidizer and fuel for the diffusion flame (L_{Diff}), and the distance associated with the fuel-oxidizer reaction time subsequent to mixing (L_{Kin}). (An alternate way of thinking about this last distance, which it is difficult to show in the figure is to picture two stacked cones in the figure, separated by the distance L_{Kin}.) A heat balance between heat feedback from these two flames and the energy requirements for heating the propellant from its initial temperature to the burning surface temperature and decomposing it yields (assuming that the heat feedback required per unit mass of propellant consumed is independent of burning rate):

$$r_o \propto \dot{q}_{feedback} \propto \frac{k_1 (T_{AP}-T_s)}{L_I} + \frac{k_2 (T_f-T_s)}{L_{Diff}+L_{Kin}} \quad (9)$$

(The rationale leading to this type of summing of flames from the two different flames is discussed in detail in Reference 53.)

The situation pictured as prevailing with a crossflow is shown in the second part of Figure 5. Since L_I and L_{Kin} are both kinetically controlled and are, thus, simply proportional to a characteristic reaction time (which is assumed to be unaffected by the crossflow) multiplied by the propellant gas velocity normal to the surface (which for a given formulation is fixed by burning rate and pressure alone), these distances are fixed for a given formulation at a given burning rate and pressure, independent of the cross-flow velocity. Of course, since crossflow velocity affects burning rate at a given pressure through its influence on the diffusion process as discussed below, L_I and L_{Kin} are influenced through the change in burning rate, but this is simply coupled into a model by expressing L_I and L_{Kin} as explicit functions of burning rate and pressure in that model. The important point is that they can be expressed as functions of these two parameters alone for a given propellant.

However, the distance of the effective mixing zone height from the propellant surface is directly affected by the crossflow. To a first approximation, L_{Diff} measured along a vector coincident with the resultant and crossflow velocities should be the same as L_{Diff} normal to the surface in the absence of a crossflow at the same burning rate and pressure. A simplified version of the reasoning leading to this conclusion is presented in Figure 6, which is essentially self-explanatory. While the time required for a parcel leaving the surface to travel the distance L_{Diff} in the flow direction θ at constant burn rate is inversely proportional to the sine of the flow angle, the characteristic mixing time is also decreased since the average concentration gradient is increased by the

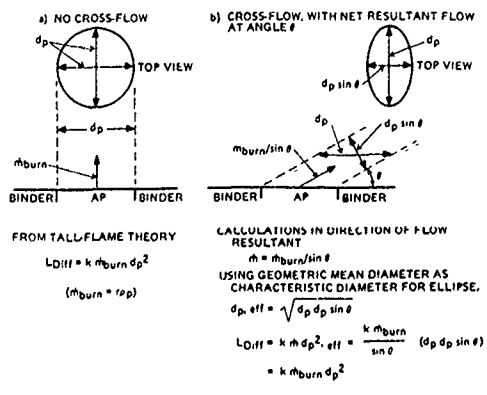

Figure 6. Procedure For Calculation of Dependency of Diffusion Distance on Flow Angle

circular cross-section (in the absence of crossflow) being converted to an elliptical cross-section with major axis d_p (oxidizer particle diameter) and minor axis $d_p \sin\theta$. Doing an exact calculation of the effect on characteristic mixing time is somewhat difficult: however, replacement of the circle diameter d_p by the geometric mean ellipse diameter $\sqrt{d_p \cdot d_p \sin\theta}$ in calculating concentration gradients does not seem unreasonable. When this is done, the magnitude of L_{Diff}, measured in the flow direction, is calculated to be independent of flow angle, θ, as shown in Figure 6. [A somewhat more rigorous (and immensely more complex) analysis has been performed, indicating that the above approximation is quite good for $\theta > 20$ degrees, but that for smaller angles (columns further pushed over), the magnitude of L_{Diff} actually begins to decrease relative to the no-crossflow value.]

At any rate, to a reasonably good approximation, the magnitude of L_{Diff} is independent of the crossflow velocity (at fixed pressure and burning rate) although its orientation is not. Thus, the distance from the surface to the "average" mixed region is decreased to $L_{Diff} \sin\theta$. (See Figure 5.) The heat balance at the propellant surface now yields:

$$\dot{r} \propto \dot{q}_{feedback} \propto \frac{k_1(T_{AP}-T_s)}{L_I} + \frac{k_2(T_f-T_s)}{L_{Diff}\sin\theta + L_{Kin}} \tag{10}$$

This picture was used as the basis of development of the first generation flame bending model for prediction of burning rate versus pressure curves at various crossflow velocities, given only a curve of burning rate versus pressure in the absence of crossflow. The general approach utilized in development of this model follows:

1. The expressions for L_I, L_{Diff}, and L_{Kin} as functions of burning rate (or burning mass flux, $\dot{m}$), pressure, and propellant properties are derived and substituted into a propellant surface heat balance.
2. The resulting equation is worked into the form of Equation 16 (developed in succeeding paragraphs) for burning in the absence of crossflow. A regression analysis using no-crossflow burning rate data is performed to obtain best fit values for A_3, A_4, and A_5, three constants appearing in this expression. (d_p is the average ammonium perchlorate particle size. For a given propellant, the burning rate data may be just as effectively regressed on A_3, A_4, and $A_5 d_p^2$, eliminating the necessity of actually defining an effective average particle size.)
3. From these results, expressions are obtained for L_I, L_{Diff}, and L_{Kin} as functions of burning rate (or $\dot{m}$) and pressure.
4. These expressions are combined with an analysis of the boundary layer flow (which gives the crossflow velocity as a function of distance from the propellant surface, mainstream velocity, and propellant burning rate) to permit calculation of the angle θ (Figure 5), L_I, L_{Diff}, L_{Kin}, and $\dot{m}$ for a given pressure and crossflow velocity.

In the derivation of burning rate for a composite propellant in the absence of a crossflow, an energy balance at the propellant surface was written as (see Figure 5):

$$\frac{\lambda_A (T_f-T_s)}{(L_{Diff}) + (L_{Kin})} + \frac{\lambda_B (T_{AP}-T_s)}{L_I} \tag{11}$$

$$= \dot{m} [C_p (T_s-T_o) + Q_{VAP}-Q_{RX}]$$

where the λ's are thermal conductivities, T_f is the final flame temperature, T_{AP} is the ammonium perchlorate monopropellant flame temperature, T_s is the surface temperature, T_o is the bulk propellant temperature, and Q_{VAP} and Q_{RX} are heat sink and source terms in the solid propellant. The first term in this equation represents heat flux from the final flame to the surface, the second represents heat flux from the ammonium perchlorate monopropellant flame, and the third represents the heat flux requirements for ablation of the propellant at the mass flux, $\dot{m}$. (Several simplifying assumptions were utilized in writing of the equation in this form, as discussed in detail in Reference 53.)

The monopropellant ammonium perchlorate flame offset distance, L_I, may be expressed as the product of a characteristic reaction time, τ_I, and the linear velocity of gases leaving the propellant surface:

$$L_I = \tau_I \frac{\dot{m}}{\rho_{gas}} \tag{12}$$

For a second-order gas-phase reaction (generally assumed), τ_I is inversely proportional to pressure, and for a given formulation, the gas density is directly proportional to pressure, yielding:

$$L_I = K_1 \dot{m}/P^2 \tag{13}$$

A similar analysis for L_{Kin} yields:

$$L_{Kin} = K_2 \dot{m}/P^2 \tag{14}$$

For a columnar diffusion flame, it may easily be shown that the diffusion cone height, L_{Diff}, may be expressed as:

$$L_{Diff} = K_3 \dot{m} d_p^2 \tag{15}$$

Equations 11 and 13-15 may be combined to yield:

$$\dot{r} = \dot{m}/\rho_s = A_3 P \left[1 + \frac{A_4}{1 + A_5 d_p^2 P^2}\right]^{1/2} \tag{16}$$

Burning rate versus pressure data for a given propellant in the absence of a crossflow may then be analyzed via a fairly complicated regression analyisis procedure to yield values of the constants A_3, A_4, and A_5 (or $A_5 d_p^2$) for that given propellant. The constants K_1, K_2, and K_3 are related to these constants in turn by:

$$K_1 = \frac{(T_{AP} - T_s)\,\lambda_B}{A_2 A_3^2 \lambda_A} \tag{17}$$

$$K_2 = \frac{(T_f - T_s)}{A_2 A_3^2 A_4} \quad (18)$$

$$K_3 = \frac{(T_f - T_s)\, A_5}{A_2 A_3^2 A_4} \quad (19)$$

where:

$$A_2 = \frac{\rho_s^2 \left[C_p (T_s - T_o) + Q_{VAP} - Q_{RX}\right]}{\lambda_A} \quad (20)$$

Data of Mickley and Davis (62) were used to develop empirical expressions for the local crossflow velocity as a function of distance from the propellant surface, mainstream crossflow velocity, and transpiration rate (gas velocity normal to the propellant surface). In this analysis, it was decided that the transpiration velocity should be calculated as the gas velocity normal to the surface at the final flame temperature. (Mickley and Davis correlations are based upon the ratio of mainstream velocity to transpiration velocity.)

The analyses described above were used in derivation of eight equations in eight unknowns for the burning of a given composite propellant at a given crossflow velocity; a computer code was developed to solve this equation set, yielding a predicted burning rate for a given pressure, crossflow velocity and set of constants A_3, A_4, and $A_5 d^2$ obtained from regression of no-crossflow data for that propellant. Details appear in Reference 53. As mentioned earlier, this model was used to successfully predict erosive burning rates for a number of composite propellants over a wide range of pressures and crossflow velocities; however, examination of some of the intermediate parameters for calculation of the various distance parameters indicated physically unrealistic values. Accordingly, this model was abandoned in favor of a more fundamental "second-generation" model, described in the next section.

4.2.2 SECOND-GENERATION COMPOSITE PROPELLANT MODEL

King's "second-generation" erosive burning model for composite propellants (31,32,54) is built on a zero-crossflow composite propellant burning model, also developed by King (63), which is, in turn, loosely based on the classic Beckstead-Derr-Price (BDP) model (64) (though with many major and minor modifications as described in detail in Reference 63). Both two-dimensional and axisymmetric versions of this erosive burning model were developed; the version described in the following paragraphs was developed for the two-dimensional slab geometry employed in the previously-described experimental program conducted by King in the Atlantic Research Corporation test apparatus. The version for treatment of cylindrically-perforated grain ports was developed via straightforward modifications to the two-dimensional model version, with the main modifications involving a change in zero-blowing skin friction coefficient expressions and modification of the momentum integral equation used in calculation of local shear stress as a function of distance from the propellant surface, and will not be discussed further. A relatively brief description of the two-dimensional model is presented below; for further details, the reader is directed to References 31, 32, 54, and 63.

The basic model centers around an energy balance, the product of burning mass flux and energy requirements to raise ingredients from ambient to surface temperature (related to burn rate by an Arrhenius function) and vaporize that fraction not consumed in subsurface reactions being equated to the sum of heat release rate from subsurface reactions and heat feedback rates from two gas flame zones (Figure 7). Thus, burning rate is controlled by three heat release zones: (1) a thin subsurface zone; (2) a gas-phase AP decomposition product monopropellant flame; and (3) a diffusion flame between AP products and binder pyrolysis products.

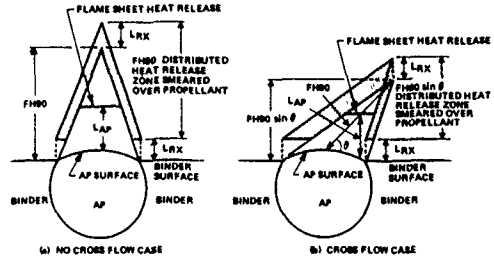

Figure 7. Schematic of Postulated Composite Propellant Flame Structure, With and Without Crossflow

Subsurface heat release is calculated using an estimated subsurface temperature profile substituted into a rate expression representing subsurface heat release data measured by Waesche and Wenograd (65). This expression is integrated from the surface to a depth where the temperature equals the AP melting point to obtain total subsurface heat release. This procedure differs from the BDP approach, in which subsurface heat release per unit mass of propellant is assumed constant, independent of burning rate.

For the gas phase, a two-flame approach was chosen (in contrast to the three-flame approach of BDP), the flames being an AP monopropellant flame and a columnar diffusion [Burke-Schumann (66)] flame. Three distances (FH90 sin θ, L_{AP} and L_{RX}) are important in determining heat feedback from these flames (Figure 7). FH90 is a distance associated with 90-percent mixing of fuel and oxidizer gases, while L_{RX} and L_{AP} are reaction distances (products of gas velocity normal to the surface and reaction times) associated with diffusion and monopropellant flames, respectively. As discussed in the previous section, describing King's "first-generation" model, crossflow-induced flame bending is postulated to reduce the mixing region height by the factor sinθ, where θ is determined by the resultant of local transpiration and crossflow velocities. AP monopropellant flame heat release is assumed to occur at

one plane, while the diffusion flame releases heat in a distributed fashion [defined by a Burke-Schumman (66) analysis] between distances L_{RX} and $L_{RX} + FH90 \sin\theta$ from the surface.

Details of equation development for the unimodal oxidizer non-metallized propellant model appear in References 54 and 63. Included in this model are three "free" constants (pre-exponentials associated with the subsurface rate expression and two rate expressions used to calculate gas-phase reaction times). Optimized values for these constants were chosen using no-crossflow burning rate data for four unimodal oxidizer AP/HTPB (hydroxy-terminated polybutadiene) formulations and subsequently used in all other calculations.

The model was extended to multimodal oxidizer formulations using a variation of Glick's "petit ensemble" approach (67). First, a multimodal oxidizer formulation is divided into subpropellants, each containing oxidizer of one size. These subpropellants are assumed to burn non-interactively, with the unimodal model being used to calculate individual mass fluxes. Oxidizer of one size is allowed to affect another subpropellant's burning rate only through possible influence on the assignment of fuel to that subpropellant. Unequal oxidizer/fuel ratios for the subpropellants are permitted via:

$$V_{f,d_i} = C_2 \left(D_{o,i}\right)^{XEXPOF} \qquad (21)$$

where V_{f,d_i} is the fuel volume assigned to a particle of diameter $D_{o,i}$, XEXPOF is an arbitrary constant, and C_2 is fixed by overall continuity. (XEXPOF = 3 results in equal oxidizer/fuel ratios for each subpropellant, while XEXPOF < 3 results in subpropellants with small oxidizer being more fuel-rich than those with large oxidizer. XEXPOF = 3 was used in the following calculations.) In averaging the individual subpropellant fluxes, Glick assumes that the average fractional surface area associated with subpropellant i is equal to its overall volume fraction. Critical analysis indicates, however, that if the subpropellants burn at different rates, slower burning ones will occupy a disproportionately higher fraction of surface. Development of this concept for XEXPOF = 3 leads to:

$$\bar{r} = 1/\Sigma \left(x_i/r_i\right) \qquad (22)$$

replacing Glick's expression:

$$\bar{r} = \Sigma x_i r_i \qquad (23)$$

r_i = Burning rate of subpropellant i
x_i = Mass fraction of overall propellant in subpropellant i
$\bar{r}$ = Average burning rate

The original model was also extended to treat metalized propellants. The metal (aluminum) is allowed to alter burning rate through heat sink effects and by conductive and radiative feedback from burning metal particles. Phenomena treated included agglomeration, particle velocity lags, ignition delay, particle combustion, conductive feedback from multiple heat release zones, and radiative feedback. For multimodal oxidizer formulations, distribution of metal among subpropellants is treated identically to that of binder.

Surface agglomeration of aluminum is calculated using equations developed by Beckstead (68). Particle ignition delays are calculated as times to heat particles from surface temperature to an assigned ignition temperature (2100°K), while particle burning rates are calculated using an expression by Belyaev (69). The transpiration gas velocity profile is calculated assuming a linear temperature profile from the surface to the end of the diffusion flame. A force balance on a particle is then integrated from the surface, utilizing a fitted drag coefficient equation assumed [based on Marshall's study (70)] to increase by a factor of 2.5 after ignition, to yield a particle time-distance history. Coupling of this analysis with ignition time and burning rate expressions permits calculation of metal combustion heat release distribution for each metal particle size (agglomerated and unagglomerated) and, finally, calculation (by superposition procedures) of the rate of conductive feedback. Radiative feedback was approximated using a cloud emissivity based on fractional area subtended by particles within an assigned distance from the surface. (For the one metalized formulation tested, radiative transfer had negligible effect on predicted burning rate.) Further details of the treatment of the effects of aluminum on composite propellant combustion are given in Reference 32.

Two postulated erosive burning mechanisms were utilized. The first, enhancement of transport properties by crossflow-induced turbulence, decreases oxidizer/fuel gas mixing distance and increases effective thermal conductivity between the heat release zones and the surface. In addition, as discussed earlier, columnar diffusion flame bending is postulated to decrease the mixing distance component normal to the surface through distortion of the mixing cone.

Calculation of crossflow effects on burning rate via these mechanisms requires a fluid flow analysis for determination of velocity and turbulence profiles. A summary of the procedures follows; details appear in Reference 54.

First, estimates of burning rate and flame height are made. A non-blowing skin friction coefficient is calculated from empirical flat-plate equations as a function of crossflow Reynolds' Number and roughness height. It should be noted in passing that there are typographical errors in the equations presented in Reference 54. Equation 29 in that reference should read:

$$C_{fo} = 0.00140 + 0.125\ Re^{-0.32} \qquad (24)$$

and Equation 30 in that reference should read:

$$C_{fo} = 0.95\ [4 \log_{10}(R/k) + 3.48]^{-2} \qquad (25)$$

A blowing parameter, b:

$$b = 2\dot{m}_p/(\rho U C_{fo}) \qquad (26)$$

U = Mainstream crossflow velocity
C_{fo} = Non-blowing skin friction coefficient

is then calculated for determination of the actual skin friction coefficient, C_f. Due to a lack of data, particularly at high blowing numbers of interest, several optional expressions relating C_f/C_{f_0} to b were initially considered. An expression, based on the work of Kutataladze and Leont'ev (14), which agreed well with limited data and gave reasonable results on extrapolation was finally selected:

$$C_f/C_{f_0} = (1 - b/10)^2/(1 + b/10)^{0.4} \qquad (27)$$

As may be noted, this expression yields negative skin fraction values for $b > 10$; this is interpreted as indicating boundary layer separation. For such cases, it is assumed that the velocity profile assumes the cosine shape measured by Yamada and Goto (12).

With C_f, wall shear stress is calculated straightforwardly and substituted into an expression (based on momentum integral analysis) for local shear stress:

$$\tau = \tau_{wall} + \dot{m}_p u - Ky \qquad (28)$$

y = Distance from propellant surface
u = Local crossflow velocity
K = Constant, function of mainstream crossflow velocity, burning rate, and channel dimensions

An eddy viscosity approach is used to relate τ to the local crossflow velocity gradient:

$$\tau = (\mu + \rho\varepsilon)\, du/dy \qquad (29)$$

With specification of an expression relating ε to y and du/dy, (discussed later) assumption of a linear temperature profile, and use of expressions relating density and viscosity to temperature, Equations 28 and 29 are then combined and numerically integrated from $u = 0$ at $y = 0$ (surface) to yield $u(y)$, $\rho(y)$, $\mu(y)$, and $\varepsilon(y)$. (Streamline shapes are also calculated, permitting calculation of the flame bending angle, θ.) The eddy viscosity distribution is then used, assuming Reynolds' analogy, to calculate total effective conductivity and diffusivity distributions. Total transport property values averaged over appropriate zones are then calculated and used in mixing and heat feedback equations to calculate revised burn rates and flame distances. This procedure is repeated to convergence. (It should be noted that the averaging procedure has been modified from that used for calculations presented in Reference 54 to better allow for the fact that the effect of gas-phase heat release on burning rate decreases exponentially with distance from the surface. In addition, effects of flame curvature on the flame bending influence have been added.)

Several eddy viscosity models for closure of the boundary layer analysis were included: All entail use of a Prandtl mixing-length expression:

$$\varepsilon = .168\,(y + y_\Delta)^2\,(DF)^2\, du/dy \qquad (30)$$

where DF is a damping factor (function of such parameters as blowing ratio, axial pressure gradient, and roughness height) while y_Δ is an offset factor dependent on roughness. The most comprehensive form of expression for DF employed was one based on a modified form of an empirical relation developed by Kays and Moffat (71) which includes the effects of blowing and axial pressure gradient but does not include the effects of wall (surface) roughness. The modifications added by King were an attempt to include the effects of roughness using approaches suggested by the works of Van Driest (60) and Cebeci and Chang (61).

As may be seen from Table II (presented in the Experimental Studies section), there were ten uncatalyzed HTPB binder composite propellant formulations studied in the Atlantic Research Corporation test apparatus, permitting extensive checkout of the model described above. (Predictions were not made for the catalyzed formulation since the model does not include the capability of treating catalysts; however, the data are included in the following discussion of the effects of various parameters on sensitivity of formulations to crossflow.) The polyester formulations were also not checked against the model since the limited data base for these formulations is inadequate for evaluation of the three "free" constants in the model, which would almost certainly be different for different binder systems. (Recall, the values of the constants for the HTPB-AP formulations were chosen using zero-crossflow data for Formulations 4525, 5051, 4685, and 5542, the four unimodal oxidizer formulations).

Erosive burning test results are presented in Figures 8 - 18, in the form of burning rate versus pressure at various crossflow velocities. In addition, theoretical predictions are presented for all but the catalyzed formulation (4869) in these figures. As may be seen, the agreement between data and predictions for the no-crossflow conditions is excellent for all formulations except 7996, where the theoretically predicted burning rates are 10 to

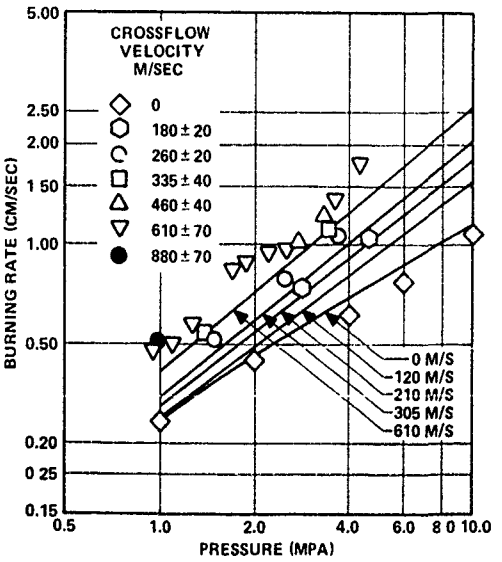

Figure 8. Burning Rate Predictions (Solid Lines) and Data (Points) For Formulation 4525 (73/27 AP/HTPB, 20 Micron AP)

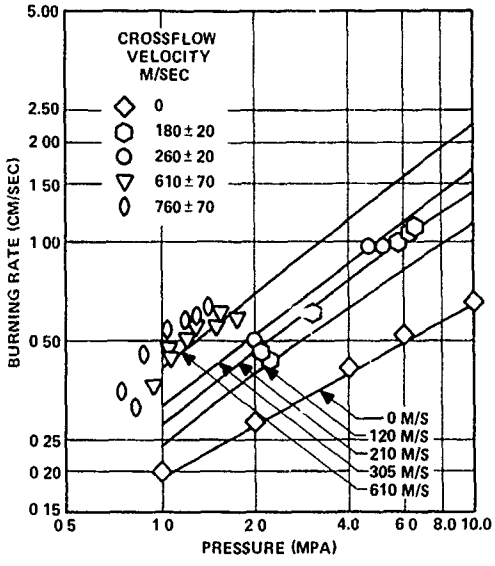

Figure 9. Burning Rate Predictions (Solid Lines) and Data (Points) For Formulation 5051 (73/27 AP/HTPB, 200 Micron AP)

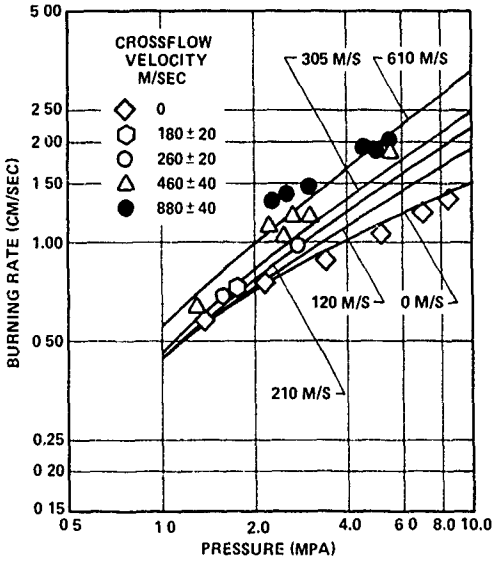

Figure 11. Burning Rate Predictions (Solid Lines) and Data (Points) For Formulation 5542 (77/23 AP/HTPB, 20 Micron AP)

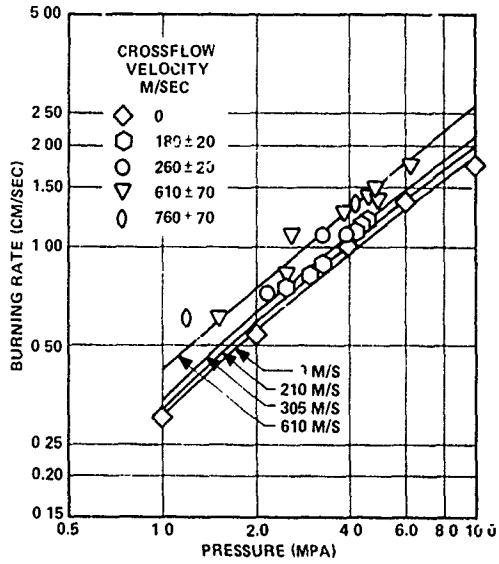

Figure 10. Burning Rate Predictions (Solid Lines) and Data (Points) For Formulation 4685 (73/27 AP/HTPB, 5 Micron AP)

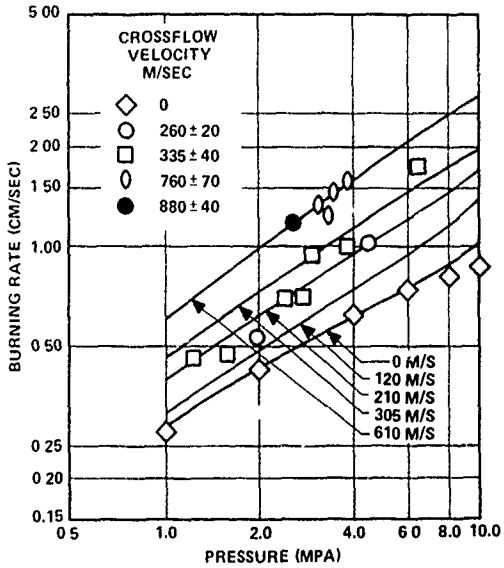

Figure 12. Burning Rate Predictions (Solid Lines) and Data (Points) For Formulation 5565 (82/18 AP/HTPB, 13.65% 90 Micron AP, 68.35% 200 Micron AP)

20 percent high. In addition, the crossflow effect predictions agree reasonably well with the data in general. With the baseline formulation (4525), the theory slightly underpredicts the effect of crossflow on burning rate, while with 5051, 4685, and 5542 (the other three non-catalyzed unimodal oxidizer formulations), agreement between theory and data is excellent. The model predicts that the high burning rate formulation (5555) should be quite insensitive to crossflow velocity, in excellent agreement with experiment. Formulation 5565, on the other hand, appears to be slightly less sensitive to crossflow than predicted, particularly at the lower pressures (1-3 MPa). Agreement between theory and data for the remaining three multimodal oxidizer, non-metalized formulations is good, except that the zero-crossflow offset between theory and data for 5526 appears to be maintained for the crossflow cases. Finally, the rather

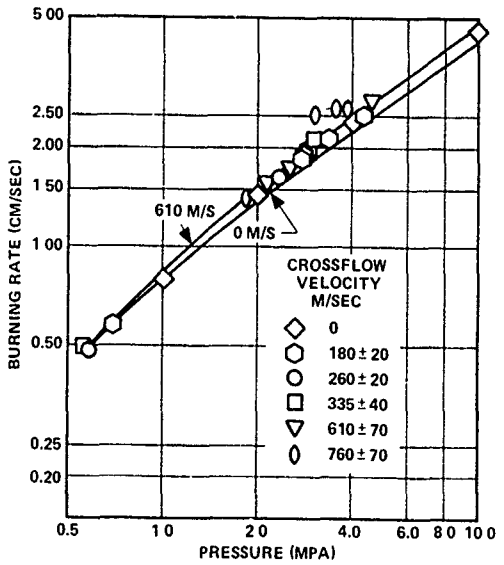

Figure 13. Burning Rate Predictions (Solid Lines) and Data (Points) For Formulation 5555 (82/18 AP/HTPB, 41% 1 Micron AP, 41% 7 Micron AP)

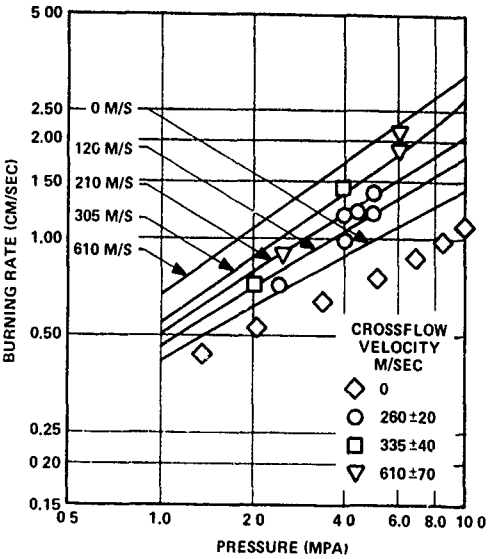

Figure 15. Burning Rate Predictions (Solid Lines) and Data (Points) For Formulation 7996 (82/18 AP/HTPB, 41% 20 Micron AP, 41% 200 Micron AP)

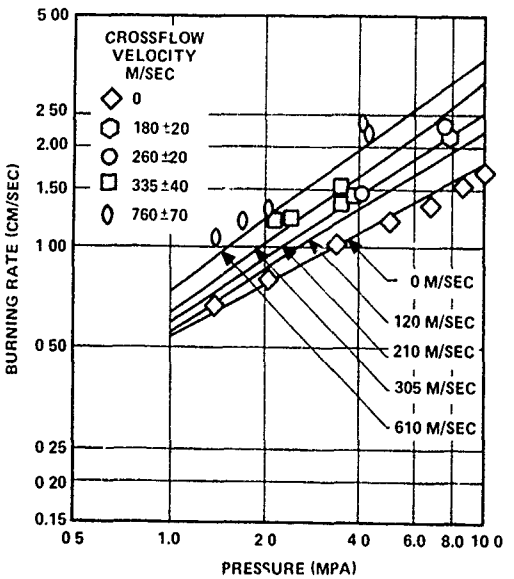

Figure 14. Burning Rate Predictions (Solid Lines) and Data (Points) For Formulation 7993 (82/18 AP/HTPB, 41% [illegible] Micron AP, 41% 90 Micron AP)

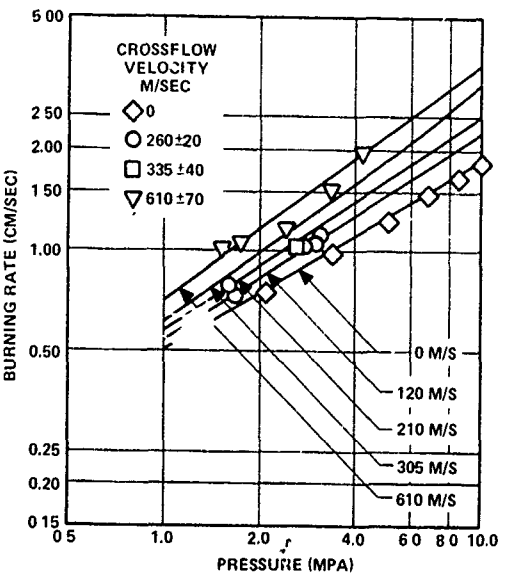

Figure 16. Burning Rate Predictions (Solid Lines) and Data (Points) For Formulation 8019 (82/18 AP/HTPB, 27.3% 1 Micron AP, 27.3% 20 Micron AP, 27.4% 200 Micron AP)

limited data for the metalized formulation (6626) appear to be in general agreement with predictions.

Results for the various formulations may be compared to identify parameters dominating the sensitivity of burning rate to crossflow. Formulations 4525, 5051, and 4685 were identical except for oxidizer particle size (and, as a consequence) base (no-crossflow) burning rate. Examination of Figures 8-10 reveals that the crossflow sensitivity increases with increasing particle size (decreasing base burning rate). For example at 200 m/sec and 5 MPa, the augmentation ratios for 4685, 4525, and 5051 are about 1.10, 1.60, and 2.00, respectively.

Comparison of data for 4525 and 4869, differing only in use of catalyst in the latter (with consequent higher base burn

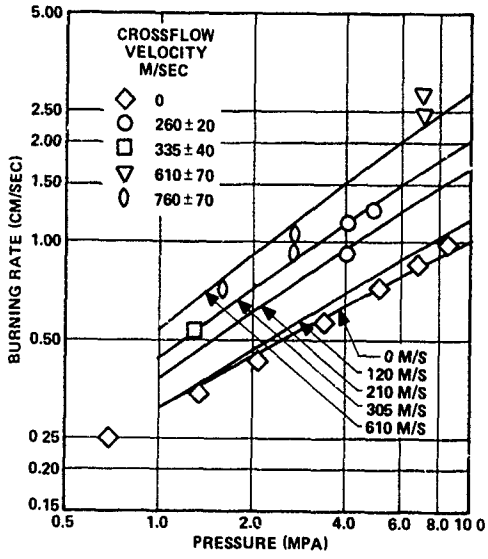

Figure 17. Burning Rate Predictions (Solid Lines) and Data (Points) For Formulation 6626 (74/21/5 AP/HTPB/Al, 70% 90 Micron AP, 4% 200 Micron AP)

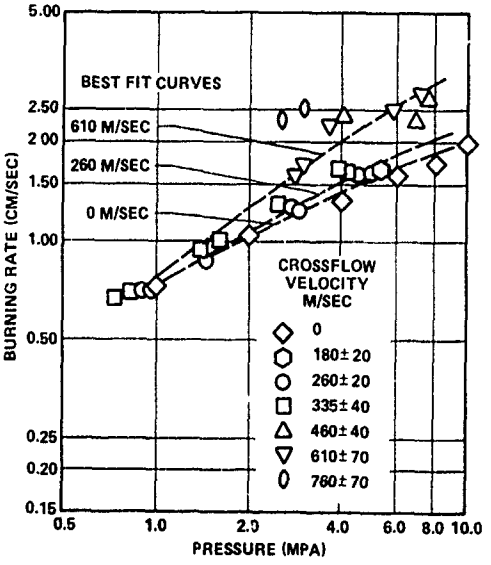

Figure 18. Burning Rate Data (No Predictions) For Formulation 4869 (72/26/2 AP/HTPB/ Iron Oxide, 20 Micron AP)

rate) again shows an increase in crossflow sensitivity with decreasing base rate. At 5 MPa and 200 m/sec, their respective burn rate augmentation ratios are 1.60 and 1.10, while at 600 m/sec, the r/r_0 values are 2.3 and 1.7. Thus, base burn rate is seen to affect erosion sensitivity even at constant oxidizer size.

Formulations 4685 and 4869 have approximately the same base burning rate at 8 MPa, although their oxidizer sizes are different. Data comparison indicates that these formulations have nearly the same sensitivity to low crossflow velocities at 8 MPa, with the catalyzed propellant being only slightly more sensitive at higher velocities. Thus, it appears that it is the base burning rate rather than the oxidizer particle size which dominates the sensitivity of this series of four 73/27 AP/HTPB formulations to crossflow, though oxidizer size itself does appear to have a slight additional effect, crossflow sensitivity decreasing with decreasing size at constant base rate.

Formulation 5542 differs from 4525 in oxidizer/fuel ratio and consequently flame temperature. Since oxidizer particle size was held constant, the higher O/F ratio results in higher base rate for 5542. The data (Figure 8 and 11) indicate that the crossflow sensitivity of 5542 is considerably lower over the entire range of conditions studied. Comparison of results for 5565 and 4525, which differ in O/F ratio, but have the same base burning behavior (due to compensating AP particle size differences), indicates that the sensitivity of these two formulations to crossflow is nearly identical. Accordingly, it may be concluded that O/F ratio (and consequently flame temperature) changes do not directly effect the erosion sensitivity of these formulations, but only affect it through their effect on base burning rate.

Formulation 6626 (metalized) has nearly the same base burning characteristics as 4525 and 5565 and approximately the same flame temperature as 5565. The data of Figures 8, 12, and 17 reveal that all three formulations have quite similar erosive burning characteristics. For example, at 760 m/sec and 2.8 MPa, the augmentation ratios for 4525, 5565, and 6626 are 2.1, 2.25, and 2.1, while at 260 m/sec and 4.0 MPa, they are 1.65, 1.55, and 1.60. These results support a conclusion that the dominant factor affecting crossflow sensitivity of composite propellants is base burning rate, largely independent of the factors determining that base rate.

Formulations 5555, 5565, 7993, 7996, and 8019 are identical in composition (82/18 AP/HTPB) differing only in oxidizer particle size blends, which were adjusted to give a range of base (zero-crossflow) burning rate versus pressure characteristics. In Figure 19, data extracted

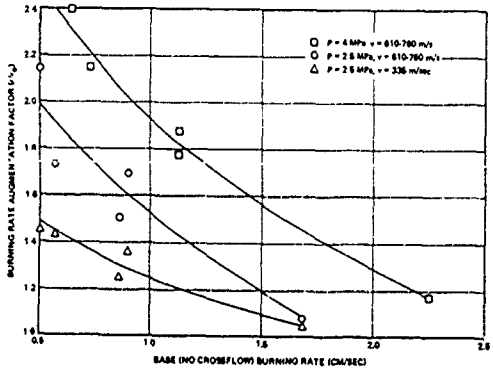

Figure 19. Summary of Results For 82/18 AP/HTPB Formulations

from Figures 12 - 16 are plotted in the form of burning rate augmentation factor (r/r_0) versus base burning rate for three combinations of pressure and crossflow velocity. As may be seen, the augmentation factor decreases monotonically and fairly smoothly with increasing base burning rate, again indicating the importance of that parameter on crossflow sensitivity.

A summary of the above comparisons, delineating the effects of various parameters on crossflow sensitivity of burning rate was presented earlier as Table III. As may be seen from Figures 8 - 18, the "second generation" composite propellant model by King predicts these observed tendencies quite well.

4.2.3 DOUBLE-BASE PROPELLANT MODEL

In the modeling of erosive burning of double-base propellants by King (55,56), effects of crossflow on a multiple heat-release zone combustion wave, as described by Rice and Ginell (72), were examined. The proposed flame structure (Figure 20) consists of three separate reaction zones. Heat feedback raises the propellant from its bulk temperature to a temperature, near the surface, at which reaction to preliminary intermediates (gas and/or spray) takes place. These fragments are further heated by the thermal wave until a second set of reactions occurs in a fizz reaction zone. Finally, there is a long induction zone (dark zone) terminated by a final thin luminous flame zone (reasonably approximated as a flame sheet). Without crossflow, the extreme length of the dark zone and the low molecular conductivity result in negligible heat feedback from the final flame, decoupling it from the burn-rate-controlling fizz zone and surface reaction zone processes. However, with crossflow, induced turbulence can increase the average effective thermal conductivity across the dark zone by one to two orders of magnitude, resulting in appreciable heat flux back to the fizz zone and raising its temperature markedly. This, in turn, accelerates reactions in this zone, causing increased heat feedback to the surface.

Crossflow may also accelerate double-base propellant burning rate by penetration of crossflow-induced turbulence into the fizz zone, increasing heat feedback from the fizz reaction zone to the surface.

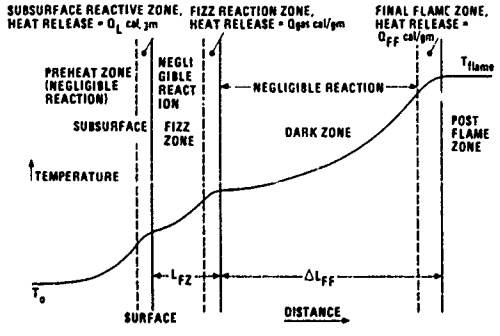

Figure 20. Postulated Double-Base Propellant Flame Structure

However, due to the gas/liquid froth structure of this zone, it is not clear how effectively such turbulence will penetrate through it. Accordingly, two limiting-case analyses were developed: (1) no turbulence penetration into the fizz zone, with the outer edge of this zone being considered to be an effective surface; and (2) treatment of the fizz zone as a gas, with boundary layer analysis beginning at the actual propellant surface. (As will be discussed later, only the second model variant gave predictions in good agreement with data.)

First, a model was developed for prediction of burning rate as a function of pressure and heat of explosion in the absence of crossflow. As indicated earlier, under no-crossflow conditions, the final flame is decoupled and the temperature gradient at the inner edge of the dark zone is zero. The fizz reaction zone is assumed to be infinitesimally thin, its distance from the surface being the product of gas outflow velocity and a characteristic reaction time. Following Beckstead (73), mass flux and surface temperature are related by:

$$\dot{m} = 5000 \exp(-10000/RT_s) \text{ gm/cm}^2\text{sec} \quad (31)$$

Solution of the Fourier equation (with no source term) between x=0 and $x=L_{fz}$, application of an energy balance at $x=L_{fz}$, with the fact that the temperature gradient at the inner side of the dark zone is zero, and application of an overall energy balance (with no feedback from the final flame) yields:

$$T_s = T_{dz} - \left[(T_{dz}-T_s) + \frac{C_{ps}}{C_{pfz}}(T_s-T_o) - \frac{Q_L}{C_{pfz}}\right](1 - e^{-\dot{m}c_{pL}\,fz/\lambda}) \quad (32)$$

where T_{dz} is the dark zone temperature, Q_L is the net surface/subsurface heat release, and T_o is the bulk propellant temperature.

Data of Aoki and Kubota (74) relating T_{dz} to pressure (P) and heat of explosion (H_{ex}) may be expressed as:

$$T_{dz} = a(P) + b\,H_{ex} \quad (33)$$

where b = 0.425°Kgm/cal and a = 720 + 125ln(P) for P < 20 atm and a = 855 + 80ln(P) for P > 20 atm. An empirical expression for Q_L based on a modification of Beckstead's expression to better allow for observed burning rate trends at low pressure was also utilized (P in atm):

$$Q_L \text{ (cal/gm)} = (65.7 + 0.013\,H_{ex})\,(P/6)^{0.08} \quad (34)$$

Finally, L_{fz} was calculated as the product of average gas velocity across the fizz zone and a characteristic reaction time:

$$L_{fz} = \frac{\dot{m}RK_{fzrx}(T_{dz}+T_s)\exp(E_{fz}/RT_{dz})}{2P^{\nu}\,(MW)\,T_{dz}} \quad (35)$$

From Aoki and Kubota (74) and Beckstead (73), E_{fz} was set equal to 40000, and the reaction order, ν, was chosen to be unity. The reaction rate constant K_{fzrx} was determined by fitting one data point

from an extensive burning rate versus pressure and heat of explosion data base generated by Miller (75).

Substitution of Equations 33 and 34 into Equations 32 and 35 results in three equations (31, 32, and 35) in three unknowns (m, L_{fz}, and T_s), which are simply solved to give burning rate as a function of pressure and heat of explosion in the absence of crossflow.

The mechanism by which crossflow is assumed to alter burning rate is by augmentation of the thermal conductivity from the surface of the propellant all the way through the final flame zone. The procedure used for calculation of the variation of this parameter with distance from the surface was the same as that described earlier for the "second generation" composite propellant erosive burning model of King. Details of the equation development and solution procedures for both scenarios mentioned earlier as regards alteration of the fizz zone transport properties by turbulence are presented in References 55 and 56.

Miller (75) has generated a systematic database for burning rates of Nitrocellulose (12.6 N)/Nitroglycerine/Secondary Plasticizer formulations as a function of pressure and heat of explosion. One of his data points (P = 35 atm, H_{ex} = 950 cal/gm) was used to calculate K_{fzrx}, the rate constant appearing in Equation 35, after which the no-crossflow model was used to predict mass burning fluxes at other pressures and H_{ex} values in his database. Predicted and measured values are presented in Figure 21; as may be seen, excellent agreement is observed between the data and predictions.

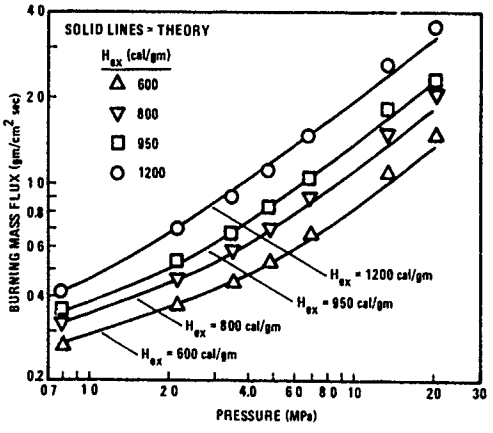

Figure 21. Comparison of Predicted Burning Rates Using a Flamesheet Model with Data of Miller (75)

In Figure 22, predictions made with the zero-crossflow version of this model are compared with data obtained by Aoki and Kubota (74) for two formulations with much higher NC/NG ratios than those tested by Miller. Agreement between data and predictions is again excellent, at least down to burning mass fluxes of 0.3 gm/cm^{2}sec, at which point predicted rates begin to exceed

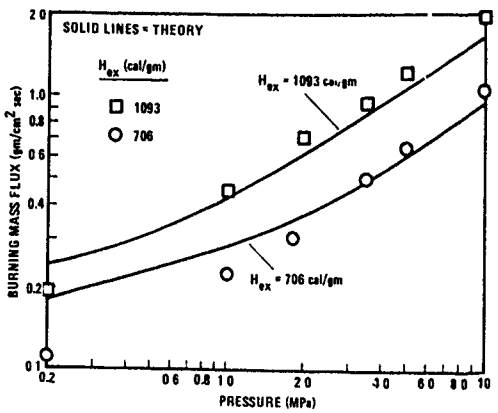

Figure 22. Comparison of Predicted Burning Rates Using a Flamesheet Model With Data of Aoki and Kubota (74)

measured ones, probably due to the fact that condensed-phase reactions (less well understood) begin to dominate at these low mass fluxes and pressures.

The two erosive burning model variants (with and without turbulence penetration into the fizz zone) have been tested against data obtained for two NG/NC propellants studied by Burick and Osborn (76). These formulations, designated as BUU and BDI, have heats of explosion of approximately 1050 and 920 cal/gm, respectively. Predicted and observed burning mass fluxes are presented in Figures 23 - 26. As may be seen from Figure 23, the no-crossflow predictions of burning rate versus pressure for BUU are excellent. In addition, the erosive burning predictions made assuming full turbulence penetration through the fizz zone are quite good, while the rigid structure fizz zone model results in drastic underprediction of crossflow effects. This is more clearly shown in

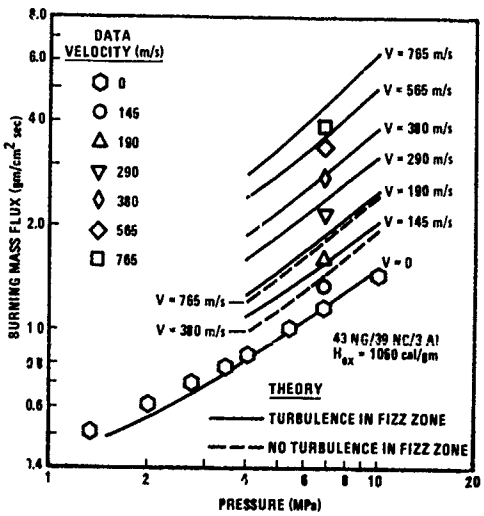

Figure 23. Predicted and Observed Burning Mass Fluxes For BUU Propellant

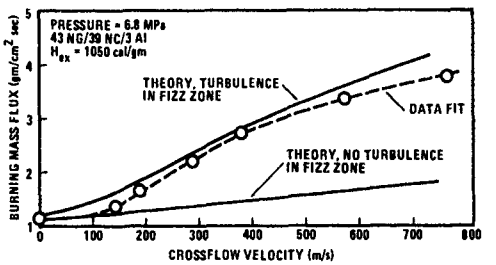

Figure 24. Predicted and Observed Effects of Crossflow Velocity on Burning Rate of RUU Propellant

Figure 24, where the burning mass flux (predicted and observed) is plotted against crossflow velocity at constant pressure. Effects of crossflow predicted assuming turbulent boundary layer development starting at the interface of the unburned propellant and the fizz zone agree quite well with data, while the alternate model fails badly. Similar results for the BDI formulation appear in Figures 25 and 26.

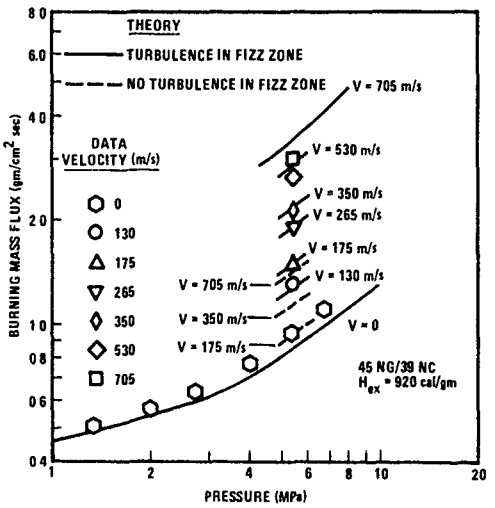

Figure 25. Predicted and Observed Burning Mass Fluxes For BDI Propellant

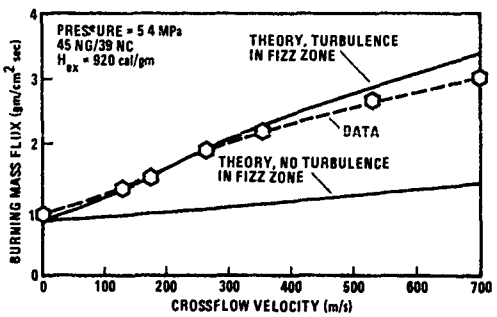

Figure 26. Predicted and Observed Effects of Crossflow Velocity on Burning Rate of BDI Propellant

In conclusion, a flame-sheet model of homogeneous double-base propellant combustion for prediction of burning rate as a function of pressure and heat of explosion in the absence of crossflow has been developed and found to yield excellent agreement between predicted and measured values. Two extensions of this model to treat crossflow have been developed, one allowing for turbulence effects in both the fizz and dark zones, the other allowing such effects only in the dark zone. The former model variant yields predictions in excellent agreement with measured data over a wide range of crossflow velocities.

5.0 CORRELATIONS BASED ON PREDICTED RESULTS FROM COMPLEX MODELS

The comparatively long computer run times associated with exercise of the more comple models described above generally preclude their direct incorporation in solid rocket motor interior ballistics analyses, where they would have to be called on thousands of times to calculate burning rates at each spatial node at each time increment utilized in such analyses. Accordingly, both Kuo, et. al (77) and King (78) have used their models to develop correlation procedures for much simpler calculations of burning rate as a function of numerous parameters. (King's procedure has been incorporated in a code for analysis of nozzleless rocket motors, as indicated in Reference 78.) These correlations are described briefly below.

The correlating expression developed by Kuo, et. al., for erosive burning of composite propellants may be expressed as (using slightly different nomenclature):

$$\frac{r_b}{r_b^o} = (1 + f_{M,P} f_{R_h} f_{PG} f_D) \exp_{\cdot}[(\sigma_p - \sigma_p^o)(T_{pi} - T_{pi,r})] \quad (35)$$

where:

$$f_{R_h} = 1.0 + 0.50 \tanh [0.063 (MP)^{0.59} R_h - 1]$$
$$= 1.0 \text{ if bracketed term is less than 0} \quad (36)$$

$$f_{PG} = 1.0 - 0.019\, \partial P/\partial X \quad (37)$$

$$f_D = 1.0 + 0.1 \exp(-2.8D) \quad (38)$$

$$f_{MP} = \frac{0.40 [(M - M_{th}) P]^{0.64}}{a p^n} \text{ for } M > M_{th}$$
$$= (0.0 \text{ for } M = M_{th}) \quad (39)$$

(In this correlation, the four f's of Equations 36-39 represent corrections for roughness height, pressure gradient, port diameter, and a combination of crossflow Mach Number and pressure, respectively.)

r_b - Burning rate at roughness height, conditioning temperature, pressure, crossflow Mach Number, axial pressure gradient, and port diameter of interest

r_b^o - Zero-crossflow burning rate at standard (baseline) conditioning temperature

σ_p - Burning-rate temperature sensitivity under crossflow conditions

σ_p^o - Strand burning-rate temperature sensitivity

T_{pi} - Propellant conditioning temperature

T_{pi}^o - Standard (baseline) propellant conditioning temperature

M - Crossflow Mach Number

M_{th} - Threshold crossflow Mach Number

P - Pressure

R_h - Roughness height

$\partial P/\partial X$ - Pressure gradient along grain port

D - Port diameter

aP^n - Base (zero-crossflow) burning rate at the given pressure

In the development of correlations by King (78) (using predictions of erosive burning made with his "second generation" model) effects of scaling (port diameter) were first examined. For any given propellant, pressure, and crossflow combination, it was found that the predicted burning rate ratio, r/r_o (burning rate with crossflow divided by zero-crossflow rate) could be related to port diameter by:

$$r/r_o]_D = r/r_o]_{D_{reference}} - B \ln (D/D_{reference}) \quad (40)$$

with B correlating as a function of the reference r/r_o value and an effective flame temperature. [For non-metalized propellants, this is the actual flame temperature, while for metalized propellants $T_{effective} = T^* + 10$ (weight percent metal), T^* being the flame temperature in the absence of burning of the metal.] In this correlation, the reference diameter was arbitrarily selected as 0.1 ft; for this choice, the correlating procedure led to:

$$B = G\sqrt{T_{effective}/100} \quad (41)$$

where:

$$G = -0.85 + 0.85\,(r/r_o)]_{D = 0.1\ ft} \quad \text{for } r/r_o \leq 1.2$$

$$= -0.0332 + 0.1694\,(r/r_o)]_{D = 0.1\ ft} \quad \text{for } r/r_o = > 1.2 \quad (42)$$

with Equation 40 becoming (D in feet):

$$r/ro]_D = r/ro]_{D = 0.1\ ft} - B \ln (10\ D) \quad (43)$$

Attention was next turned to development of a correlation for r/r_o at the 0.1 ft port diameter reference condition as a function of pressure, crossflow velocity, and propellant parameters. A large number of calculations were performed with the full model, covering a wide range of pressures, crossflow velocities and propellant types. Fortunately, it was found that for any given pressure and crossflow velocity, erosive burning ratio could be correlated almost perfectly with just two propellant parameters, base (zero-crossflow) burning rate and effective flame temperature (with the effect of the second parameter being much less than that of the first). Careful study revealed that r/r_o could be fit quite well by:

$$r/ro]_{D = 0.1\ ft} = A_1/r_o^{A_2} \quad (44)$$

where A_2 is a function of crossflow velocity and effective flame temperature and A_1 is a function of these two parameters and velocity. Closed-form correlations of A_1 and A_2 as functions of P (in atmospheres) and V (in feet/second) were developed for several flame temperatures, where the constants in these expressions, k_1 - k_6 are functions of flame temperature (as tabulated in Table V).

$$A_1 = k_3 V^{k_4} P^{[k_5 + k_6 \ln V]} \quad (45)$$

$$A_2 = 1 - k_1 V^{-k_2} \quad (46)$$

(It should be noted that these expressions were inadvertantly reversed and the bracketed term was incorrectly not written as a superscript to P in Reference 78; the corrections were later noted in an Erratum in JSR, 22, pp 394-5, 1985.)

Table V. Values of k_1-k_6 (Eqns 45 & 46) At Various Temperatures

T_{eff}(K)	k_1	k_2
1667	86 3	0 929
2017	10 93	0 577
2534	2 07	0 279
2974	0 805	0.139

T_{eff}(K)	V-range	k_3	k_4	k_5	k_6
1667	>2000	0 00255	0.457	0 913	-0 0217
	<2000	0.258	-0.151	-0 0894	+0.1103
2017	>1500	0.100	0.040	0.0124	0.0873
	<1500	0 363	-0.136	-0 267	0.1255
2534	All	0.0973	0.100	-0 091	0.089
	—	—	—	—	—
2974	>700	0.0131	0.378	0 345	0 0287
	<700	1.122	-0.30	-0.622	0.176

With Equations 41-46, the following procedure is used to calculate burning rate ratio (and thus total burning rate) for specified pressure, crossflow velocity, channel (port) diameter, and propellant. First, logarithmic interpolation of a base (zero-crossflow) burning rate versus pressure table is used to obtain the base burning rate, r_o. Next, A_1 and A_2 are evaluated for tabular values of flame temperature bracketing the actual value using Equations 45 and 46, and the r/r_o values for a port diameter of 0.1 ft are calculated for these bracketing values using Equation 44. Linear interpolation is finally used to obtain the reference diameter r/r_o value at the actual temperature and Equations 41-43 are then used to correct to the actual port diameter. If this procedure leads to a calculated r/r_o value of less than unity, it is assumed that this represents being in a boundary-layer blowoff regime, and the r/r_o value is defaulted to unity.

6.0 SCALING

The detailed models of King and Kuo, et. al. (and the correlations based on them) discussed earlier include capability for prediction of effects of motor scale on erosive burning. Both of the correlation procedures discussed in the previous section can readily be shown to predict a decrease in erosive effects with increasing port diameter. In addition, the "second-generation" model of King and the correlation procedure based on it show an increase in threshold velocity (minimum crossflow velocity below which erosive burning effects are not predicted) with increased port diameter as demonstrated in calculation results presented in Reference 32. Both of these predicted trends are in at least qualitative agreement with observations from motor scaleup studies.

In Reference 10, Beddini presents an approximate analysis for scaling erosive burning threshold conditions as a function of the base (zero-crossflow) burning rate and motor size. One goal of this analysis which was met was prediction of the observed fact that the threshold value of crossflow mass flux increases with increased propellant burning rate and increased motor size (port diameter). In this study, it was concluded that the threshold conditions for erosive burning are related to a critical value of the blowing parameter, b (defined by Equation 26); for values of this parameter above the critical value, the mainstream turbulence does not penetrate (subside) into the near-surface flame regions. (As noted earlier, King refers to this condition of $b > b_{critical}$ as representing boundary layer blowoff and also concludes that erosive burning effects are negligible in this case; thus the King "second generation" model yields scaling predictions consistent with those of Beddini.) Details of Beddini's application of this criterion to determination of threshold crossflow velocity for erosive burning are presented in Reference 10. His final scaling relationship indicates that the value of the crossflow Reynolds' Number at the threshold point scales mainly with the surface-transpiration Reynolds' Number to the 1.25 power; this in turn corresponds to the critial crossflow mass flux being approximately proportional to port diameter to the 0.25 power and to burning rate to the 1.25 power. Accordingly, this relationship predicts the absence of erosive burning for very large motors (such as space booster solid motors) as observed. (As pointed out by Beddini, none of the large (120-, 156-, 260-inch motors) fired up to the time of his publication had exhibited any erosive burning, consistent with his predictions.) In addition, the relationship developed by Beddini indicates strongly increasing values of threshold crossflow mass flux with increased zero-crossflow propellant burning rate, as predicted and observed in the studies by King discussed in Section 4 2.2.

Recently, Strand and Cohen (22) have been conducting a series of tests with long segmented motors to measure the transition length threshold conditions (axial location at which deviation from non-erosive burning begins) while systematically varying parameters considered to influence the erosive burning phenomenon. From these experimental studies, they have concluded that the threshold conditions can be correlated in terms of critical crossflow Reynolds' Number, surface transpiration Reynolds' Number and motor local length-to-radius (or diameter) ratio by a linear expression:

$$Re_c = K\ (L/R)\ Re_s' \qquad (47)$$

where Re_c is the critical crossflow Reynolds' Number,

$$Re_c = \frac{\rho_g\ U_{crit}\ R_{port}}{\mu_g} \qquad (48)$$

and Re_s' is a reduced surface transpiration (burning rate) Reynolds' Number:

$$Re_s' = \frac{\phi\ \rho_s\ r\ R_{port}}{\mu_s} \qquad (49)$$

(with r being the propellant burning rate). This differs from the Beddini correlation as regards the exponent on the transpiration Reynolds' Number (1.0 versus 1.25) and, more importantly, inclusion of the length/radius ratio term. As a result, in this correlation, the critical crossflow mass flux for onset of erosive burning is directly proportional to propellant burning rate and to the local length to diameter ratio - thus the L/R ratio rather than the port radius itself is the critical geometrical scaling parameter and large motor diameter alone will not serve to avoid the erosive burning regime. The authors claim that this conclusion is corroborated by the fact that erosive burning does indeed occur in the early phases of operation of the very large space shuttle SRM.

Accordingly, it appears that at this time there is some controversy as regards motor scale effects on threshold crossflow mass flux required for onset of erosive burning, with Beddini claiming that port diameter is the critical scaling parameter, while Strand and Cohen claim that length-to-diameter ratio is the critical scaling parameter; the first scenario leads to the conclusion that large diameter motors are not susceptible to erosive burning, while the latter scenario contradicts this

conclusion. Further study to resolve this conflict is of considerable importance as regards scaling of erosive burning data from small (relatively inexpensive) motor tests to large motors.

REFFRENCES

1. Marklund, T., and Lake, A., "Experimental Investigation of Propellant Erosion," ARS Journal, 30, 173, 1960.

2. King, M. K., "Effects of Crossflow on Solid Propellant Combustion: Interior Ballistic Design Implications," 1976 JANNAF Propulsion Meeting, Dec. 1976, CPIA Publication 280, Vol. V, p 341.

3. Ayris, J., and Petrovic, S., "Erosive Burning in Solid Propellant Rocket Motors," AIAA Paper 90-2215, AIAA/SAE/ASME/ASEE 26th Joint Propulsion Conference, Jul. 1990.

4. Razdan, M. K., and Kuo, K. K., "Erosive Burning of Solid Propellants," Chapter 10 (pp 515-598), Fundamentals of Solid Propellant Combustion, Editors: Kuo, K. K., and Summerfield, M., AIAA, NY, NY, 1984.

5. Parkinson, R. C., and Penny, P. D., "Boundary-Layer Models of Erosive Burning," Paper 10, AGARD Conference on Solid Rocket Motor Technology, Oslo, Norway, Apr 2-5, 1979 (AGARD CP-259).

6. Parkinson, R. C., "Erosive Burning as a Boundary Layer Phenomenon in Rocket Motors," AIAA Paper 80-1208, AIAA/SAE/ASME 16th Joint Propulsion Conference, Hartford, CT, June 30 - July 2, 1980.

7. Traineau, J-C., and Kuentzman, P., "Ultrasonic Measurements of Solid Propellant Burning Rates in Nozzleless Rocket Motors," Journal of Propulsion and Power, 2, 3, pp 213-222, May-Jun. 1986.

8. Beddini, R. A., "Reacting Turbulent Boundary-Layer Approach to Solid Propellant Erosive Burning," AIAA Journal, 16, 9, pp 898-905, Sept. 1978.

9. Beddini, R. A., "Aerothermochemical Analysis of Erosive Burning in a Laboratory Solid-Rocket Motor," AIAA Journal, 18, 11, pp 1346-1353, Nov. 1980.

10. Beddini, R. A., "On the Scaling of Solid Propellant Erosive Burning: The Threshold Condition," 15th JANNAF Combustion Meeting, CPIA Publ. 297, Vol. II, p. 199, Feb. 1979.

11. Culick, F. E. C., "Rotational Axisymmetric Mean Flow and Damping of Acoustic Waves in a Solid Propellant Rocket," AIAA Journal, 4, 8, p 1462, Aug. 1966.

12. Yamada, K., Goto, M., and Ishikawa, N., "Simulative Study on the Erosive Burning of Solid Rocket Motors," AIAA Journal, 14, 9, p 1170, Sept. 1976.

13. Dunlap, R., Willoughby, P. G., and Hermsen, R. W., "Flowfield in the Combustion Chamber of a Solid Propellant Rocket Motor," AIAA Journal, 12, 10, p 1440, Oct. 1974.

14. Kutatladze, S. S., and Leont'ev, A. I., Turbulent Boundary Layers in Compressible Gases, Academic Press, NY, 1964.

15. Viles, J. M., "Prediction of Rocket-Motor Chamber Pressures using Measured Erosive-Burning Rates," Technical Report S-275 (Contract DAAH01-70-C-0152) Rohm and Haas Co., Huntsville, Alabama 35807, Oct. 1970.

16. Zucrow, M. J., Osborn, J. R., and Murphy, J. M., "An Experimental Investigation of the Erosive Burning Characteristics of a Nonhomogeneous Solid Propellant," AIAA Journal, 3, 523, 1965.

17. Vilyunov, V. N., Dvoryashin, A. A., Margolin, A. D., Ordzhonikidze, S. K., and Pokhil, P. F., "Burning of Ballistite Type H in Sonic Flow," Fizika Goreniya i Vzryva, 8, 4, 501-5, Oct.-Dec. 1972.

18. Saderholm, C. A., "A Characterization of Erosive Burning for Composite H-Series Propellants," AIAA Solid Propellant Rocket Conference, Palo Alto, California, Jan. 29, 1964.

19. Green, L., "Erosive Burning of Some Composite Solid Propellants," Jet Propulsion, 24, pp 9-15, 1954.

20. Kreidler, J. W., "Erosive Burning: New Experimental Techniques and Methods of Analysis," AIAA Paper 64-155, Solid Propellant Rocket Conference, Palo Alto, CA, Jan. 1964.

21. Peretz, A., "Investigation of the Erosive Burning of Solid-Propellant Grains with Variable Port Area by Means of Interrupted Burning Experiments," Israel Journal of Technology, 3, pp 94-101, 1965.

22. Strand, L., and Cohen, N., "Erosive Burning Threshold Conditions in Solid Rocket Motors," AIAA Paper 89-2528, AIAA/ASME/SAE/ASEE 25th Joint Propulsion Conference, Jul. 1989.

23. Strand L., Nguyen, M. H., and Cohen, N. S., "The Scaling of the Threshold Conditions for Solid Propellant Erosive Burning," AIAA Paper 88-3254, AIAA/ASME/SAE/ASEE 24th Joint Propulsion Conference, Jul. 1988.

24. Waesche, W., and O'Brien, W. F., "Evaluation of Techniques for Direct Measurement of Burning Rates in Nozzleless Motors," 24th JANNAF Combustion Meeting, CPIA Publication 476, Vol. I, pp 281-292, Oct. 1987.

25. Stokes, B. B., Hessler, R. O., and Caveny, L. H., "Erosive Burning of Nonmetallized Composite Propellants," 13th JANNAF Combustion Meeting, CPIA Publication 281, Vol. II, pp 437-451, Sept. 1976.

26. Razdan, M. K., and Kuo, K. K., "Measurements and Model Validation for Composite Propellants Under Crossflow of Gases," AIAA Journal, 18, 6, pp 669-677, Jun. 1980.

27. King, M., "Erosive Burning of Composite Propellants," 13th JANNAF Combustion Meeting, Monterey, California, CPIA Publ. 281, Vol. II, p 407, Sept. 1976.

28. Peretz, A., "Experimental Investigation of the Erosive Burning of Solid Propellant Grains with Variable Port Area," AIAA Journal, 6, 910, 1968.

29. Dickinson, L. A., Jackson, F., and Odgers, A. L., "Erosive Burning of Polyurethane Propellants in Rocket Engines," Eighth Symposium (International) on Combustion, 754, Williams and Wilkins, Baltimore, 1962.

30. Schultz, R., Green, L., and Penner, S. S., "Studies of the Decomposition Mechanism, Erosive Burning, Sonance and Resonance for Solid Composite Propellants," Combustion and Propulsion, 3rd AGARD Colloquium, Pergamon Press, NY, 1958.

31. King, M. K., "Experimental and Theoretical Study of the Effects of Pressure and Crossflow Velocity on Composite Propellant Burning Rate," Eighteenth Symposium (International) on Combustion, The Combustion Institute, Pittsburgh, PA, pp 207-215, 1981.

32. King, M. K., "Predicted and Measured Effects of Pressure and Crossflow Velocity on Composite Propellant Burning Rate," 17th JANNAF Combustion Meeting, CPIA Publication 329, Vol. I., pp 99-122, Nov. 1980.

33. King, M. K., "An Investigation of the Effects of Formulation Parameters on Erosive Burning of Composite Propellants," 16th JANNAF Combustion Meeting, CPIA Publication 308, Vol. II, pp 171-191, Dec. 1979.

34. Lenoir, J. M., and Robillard, G., "A Mathematical Method to Predict the Effects of Erosive Burning in Solid-Propellant Rockets," Sixth Symposium (International) on Combustion, 663, Reinhold Publishing Corp., New York, 1957.

35. Zucrow, M. J., Osborn, J. R., and Murphy, J. M., "The Erosive Burning of a Nonhomogeneous Solid Propellant," AICHE Symposium Series No. 52, 23-29, 1964.

36. Saderholm, C. A., Biddle, R. A., Caveny, L. H., and Summerfield, M., "Combustion Mechanisms of Fuel Rich Propellants in Flow Fields," AIAA Paper No. 72-1145, presented at AIAA/SAE 8th Joint Propulsion Specialist Conference, New Orleans, Louisiana, Nov. 29, 1972.

37. Lengelle, G., "Model Describing the Erosive Combustion and Velocity Response of Composite Propellants," AIAA Journal, 13, 3, 315-322, Mar. 1975.

38. Corner, J., Theory of the Interior Ballistics of Guns, John Wiley and Sons, Inc., New York, 1950.

39. Vandenkerchove, J., "Erosive Burning of a Colloidal Solid Propellant," Jet Propulsion, 28, 599, 1958.

40. Zeldovich, Y. B., "Theory of Propellant Combustion in a Gas Flow," Fizika Goreniya i Vzryva, 7, 4, 463-76, Oct.-Dec. 1971.

41. Geckler, R. E., et. al, Aerojet Engineering Corporation Report 455, 1950.

42. Parkinson, R. C., and Penny, P. D., "A Transpired Boundary Layer Model of Erosive Burning," AIAA Paper 78-980, AIAA/SAE 14th Joint Propulsion Conference, Jul. 1978.

43. Tsuji, H., "An Aerothermochemical Analysis of Erosive Burning of Solid Propellant," Ninth International Symposium on Combustion, 384-393, 1963.

44. Klimov, A. M., "Erosive Burning of Propellants," Combustion, Explosion and Shock Waves, 11, 5, p 678, Oct. 1976. (Translated from Fizika Goreniya i Vazyva, 11, 5, p 793, Sep.-Oct. 1975.)

45. Molnar, O., "Erosive Burning of Propellant Slabs," AIAA/SAE 8th Joint Propulsion Specialist Conference, New Orleans, Louisiana, AIAA Paper 72-1108, Nov. 1972.

46. Miller, E., "Erosive Burning of Composite Solid Propellants," Combustion and Flames, Vol. 10, p 330, Dec. 1966.

47. King, M., "A Modification of the Composite Propellant Erosive Burning Model of Lenoir and Robillard," Combustion and Flame, 24, 365-368, 1975.

48. King, M. K., "Erosive Burning of Composite Solid Propellants: Experimental and Modeling Studies," Journal of Spacecraft and Rockets, 16, 3, pp 154-162, May-Jun. 1979.

49. Razdan, M. K., and Kuo, K. K., "Erosive Burning Study of Composite Solid Propellants by Turbulent Boundary Layer Approach," AIAA Journal, 17, 11, pp 1225-1233, Nov. 1979.

50. Razdan, M. K., and Kuo, K. K., "Turbulent Flow Analysis of Erosive Burning of Cylindrical Comdposite Solid Propellants," AIAA Journal, 20, 1, pp 122-128, Jan. 1982.

51. Kamath, H., Arora, R., and Kuo, K. K., "Erosive Burning Measurements and Predictions for a Highly Aluminized Composite Solid Propellant," AIAA Paper 82-1111, AIAA/SAE/ASME 18th Joint Propulsion Conference, Jun. 1982.

52. Wu, X., Kumar, M., and Kuo, K. K., "A Comprehensive Erosive Burning Model for Double-Base Propellants in Strong Turbulent Shear Flow," Combustion and Flame, 53, pp 49-63, 1983.

53. King, M. K., "A Model of Erosive Burning of Composite Propellants," Journal of Spacecraft and Rockets, 15, 3, pp 139-146, May-Jun. 1978.

54. King, M. K., "A Model of the Effects of Pressure and Crossflow Velocity on Composite Propellant Burning Rate," AIAA Paper 79-1171, AIAA/SAE/ASME 15th Joint Propulsion Conference, Jun. 18-20, 1979.

55. King, M. K., "Model for Prediction of Double-Base Propellant Burn Rate Including Crossflow Effects," AIAA Journal, 20, 10, pp 1432-1439, Oct. 1982.

56. King, M. K., "A Burning Rate Model for Double-Base Propellants With and Without Product Crossflow," Paper No. 7, First Specialists Meeting (International) of the Combustion Institute, Vol. I, Section Francaise du "Combustion Institute," pp 37-42, Jul. 1981.

57. Renie, J. P., Condon, J. A., and Osborn, J. R., "Oxidizer Size Distribution Effects on Propellant Combustion," AIAA Journal, 17, pp 877-883, Aug. 1979.

58. Renie, J. P., Barger, M. E., and Osborn, J. R., "Effect of Erosive Burning on Pressure and Temperature Sensitivity," 16th JANNAF Combustion Meeting, CPIA Publication 308, Vol. II, pp 153-169, Sept. 1979.

59. Renie, J. P., and Osborn, J. R., "Erosive Burning," AIAA Journal, 21, 12, pp 1681-1689, Dec. 1983.

60. Van Driest, E. R., "On Turbulent Flow Near a Wall," Journal of Aeronautical Science, 23, pp 1007-1011, Nov. 1956.

61. Cebeci, T., and Chang, K. C., "Calculation of Incompressible Rough-Wall Boundary-Layer Flows," AIAA Journal, 16, pp 730-735, Jul. 1978.

62. Mickley, H. S., and Davis, R. S., "Momentum Transfer for Flow Over a Flat Plate With Blowing," NACA Technical Note 4017, Nov. 1957.

63. King, M., "Model for Steady State Combustion of Unimodal Composite Solid Propellants," AIAA Paper 78-216, Jan. 1978.

64. Beckstead, M. W., Derr, R. L., and Price, C. F., Thirteenth Symposium (International) on Combustion, p 1047, the Combustion Institute, 1971.

65. Waesche, R. H. W., and Wenograd, J., "Calculation of Solid Propellant Burning Rates from Condensed-Phase Decomposition Kinetics," AIAA paper 69-145, Jan. 1969.

66. Burke, S. P., and Schumann, T. E. W., Ind Eng Chem, 20, 998 (1928); also First/Second Symposium Combustion, p 2, The Combustion Institute, Reprinted 1965.

67. Glick, R. L., and Condon, J. A., "Statistical Analysis of Polydisperse, Heterogeneous Propellant Combustion: Steady-State," 13th JANNAF Combustion Meeting, CPIA Publication No. 281, Vol. II, p 313, Dec. 1976.

68. Beckstead, M. W., "A Model for Solid Propellant Combustion," 14th JANNAF Combustion Meeting, CPIA Publication No. 292, Vol. I, p 281, Dec. 1977.

69. Belyaev, A. F., Frolov, Yu, V., and Korotkov, A. I., Fizika Goreniya i Vzryva, 4, 3, 323-329, 1968.

70. Marshall, R. L., Pellet, G. L., and Saunders, A. S., "An Experimental Study of the Drag Coefficient of Burning Aluminum Droplets," Air Force Rocket Propulsion Laboratory Report AFRPL-TR-67-223, Vol. II, p 843, Aug. 1967.

71. Kays, W. M., and Moffat, R. J., "The Behavior of Transpired Turbulent Boundary Layers," Report HMT-20, Thermosciences Division, Dept. of Mech. Eng., Stanford Univ., Stanford, CA, Apr. 1975.

72. Rice, O. K., and Ginell, R., J. Phys. Chem., 54, pp 885-917, 1950.

73. Beckstead, M. W., AIAA Paper 80-1164, AIAA/SAE/ASME 16th Joint Propulsion Conference, Jul. 1980.

74. Aoki, I., and Kubota, N., AIAA Paper 80-1165, AIAA/SAE/ASME 16th Joint Propulsion Conference, Jul. 1980.

75. Miller, R. R., and Foster, R. L., Personal Communication, Hercules/ABL, Cumberland, MD, 1980.

76. Burick, R. J., and Osborn, J. R., 4th ICRPG Combustion Conference, CPIA Publication 162, Vol. II, pp 57-69, Dec. 1967.

77. Arora, R., Wu, X., White, F. X., and Kuo, K. K., "Erosive Burning of Composite Solid Propellants: Mechanism, Correlation, and Grain Design Applications," Journal of Spacecraft and Rockets, 20, 1, pp 43-48, Jan.-Feb. 1983.

78. King, M. K., "Prediction of Burning Rates in Nozzleless Rocket Motors," Journal of Spacecraft and Rockets, 22, 4, pp 394-395, Jul.-Aug. 1985. (Also AIAA Paper 82-1200.)

EFFECTS OF WIRES ON SOLID PROPELLANT BALLISTICS

Merrill K. King
4634 Tara Drive
Fairfax, Virginia 22032
USA

SUMMARY

Metallic wires have been employed in numerous end-burning solid propellant rocket motors over the last thirty years to provide desired burning rate amplifications needed for certain applications. These wires provide such amplification by serving as a thermal "short-circuit" between the hot final products of the propellant combustion and the unburned solid material, with resultant development of cones penetrating into the propellant adjacent to the wires (creating an increase in burning surface area) which lead the propellant regression. A brief review of models developed by others and of a systematic data base as regards burning of wired strands is presented. The major emphasis o this lecture, however, is modeling activity carried out by the author during the last two years. First, a model of the processes by which wires amplify the burning of strands (at fixed pressure) was developed and applied to analysis of the systematic data base referred to above, with excellent agreement being found between predicted and measured effects of wire type, wire diameter, and pressure on quasi-steady-state burning rates. This model is also capable of treating unsteady-state phenomena and the effects of local (sporadic) gaps between wire and propellant, caused by partial wire unbonds from the surrounding propellant (possibly resulting from extreme temperature cycling). Accordingly, the strand model was subsequently coupled wih a chamber ballistic analysis and a geometrical analysis as regards cone shape evolution to permit prediction of pressure-time histories in wired motors with various dstributions along the wire of gaps between the wire and the propellant.

LIST OF SYMBOLS

$A_{s,Total}$	total propellant surface area (cone plus flat)
A_t	throat area
C_D	propellant product discharge coefficient
$C_{p,wire}$	wire specific heat
$C_{p,prod}$	propellant product specific heat
D_{wire}	wire diameter
$h_{contact}$	heat transfer coefficient between wire and propellant
k_{prop}	thermal conductivity of propellant
M	product molecular weight
$\dot{M}_{in}$	mass generation rate of propellant products
$\dot{M}_{out}$	mass flow rate out of motor
P	motor pressure [f(t)]
R	universal gas law constant
q"	heat flux into wire from gas or propellant [f(t,z)]
r	radius (Fig. 1)
r_{wire}	wire radius
r'_b	burning rate
r'_{298}	burning rate at 298K
r'_{matrix}	matrix (unwired propellant) burning rate
r'_{wire}	burning rate of propellant along wire
t	time
T	temperature
T_{gas}	product gas temperature
T_{auto}	propellant autoignition temperature
T_{prop}	local temperature in propellant [f(t,z,r)]
$T_{prop,interface}$	propellant temperature at wire interface [f(t,z)]
T_{wire}	wire temperature [f(t,z)]
T_{bulk}	propellant bulk (conditioning) temperature
$\tilde{T}$	temperature relative to propellant conditioning temperature ($T-T_{bulk}$)
$\tilde{T}_{prop,interface}$	$T_{prop,interface} - T_{bulk}$
U_{wire}	velocity of product gases immediately adjacent to wire
u	average axial velocity of gases in cone
V_c	free volume of motor chamber [f(t)]
$V_{surface}$	velocity of gases leaving propellant surface (normal to surface)
z	axial direction (Fig. 1)
α_{prop}	propellant thermal diffusivity
β	constant in Eqn. 10
δ	penetration thickness of thermal wave associated with heat transfer from wire [f(t,z)]
Δ_{tj}	jth time increment
η	non-dimensional thermal penetration thickness [f(t,z)]
θ	cone angle (Fig. 1)
μ_{gas}	viscosity of product gases
ρ_{gas}	gas density
ρ_{prop}	propellant density
ρ_{wire}	wire density
σ_p	temperature sensitivity of matrix propellant burning rate

1. BACKGROUND

Solid propellants are generally burned in rocket motors in one of two basic configurations, either in the form of an end-burning grain or as a centrally perforated grain. In the end-burner (cigarette-burner) mode, a solid cylinder of propellant is ignited on one end face and burns back along the cylinder parallel to the centerline. In the centrally-perforated mode, the propellant cylinder contains a port along the

centerline (which may be a simple circular port or may have a much more complex shape such as a star or a wagon wheel) with burning being initiated on the inside of this port, followed by burnback through the cylinder radially to the motor wall. As might be expected, for typical tactical motor length/diameter ratios, the end-burning configuration tends to lead to relatively high action times, while the centrally-perforated configurations yield much shorter times. Due to limited variability of propellant burn rate via formulation adjustment (particularly in the presence of other design constraints) the motor designer sometimes finds himself in a situation where the action times achievable with an end-burner are unacceptably long, while those achievable with a centrally-perforated grain are unacceptably short (within given constraints on motor geometry) for his mission. (In addition, end-burning configurations lead to higher mass fractions, often of considerable importance, a factor driving the designer to prefer their use.) One way around the problem of excessively long action times for endburners is to embed metallic wires in the propellant, parallel to the motor centerline, to increase effective burning rate.

These embedded metallic wires lead to amplification of the mass burning rate by providing augmented heat feedback from the product gases to the propellant immediately adjacent to the wires, thus resulting in local burn rate increases in the direction along the wire with consequent formation of cones in the propellant with half-angles equal to the arcsine of the base propellant burn rate divided by burn rate along the wires. The propellant not immediately adjacent to the wire of course burns at its normal rate perpendicular to the cone surface, but because of the increased surface area associated with the cone, the mass generation rate and "effective" burn rate are increased. (See Figure 1.) An offshoot of this approach to burn rate enhancement is the use of chopped metallic fibers (oriented or unoriented) in formulations. (In the oriented-fiber approach, advanced casting technology is applied to cause the fibers to orient themselves preferentially parallel to the direction of burning.)

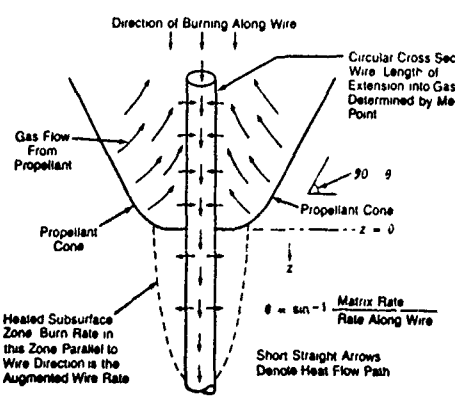

Figure 1 Schematic of Wired Propellant Combustion

Over the past thirty years, Atlantic Research Corporation has applied the approach of embedding metallic wires in end-burning propellant grains to enhance burning rates to a number of tactical solid rocket motors, the most notable of these being the Stinger Missile and its predecessor, the Redeye Missile, both shoulder-fired surface-to-air weapons. Additional applications include the MK30 (Terrier) Missile, the AGM-130, and the Tiger II.

Rumbel and coworkers at Atlantic Research[1-3] pioneered the use of embedded metallic wires to enhance solid propellant burning rates in the mid-1950s, first applying this technology to extrudable polyvinyl-chloride-based composite propellants (designated Arcites). In the course of these early studies, these investigators developed an extensive data base for two formulations, Arcite 155 and 322 (similar formulations differing only in ammonium perchlorate particle size and thus matrix burn rate versus pressure characteristics), utilizing wired strands of propellant burned in a pressurized bomb. This data base encompassed a wide range of pressures, wire diameters, and wire materials (silver, aluminum, copper, tungsten, platinum, molybdenum). It was found that the burning rate enhancement was for the most part proportional to the wire thermal diffusivity, with wire melting temperature having a secondary influence (higher melting point leading to higher rate). For very small diameter wires, burn rate enhancement was found to increase with increasing wire diameter, up to a diameter of about 5 mils (.0127 cm), with subsequent decrease in enhancement for further increases in wire diameter.

Subsequently, considerable additional (though not nearly as systematic) data on the effects of wires on burning rates of other composite propellants, notably polybutadiene-based systems, have been amassed at Atlantic Research. In general, however, these studies have been limited to one type of wire and one (or at most, two) sizes, with minor formulation adjustments being made in search of a specific wired rate for a specific application. In 1982, Kubota and coworkers[4] published a paper summarizing an experimental study of effects of embedded metal wires on the burning of a series of double-base propellants; wire materials used in this study included silver, tungsten, and nickel, with silver being studied most extensively. (This paper did not include enough information regarding the propellant characteristics to permit comparison of data with predictions by this lecturer's model, described in detail below.) The wire sizes utilized were all well in excess of 5-mil diameter; augmentation ratios were found to decrease with increasing wire diameter, consistent with the results of Rumbel, et al in this regime. In addition, augmentation ratio was seen to increase with increasing wire thermal diffusivity, again consistent with previous observations.

Hsing, Wa, and Kuo[5], in 1990, published results of a limited study of the effects of silver and copper wires on end-burning HTPB composite propellant grains in a motor, using an X-ray imaging system to track the development of cones around the wires. In their studies they found somewhat larger wire diameters for maximization of

burn rate augmentation, approximately 0.6 mm (25 mils) compared to the 5 mil optimum observed in the extensive studies of Rumbel, et al. As part of their work, Hsing and coworkers developed an empirical expression relating the burning rate augmentaion to the wire thermal diffusivity, wire size, base (unwired) rate, and effective spacing between wires (effective diameter influenced by a single wire).

As part of the early studies by Rumbel and coworkers,[2,3] a simplified heuristic model was developed to qualitatively explain the observed trends regarding effects of wire diameter and type on burning rate enhancement. This description did qualitatively describe the observations, but required artificial adjustments of parameters not calculated from first principles to actually fit the data. In addition, this model was strictly a steady-state one, incapable of treating transient effects, such as startup or encountering of contact resistances associated with local wire unbonds from the surrounding propellant.

In 1967, Caveny and Glick[6] published a paper describing the effects of embedded metal fibers (actually flat ribbons with a high ratio of one surface dimension to the other, leading to treatment of conduction of heat from the wire into the propellant as a one-dimensional process at each axial location along the wire) on the burning rate of solid propellants. In this analysis, they assumed that the burn rate along the wire is simply the rate at which the point along the wire at which the temperature is equal to some arbitrarily assigned "ignition temperature" propagates along the wire. (This is not to imply that the analysis is simple--it is not.) In addition, no consideration was given to the possibility of a "contact resistance" between the wire and the propellant, a likely result of wire/propellant unbonds which may well occur, for example, as a result of temperature cycling. This model is capable of treating transient effects, being mainly aimed at analysis of the effects of short chopped metallic fibers on burning rate.

Rybanin and Stesik[7] also analyzed the effects of flat heat-conducting elements on combustion of solid propellants, using an asymptotic solution approach; their analysis is limited to steady-state behavior. More recently, Gossant and coworkers[8] developed a simplified analysis of the effects of circular metal wires on propellant burning rate. Unfortunately, this model encompasses several simplifications which are strongly at odds with experimental observations, the most notable of which are an assumption that the wire does not project above the propellant surface into the gas and a second assumption that the temperature of the wire at the propellant surface is the melting temperature of the wire. With respect to the first assumption, movies of the burning of wired strands have shown that there is significant protrusion of the wires above the propellant surface; the second assumption comes to grief as regards the use of wires with high melting temperatures (e.g., tungsten) which would result in absurdly high propellant temperatures near the propellant-wire-surface interface.

2. OUTLINE OF INTEGRATED STUDIES BY THIS LECTURER

In the course of this lecturer's studies of the effects of wires on solid propellant burning rate, a model of the effects of wires on burning of strands with wires embedded along their centerlines was first developed.[9] This model was then checked/calibrated against the previously mentioned extensive data base of Rumbel, et al. Finally, the model was extended to treatment of motor ballistics in the presence of wires, with particular attention being paid to the possible effects of local gaps (along the length of the wire) between the wire and the surrounding propellant.[10,11]

3. WIRED STRAND MODEL DEVELOPMENT

In this analysis, circular cross-section wires were treated since these are by far the most commonly used in practice. A transient analysis, with an initially flat surface (θ = 90 degrees in Fig. 1) and an arbitrarily specified initial projection distance of the wire above the propellant surface was developed, utilizing the following general strategy.

First, the known product gas temperature and the initial temperature distribution in the wire (to date, the analysis is performed assuming the initial temperature throughout the wire to be equal to the propellant conditioning temperature) are used with a gas-phase heat transfer analysis (described later) to calculate the heat flux into the wire at each axial location along the part of the wire extending into the gas. This flux distribution is assumed to remain constant through one time step, which is calculated as the quotient of the user-input axial node spacing divided by the current burn rate along the wire (equal to the matrix rate for the first time step).

A transient analysis of the heat transfer along the wire and into the propellant (again described later) is then carried out for this first time step, yielding a resultant axial and radial distribution of temperature in the propellant at the end of the time step. The first axial increment of the propellant (increment closest to the surface) is dropped at this point, and the radial temperature distribution at the next node is used to calculate a mean temperature at the "new surface" across a radial thickness equal to three characteristic matrix thermal profile thicknesses (3 times propellant diffusivity divided by matrix burn rate). This mean temperature is then used with an expression relating burn rate to temperature (based on the matrix burn rate temperature sensitivity and autoignition temperature as described later) to calculate a new regression rate value along the wire. This rate is then used in combination with the matrix rate to calculate a new cone angle (θ = arcsine (Matrix Rate/Wire Rate)). The distribution of heat flux into the wire for the next time step is then calculated using the new temperature distribution in the exposed part of the wire and the new cone angle, a new time step is calculated as the quotient of the axial node spacing and the new burning rate along the wire, and the

transient heat transfer analysis in the wire and propellant is restarted and run for this new time increment. A new surface temperature radial distribution is thus defined as that at the next axial node at the end of this time increment, a new mean surface temperature and burning rate along the wire are calculated, and the next calculation loop is started. For calculation of a steady-state wired rate in strands, the analysis is repeated until an asymptotic limit rate is reached.

3.1 MAJOR ASSUMPTIONS/APPROXIMATIONS

At any given time step through the analysis, the geometry in the vicinity of the wire will have the generic shape of Fig. 1 (with, as mentioned, time zero representing a limiting case where $\theta = 90$ degrees and the cone walls are horizontal). This figure is instructive in listing the major assumptions/approximations associated with the analysis:

(1) Heat conduction in the propellant parallel to the wire (axial conduction) is neglected.

(2) The wire itself is assumed to be thermally thin (no radial temperature gradients in the wire).

(3) Gas-phase reaction contributions to the heat balance in the near-wire region are neglected.

(4) Radiative heat transport between the wire and surrounding flow is neglected. (Note that this is not the same as neglecting radiative heat feedback to the propellant surface in regions not directly affected by the wire - any contribution in this area is lumped into the empirically input matrix burning rate versus pressure characteristics.) An order-of-magnitude analysis indicates that for a typical wire diameter of 5 mils (0.0125 cm) with a mass flux along the wire of approximately 5 gm/cm^2/sec, the conductive/convective heat transfer coefficient between the wire and surrounding flow will be about 0.1 cal/cm^2/sec/K, which with a typical temperature difference of approximately 2000K leads to a heat flux into the wire of about 200 cal/cm^2/sec. With an emissivity-absorptivity product of unity, radiative transport, for a gas temperature of 2500K, will lead to a flux of about 50 cal/cm^2/sec, only one-fourth of the conductive/convective flux. Moreoever, for more realistic values of the emissivity-absorptivity product of 1 or less[12,13] (even for highly metalized propellants, which are not being treated in this study to date) radiative transport contributions will be less than 3 percent of the conductive/convective contributions.

(5) All propellant thermal properties are constant (temperature independent) and isotropic.

(6) All wire thermal properties are constant (temperature independent).

(7) All wire nodes which reach the melting temperature of the material are assumed to disappear (break off).

(8) It is assumed that a unique relationship exists between the burn rate along the wire and a mean temperature (calculated over three matrix thermal profile thicknesses around the wire) for any given formulation.

The last assumption requires further discussion. It is considered that the heating of the propellant adjacent to the wire is equivalent to local raising of the conditioning temperature of the propellant. Thus, for moderate values of "superheat," it is assumed that the matrix propellant burn rate temperature sensitivity (σ_p) can be used to calculate the augmented rate. However, available temperature sensitivity data in general are only good up to about 50 degrees (Kelvin) of superheat. Accordingly, it was decided to use the autoignition temperature of the propellant as an additional data point, with burn rate set equal to infinity at this temperature. It is assumed that the relationship between burning rate and "effective conditioning temperature" can be expressed in the form:

$$\frac{1}{r_b'} = k_1 + k_2 T + k_3 T^2 \qquad (1)$$

with the burn rate at 298K, the temperature sensitivity over a 50°K range, and the autoignition temperature being used to calculate k_1, k_2 and k_3 for a given formulation from:

$$\frac{1}{r_{298}'} = k_1 + 298\, k_2 + (298)^2 k_3 \qquad (2a)$$

$$\frac{1}{r_{298}' \exp(50\sigma_p)} = k_1 + 348\, k_2 + (348)^2 k_3 \qquad (2b)$$

$$0 = k_1 + T_{auto}\, k_2 + (T_{auto})^2 k_3 \qquad (2c)$$

Next, one is faced with the question of defining an appropriate temperature for use in Eqn. 1 for calculating the burning rate along the wire. One might consider using the surface temperature at the wire-propellant interface, but it seems apparent that this is not really appropriate since it represents the temperature of only an infinitesimal amount of propellant. (In addition, it can be shown that use of such a temperature will result in the predicted rate rising monotonically with decreasing wire diameter all the way to a wire diameter of zero, a result in conflict with observation (and with common sense).) It appears logical that a mean temperature over a thickness of propellant proportional to the characteristic matrix thermal profile thickness is more appropriate - a thickness equal to three times the propellant diffusivity divided by the matrix rate (equivalent to 95 percent of the total matrix thermal profile) was chosen as appropriate for the averaging process, giving:

$$\bar{T} = \int_{r_{wire}}^{r_{wire} + 3\alpha_{prop}/r'_{matrix}} r\,T\,dr \Big/ \int_{r_{wire}}^{r_{wire} + 3\alpha_{prop}/r'_{matrix}} r\,d\,r \qquad (3)$$

3.2 ANALYSIS OF HEAT TRANSFER INTO WIRE

An approximate analysis of the gas flow field in the cone surrounding the wire (Fig. 1) indicates that the velocity component parallel to the wire immediately adjacent to it is proportional to the bulk (average) axial velocity in the cone, with the proportionality constant depending on the cone angle, varying from unity for a flat surface (θ = 90 degrees) to approximately 2.0 for cone angles less than or equal to 45 degrees. In addition, the average axial velocity in the cone is related to the gas velocity leaving the cone surfaces by:

$$\bar{u} = \frac{V_{surface}}{\sin\theta} \qquad (4)$$

With substitution of $\sin\theta = r'_{matrix}/r'_{wire}$ and $\rho_{propellant}\, r'_{matrix} = \rho_{gas}\, V_{surface}$, the velocity adjacent to the wire can thus be expressed as:

$$U_{wire} = \frac{K\, V_{surface}\, r'_{wire}}{r'_{matrix}} = \frac{K \rho_{propellant}}{\rho_{gas}}\, r'_{wire} \qquad (5)$$

where K is a function of the cone angle ranging from 1.0 to 2.0. (An empirical fit to the results of the flow analysis is utilized for calculation of K for any given cone angle.)

The velocity adjacent to the wire is used in calculation of a friction factor and, using Reynolds' analogy, a heat transfer coefficient for heat transport from the product gases into the wire. Laminar flow equations are employed for a Reynolds' Number (based on wire diameter and axial velocity adjacent to the wire) of less than 2000, while a constant friction factor of 0.008 is used for higher Reynolds' Number values, leading to:

[Laminar]

$$q'' = \frac{4\, K\, C_{p,prod\ gas}}{D_{wire}} (T_{gas} - T_{wire}) \qquad (6a)$$

[Turbulent]

$$q'' = .008\, \rho_{prop}\, r'_{wire}\, C_{p,prod}\, (T_{gas} - T_{wire}) \qquad (6b)$$

[Slight modification of this analysis to allow for differences between the angle at the tip of the cone and the "average" angle over the entire cone was carried out during extension of the model to treatment of the effects of wires on motor ballistics.]

3.3 TRANSIENT THERMAL ANALYSIS OF WIRE AND PROPELLANT

Rigorous analysis of the transient heat transfer in the propellant and wire would be extremely difficult, even with the simplifying assumptions listed earlier, involving simultaneous treatment of axial derivative terms in the wire, radial derivative terms in the propellant, and time derivatives in both media. Accordingly, following the lead of Caveny[6], the author employed an integral method based on the work of Goodman[14] and Lardner and Pohle[15] to reduce the order of the problem by replacing the differential equations describing the radial heat transfer in the propellant with integral equations based on assumption of a fixed form for the shape of the radial temperature distribution in that region. With this approach, expressions relating the radial heat flux into the propellant at any given axial location and time to the current propellant temperature adjacent to the wire at that axial location and the time-integrated value of local flux up to that time can be used to replace rigorous analysis of the propellant region in supplying needed boundary conditions for solution of the partial differential equation (in time and axial coordinate) governing heat transfer in the wire. (It should be noted in passing that the integral analysis is somewhat more difficult to apply in the current cylindrical geometry than in the one-dimensional geometry treated in Caveny's analysis due to the transcendental nature of the integral equations in the cylindrical geometry case.)

Application of an unsteady-state heat balance to the wire results in the following partial differential equation in temperature (function of time and axial location) along the wire:

$$\rho_{wire} c_{p,wire} \frac{\partial T_{wire}}{\partial t} = k_{wire} \frac{\partial^2 T_{wire}}{\partial z^2} + \frac{4}{D_{wire}}\, q'' \qquad (7)$$

where the sign convention for q" is such that it represents heat flux into the wire at any axial location. (Recall the assumption of a thermally thin wire, which reduces the wire analysis to a one-dimensional transient problem through neglect of radial temperature gradients in the wire itself.) The boundary conditions for the part of the wire projecting into the gas product stream were discussed in the previous section. For the submerged part of the wire, the heat flux into the wire at any axial location may be expressed as:

$$q'' = h_{Contact}(T_{prop,interface} - T_{wire}) = k_{prop} \frac{\partial T_{prop}(r_{wire}, t)}{\partial r} \qquad (8)$$

where q", $T_{prop,interface}$, T_{wire}, $h_{contact}$, and $\partial T_{prop}/\partial r$ are all functions of axial location (z) and time. The integral method outlined below is used to relate q" (z,t) to

$T_{prop,interface}(z,t)$ at each axial location and time, and Eqn. 8 is then used to eliminate $T_{prop,interface}$ to establish a relationship between $q''(z,t)$ and $T_{wire}(z,t)$; Eqn. 7 can then be solved numerically using an implicit scheme involving solution of a tridiagonal matrix at each time step.

With neglect of axial temperature gradients in the propellant (Assumption 1) the governing equation for temperature distribution in the propellant at any axial location is:

$$\frac{\partial(rT)}{\partial t} = \alpha_{prop} \frac{\partial}{\partial r}\left(r\frac{\partial T}{\partial r}\right) \tag{9}$$

Following the method of Lardner and Pohle[15] for integral method analysis in cylindrical coordinates, it is assumed that the temperature profile shape at any given time and axial location may be expressed as:

$$\tilde{T} = T - T_{bulk} = \beta\left(\frac{\delta + r_{wire} - r}{r_{wire}}\right)^2 \ln\left(\frac{r}{r_{wire} + \delta}\right) \tag{10}$$

where $\delta(z,t)$ is the thermal wave thickness in the propellant and β is a constant determined by the boundary conditions. These boundary conditions are:

$$r = r_{wire} + \delta \;:\; \tilde{T} = 0\,,\quad \frac{\partial \tilde{T}}{\partial r} = 0$$
$$r = r_{wire} \;:\; q'' = k_{prop}\frac{\partial \tilde{T}}{\partial r} \tag{11}$$

Application of these boundary conditions, and substitution of $\eta(z,t) = (\delta(z,t) + r_{wire})/r_{wire}$ leads to:

$$\tilde{T} = \frac{(q''r_{wire}/k_{prop})(\eta - r/r_{wire})^2 \ln(r/r_{wire}\eta)}{(\eta-1)(2\ln\eta + \eta - 1)} \tag{12}$$

which when evaluated at the propellant-wire interface ($r = r_{wire}$) yields:

$$\tilde{T}_{prop,interface} = \frac{-(q''r_{wire}/k_{prop})(\eta-1)\ln\eta}{2\ln\eta + \eta - 1} \tag{13}$$

Integration of both sides of Eqn 9 over the thermal wave thickness (r_{wire} to $r_{wire} + \delta$), followed by substitution of the flux boundary condition at the wire-propellant interface (second part of Eqn. 8) and considerable mathematical manipulation leads to an expression relating the thermal profile thickness at a given time, the flux at that time, and the time integral of the flux up to that time (all at a given axial location):

$$-\alpha_{prop}/r^2_{wire}\,q'' \int_0^t q''dt = f(\eta) \tag{14}$$

where

$$f(\eta) = \frac{(\eta^2 - 96\eta + 36)\ln\eta + 36\eta^2 - 13\eta^4 - 32\eta + 9}{144(\eta-1)(2\ln\eta + \eta - 1)} \tag{15}$$

The heart of the integral analysis lies in breaking the integral of Eqn. 14 down to:

$$\int_0^t q''dt = \int_0^{t-\Delta t_j} q''dt + \frac{q''(t-\Delta t_j) + q''(t)}{2}\Delta t_j \tag{16}$$

with the integral on the right-hand side of the equation being updated and stored at each time step.

A brief outline of the procedure for analyzing heat transport in the wire and propellant using the integral method for the propellant follows. For any time step (Δt_j) new values of T_{wire} are calculated at each axial node along the wire using one time step of numerical integration of Eqn. 7 with the old (previous time step) flux values (lagging solution). New values of propellant temperature at the wire-propellant interface, η (dimensionless thermal wave penetration), and flux are then calculated at each axial location using Eqns 13-16 along with the first part of Eqn. 8 in a trial-and-error-loop calculation. (For cases with very small or no gap between the wire and propellant, the old flux values could be used to calculate the temperatures via Eqn. 8, with subsequent solution of Eqns. 13-16 for new flux values, but with gaps of more than a few microns, this simpler procedure was found to break down.) The new values of flux are then used to update the flux-time integrals at each node and are also used as boundary conditions in treatment of the next time step in the integration of Eqn. 7 with respect to time.

3.4 TREATMENT OF MELTING WIRE EFFECTS

Some of the wire materials employed in wired propellant grains have fairly low melting points (e.g., 930°K for aluminum, 1230°K for silver, 1355°K for copper); early calculations with a computer code based on the analysis described in the preceding sections showed that these temperatures would be quickly exceeded at the outer reaches of the exposed wires as the propellant receded back around them. It is postulated that the shear forces associated with the product flow along the wires (out of the cones) will instantaneously remove any wire nodes whose temperature rises above the melting point of the material being used. Accordingly, the code was modified to drop at each time step any wire nodes predicted to rise above the melting temperature during the preceding time increment. In this analysis, the heat of melting is straightforwardly decremented from the heat balance on the wire via modification of the wire tip boundary condition to include a heat of melting term for the mass associated with the dropped nodes.

3.5 COMPARISON OF MODEL PREDICTIONS WITH STRAND DATA

As indicated earlier, an extensive data base on the effects of wires on propellant

burning rates was developed by Rumbel, et al for two polyvinylchloride-ammonium perchlorate solid propellant formulations in the 1950's. In this investigation, in which wired propellant strands were burned in a pressurized bomb, wire type, wire diameter, and pressure were systematically varied independently; thus, this data base provides an excellent test vehicle for the model described above. In addition, data obtained more recently by Atlantic Research for a polybutadiene-based composite propellant are examined. Compositions for the three formulations studied along with propellant properties needed for model inputs are given in Table I. As may be seen, the two polyvinyl chloride formulations (Arcites 155 and 322) are nearly identical, differing only in ammonium perchlorate size distribution (and thus matrix burning rate). Data obtained with six different wire materials (silver, copper, tungsten, platinum, aluminum, and molybdenum) were compared to model predictions in this study; properties of these materials required as model inputs are tabulated in Table II.

As mentioned in discussion of the model development, allowance was made in the model for a finite contact resistance (variable with axial distance along the wire via user input) between the wire and propellant to permit simulation of the effects of gaps resulting from wire unbonds (caused in motor situations, for example, by temperature cycling resulting in different expansions/contractions of the propellant and the metallic wires which tend to have large differences in coefficients of thermal expansion). All calculations presented in this section were performed using a negligible contact resistance (very high value of $h_{contact}$) under the logical assumption that no such unbonds were present with the wired strands. In all cases, the model was run until an asymptotically limiting value of burn rate along the wire was achieved (generally at 0.5 to 1.0 cm of total regression along the wire).

The one needed propellant property which is not well documented (and, in fact, not even very well defined) is the autoignition temperature, required for evaluation of the constants appearing in the burning rate versus temperature equation (Eqn. 1). Discussions with various propellant developers indicate that physically realistic values of this parameter probably are bounded by 450 and 600°K (350-620°F). A rough optimization of choice of value for this parameter was carried out by comparison of model predictions with data obtained at 1000 psia with various diameter tungsten wires, resulting in a chosen value for autoignition temperature of 520°K (475°F) for the Arcites. Sensitivity of predicted augmentation ratios (wired rate/matrix rate) to this parameter was examined; results of this sensitivity study for 3 mil diameter tungsten wires in Arcite 155 are presented in Fig 2. As may be seen, variation of the autoignition temperature value from 480 to 560°K (± 40°K around the selected 520°K value) leads to a variation in augmentation ratio from 4.8 to 2.9 (± 30 percent around the 3.65 value). Thus it may be seen that the sensitivity of predicted wired rates to this parameter, while not overwhelming, is certainly not negligible; further information for fitting of the constants in Eqn. 1 (for example, temperature sensitivity data out to much higher temperatures than normally examined) would be highly desirable.

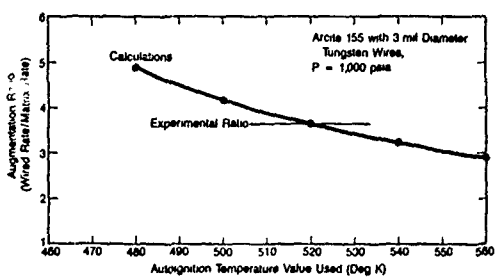

Figure 2 Sensitivity of Calculated Wired Propellant Burn Rate to Input Autoignition Temperature

In Table III, predicted 1000 psia burning rates and augmentation ratios are compared with data for Arcite 322 containing 5 mil diameter wires of different materials (silver, copper, tungsten, platinum, and aluminum). In all model runs, the autoignition temperature of the propellant is held at the 520°K value established from the earlier analysis of the tungsten wire data with Arcite 155. As may be seen, the model does a reasonably good job of predicting the effects of the various materials on wired burning rates, though it does overpredict the augmentation ratio by about 17 percent for silver and 27 percent for aluminum, while underpredicting the effect of platinum by about 22 percent. It should be noted that the conductivity value used for aluminum may well be too high. It has been observed that electrical conductivity of aluminum is strongly decreased in the presence of even low levels of impurities, and it is generally found that thermal con-

Table 1. Propellant Properties of Formulations Examined

	Arcite 155, 322	Arcadene 426
Mixing* Composition	74.62 AP 12.44 PVC Resin 12.44 Dibutyl Sebacate 0.50 Stabilizer	45.0 AP 12.5 HTPB 2.5 Dioctyladipate
Flame Temperature (°K)	2,471	2,838
Product specific heat (cal/gm °K)	0.43	0.445
Density (gm/cm^3)	1.645	1.67
Propellant specific heat (cal/gm °K)	0.385	0.375
Propellant thermal conductivity (cal/cm sec K)	0.0006?	0.0007?
ρ (% per °K)	0.22	0.25
Matrix rates at 1,000 psia (cm/sec)	1.14, 1.27	1.70

Table 2. Wire Properties for Wire Materials Used

Material	Thermal Conductivity (cal/cm sec K)	Density (gm/cm^3)	Specific Heat (Cal/gm °K)	Thermal Diffusivity (cm^2/sec)	Melt Temperature (°K)	Heat of Melting (cal/gm)
Silver	0.95	10.50	.088	1.33	1,230	26
Copper	0.90	8.92	.106	0.95	1,355	50
Tungsten	0.42	19.35	.035	0.62	3,950	46
Platinum	0.28	21.45	.038	0.37	2,030	24
Aluminum	0.55	2.70	.214	0.70	930	95
Molybdenum	0.35	10.20	.070	0.49	3,160	73

Table 3. Comparison of Predicted and Experimental Burn Rates for Arcite 322 with Various 5 mil Diameter Wires at P = 1,000 psia

Wire Type	Burn Rate (cm/sec) Expt.	Burn Rate (cm/sec) Calc.	Augmentation Ratio Expt.	Augmentation Ratio Calc.	
Silver	6.73	7.85	5.30	6.18	(17% High)
Copper	5.89	5.40	4.63	4.25	(8% Low)
Tungsten	4.62	4.39	3.64	3.46	(5% Low)
Platinum	3.71	2.88	2.92	2.27	(22% Low)
Aluminum	2.95	3.75	2.32	2.95	(27% High)

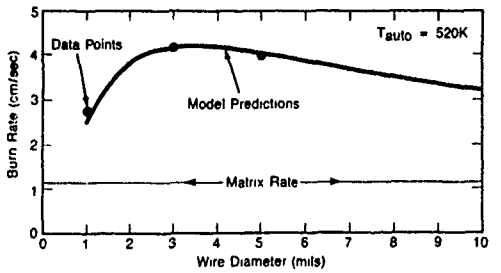

(a) Arcite 155 with Tungsten Wires, P = 1,000 psia

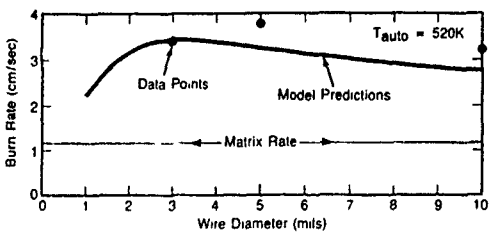

(b) Arcite 155 with Molybdenum Wires P = 1,000 psia

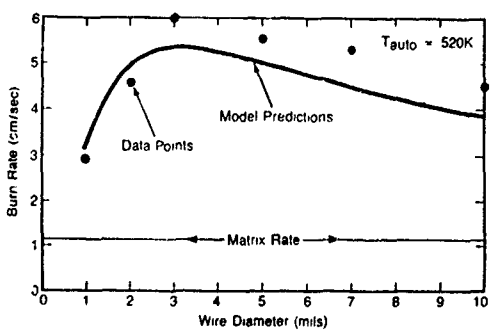

(c) Arcite 155 with Copper Wires, P = 1,000 psia

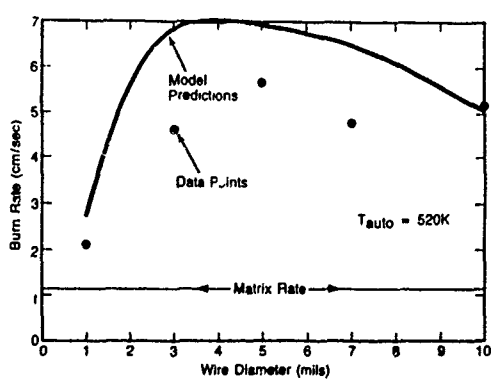

(d) Arcite 155 with Silver Wires, P = 1,000 psia

Figure 3 Predicted and Observed Effects of Various Wires on Burning Rate

ductivity tracks well with electrical conductivity. Thus, if there were impurities in the aluminum wire used the thermal conductivity may well have been lower than the value used in the modeling exercise; reduction of this value from 0.55 to 0.45 cal/cmsec °K would result in excellent agreement between model predictions and data.

In Fig. 3, predicted and experimental wired burning rates for Arcite 155 at 1000 psia are plotted against wire diameter for tungsten, molybdenum, copper, and silver wires. As may be seen, the model predicts the existence of a wire diameter for which the rate is maximized, with the rate rolling off fairly quickly for smaller diameters and more gradually for larger diameters; for the four wire materials studied, the rate-maximizing diameters are predicted to be 3 to 4 mils. In general, the model predictions agree reasonably well with the data both in terms of general magnitude of the wire effect and wire diameter dependency. With tungsten wires, agreement between theory and data is exellent while with molybdenum and copper the degree of agreement is certainly respectable. Even with silver wires the trends appear to be correctly predicted though the magnitude of the wire effect is overpredicted for silver wires as with Arcite 322. On the whole, the model predictions appear to be quite acceptable, particularly considering the lack of adjustable parameters.

A predicted burning rate versus pressure curve for Arcite 155 with 3 mil diameter tungsten wires is plotted along with five data points in Fig. 4; as may be seen, the degree of agreement is outstanding. In Fig. 5, a similar burning rate versus pressure presentation of data and predictions is made for Arcadene 426 with 10 mil diameter silver wires. Due to major differences in this formulation from the Arcites (Table I), it is reasonable to expect that the effective autoignition temperature of this propellant might well differ from the 520°K value used for the Arcites. Predicted burning rate versus pressure curves calculated using autoignition temperatures of 550, 600, and 620°K are presented, along with wired propellant and matrix data, in Fig. 5. It is observed that reasonably

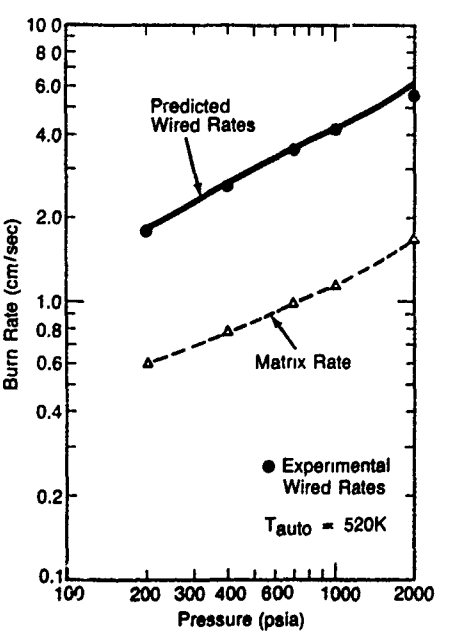

Figure 4. Arcite 155 with 3 mil Diameter Tungsten Wires

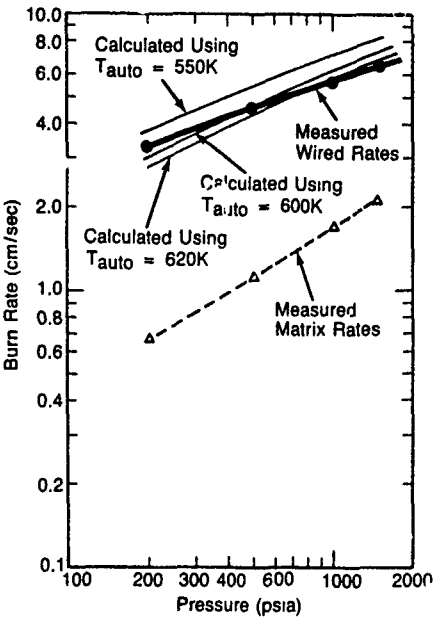

Figure 5. Arcadene 426 with 10 mil Diameter Silver Wire

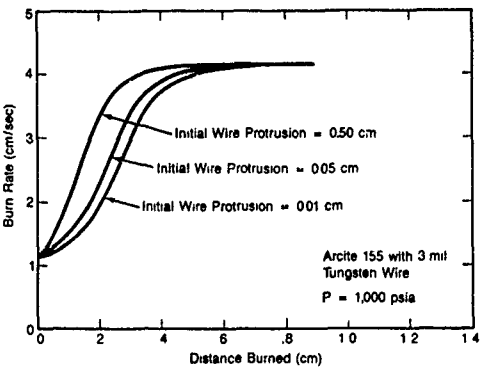

Figure 6. Examination of Effects of Initial Wire Protrusion on Burn Rate vs Distance Burned

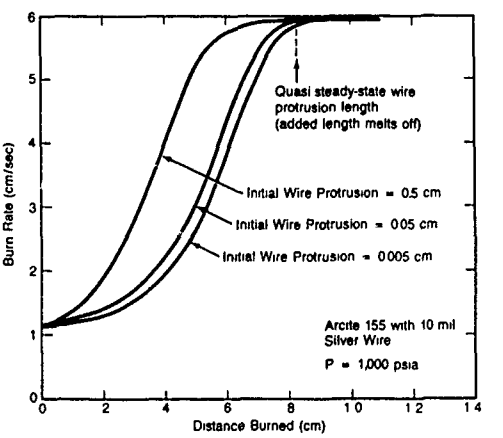

Figure 7 Examination of Effects of Initial Wire Protrusion on Burn Rate vs Distance Burned

good agreement between theory and data is found with T_{auto} = 600 or 620 degrees Kelvin, while use of T_{auto} = 550 degrees Kelvin leads to overprediction of augmentation ratio by about 15-20 percent. It should be recalled, however, that the effect of silver wires was overpredicted for the Arcite formulations. Thus it might be that the 550 degree value would prove to be more reasonable in predictions of Arcadene 426 behavior with other wire materials; unfortunately data for such a comparison have not been found.

Figures 6 and 7 demonstrate some of the transient prediction capability of the model described in this paper, as well as showing how the approach to the steady-state wired rate in a strand is influenced by the initial protrusion of the wire into the gas product stream above the initially flat surface. In Figure 6, burning rate of Arcite 155 at 1000 psia along a 3 mil diameter tungsten wire is plotted against cumulative distance burned for three different initial wire projections (.01, .05, and .50 cm). As might be expected, the burn rate asymptotes to the steady-state value in a shorter burnback distance for greater initial wire protrusion, with the required burnback distance varying from about 0.4 cm for the 0.50 cm initial protrusion to 0.6 cm for the 0.01 initial protrusion. Figure 7 presents similar results for a 10 mil diameter silver wire; since silver has a melting temperature of only 1230°K, well below the propellant flame temperature (unlike tungsten, whose melt temperature exceeds the flame temperature), it eventually attains a steady-state projection distance into the gas (approximately 0.83 cm as indicated in the figure) with one wire node melting and dropping off for each increment of propellant burned. Again, larger values of initial protrusion of the wire into the product gases lead to quicker approach to a steady-state burning rate along the wire.

3.6 PREDICTED EFFECTS OF GAPS ON WIRED STRAND RATES

Following completion of the calibration of the strand version of the wired burning rate model with respect to the data base described in the previous section, parametric studies of the effects of gaps between the wire and surrounding propellant on strand burning rate were carried out. Arcadene 426 burning at 200 psi with an embedded 10 mil diameter silver wire was arbitrarily chosen for these studies. An autoignition temperature for this formulation of 560°K, based on the rationale presented in the last section was used in generation of the results presented here; trends observed were only slightly affected by use of autoignition temperatures over the range presented in Fig. 5. In calculation of the heat transfer coefficient across the gap ($h_{contact}$ in Eqn. 8, the quotient of the thermal conductivity of the gap medium and the gap width) a value of 0.0001 cal/cm/sec/K was used for the thermal conductivity of the gap gases (corresponding to nitrogen at about 400°K), again somewhat arbitrarily. [Obviously, if a different value is chosen the results presented can be easily adjusted by ratioing gap widths proportionally to the conductivity values.]

In Fig. 8, the effect of the gap size on strand burning rate versus distance burned (again assuming an initially flat surface) is presented. Included for reference are the matrix rate for Arcadene 426 at 200 psi and the predicted burn rate versus distance burned for perfect contact between the wire and the propellant (no gap). As may be seen, the shapes of the curves for the various gap widths are somewhat similar, though the overshoot in burn rate predicted at zero or small gap width (resulting from the finite time required for the quasi-steady temperature profile in the wire to be established) does disappear for gap widths in excess of about 5-10 microns (0.2-0.4 mils). As also shown by this figure and Figure 9, the asymptotic strand rate decreases monotonically with increasing gap width, as expected, with the augmentation ratio (wired rate divided by matrix rate) decreasing from about 7 in the case of no gap to 4 for a 5 micron (0.2 mil) gap to 2 for a 33 micron (1.3 mil) gap.

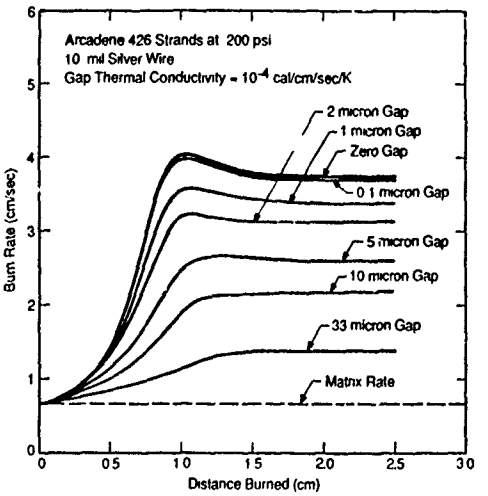

Figure 8. Effect of Gap Between Wire and Propellant on Burn Rate Versus Distance Burned

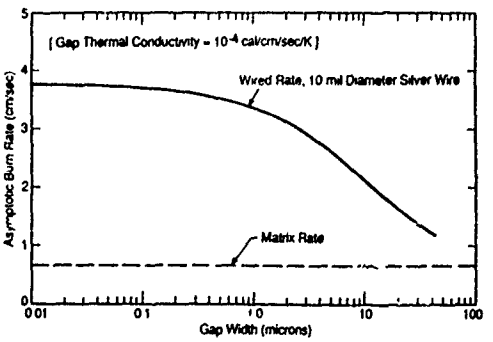

Figure 9 Effect of Gap Width on Asymptotic Strand Burn Rate For Arcadene 426 at 200 psi with 10 mil Silver Wire

In Figure 10, results of examination of the effects of step changes in gap size along the propellant strand are presented. In these studies, the gap width was held at zero for the first two centimeters along the strand, suddenly increased to some non-zero value and held constant at that value for the next 1.5 cm, and then suddenly returned to zero, representing a small local unbond region. Three gap widths (1, 2, and 5 microns) were examined. As the region with the gap is approached, the model predicts an upturn in the burning rate (due to less heat loss along the wire downstream of the beginning of the gap). As soon as the gap is reached, burning rate drops precipitously, wih a strong overshoot, before rebounding to the quasi-steady-state rate for the given gap width (compare the intermediate flat region to figures 8 and 9). Toward the end of the gap region the predicted rate decreases for a short period due to increased losses in the downstream region where the gap has returned to zero; a strong overshoot is then predicted just downstream of the end of the gap with, finally, an asymptotic return to the zero-gap burning rate. Thus, it may be seen that local gaps can have dramatic effects on predicted burn-rate versus distance burned along a strand, particularly for step changes in gap width.

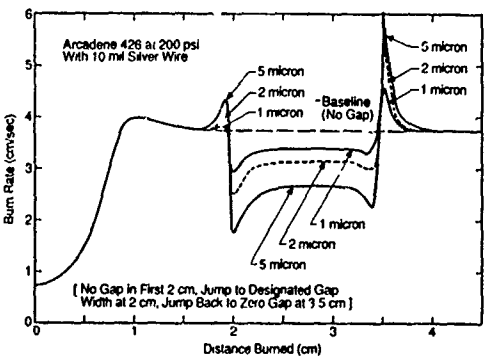

Figure 10 Effect of Step Changes in Gap Width on Strand Burn Rate Versus Distance Burned

It is recognized, however, that such step changes are somewhat idealized limiting cases; accordingly a second scenario as regards gap width distribution along a wire was studied. In this scenario (for which results are presented in Fig. 11), the gap is again held at zero for the first two centimeters along the wire, with a ramp up to a designated value over the next two

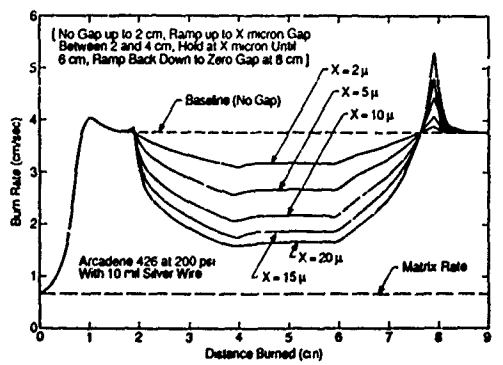

Figure 11. Effect of Ramp Changes in Gap Width on Strand Burn Rate Versus Distance Burned.

centimeters, followed by a hold at the designated value for the next two centimeters, and finally a ramp back to zero gap width over the next two centimeters. Designated gap width values examined in this part of the study were 2, 5, 10, 15, and 20 microns. As may be seen, overshoots are somewhat reduced (though not eliminated) by the more realistic use of ramp changes in gap width. The flat portions of the burning rate versus distance burned curves, appearing over most of the period of constant gap width, again agree well with the quasi-steady-state values for the corresponding gap widths presented in Figures 8 and 9.

4. EXTENSION OF MODEL TO CALCULATION OF MOTOR BALLISTICS

Extension of the model described above, developed for calculation of the effects of wires on propellant strand rates (fixed pressure) with and without gaps between the wire and the propellant, to treatment of motor ballistics (with time-dependent pressure and matrix rate) involves addition of geometric (cone development) and ballistic analysis steps (along with the slight modification of the analysis of heat transfer from product gases into the wire, alluded to earlier). For simplicity (at least at present) the motor analysis is currently limited to treatment of a cylindrical end-burning grain with a single wire down its center. (Gap width between the wire and surrounding propellant is allowed to vary with distance along the wire for parametric study of the influence of non-constant gaps on ballistics.)

4.1 MODEL DEVELOPMENT

As the propellant burns back along the wire, successive segments of propellant surface with orientations determined by the angle at the tip of the cone at the time of their generation are added to the developing cone. These segments subsequently burn back normal to their orientations at the pressure-dependent matrix burning rate (function of time through dependence of pressure on time). At each successive time point, each segment is moved back normal to its orientation by a distance equal to the product of the instantaneous matrix rate and the time increment, and new intersections of adjacent segments are calculated for definition of a new cone surface profile. (As part of this procedure, segments can of course disappear upon convergence of their normal bisectors - this is treated in the geometrical analysis.) As the intersection of the first segment generated with the remaining initial flat surface (which is of course also receding) moves outward, the motor wall is eventually reached (no more surface normal to the motor axis) and treatment of successive intersections of the cone with the wall is brought into the geometrical analysis.

Definition of the full shape of the cone and the amount of flat surface not yet engulfed (up to the point at which the cone intersects the wall) permits straightforward calculation of total propellant surface area at any given time. This value is then used in a simplified chamber ballistics analysis (in which product temperature variations due to pressurization/depressurization are neglected) to calculate the evolution of motor pressure and free volume with time using Eqns. 17-20.

$$\dot{m}_{in} = \rho_{prop} r'_{matrix} A_{s,Total} \tag{17}$$

$$\dot{m}_{out} = C_D A_t P \tag{18}$$

$$V_c \frac{M}{RT_{gas}} \frac{dP}{dt} = \dot{m}_{in} - \dot{m}_{out} \tag{19}$$

$$\frac{dV_c}{dt} = \dot{m}_{in}/\rho_{prop} \tag{20}$$

4.2 PREDICTION OF MOTOR PRESSURE BEHAVIOR

Next, the complete model, including treatment of cone shape development and motor chamber ballistics coupled with the analysis of wire heating effects on propagation of the cone tip along the wire was utilized in a limited study of the effects of wires on motor ballistic behavior, with and without the presence of gaps between wire and propellant. The Arcadene 426 propellant (Table I) with a single 10 mil diameter silver wire embedded along the motor axis was used for this study; motor parameters chosen are summarized in Table IV. A fairly small motor was used in this study since larger motors generally use more than one wire, a scenario not yet treatable with this model. An initially flat surface (no preconing) was assumed; the chosen motor parameters yield an initial motor pressure (steady-state pressure without the wire) of about three atmospheres. It should be noted that the pressure exponent of the chosen propellant is fairly high (0.577) leading to strong magnification of wire effects on motor operating pressure.

Table 4. Motor Parameters For Motor Pressure-Time History Cases Studied.

Arcadene 426 Propellant
10 mil Diameter Silver Wire
BR (cm/sec) = 0.149 $P^{0.577}$ (P in atmospheres)
Product MW = 24.65
C-Star = 4900 ft/sec
Throat Area = 0.041 cm^2
Motor ID = 1.5 cm
Initial Free Volume = 10 cm^3
Equil. Pressure w/o Wire = 2.938 atm
Initially, Flat Surface (No Precone)
One Wire

First, the effects of various constant gap widths between wire and propellant were examined; results are presented in Fig. 12 (pressure versus distance burned) and Fig. 13 (asymptotic pressure levels attained versus gap width). As may be seen from Fig.

12, the model predicts considerable (order of 20 percent) overshoot in pressure above the asymptotic value due to interactions between wire heatup processes and cone development processes. The asymptotic pressure level is predicted to decrease strongly with increasing gap width, due to a combination of the strong sensitivity of propagation rate along the wire to gap width (shown earlier) and the relatively high burning rate-pressure exponent.

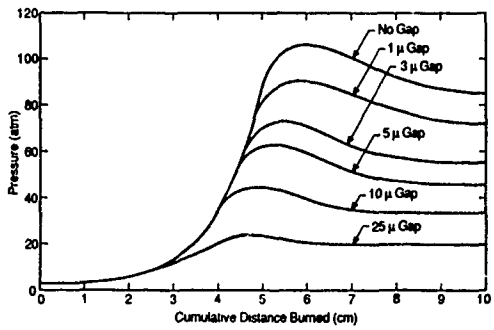

Figure 12 Baseline Motor Test Case - Various Gap Widths

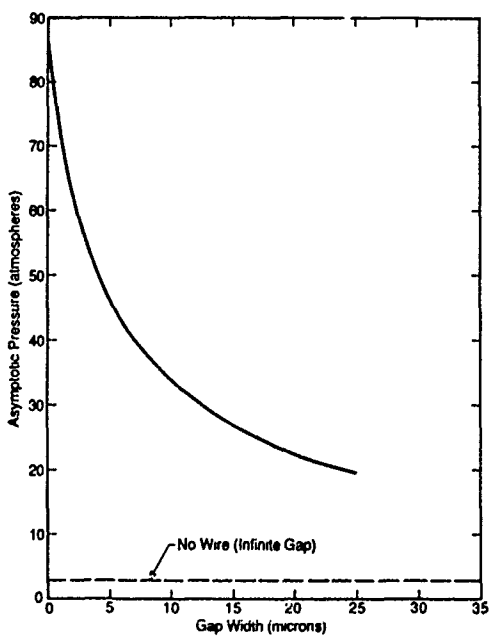

Figure 13. Asymptotic Equilibrium Pressure Versus Gap Width For Baseline Motor Test Case.

Finally, the effects of several scenarios as regards gap width distribution along the wire were examined; results of these studies are presented in the five-part Fig. 14. In each part of this figure, the gap width versus distance burned profile is presented at the bottom of the panel, with the resulting predicted pressure being presented at the top of the panel. (The first 8 cm of each case are omitted since the gap width in all cases was zero over this

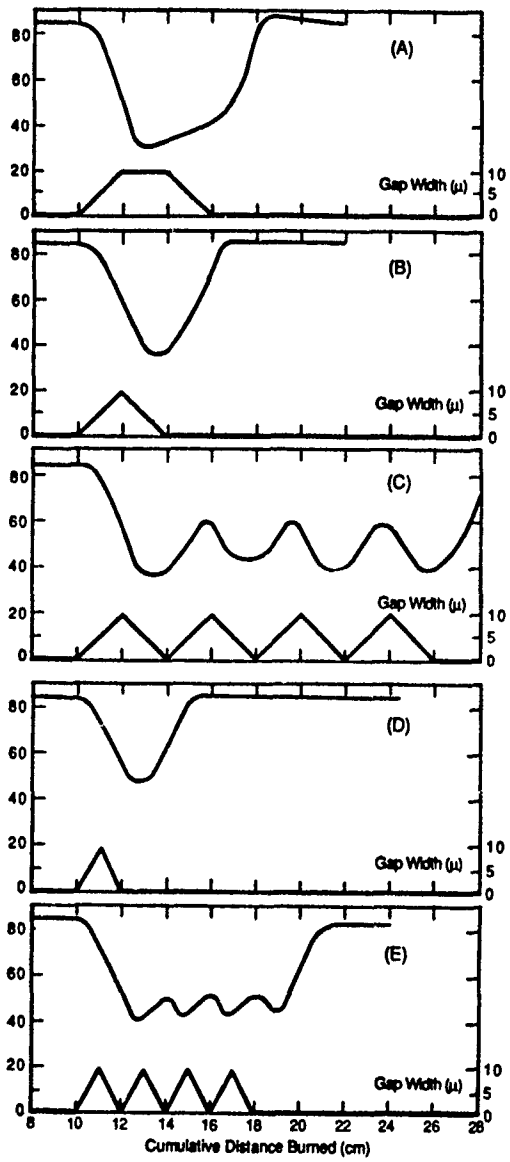

Figure 14.

Pressure (Atmospheres) Versus Cumulative Distance Burned for Various Gap Width Schedules.

portion of the run, leading to identical results). In all cases examined, the maximum gap width was 10 microns (0.4 mils).

As may be seen from Panel A, a 2 cm ramp up to 10 micron gap width, followed by 2 cm at this gap width, followed by a 2 cm ramp back to zero gap results in a slightly distorted pressure versus time pattern, with a modest undershoot in pressure relative to the 10 micron gap asymptotic value. With a 2 cm ramp-up followed by an immediate 2 cm ramp back to zero gap (Panel B) a fairly

regularly waveform is obtained, with pressure not quite dropping to the aymptotic value of 33 atm. associated with a 10 micron gap. Skipping to Panel D, where the ramp times are halved, we again see a regular waveform, but the minimum pressure produced in this case is even further above the 10 micron gap asymptotic value.

In Panels C and E, the effects of repeated sawtooth ramps corresponding to the single sawtooth patterns of Panels B and D are presented; as may be seen, approximately the same pressure minima are predicted, but the pressure does not return to anywhere near the zero-gap asymptotic value during the intermediate returns of gap width to zero, only returning to that value after cessation of the gap width cycling.

This preliminary study demonstrates that the existence of gaps between the wire and propellant in wired motors can have major impact on motor pressure behavior, with considerable variation of pressure with time and considerable reduction in average operating pressure (and thus mass flow and thrust). Such behavior has indeed been observed in high L/D wired motors which have been temperature cycled and then fired at low temperature conditions (but not when the motors are temperature cycled and fired at normal ambient or high temperature). It is suspected that the temperature cycling, due to large differences in thermal expansion coefficient of wire and propellant, leads to unbonds between wire and propellant causing sporadic gaps between the wire and the propellant which cannot relax back to zero gap at low temperature conditions where the propellant is considerably less elastic than at normal ambient or high temperature conditions.

REFERENCES

1. Rumbel, K.E., Cohen, M., Henderson, C.B., and Scurlock, A.C., "A Physical Means of Attaining High Burning Rate in Solid Propellants," Eleventh Army-Navy-Air Force Solid Propellant Meeting, May 1955, p. 155.

2. Grover, J.H., et al, Research and Development Programs in Fields of Solid Propellants and Interior Ballistics, Supplement to QPR No. 26, Report to US Navy Bureau of Ordnance, May, 1960.

3. Friedman, R., Henderson, C.B., and Rumbel, K.F., "Factors Governing Burning Characteristics of Composite Solid Propellant," 1959 JANAF Meeting.

4. Kubota, N., Ichida, M., and Fujisawa, T., "Combustion Processes of Propellants With Embedded Metal Wires," AIAAJ, 20, 1, January 1982, p. 116.

5. Hsing, Y., Wu, S., and Kuo, J., "Burning Rate of HTPB Composite Propellant Grains with Embedded Metal Wires," AIAA Paper 90-2201, AIAA/SAE/ASME/ASEE 26th Joint Propulsion Conference, Orlando, FL, July 16-18, 1990.

6. Caveny, L.H. and Glick, R.L., "Influence of Embedded Metal Fibers on Solid-Propellant Burning Rate," J Spacecraft and Rockets, 4, 1, January 1967, p. 79.

7. Rybanin, S.S. and Stesik, L.N., "Theory of Combustion of a Condensed Propellant With a Flat Heat-Conducting Element," Combustion, Explosion and Shockwaves, 10, 5, February 1976, p. 553.

8. Gossant, B., Godfrey, F., and Robert, P.H., "Theoretical Calculus of Burning Rate Ratio in Grains with Embedded Metal Wires," AIAA/ASME/SAE/ASEE 24th Joint Propulsion Conference, July 11-13, 1988, AIAA-88-3255.

9. King, M.K., "A Model of the Effects of Wires on Solid Propellant Burning Rate," 25th JANNAF Combustion Meeting, Huntsville, AL, Oct., 1988, CPIA Publication 498, Volume I, p. 95.

10. King, M.K., "Analytical Modeling of Effects of Wires on Solid Motor Ballistics," AIAA Paper 89-2784, AIAA/ASME/SAE/ASEE 25th Joint Propulsion Conference, Monterey, CA, July, 1989.

11. King, M.K., "Analytical Modeling of Effects of Wires on Solid Motor Ballistics," accepted for publication in late 1990 or early 1991 by Journal of Propulsion and Power.

12. Zennin, A.A., Glaskova, A.P., Leipunskyi, O.I., and Bobolev, V.K., "Effects of Metallic Additives on the Deflagration of Condensed Systems," Twelfth Symposium (Intl) on Combustion, The Combustion Institute, Pittsburgh, PA., 1969, p. 27.

13. Felton, R.F., and Hitchcock, J.E., "An Optical Technique to Measure Radiant Energy Incident on a Burning Solid Propellant Surface," AIAA 6th Thermophysics Conference, Tullahoma, TN, April 1971. AIAA Paper No. 71-469.

14. Goodman, T.R., "Applications of Integral Methods to Transient Nonlinear Heat Transfer," Advances in Heat Transfer, Academic Press, NY, NY, 1964, p. 52.

15. Lardner, T.J. and Pohle, F.V., "Application of the Heat Balance Integral to Problems of Cylindrical Geometry," Transactions of the ASME (Journal of Applied Mechanics), June 1961, p. 310.

INSTABILITES DE COMBUSTION

Paul KUENTZMANN

Office National d'Etudes et de Recherches Aérospatiales
29, Avenue de la Division Leclerc

92320 CHATILLON (FRANCE)

RESUME

L'apparition d'une instabilité de combustion lors de l'essai d'un moteur à propergol solide constitue toujours un événement majeur par ses possibles répercussions sur le délai et le coût de développement du système. Depuis plus de quarante ans, de nombreuses observations sur moteurs ont été accumulées, des méthodes d'analyse ont été développées pour comprendre et décrire les observations et des outils de prévision en ont été dérivés. Malgré des progrès significatifs, il arrive encore que des moteurs conçus stables se révèlent instables lors des premiers essais. Les outils de conception ne présentent donc pas encore le niveau de fiabilité requis par les industriels et des progrès restent nécessaires tant dans la compréhension des phénomènes que dans la mise au point d'outils améliorés de conception.

Cette conférence vise un bilan objectif de l'état des connaissances et des moyens, ainsi que la mise en évidence des phénomènes les plus critiques et des axes de recherche prioritaires. La première partie rappelle les notions générales sur les instabilités de combustion des moteurs à propergol solide et tente de dégager les lignes des approches les plus utilisées. La seconde partie met en relief les progrès intervenus dans les dernières années sur les phénomènes élémentaires mis en jeu en cours d'instabilité. La troisième partie illustre, en continuité avec ce qui précède, les travaux de l'ONERA sur trois types d'instabilité de complexité croissante : instabilité en volume, instabilité longitudinale d'un moteur sans tuyère en description monodimensionnelle semi-analytique, instabilité longitudinale radiale d'un moteur en description bidimensionnelle numérique.

1. INTRODUCTION

La plupart des systèmes propulsifs présentent une tendance à des comportements instationnaires imprévus lors de leur conception. Un point de fonctionnement stationnaire, caractérisé par une consommation du combustible (ou du propergol) et par une poussée, ou l'évolution lente des grandeurs propulsives dans le cas d'un moteur à propergol solide, est généralement visé lors de la conception, alors qu'un fonctionnement organisé de façon oscillatoire se manifeste parfois lors des essais. Le nom générique d'"instabilité de combustion" est donné à ce type de fonctionnement oscillatoire.

Une revue très complète des instabilités dans les systèmes à combustible ou propergol liquide -chambres de post-combustion de turboréacteur, statoréacteurs, moteurs fusées à ergols liquides- a récemment été réalisée par F.E.C. Culick lors d'une conférence AGARD (réf. 1). Cette revue dégage très clairement la démarche suivie au cours des années pour parvenir à comprendre la physique qui contrôle les instabilités de combustion et le formidable défi scientifique que représente leur complète maîtrise. Ces mêmes caractères sont retrouvés dans les ouvrages de référence qui jalonnent l'histoire des moteurs à propergol solide et qui font une place importante aux instabilités de combustion (réf. 2 à 4). Tous les moteurs-fusées chimiques impliquent la transformation de l'énergie stockée dans les liaisons des molécules en énergie mécanique pour créer l'effet propulsif direct. Cette transformation se produit pour des débits élevés de propergol, dans de très faibles volumes, elle correspond à une puissance énorme ; il n'est pas surprenant qu'une très faible fraction de cette puissance puisse être utilisée au cours du processus de transformation pour déclencher et entretenir des phénomènes oscillatoires. Le rôle actif des mécanismes de combustion dans l'instabilité a été très tôt reconnu, tant dans les moteurs à ergols liquides que dans les moteurs à propergol solide. Toutefois il est manifeste qu'un mode d'instabilité est toujours dépendant de son environnement et spécialement de la géométrie du moteur. Aussi serait-il plus justifié de parler d'instabilité de fonctionnement, de système ou de moteur que d'instabilité de combustion. Le terme d'instabilité de combustion sera toutefois conservé ici en raison de sa large diffusion.

L'apparition d'instabilités de combustion au cours de la phase de développement d'un moteur à propergol solide constitue toujours un problème sérieux par ses conséquences directes et indirectes. Les conséquences directes sont soit internes, soit externes. Du point de vue du fonctionnement propre du moteur, une instabilité de combustion peut accroître la consommation des protections thermiques internes et dans les cas les plus sévères (mode acoustique tangentiel) induire une dérive des grandeurs stationnaires. Une instabilité se traduit également par une oscillation de la poussée, l'ensemble du moteur rentre en vibration et les niveaux vibratoires peuvent dépasser le seuil de tolérance de certains équipements ou même de la charge utile. Les conséquences indirectes se mesurent en termes de temps et d'argent car, pour éliminer ou atténuer les instabilités, il faut modifier généralement l'architecture du chargement et/ou son propergol puis reprendre les essais. Il est donc justifié de considérer que les instabilités de combustion constituent une maladie endémique des moteurs à propergol solide qu'il convient de prévoir et éventuellement de guérir. Chaque industriel possède une expérience et des règles de l'art qui le guident dans la conception d'un nouveau moteur. Toutefois cette connaissance empirique s'avère limitée lorsqu'apparaissent de nouvelles architectures ; la recherche conjointe d'une fiabilité accrue et d'une diminution des coûts de développement rend en outre nécessaire une démarche plus théorique et plus quantifiée. Cette démarche scientifique passe nécessairement par la compréhension détaillée des mécanismes mis en jeu au cours d'une instabilité et débouche sur la mise au point d'outils analytiques ou numériques de conception.

Malgré l'ampleur des efforts menés sur le problème des instabilités de combustion depuis plus de quarante ans, l'état actuel des connaissances et des outils n'est pas à la mesure des ambitions industrielles et des enjeux économiques et la maîtrise des instabilités continue à être considérée comme un point-clef de la technologie des moteurs-fusées à propergol solide des années 90 (réf. 5). Il n'est guère possible de présenter une liste exhaustive des moteurs qui ont connu des instabilités de

combustion dans les différents pays. On peut toutefois signaler que certains moteurs de grandes dimensions, affectés par des instabilités longitudinales de niveau modéré, sont parvenus sans modification au stade opérationnel ; c'est en particulier le cas pour plusieurs moteurs segmentés pour lanceurs spatiaux, prédits stables lors de leur conception et observés instables lors des essais.

L'état de l'art de l'analyse des instabilités de combustion doit beaucoup aux Etats-Unis. C'est en particulier dans ce pays que sont apparus, peu après la deuxième guerre mondiale, les premiers travaux fondamentaux et qu'ont été mis au point les outils prédictifs, tels que le bilan acoustique et ses variantes, aujourd'hui universellement utilisés. L'avance des Etats-Unis doit certainement beaucoup au dialogue organisé entre les équipes scientifiques de haut niveau des Universités et celles des Centres des Forces Armées (Air Force, Navy) et des Industriels. La France, qui possède une longue tradition dans la propulsion par propergol solide, a été confrontée à des problèmes d'instabilité dans le cadre de ses programmes de missiles. Les premiers travaux de l'ONERA ont été initiés vers les années 1960 par M. Barrère et se poursuivent actuellement ; en 1986, de nouvelles études ont démarré pour le CNES, dans le cadre du développement du Moteur à Propergol Solide du lanceur européen Ariane 5. On trouvera en référence 6 une synthèse des travaux de l'ONERA réalisés jusqu'en 1979 et en référence 7 le point de vue de la SNPE. La compétence des autres pays ne peut être appréciée qu'à partir de la littérature ouverte et des échanges bilatéraux, elle est très liée aux programmes militaires et civils nationaux. La rapide synthèse qui suit sera limitée aux pays participant à l'AGARD ; l'impression qui s'en dégage est l'existence de centres de compétence orientés vers la résolution de problèmes spécifiques soit au niveau appliqué, soit au niveau fondamental. La Grande Bretagne, dont les travaux sur les instabilités tangentielles faisaient autorité dans le passé (réf. 8), parait avoir concentré ses efforts dans la formulation des propergols solides. Le Canada semble maintenir une grande expérience pratique sur les instabilités longitudinales présentant un caractère non linéaire, c'est-à-dire associées à des amplitudes élevées de pression ou à des fronts raides (réf. 9). L'Italie poursuit des travaux fondamentaux sur les mécanismes instationnaires de combustion (réf.10) et est très présente par la firme BPD dans les programmes spatiaux européens. Les Pays Bas ont particulièrement publié sur les instabilités en volume (réf. 11).

Si les recherches sur les instabilités de combustion gardent une certaine vigueur, notamment aux Etats Unis, on peut s'interroger sur l'adéquation des moyens engagés à la complexité du problème. Plusieurs remarques peuvent être proposées sur ce point. La première est que le problème des instabilités ne redevient souvent prioritaire pour les décideurs qu'en période de crise, ce qui n'est pas forcément choquant mais restreint l'ampleur des travaux qui permettraient justement de faire face à une situation d'urgence. La seconde remarque est liée au fait que le progrès ne peut résulter que d'investissements assez lourds sur les plans théorique, numérique et expérimental et que ce progrès est lent, ce qui conduit à étaler les programmes de recherches. Un bon équilibre doit être trouvé entre une description détaillée des phénomènes physiques, suivi de leur traitement sans biais, et l'acquisition des données d'entrée indispensables. On notera également qu'il existe un couplage étroit entre les moyens d'essais chargés de fournir les données d'entrée et les outils de simulation à caractère prédictif puisque les mêmes descriptions théoriques sont utilisées soit en mode direct (prévision) soit en mode inverse (exploitation des essais) ; ce couplage est particulièrement net pour tout ce qui touche la combustion instationnaire.

Les considérations générales qui précèdent visaient à resituer le problème des instabilités de combustion dans un contexte général. Le choix volontairement fait pour la suite de l'exposé a été de privilégier la description physique, au détriment des développements mathématiques, et d'assurer la liaison entre les considérations théoriques et les observations. On trouvera donc successivement :

- dans le chapitre 2, un rappel des bases de l'analyse des instabilités de combustion,
- dans le chapitre 3, une synthèse des progrès réalisés sur la compréhension des phénomènes élémentaires,
- dans le chapitre 4, l'illustration de quelques travaux récents de l'ONERA.

La combustion instationnaire du propergol solide, faisant l'objet d'une autre conférence, ne sera traitée que succintement.

2. NOTIONS GENERALES SUR LES INSTABILITES DE COMBUSTION DES MOTEURS A PROPERGOL SOLIDE

L'examen des récents développements de l'analyse des instabilités de combustion (chapitre 3) nécessite le rappel d'un certain nombre de connaissances et d'observations élémentaires. Ce rappel synthétique s'efforcera de dégager les problèmes les plus importants, dans une logique chronologique. Un parallèle sera fait en particulier entre les différents objectifs de l'analyse des instabilités de combustion et les différentes approches théoriques qui leur correspondent, ainsi qu'entre les observations et les prévisions théoriques.

2.1. Démarche

Telle que perçue par l'expérimentateur, toute instabilité de combustion possède ses caractéristiques propres : les phénomènes sont organisés sur une fréquence fondamentale, avec une amplitude pouvant éventuellement lentement varier dans le temps, un contenu fréquentiel lié à la forme des signaux observés, etc... Certaines instabilités de combustion possédant des caractéristiques similaires sont réputées appartenir à une même famille de modes d'instabilité.

La détermination des modes d'instabilité suit une logique qui rappelle les observations et qui procède selon les étapes suivantes :

- recherche des fréquences des modes d'instabilités susceptibles de se manifester naturellement au cours du fonctionnement ou modes potentiels,

- recherche de la stabilité de chaque mode potentiel c'est-à-dire de sa faculté à apparaître réellement ou non,

- recherche, pour les modes identifiés comme instables, d'une éventuelle stabilisation de l'amplitude (cycle limite) et d'une évolution des grandeurs moyennes,

- recherche de la stabilité du moteur après une perturbation de grande amplitude et en cas d'instabilité déclenchée, recherche du cycle limite.

On peut donc distinguer deux types de stabilité que nous nommerons, en référence à l'usage pour les moteurs à ergols liquides, stabilité statique et stabilité dynamique (fig.1).

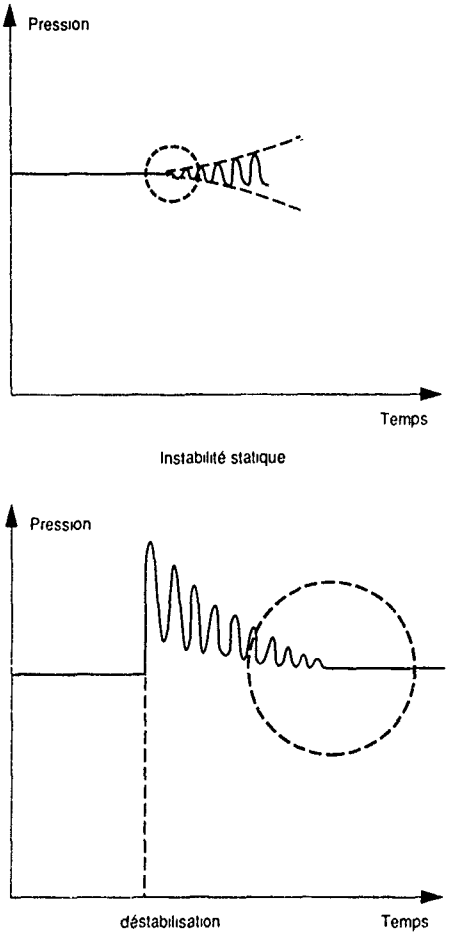

Figure 1 - Types de stabilité / instabilité

2.1.1. Stabilité statique

La stabilité statique s'intéresse à la naissance spontanée et au développement initial de l'instabilité, elle est donc caractérisée par de très faibles amplitudes des oscillations autour du régime permanent initial. Le fait de considérer de très faibles amplitudes a une répercussion immédiate sur l'analyse théorique de la stabilité puisqu'elle conduit à décomposer toute grandeur f en une composante stationnaire ou moyenne, $\bar{f}$, qui est celle définie par le régime permanent, et une perturbation f', caractéristique de l'instabilité et donc instationnaire :

$$f(\vec{r},t) = \bar{f}(\vec{r}) + f'(\vec{r},t) \,, \qquad (2.1)$$

où $|f'/\bar{f}| \ll 1$

A cette hypothèse de base correspond la possibilité de linéariser les équations décrivant le problème qui sont principalement de nature aérothermochimique et donc fortement non-linéaires. Cette linéarisation conduit à ne retenir dans les produits de grandeur que les termes du premier ordre pour les perturbations, c'est-à-dire à écrire :

$$fg = \bar{f}\bar{g} + f'\bar{g} + \bar{f}g' \qquad (2.2)$$

La linéarisation autorise de nombreux développements mathématiques et en particulier :

- elle permet de considérer tout phénomène comme la superposition d'un phénomène stationnaire et d'un phénomène instationnaire ; le phénomène stationnaire peut être traité indépendamment du phénomène instationnaire mais le phénomène instationnaire dépend en principe du phénomène stationnaire,

- dans le phénomène instationnaire global peuvent être mises en évidence les contributions additives de phénomènes instationnaires élémentaires.

La naissance proprement dite de l'instabilité n'est pas dans ce cadre un problème important car un moteur à propergol solide comporte de multiples possibilités de destabilisation de très faible amplitude : bruits de la combustion et de l'écoulement, détachement accidentel d'un petit morceau de propergol ou de protection thermique, obstruction partielle et momentanée de la tuyère due au passage d'un élément de l'allumeur...

Une perturbation initiale va donner naissance à des ondes propagatives dans l'écoulement qui vont se réfléchir sur la surface de combustion, les parois du propulseur et la tuyère, se composer pour finalement s'organiser sous forme d'onde stationnaire. A ce régime stationnaire, au sens de l'acoustique, correspond la possibilité de séparer les variables spatiales et temporelle sous la forme complexe :

$$f'(\vec{r},t) = \tilde{f}(\vec{r})\, e^{i\omega t}\, e^{\alpha t} \qquad (2.3)$$

$\tilde{f}(\vec{r})$ est l'amplitude complexe qui dépend de la position considérée, $\omega = 2\pi f$ est la pulsation et α est l'amplification temporelle.

Le problème mathématique se réduit donc de la recherche de la solution d'un système d'équations différentielles sur $\vec{r}$ et t, à la résolution d'un système d'équations différentielles sur $\vec{r}$ et à la détermination de valeurs propres complexes ω-$i\alpha$.

L'analyse linéaire ne permet donc pas de prévoir l'amplitude absolue de l'instabilité mais sa tendance à diverger ou au contraire à s'amortir, par l'intermédiaire de α, sa fréquence et la répartition relative des amplitudes.

Un mode linéaire sera dit stable si $\alpha < 0$, instable si $\alpha > 0$. Le mode sera considéré comme marginalement stable si α est autour de zéro ; la SNPE utilise plutôt la terminologie "mode à risque" si :

$$-0{,}1\, f < \alpha < +0{,}1\, f \qquad (2.4) \text{ (réf. 7)}$$

Lorsque l'amplitude d'un mode linéaire atteint un certain niveau, l'analyse linéaire devient insuffisante et ce sont les méthodes signalées pour la stabilité dynamique qu'il convient d'utiliser. La transition entre linéaire et non-linéaire ne peut être rigoureusement définie ; expérimentalement elle se manifeste par un changement de l'amplification dans le temps et une divergence de la forme des signaux oscillatoires par rapport à la sinusoïde pure.

2.1.2. Stabilité dynamique

La stabilité dynamique vise le comportement asymptotique du moteur à la suite d'une déstabilisation provoquée mettant en jeu des amplitudes élevées. Le comportement du moteur au cours du temps ne peut plus se résumer à une fréquence complexe et ceci pour deux raisons :

- la déstabilisation est rarement harmonique et la fréquence fondamentale peut varier au fur et à mesure de l'organisation de l'instabilité non-linéaire,

- les signaux de fortes amplitudes présentent généralement un fort contenu fréquentiel et peuvent même dégénérer en fronts raides ou en ondes de choc.

A cette complexité s'ajoute la possibilité des grandeurs stationnaires de s'écarter notablement des valeurs du régime permanent, la notion de stationnaire recouvrant alors celle de moyenne temporelle sur un nombre entier de périodes.

Les méthodes linéaires sont en défaut dans le cas de l'instabilité dynamique mais on peut leur donner un prolongement par des développements dépassant le premier ordre des perturbations. On peut aussi recourir à l'intégration numérique des équations aux dérivées partielles.

Il n'est pas possible d'opposer stabilité statique et stabilité dynamique qui représentent au contraire deux aspects d'un même phénomène général. Un moteur peut s'avérer stable statiquement et instable dynamiquement en pratique. La figure 2 est classique et illustre un tel type de situation conduisant à un cycle limite c'est-à-dire à la stabilisation des amplitudes par des effets non-linéaires. De manière schématique, la dérivée temporelle d'une amplitude caractéristique $\mathcal{E}$ d'un mode simple est portée en fonction de $\mathcal{E}$. La portion AA' de la courbe tracée peut être décrite par :

$$\frac{d\mathcal{E}}{dt} = k\mathcal{E} \qquad (2.5)$$

ou $$\mathcal{E} = C\exp(kt) \qquad (2.6)$$

elle décrit donc bien une instabilité linéaire.

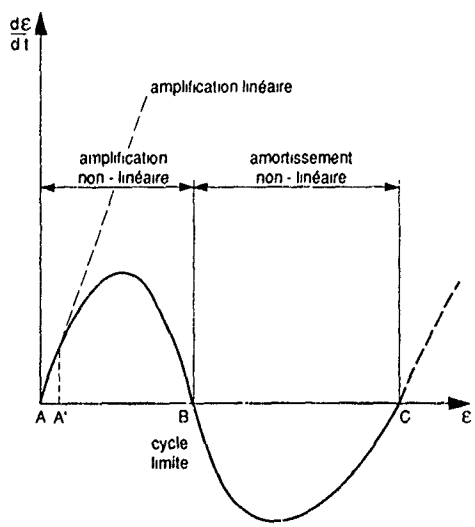

Figure 2 - Comportement schématique d'un mode simple en fonction de l'amplitude

En raison des non-linéarités dans les mécanismes d'entretien ou d'amortissement de l'instabilité, la courbe est supposée prendre une courbure négative de A' à B puis positive de B à C. Toute situation de départ comprise entre A et C conduit au point B où l'amplitude restera constante et qui correspond à un cycle limite accessible soit par instabilité spontanée, linéaire puis non-linéaire, soit par une déstabilisation importante suivie d'un amortissement non-linéaire. Le point C ne reproduit aucune situation stabilisée puisqu'on tend toujours à s'en écarter. Il est bien entendu possible d'envisager, selon la même approche, des formes de courbe qui traduiraient un amortissement linéaire joint à un comportement non-linéaire conduisant ou non à un cycle limite.

2.1.3. Remarque sur les échelles de temps

Les moteurs à propergol solide possèdent la particularité d'être des moteurs à géométrie variable puisque le volume occupé par les produits de combustion croît avec la régression de la surface de combustion. On pourrait donc supposer que le fonctionnement est toujours instationnaire. En réalité, quelques considérations d'ordres de grandeur permettent de simplifier le problème :

- le temps de fonctionnement est généralement supérieur de trois ordres de grandeur à la période de l'instabilité,

- la vitesse de régression de la surface (vitesse de combustion du propergol) est généralement inférieure de trois ordres de grandeur à la vitesse des produits de combustion émis de la surface.

Il est donc légitime, pour l'analyse des instabilités, de considérer fixe la géométrie du chargement, débitante la surface de combustion et constantes les grandeurs stationnaires (en régime linéaire). L'analyse des instabilités doit être en conséquence répétée pour différents temps de fonctionnement ou différentes épaisseurs brûlées de propergol, ce qui pose des contraintes pratiques limitant la sophistication des moyens de prévision d'usage courant.

2.1.4. Remarque sur les échelles d'espace

Le système de flammes au-dessus de la surface de combustion d'un propergol solide possède, dans les conditions normales de fonctionnement, une hauteur inférieure au 1 mm et donc généralement très inférieure à une dimension caractéristique du moteur. Vis-à-vis de l'instabilité qui intéresse tout le volume de la cavité, la tentation est grande de considérer que le phénomène d'ensemble comme un phénomène de champ essentiellement aérodynamique soumis à des conditions limites pilotées par la combustion. Cette vision amène à représenter, en première approximation, une instabilité par une boucle fermée, au sens des automaticiens (fig. 3). L'apparition de phénomènes instationnaires dans l'écoulement de cavité modifie la vitesse de combustion du propergol, le changement de vitesse de combustion réagit à son tour sur l'écoulement instationnaire et, pourvu que les gains et les déphasages soient adaptés, la boucle est instable.

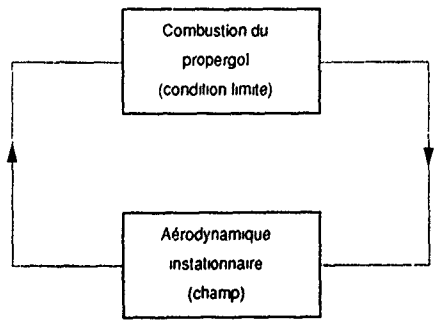

Figure 3 - Boucle d'instabilité

Cette décomposition possède l'avantage de la simplicité et de la séparation des disciplines scientifiques. Elle se trouve cependant en défaut sur au moins deux points :

- si le propergol possède une charge métallique, la combustion de cette charge se produit plutôt en volume qu'en surface. Pour l'aluminium par exemple et certains moteurs, le problème est souvent évoqué de savoir, dans les premiers instants du fonctionnement, si tout l'aluminium a brûlé avant son éjection par la tuyère. La question de l'influence de la combustion distribuée de l'aluminium se pose également pour la stabilité,

- certains phénomènes de couplage entre écoulement et combustion ne permettent pas une séparation aussi tranchée. C'est le cas de la combustion érosive en stationnaire et du couplage-vitesse en instationnaire.

2.2. Description théorique des instabilités de combustion

La description théorique des instabilités de combustion n'est pas indépendante de la nature des mesures qui peuvent être réalisées sur moteur. Le milieu à étudier est particulièrement hostile : pression élevée, température des produits de combustion dépassant couramment 3000 K, phases condensées (propergols métallisés), géométrie évoluant au cours du temps, expérimentation requérant des installations spécialisées pour des raisons de sécurité, etc... L'instrumentation classique est donc limitée à la mesure de pressions statiques sur la paroi du propulseur, elle permet d'accéder aux fréquences, aux amplitudes et aux déphasages de pression. Il n'est pas par contre possible de mesurer simplement d'autres grandeurs de champ telles que la vitesse. Cette limitation de l'instrumentation sur moteur à deux conséquences :

- elle tend à privilégier le rôle de la pression dans la comparaison théorie-expérience bien que cette grandeur n'apparaisse pas a posteriori la plus significative ; l'étude des phénomènes d'interaction entre champs stationnaire et instationnaire montre en particulier qu'un champ de pression instationnaire proche du champ acoustique élémentaire peut être associé à un champ de vitesse instationnaire très éloigné du champ acoustique associé (paragraphe 3.1.1),

- elle contraint à une démarche intellectuelle spéculative pour la compréhension fine des phénomènes de champ.

Il existe, pour les objectifs de recherche, des possibilités en nombre limité d'accès à d'autres grandeurs physiques. La première voie est celle de la simulation gazeuse et intéresse uniquement les phénomènes d'origine aérodynamique ; elle consiste à reproduire l'écoulement dans la cavité du moteur par l'injection au travers d'une paroi poreuse. Cette technique, utilisée par de nombreux chercheurs pour l'étude de l'écoulement stationnaire, a également donné lieu à quelques travaux visant les phénomènes aérodynamiques instationnaires (réf. 12 et 13). Les résultats obtenus sont précieux d'un point de vue qualitatif, peut être un peu plus limités d'un point de vue quantitatif en raison de certaines limitations de similitude entre écoulements réel et simulé, de mesure et de représentativité de la surface poreuse par rapport à la surface de combustion du propergol. Une autre voie de recherche, assez peu suivie, est la visualisation de l'écoulement sur une chambre à parois transparentes. La figure 4 illustre un résultat déjà ancien obtenu à l'ONERA sur un petit montage équipé d'un chargement à encoches (réf. 14). Le film montre l'existence de lignes sombres et instables émis des angles du chargement, laissant supposer l'existence d'instabilités hydrodynamiques. Les informations recueillies par cette technique sont uniquement qualitatives et sujettes à caution puisque la visualisation favorise l'observation des phénomènes se produisant près du hublot.

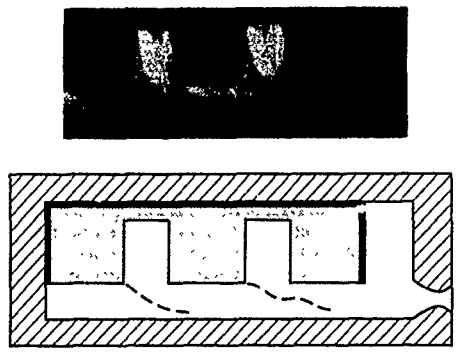

Figure 4 - Visualisation sur chambre à voyants

2.2.1. Classement des modes d'instabilités

A une fréquence d'instabilité correspond directement une longueur d'onde donnée par :

$$\lambda = \frac{a}{f} \qquad (2.7)$$

où a est la célérité du son dans les produits de combustion. La comparaison de λ et d'une dimension caractéristique L du moteur permet de faire apparaître deux types de mode d'instabilité :

- si λ est très supérieur à L et si l'écoulement stationnaire dans la cavité est à faible nombre de Mach, le mode d'instabilité est un mode en volume,

- si λ est de l'ordre de L ou inférieur, le mode est réputé acoustique c'est-à-dire organisé, conformément aux mesures de pression, au voisinage d'un mode acoustique de cavité.

Un mode de volume se manifeste par des oscillations de pression qui ont même amplitude et même phase en chaque point de la cavité alors qu'un mode acoustique fait apparaître une structure de mode caractérisée par une répartition des amplitudes et des phases.

La classification des modes acoustiques d'instabilité suit celle des modes acoustiques de cavité. Au champ de pression acoustique de cavité est associé un champ de vitesse acoustique et suivant les composantes de vitesse acoustique on distingue des modes :

- longitudinaux : si la vitesse acoustique ne possède qu'une composante suivant l'axe du moteur,

- radiaux : si la vitesse acoustique est dans un plan perpendiculaire à l'axe du moteur et intercepte cet axe,

- tangentiels : si la vitesse acoustique est dans un plan perpendiculaire à l'axe du moteur sans composante radiale,

- couplés : si la vitesse acoustique possède plusieurs composantes.

L'existence de modes acoustiques purs, c'est-à-dire à une seule composante de vitesse acoustique, n'est possible que dans une cavité cylindrique. Pour des géométries de cavité plus complexes et plus réalistes, les modes acoustiques sont toujours des modes couplés.

Remarque sur la classification des modes acoustiques

La classification traditionnelle des modes acoustiques d'instabilité est une double source de confusion.

La première confusion consiste à assimiler mode acoustique d'instabilité et mode acoustique de cavité alors que la dénomination acoustique ne traduit qu'une proximité. En fait, dans une cavité cylindrique, il peut exister des modes longitudinaux de cavité mais les modes d'instabilité correspondants impliqueront des mouvements à la fois longitudinaux et radiaux (paragraphe 3.1.1.).

L'autre confusion porte sur la description du mode d'un point de vue physique et la façon dont sont traitées les équations, de manière plus ou moins simplifiée, et bien qu'il existe certaines correspondances. L'espace physique comporte trois dimensions et les équations locales de base sont décrites suivant une dimension de temps et les trois dimensions d'espace. Les réductions des équations générales peuvent être établies :

- par intégration sur le volume complet de la cavité : des équations différentielles ordinaires sur le temps, dites zérodimensionnelles (0D), sont obtenues ; ce sont typiquement celles utilisées pour décrire les modes de volume,

- par intégration sur la section perpendiculaire à l'axe de la cavité : des équations dépendant du temps et de l'abscisse, pour des grandeurs moyennes sur une section sont obtenues. On parle alors d'écoulement par tranches ou de résolution par équations monodimensionnelles (1D). Cette approche est souvent utilisée pour la description des instabilités dans un moteur dont le canal est cylindrique. De nombreux problèmes théoriques trouvent leur origine dans le traitement 1D des instabilités car la moyenne réalisée sur une section gomme tous les phénomènes se développant radialement.

Il faut donc en définitive qualifier les modes d'instabilités par les adjectifs acoustiques à partir de la prédominance du mouvement instationnaire dans une ou plusieurs directions, prédominance par ailleurs présupposée ou établie à partir de la fréquence observée. Les dénominations établies dans cet esprit se retrouvent sur la figure 5 qui donnent quelques modes d'instabilité fréquemment rencontrés.

2.2.2. Analyse linéaire de la stabilité

L'analyse linéaire de la stabilité commence par la détermination des modes potentiels d'instabilité. Cette détermination n'est pas possible pour les modes de volume indépendamment de la réponse instationnaire du propergol (paragraphe 4.1.1.). On envisagera donc ici le seul cas des modes acoustiques d'instabilité ; pour ceux-ci il s'avère réaliste de calculer une première approximation des fréquences par les modes acoustiques de la cavité constituée par la surface de combustion, les parois du propulseur et une surface de fermeture dans la tuyère. Le calcul s'effectue classiquement avec les hypothèses suivantes :

- parois rigides,
- vitesse du son uniforme,
- propagation dans un milieu au repos.

Les équations dérivent directement par linéarisation des équations plus générales de la mécanique des fluides. Le problème acoustique se ramène à l'équation d'Helmoltz :

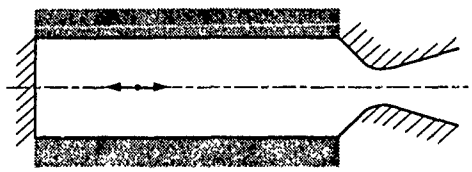

Cavité cylindrique mode longitudinal

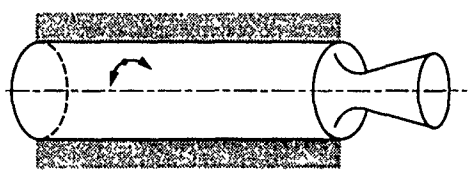

Cavité cylindrique mode tangentiel

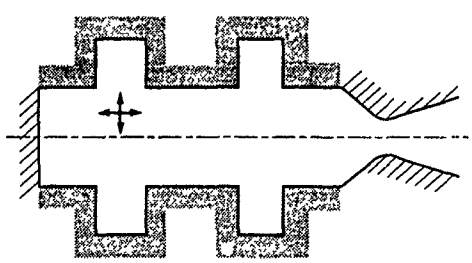

Cavité axisymétrique mode longitudinal - radial

Figure 5 - Quelques modes d'instabilité acoustique simples

$$\Delta \tilde{p}_N + \frac{\omega_N^2}{a^2} \tilde{p}_N = 0 \quad \text{dans la cavité}$$
$$\frac{\partial \tilde{p}_N}{\partial n} \quad \text{sur la surface} \qquad (2.8)$$

où ω apparaît comme valeur propre.

Des solutions analytiques peuvent être obtenues pour des cavités de géométries très simples (cylindre circulaire, parallélépipède) ; pour des cavités plus complexes, il faut recourir au calcul numérique, par exemple aux éléments finis (fig.6). On notera que le problème mathématique peut être posé sous forme adimensionnée et que des pulsations réduites sont alors calculées :

$$\Omega = \frac{\omega_N L}{a} \qquad (2.9)$$

Cette propriété est utilisée pour déterminer expérimentalement les fréquences de cavité par l'intermédiaire d'une maquette rigide reproduisant le moteur à un instant de son fonctionnement et soumise à une excitation forcée, par exemple par l'intermédiaire d'un haut-parleur. Un mode de cavité est mis en évidence par un maximum de l'amplitude du signal d'un microphone ou d'un capteur de pression lorsque la fréquence varie. Calcul numérique et méthode expérimentale donnent des résultats en bon accord, c'est-à-dire une suite discrète théoriquement infinie de fréquences et de modes acoustiques de cavité.

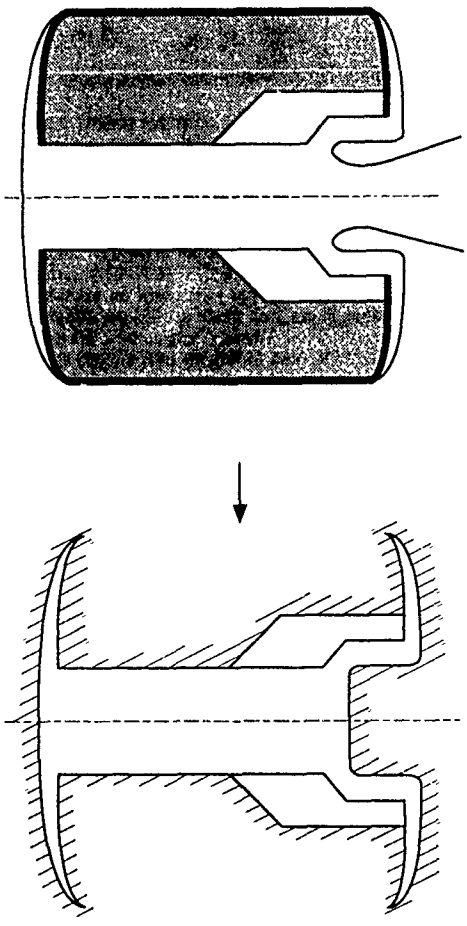

Figure 6 - Détermination des modes de cavité

L'approximation des fréquences d'instabilité potentielle par les fréquences acoustiques de cavité est souvent excellente. Elle pose toutefois quelques problèmes spécifiques souvent passés sous silence et qui sont directement liés aux hypothèses de départ :

- choix de la surface de fermeture dans la tuyère : la théorie impose de choisir cette surface dans une zone où le nombre de Mach moyen reste très inférieur à 1. Si la tuyère est intégrée, le nombre de Mach à l'entrée de la tuyère est proche de 0,3 et il est conseillé de choisir le plan de fermeture dans la section d'entrée de la tuyère (voir aussi paragraphe 3.1.3.1.),

- parois rigides : les ondes mécaniques se transmettent également dans le chargement et il faut envisager la possibilité de vibrations acousto-élastiques. Cette possibilité a été prouvée théoriquement dans différents cas en considérant un chargement élastique. Cependant le couplage acoustico-élastique ne se produit que dans des circonstances exceptionnelles et le propergol possède plutôt un comportement visco-élastique qu'élastique. On peut donc penser qu'un couplage reste, dans les conditions normales d'utilisation, peu probable et compte-tenu de la dissipation visco-élastique du propergol, peu propice à l'entretien des instabilités. Des expériences comparatives réalisées sur maquettes rigides et souples, en matériau polymère, n'ont pas en outre mis en évidence d'écarts significatifs de fréquence,

- vitesse du son uniforme : cette hypothèse peut être remise en question si la charge métallique du propergol brûle dans une fraction notable du volume de la cavité. Par chance, la célérité du son dans les produits de combustion de la matrice du propergol (composants du propergol à l'exception de la charge métallique) reste, par le jeu des masses molaires, voisine de la célérité du son dans les produits de combustion du propergol complet. L'influence des hétérogénéités de la célérité du son sur les fréquences n'est donc pas importante pour la majorité des moteurs. Le seul contre-exemple à signaler est celui d'un montage d'étude possédant un volume mort au fond avant dont la température ne s'équilibrait pas avec celle des produits de combustion,

- milieu au repos : cette hypothèse est raisonnable pour les moteurs classiques, notamment après le début du fonctionnement. Elle est par contre en défaut dans le cas du moteur sans tuyère puisque l'écoulement dans le canal du chargement atteint le supersonique (paragraphe 4.2).

Les modes potentiels d'instabilité étant déterminés par leurs fréquences, il s'agit maintenant d'étudier la stabilité linéaire de chacun d'entre eux. La méthode la plus utilisée est celle du bilan acoustique, mise sous une forme achevée par F.E.C. Culick, d'abord pour une description monodimensionnelle de l'écoulement (réf. 15) puis pour une description multidimensionnelle (réf. 16). Comme cette méthode est maintenant bien connue, seule la démarche sera rappelée et commentée.

Les équations de continuité, de quantité de mouvement et d'énergie sont d'abord écrites pour la phase gazeuse et la phase condensée, assimilée à un milieu continu en interaction avec la phase gazeuse et échangeant quantité de mouvement et énergie (traînée des particules et transfert thermique entre gaz et particules). Après quelques transformations, il vient :

$$\frac{\partial p}{\partial t} + \left(\frac{r_m}{Cv_m} + 1\right) p \vec{\nabla}.\vec{u} + \vec{u}.\vec{\nabla}p = \frac{n}{Cv_m}\delta Q_p$$
$$\rho_m \frac{\partial \vec{u}}{\partial t} + \rho_m \vec{u}.\vec{\nabla}\vec{u} + \vec{\nabla}p = \delta \vec{F}_p \qquad (2.10)$$

où p est la pression,
r_m et Cv_m sont la constante du gaz équivalent et sa chaleur massique à volume constant,
$\vec{u}$ est la vitesse du gaz,
ρ_m est la masse volumique du mélange,
$\delta \vec{F}_p$ est la force de traînée exercée par le gaz sur les particules par unité de volume,
δQ_p est la puissance thermique transmise du gaz aux particules par unité de volume.

La linéarisation des équations n'est possible qu'en utilisant deux paramètres de perturbations : ε pour l'amplitude des oscillations et $\bar{M}$ nombre de Mach de l'écoulement stationnaire du gaz équivalent. Le champ stationnaire n'est décrit qu'au premier ordre de $\bar{M}$. Une équation d'onde est établie pour la perturbation p' de pression, puis supposant un phénomène stationnaire organisé sur la fréquence complexe $\omega = 2\pi f - i\alpha$ on parvient à :

$$\Delta\tilde{p} + \frac{\omega^2}{a^2}\tilde{p} = \tilde{h} \qquad \text{dans la cavité,} \qquad (2.11)$$

$$\frac{\partial \tilde{p}}{\partial n} = -\tilde{f} \qquad \text{sur la surface,}$$

où $\tilde{h} = \frac{i\omega}{a^2}\vec{u}.\vec{\nabla}\tilde{p} - i(\gamma-1)\frac{\omega}{a^2}\delta\tilde{q}_p + \vec{\nabla}.\tilde{F}_p$

$$-\rho\vec{\nabla}.(\vec{u}.\vec{\nabla}\vec{u} + \vec{u}.\vec{\nabla}\vec{u}) \qquad (2.12)$$

$$\tilde{f} = i\omega\rho\vec{n}.\vec{u} - \vec{n}.\delta\tilde{F}_p + p\vec{n}.(\vec{u}.\vec{\nabla}\vec{u} + \vec{u}.\vec{\nabla}\vec{u})$$

Cette équation et sa condition limite peuvent être rapprochées de celles décrivant le phénomène acoustique de cavité (2.8). Une combinaison des équations (2.8) et (2.11) suivie d'une intégration sur le volume V de la cavité de surface S, conduit, après quelques simplifications résultant des ordres de grandeur, à l'expression directe de ω par :

$$\frac{\omega^2-\omega_N^2}{a^2}E_N^2 = -\frac{i\omega_N}{a}\int_S (A+\bar{M})\tilde{p}_N^2\,ds$$

$$-\int_V \delta\tilde{F}_p.\vec{\nabla}\tilde{p}_N\,dv - i(\gamma-1)\frac{\omega_N}{a^2}\int_V \delta\tilde{q}_p\tilde{p}_N\,dv\,, \qquad (2.13)$$

où : $E_N^2 = \int_V \tilde{p}_N^2\,dv$,

A est l'admittance de surface $\tilde{p} = \frac{\vec{u}.\vec{n}}{A}$,

$\bar{M}$ est le Mach d'injection ou de succion en surface.

Il est important de signaler la simplification :

$$\vec{u} \simeq \vec{u}_N = \frac{i}{\rho\omega_N}\vec{\nabla}\tilde{p}_N \qquad (2.14)$$

Cette simplification annule les produits $(\vec{\nabla}\wedge\vec{u})\wedge\vec{u}$ et $((\vec{\nabla}\wedge\vec{u})\wedge\vec{u})$. $\vec{\nabla}p_N$, issus du développement et de la linéarisation du terme $\vec{u}.\vec{\nabla}\vec{u}$ des équations (2.10) et (2.12), et fait donc disparaître toute trace de vorticité des écoulements !

La séparation des parties réelle et imaginaire de (2.13) conduit à l'expression de l'amplification α sous forme additive, pourvu que $\alpha \ll \omega$:

$$\alpha = \alpha_{PC} + \alpha_N + \alpha_{PD} \qquad (2.15)$$

où : $\alpha_{PC} = \frac{a}{2E_N^2}\int_{S_p}(A_{PC}^{(r)} + \bar{M}_z)\tilde{p}_N^2\,ds$, (2.16)

terme lié à la réponse du propergol au couplage pression,

$$\alpha_N = -\frac{a}{2E_N^2}\int_{S_T}(A_T^{(r)} + \bar{M}_T)\tilde{p}_N^2\,ds\,, \qquad (2.17)$$

terme correspondant au rayonnement et à la convection des ondes acoustiques dans la tuyère,

$$\alpha_{PD} = \frac{a^2}{2\omega_N E_N^2}\int_V (\delta\tilde{F}_p.\vec{\nabla}\tilde{p}_N)^{(i)}dv$$

$$+\frac{\gamma-1}{2E_N^2}\int_V (\delta\tilde{q}_p\,\tilde{p}_N)^{(i)}dv\,, \qquad (2.18)$$

terme dépendant des échanges entre phases.

D'autres termes sont souvent introduits en supplément. Les plus classiques sont le terme lié au couplage-vitesse et le terme de "Flow Turning" qui représente l'énergie acoustique dissipée par l'écoulement émis de la surface de combustion pour acquérir la vitesse acoustique locale.

Remarque sur le terme de "Flow Turning"

Le terme de "Flow Turning" du bilan acoustique est dégagé rationnellement des équations monodimensionnelles et est directement lié au choix de la composante longitudinale u' de vitesse des produits émis par la surface de combustion ; il s'exprime proportionnellement à l'intégrale :

$$\int_0^L \tilde{\mu}\frac{d\tilde{p}_N}{dx}S_x\,dx \qquad (2.19)\ (\text{réf. 16})$$

où $\tilde{\mu}$ est lié à $\tilde{u}_N$ en écoulement monophasique.

La méthode du bilan acoustique conduit à utiliser la relation acoustique (2.14) et donne donc une intégrale où apparaît le carré du gradient de pression acoustique et correspondant à une perte acoustique.

L'extension au tridimensionnel proposée par F.E.C. Culik (réf. 16) est fondée sur la prise en compte de l'incidence des ondes acoustiques vis-à-vis de la surface de combustion, ce qui n'est pas sans poser un problème de définition dans le cas d'un mode acoustique stationnaire. Le problème du "Flow Turning" a également été examiné en détail par W.K. Van Moorhem (réf. 17) qui aboutit à des interrogations d'ordres physique et mathématique.

Les remarques suivantes peuvent être avancées :

- la notion de "Flow Turning" tente de décrire globalement et de manière approchée l'adaptation du champ instationnaire près de la surface de combustion au champ acoustique de cavité, que ce soit en description monodimensionnelle ou tridimensionnelle,

- la démarche mathématique contraint à utiliser une relation acoustique qui suppose le champ instationnaire irrotationnel.

Tout le problème du "Flow Turning" tient donc au paradoxe qui est illustré par la figure 7 et qui est intimement lié à la représentation du mode d'instabilité par un mode acoustique près de la surface de combustion. Le mode acoustique est par nature irrotationnel et correspond donc à une condition de glissement sur la surface. La physique de la combustion impose quant à elle que les produits de combustion soient émis perpendiculairement à la surface de combustion, par simple application du théorème des quantités de mouvement. Il doit donc exister une zone d'adaptation possédant un caractère rotationnel où la vitesse acoustique subit une transition et qui fait passer le mouvement instationnaire de normal à parallèle à la surface.

Mode de cavité irrotationnel

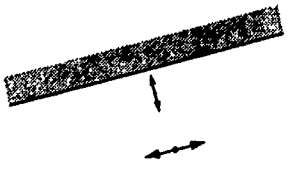

Mode d'instabilité . rotationnel

Figure 7 - Un mode acoustique de cavité donne t - il une bonne représentation du mode d'instabilité près de la surface de combustion ?

Ce paradoxe est également lié à la définition précise de la position de la surface de contrôle délimitant le volume où est réalisé le bilan acoustique et sa résolution donne lieu à deux approches (paragraphe 3.1.1.) :

- soit cette surface est définie à la frontière extérieure de la zone d'adaptation, ce qui suppose implicitement cette zone suffisamment fine, et des conditions limites modifiées sont introduites sur cette surface : c'est la théorie de la couche limite acoustique,

- soit cette surface est définie immédiatement après la zone de combustion et sur la frontière intérieure de la zone d'adaptation, ce qui impose une description rotationnelle du champ instationnaire.

2.2.3. Analyse non-linéaire de la stabilité

L'analyse non-linéaire de la stabilité a donné lieu depuis dix ans à de nombreux travaux qu'il est possible de classer en deux catégories :

- les travaux se situant dans le prolongement direct du bilan acoustique, utilisant une formulation analytique du problème et le recours ultime au calcul numérique,

- les travaux reposant sur le traitement numérique des équations de la mécanique des fluides.

Ces travaux peuvent aussi être décomposés suivant les objectifs. Certains d'entre eux visent plutôt à dégager les phénomènes fondamentaux importants qui contrôlent l'instabilité non-linéaire : c'est par exemple le cas de la méthode de l'"Averaging" qui explique la saturation du niveau d'une instabilité d'abord linéaire par un couplage de modes. D'autres travaux s'intéressent en priorité à la stabilité dynamique, par exemple ceux portant sur le traitement numérique monodimensionnel. D'autres enfin cherchent à concilier l'aspect fondamental et l'aspect appliqué et sont illustrés par les exemples du paragraphe 4.3.

2.2.3.1. Prolongement du bilan acoustique

Le principe conceptuel des approches non-linéaires dérivées du bilan acoustique peut être résumé comme suit (réf. 18) : le couplage de mode est le phénomène par lequel des modes d'amplitudes finies interagissent pour produire un changement d'amplitude des modes isolés. Lorsqu'un mode initialement linéaire croît en amplitude, les effets non-linéaires vont amener un transfert partiel de son énergie vers d'autres modes, l'autorisant ainsi à évoluer vers une amplitude stabilisée (cycle limite).

La démarche mathématique a fait l'objet de nombreuses publications, notamment des chercheurs du Caltech et de Penn State University (réf. 19 à 23). Elle ne sera que rappelée ici.

Les grandeurs sont développées par une méthode de perturbation du type :

$$\begin{aligned} \rho &= \bar{\rho}_0 + \mu^a \bar{\rho}_1(\vec{r}) + \varepsilon \rho'(\vec{r},t) \\ \vec{u} &= \mu \vec{u}(\vec{r}) + \varepsilon \vec{u}'(\vec{r},t) \\ p &= \bar{p} + \mu^2 \bar{p}_1(\vec{r}) + \varepsilon p'(\vec{r},t) \end{aligned} \qquad (2.20)$$

où μ est un paramètre caractéristique de l'écoulement stationnaire et ε un paramètre mesurant l'amplitude des oscillations. Par développement des équations de base, une équation d'onde est formée comme pour l'analyse linéaire :

$$\Delta p' - \frac{1}{a^2}\frac{\partial^2 p'}{\partial t^2} = h' , \qquad (2.21)$$

où h' est maintenant développé au second ordre.

La solution de cette équation est exprimée par une somme des modes acoustiques de cavité pondérés par des fonctions du temps :

$$\begin{aligned} p'(\vec{r},t) &= \bar{\rho}_0 \sum_{N=1}^{\infty} \eta_N(t) \tilde{p}_N(\vec{r}) \\ \vec{u}'(\vec{r},t) &= \frac{a^2}{\delta} \sum_{N=1}^{\infty} \frac{1}{\omega_N^2} \dot{\eta}_N(t) \vec{\nabla} \tilde{p}_N(\vec{r}) \end{aligned} \qquad (2.22)$$

Les fonctions $\eta_N(t)$ sont exprimées par :

$$\eta_N(t) = A_N(t)\sin(\omega_N t) + B_N(t)\cos(\omega_N t) \qquad (2.23)$$

et l'intégration est réalisée sur une période du mode fondamental, en supposant des variations "lentes" de A_N et B_N dans le temps, pour donner des équations différentielles ordinaires du type :

$$\begin{aligned} \frac{dA_N}{dt} &= \alpha_N A_N + \beta_N B_N + \text{(termes quadratiques en } A_N, B_N) \\ \frac{dB_N}{dt} &= -\beta_N A_N + \alpha_N B_N + \text{(termes quadratiques en } A_N, B_N) \end{aligned} \qquad (2.24)$$

Les solutions des équations différentielles non-linéaires sont recherchées analytiquement ou numériquement.

Les développements peuvent être poussés au troisième ordre des développements (réf. 21 et 22) mais le troisième ordre ne semble affecter que l'amplitude du cycle limite et le domaine de stabilité (réf. 21).

Cette méthode est intéressante parce qu'elle permet de pousser assez loin les calculs analytiques et d'en dominer parfaitement la signification. Les observations suivantes doivent cependant être faites :

- représentativité des modes d'instabilité linéaire par des modes de cavité : ce point a déjà été évoqué précédemment, la représentation n'est que partielle.

- développement aux ordres supérieurs des paramètres de perturbation : une hypothèse doit être faite sur les ordres de grandeur comparés de μ et ε pour conduire rationnellement le calcul, ce qui conduit à restreindre la portée des solutions obtenues.

- nombre de modes de cavité : les applications ne retiennent en général qu'un nombre limité de modes dont certains doivent être linéairement stables pour qu'un cycle limite puisse être atteint.

- développement des phénomènes élémentaires : tous les phénomènes intervenant dans la stabilité linéaire, dissipation biphasique, réponse du propergol..., doivent recevoir une description aux ordres élevés des développements. Ceci est réalisé par exemple par G.M.H.J.C. Gadiot et A. Gany (réf. 24 et 25) sur une base entièrement théorique mais malheureusement sans possibilité de vérification expérimentale autre que par les conséquences globales.

- évolution de la fréquence du mode prééminent : les modes de cavité ne sont en progression arithmétique que dans le cas des modes longitudinaux purs ce qui pose problème pour la moyenne dans le temps permettant d'établir les équations différentielles (2.24) et rend imprécis le transitoire d'établissement du cycle limite, sans doute un peu moins le cycle limite proprement dit.

2.2.3.2. Calcul numérique

L'intégration des équations de la mécanique des fluides permet en principe d'éviter toute hypothèse simplificatrice et devrait conduire à terme à des moyens d'analyse et de prévision performants. La simulation numérique des systèmes est une activité en évolution très rapide et le traitement numérique des instabilités de

combustion se heurte à des difficultés de nature générale et à des difficultés spécifiques :

- difficultés générales : les phénomènes de type convectif et de type propagatif doivent être pris en compte avec un égal soin, ce qui implique l'utilisation de schémas numériques adaptés et de maillage relativement raffinés. Les caractéristiques instationnaires du schéma numérique utilisé doivent être parfaitement maîtrisées pour que l'amortissement des phénomènes oscillatoires donné par le calcul corresponde bien au problème physique traité et non pas aux propriétés dissipatives et dispersives du schéma. Les maillages raffinés conduisent à des temps de calcul élevés, même sur les ordinateurs les plus puissants, et à des coûts élevés.

- difficultés spécifiques : l'expérience et la physique suggèrent de resserrer le maillage dans certaines zones sensibles telles que le proche voisinage de la surface de combustion et les angles vifs du chargement. Deux types de conditions limites font l'objet d'une attention spéciale : le raccordement de la chambre et de la tuyère et la surface de combustion. Pour le raccordement chambre-tuyère, on peut, pour les objectifs de recherches, imposer une pression statique oscillante ou des conditions reproduisant de manière approchée le fonctionnement instationnaire de la tuyère ; pour des applications, il semble plus sain de traiter simultanément chambre et tuyère (paragraphe 3.1.3). La surface de combustion pose le problème de la mise au point d'un modèle permettant de calculer la vitesse instantanée de combustion pour toute variation temporelle des grandeurs aérodynamiques locales, ce qui implique l'utilisation de méthodes numériques ; les modèles de couplage pression non-linéaires, comme ceux rappelés dans la référence 26, imposent au moins, en chaque point de la surface de combustion, l'intégration numérique d'une équation instationnaire de conduction thermique.

Les difficultés mentionnées limitent actuellement les ambitions à deux classes de problèmes : la simulation des instabilités non-linéaires dans les géométries simplifiées à l'aide d'une description monodimensionnelle et la simulation monophasique des instabilités non-linéaires d[illegible] des géométries axisymétriques. Le traitement rigoureux de géométries tridimensionnelles réalistes et d'écoulement diphasique ne semble pas encore avoir été abordé.

2.2.3.2.1. Simulation monodimensionnelle

La simulation monodimensionnelle ne permet pas de distinguer les niveaux de description du fluide (non visqueux, visqueux laminaire, turbulent) et a donné lieu à de nombreux travaux parmi lesquels il faut citer ceux de J.D. Baum, J.N. Levine et R.L. Lovine (réf. 27 à 31) pour deux raisons : le soin apporté au contrôle du schéma numérique et la comparaison entre calculs et essais. Les essais ont profité également de la mise au point de dispositifs de déstabilisation dynamique aux caractéristiques bien contrôlées.

La qualité des comparaisons entre calcul et expérience, pour des moteurs simplifiés déstabilisés, est plutôt satisfaisante compte-tenu des incertitudes sur le modèle de combustion (réf. 30) et des limites de l'approche 1D.

2.2.3.2.2. Simulation bidimensionnelle

Les travaux récents réalisés en simulation bidimensionnelle sont peu nombreux et se distinguent par les géométries traitées et le niveau de description du fluide. La géométrie bidimensionnelle (canal plan ou cylindrique de section constante) simplifie le maillage du champ et sert aux objectifs de recherche, la géométrie axisymétrique se rapprochant plus des applications. Le fluide peut être décrit soit compressible non visqueux (équations d'Euler), soit compressible visqueux laminaire (équations de Navier-Stokes), soit turbulent par l'intermédiaire d'un modèle classique (algébrique ou k-ε).

J.D. Baum (réf. 32) s'est intéressé à un canal cylindrique et a étudié de façon extrêmement détaillée l'interaction des champs stationnaire et instationnaire ; ses résultats sont repris au paragraphe 3.1.1.

R.A. Beddini (réf. 33) a, dans la même situation, réalisé un couplage entre l'écoulement instationnaire turbulent et une flamme simplifiée en vue d'expliquer la transition à la turbulence dans le cas d'une instabilité et d'approfondir le couplage-vitesse.

L'ONERA s'est intéressé à des géométries axisymétriques. Dans un premier temps, une tentative a été faite pour étendre au bidimensionnel le calcul monodimensionnel tenant compte du couplage pression non-linéaire. Plus récemment, les travaux ont été réorientés vers la description fine des phénomènes aérodynamiques de champ ; quelques résultats sont présentés au paragraphe 4.3.

2.3. Observations expérimentales et imperfections de l'analyse des instabilités de combustion

Les différentes recherches sur la stabilité non-linéaire statique ou dynamique n'ont pas encore donné naissance à des outils utilisables pour la conception des moteurs, mise à part la méthode de l'"Averaging". Le bilan acoustique et l'"Averaging" ne donne des résultats réalistes que si la base des modes linéaires est elle-même réaliste. Ce chapitre sera consacré à la comparaison d'observations expérimentales et des prévisions linéaires correspondantes, en mettant en relief quelques exemples significatifs où la prévision a été contredite par l'expérience.

2.3.1. Observations générales

Les instabilités de combustion se manifestent dans un domaine de fréquence de 10 Hz à plus de 10000 Hz suivant la taille et l'architecture du propulseur. Même si les phénomènes physiques mis en jeu à ces diverses fréquences présentent une unité certaine, la maîtrise de toutes les instabilités susceptibles d'être rencontrées, avec des outils communs, constitue un véritable défi, ne serait-ce qu'au niveau des données d'entrée. Cependant les moteurs présentent des spécificités selon les missions visées et il leur correspond généralement des modes particuliers d'instabilité :

- moteurs de premier étage de lanceur : le diamètre atteint 4 m, la longueur près de 30 m, le propergol aujourd'hui universellement retenu est un composite perchlorate d'ammonium/aluminium/polybutadiène, la fabrication utilise fréquemment la segmentation ; les segments sont à géométrie cylindro-conique sauf pour l'un d'entre eux à motif étoilé ou à ailettes. Les premières fréquences mises en jeu sont faibles, 15 à 25 Hz, et les moteurs opérationnels légèrement instables naturellement, avec des niveaux stabilisés modérés. L'opinion est répandue que la segmentation peut favoriser l'instabilité sur les premiers modes longitudinaux.

- moteurs pour missiles stratégiques : le diamètre peut dépasser 2m, la longueur varie suivant l'étage, le propergol est un composite métallisé à liant inerte ou énergétique, le chargement est monobloc. La géométrie Finocyl a tendance à s'imposer aujourd'hui. La France

fait également usage de chargements axisymétriques usinés ; des instabilités ont été observées dans la gamme des moyennes fréquences, à partir d'environ 100 Hz, c'est-à-dire sur des modes longitudinaux-radiaux, avec des niveaux stabilisés tolérables.

- moteurs pour missiles tactiques : il existe une grande diversité de taille, de propergol et de chargement, qui rend difficile toute généralité. On note toutefois que la tendance à utiliser des propergols "sans fumée" ou à "fumée-réduite" conduit à supprimer ou à réduire la charge métallique qui joue un rôle important dans l'amortissement des instabilités à moyenne et haute fréquence ; aussi doit-on quelquefois réintroduire un faible pourcentage de particules d'oxyde réfractaire dans le propergol pour stabiliser le fonctionnement. Les modes tangentiels, généralement tournants, entraînent souvent une dérive de la pression stationnaire et sont particulièrement redoutés.

2.3.2. Reproductibilité des instabilités

La reproductibilité des instabilités ne peut être rigoureusement déterminée que dans des conditions très strictes : même géométrie du propulseur, même lot de propergol, mêmes conditions d'essais. Ces conditions sont rarement réunies.

La reproductibilité est généralement bonne sur les fréquences, moins satisfaisante sur les niveaux d'instabilité. Les instabilités tangentielles conduisent à plus de dispersion. On peut signaler des essais de moteurs à chargement usiné dont les instabilités pouvaient appartenir à deux classes ; aucune explication satisfaisante n'a jamais été trouvée à cette ambivalence.

2.3.3. Reproductibilité des fréquences et de la stabilité statique

2.3.3.1. Moteur d'étude

L'exemple choisi porte sur un petit moteur d'étude de l'ONERA utilisé pour déterminer la réponse d'un propergol solide au couplage pression à haute fréquence (réf. 34 et 77) ; le moteur, stable naturellement, est destabilisé périodiquement sur son premier mode longitudinal et l'amortissement mesuré donne la réponse par l'intermédiaire d'un bilan acoustique. Ce moteur sert également de cas d'école pour la mise au point de la simulation numérique bidimensionnelle et l'analyse théorique des phénomènes aérodynamiques.

La fréquence croît naturellement au cours du fonctionnement. La figure 8 donne une comparaison des fréquences calculées par l'analyse linéaire 1D et mesurées. L'accord est satisfaisant, les écarts pouvant être imputés à des phénomènes mal contrôlés (ablation de l'inhibiteur...) ou au calcul de la fréquence acoustique (paragraphe 3.1.3.1.). La reproductibilité des fréquences est excellente, celle des amortissements acceptable pour ce type d'essai. L'observation est assez générale : des moteurs de géométries simples, conduisant à des évolutions régulières de fréquence et stables statiquement, présentent une bonne reproductibilité.

2.3.3.2. Moteurs segmentés

Les moteurs segmentés les mieux documentés sont ceux équipant les systèmes de lancement américains Titan III et Navette Spatiale. Le MPS d'Ariane doit faire l'objet d'un premier essai prochainement, il a été précédé d'un essai sur une maquette segmentée qui a démontré une légère instabilité.

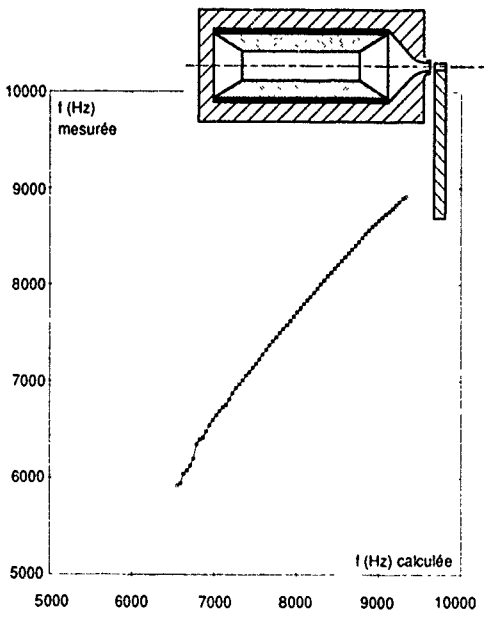

Figure 8 - Fréquences calculées et mesurées sur un moteur d'étude ONERA

La figure 9 relative au Titan 34D est extraite de la référence 35 et reproduit l'analyse de la composante instationnaire de pression enregistrée sur un capteur Kistler. Les fréquences observées se situent au voisinage des fréquences acoustiques mais leur évolution n'est pas continue : un phénomène en cascade est observé, caractérisé par une suite de décroissances de la fréquence entrecoupées de brutales remontées et suggérant des transitions entre des régimes d'instabilité. L'amplitude de l'oscillation de pression n'a pas dépassé 2 % de la pression moyenne. Un phénomène tout à fait comparable a été observé sur le Space Shuttle Booster (réf. 36), l'amplitude de pression atteinte n'a pas dépassé 3 % de la pression moyenne.

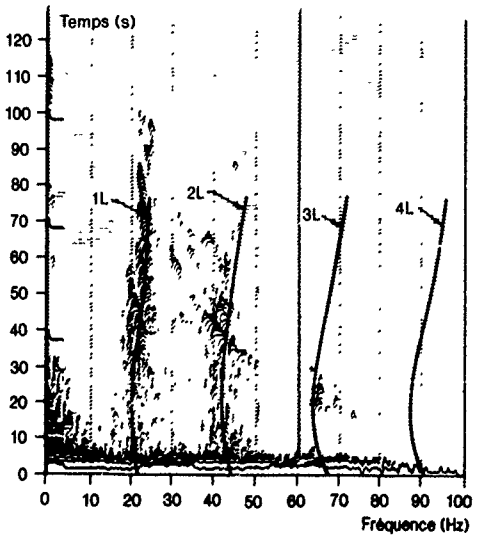

Figure 9 - Fréquences observées sur Titan 34D (réf. 35)

L'instabilité naturelle des moteurs segmentés a été une mauvaise surprise puisque les prévisions donnaient un comportement stable. Les tableaux 2.1 et 2.2 donnent une synthèse des calculs de bilan acoustique pour le premier mode longitudinal (réf. 35 et 37), α_{pc} et α_{vc} sont les contributions linéaires des couplages pression et vitesse, α_{tu} l'amortissement dû à la tuyère, α_{is} celui dû aux particules d'alumine et α_{ft} est le terme de "Flow Turning". Quelle que soit l'opinion qu'on puisse avoir sur le terme de "Flow Turning", on remarque que sa suppression ne change pas le signe de α ; l'amortissement est dans les deux cas presque exclusivement dû à la tuyère. Le désaccord entre prévision et observation a été à l'origine d'une remise en cause du bilan acoustique sous sa forme classique et a amené à incriminer un possible couplage entre l'acoustique et l'émission de structure tourbillonnaire ; ce phénomène fera l'objet du paragraphe 3.1.2.

La similitude des comportements observés à échelle 1 et à échelle réduite a surpris les chercheurs de l'ONERA et les experts étrangers en raison de la forte non-linéarité des phénomènes avec la fréquence. Ce point doit être réexaminé à la lumière de l'hypothèse d'un entretien de l'instabilité par l'émission tourbillonnaire, laquelle obéit à une similitude de Strouhal :

$$S_t = \frac{fL}{u} = Cte \qquad (2.25)$$

où u est une vitesse de référence.

2.3.3.4. Moteurs à chargement tridimensionnel Finocyl

La dénomination Finocyl résulte de la contraction de Fin (ailette) et cyl (cylindre), elle décrit un chargement

Tableau 2.1 - Prévision de la stabilité du SRM du Titan 34D (réf. 35)

Epaisseur brûlée (%)	Fréquence (Hz)	α_{PC} (s^{-1})	α_{VC} (s^{-1})	α_{N} (s^{-1})	α_{PD} (s)	α_{FT} (s^{-1})	α (s^{-1})
0	22,2	2,66	0,46	- 15,78	- 2,22	- 5,53	- 20,41
21,5	20,31	1,08	- 0,17	- 7,73	- 2,03	- 4,13	- 12,98
45	21,81	0,60	- 0,22	- 5,07	- 2,18	- 3,43	- 10,30
73,9	23,74	0,44	- 0,18	- 3,88	- 2,37	- 2,43	- 8,42

Tableau 2.2 - Prévision de la stabilité du SRB de la Navette Spatiale (réf. 36)

Epaisseur brûlée (%)	Fréquence (Hz)	α_{PC} (s^{-1})	α_{VC} (s^{-1})	α_{N} (s^{-1})	α_{PD} (s)	α_{FT} (s^{-1})	α (s^{-1})
0	15,25	2,87	0,05	- 15,14	- 0,62	- 3,92	- 16,76
45	13,17	0,46	- 0,01	- 8,38	- 0,57	- 2,29	- 10,79
80	16,18	0,31	—	8,06	- 0,66	- 1,49	- 9,90

2.3.3.3. Moteurs à chargement axisymétrique usiné

Spécialité française, ce type de moteur a donné lieu à de nombreuses observations dont une synthèse peut être trouvée dans les références 6 et 38. La figure 10 rappelle la géométrie du chargement ; il s'agit ici de la maquette à l'échelle 1/6 essayée en structure lourde. La figure 11 donne une synthèse des fréquences observées tant sur moteur réel que sur maquette ainsi que la fréquence acoustique calculée pour le premier mode (les temps et les fréquences sont ramenés à l'échelle 1).

On retrouve un phénomène d'évolution de la fréquence en cascade. La décroissance des modes supérieurs en fonction du temps n'est pas retrouvée par le calcul acoustique ; il faut toutefois remarquer qu'il est difficile de séparer les composantes harmoniques du mode le plus bas des modes supérieurs (certains essais à échelle réduite ont conduit à une amplitude maximale d'oscillation de pression crête à crête de près de 10 % de la pression moyenne). L'essai réalisé avec un propergol non métallisé est parti en instabilité tangentielle après deux secondes de fonctionnement : fréquence voisine de 7000 Hz, amplitude crête à crête supérieure à 80b, pression moyenne augmentée de plus de 80b !

constituée d'un canal cylindrique circulaire raccordé à un motif à ailettes ; la dénomination Conocyl est parfois rencontrée, le chargement peut également présenter des gorges circonférentielles supplémentaires. Ces chargements utilisés sur les moteurs modernes conduisent à des écoulements fortement tridimensionnels.

Un mode en cascade a été observé sur le premier étage du missile Poseidon, il y a près de 20 ans (réf. 39, figure 1). La fréquence mesurée était au voisinage de 80 Hz, entre 8 et 12s de fonctionnement. Des amplitudes de vibration supérieure à 20g crête sur la tuyère ont été relevées.

Le moteur du troisième étage du missile Minuteman III a également exhibé, dans sa première version, un mode en cascade (réf. 32 et 40). Comme visible sur la figure 12, les fréquences varient fortement et s'éloignent de la fréquence calculée pour le premier mode longitudinal de cavité.

A contrario, certains moteurs pour étages supérieurs de lanceurs, caractérisé par un faible allongement ont manifesté une stabilité statique en essais alors que le bilan acoustique prévoyait l'instabilité (réf. 41). Les

chercheurs ont incriminé la faible représentativité du terme de "Flow Turning" pour la prédiction de l'interaction entre le champ stationnaire et l'acoustique ainsi qu'une forte surestimation du couplage-vitesse.

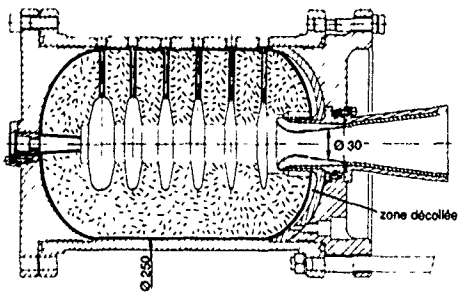

Figure 10 - Maquette de moteur à chargement axisymétrique usiné

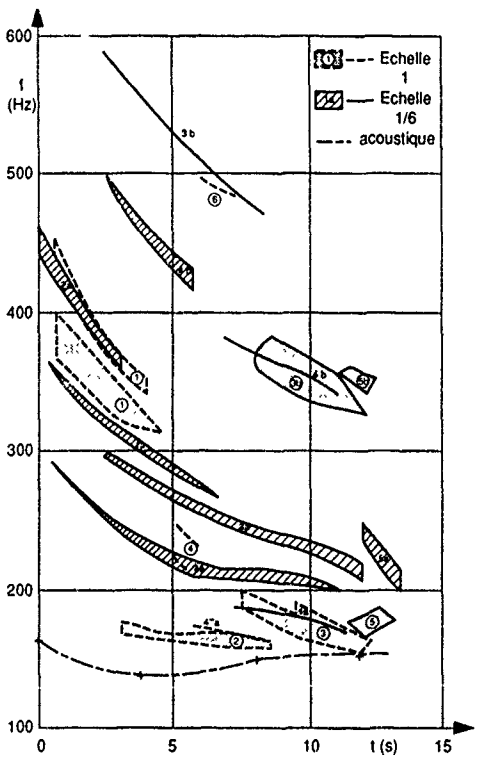

Figure 11 - Fréquences observées sur moteurs à chargement axisymétrique usiné

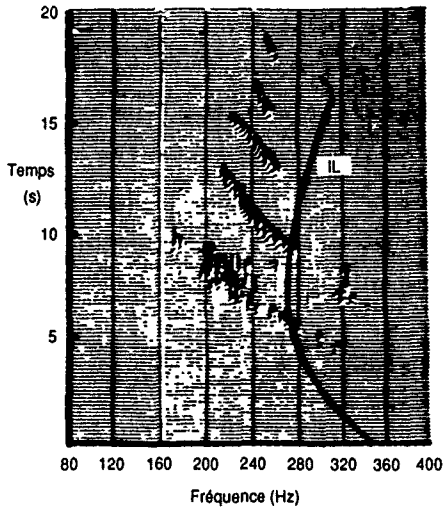

Première version

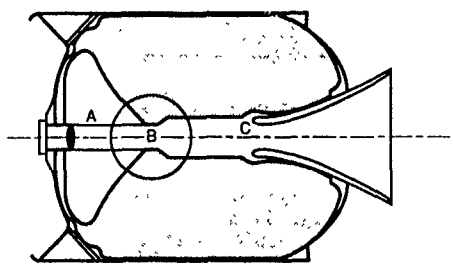

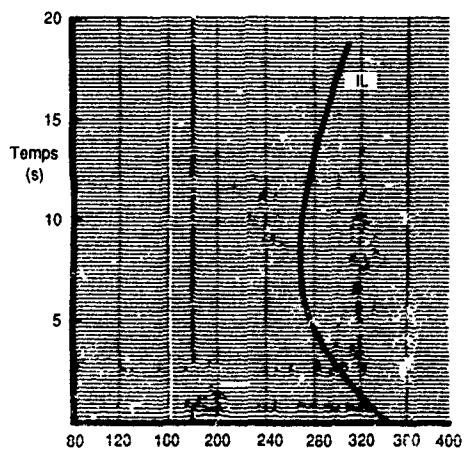

Version modifiée

Figure 12 - Fréquences observées sur le troisième étage du Minuteman III

2.3.3.5. Sensibilité des instabilités à des modifications géométriques du chargement

Deux exemples méritent d'être signalés. Le premier porte sur le moteur à chargement axisymétrique représenté sur la figure 10, la géométrie modifiée est donnée sur la figure 13. Le rôle moteur de l'émission tourbillonnaire sur les instabilités n'était pas connu à l'époque des essais ; par contre un essai avait été interrompu par détente et il avait été observé une combustion anormalement élevée sur la partie aval des gorges, au raccordement avec le canal central, ce qui laissait craindre un couplage-vitesse important. Les angles du chargement ont en conséquence été abattus dans cette zone. Le mode le plus bas est apparu exceptionnellement tard et les niveaux des modes supérieurs ont été atténués.

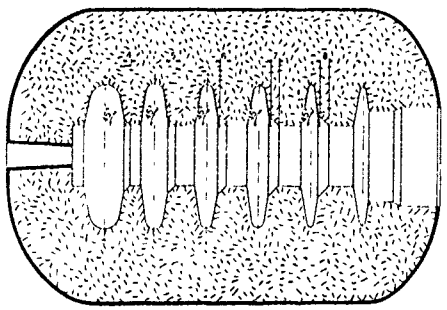

Figure 13 - Modification de la géométrie du chargement de la figure 10

L'autre exemple, beaucoup plus net, est lié au troisième étage du Minuteman III. L'explication du comportement instable avait été recherchée dans l'émission tourbillonnaire susceptible de prendre naissance au raccordement du motif à ailettes avec le canal central, en raison d'un fort étranglement. La diminution de l'étranglement aurait permis de diminuer sensiblement le niveau d'instabilité (réf. 40) ; on ne sait pas si la version modifiée dont les résultats sont reportés sur la figure 11 correspond à ce seul changement

2.3.4. Récapitulation

L'application du bilan acoustique pour la prévision de la stabilité linéaire a donné lieu à quelques déboires, surtout pour des géométries de chargement mettant en jeu des structures bidimensionnelles ou tridimensionnelles d'écoulement. L'apparition de modes en cascade pour des moteurs dont le diamètre s'échelonne de 250mm à 4m et pour des fréquences de 15 à plus de 1000 Hz conduit à s'interroger sur la validité du dénombrement classique des phénomènes élémentaires. Certains phénomènes comme le "Flow Turning" et le couplage-vitesse demandent également un réexamen.

3. PROGRES RECENTS DANS LA PHYSIQUE DES PHENOMENES ELEMENTAIRES

Le bilan acoustique met en évidence des contributions liées au champ aérodynamique instationnaire et des contributions liées à la combustion du propergol. Bien qu'obligatoirement simplifiée, cette distinction entre phénomènes aérodynamiques et phénomènes de combustion est retenue pour la présentation. L'accent sera mis sur les phénomènes aérodynamiques, dont la maîtrise semble aujourd'hui constituer un préalable indispensable à l'approfondissement des phénomènes de combustion.

3.1. Phénomènes aérodynamiques

L'aérodynamique interne des moteurs à propergol solide est très particulière car l'écoulement naît sur la surface de combustion. Cette particularité confère à l'écoulement stationnaire un caractère rotationnel qui devrait trouver un prolongement en instationnaire. Les connaissances sur les écoulements acquises dans d'autres secteurs d'activité requièrent un travail d'adaptation qui commencent généralement par une recherche dans des conditions simplifiées facilitant l'interprétation physique des résultats. Quatre problèmes seront successivement examinés : l'interaction entre les champs stationnaire et oscillatoire au voisinage de la surface de combustion, les instabilités hydrodynamiques de l'écoulement, le comportement instationnaire de la tuyère et l'aspect diphasique de l'écoulement. Les deux premiers problèmes restent encore ouverts et ont donné lieu à différentes approches qui seront commentées en vue de dégager les acquis et leurs conséquences pratiques.

3.1.1. Interaction entre champs stationnaire et oscillatoire en surface de combustion

Cette interaction recouvre plusieurs phénomènes complémentaires pour lesquels il existe encore plusieurs approches. Pour la clarté de la présentation, nous distinguerons successivement les approches linéaires des approches non-linéaires.

3.1.1.1. Théories linéaires

Les théories linéaires traitent par le calcul analytique la couche d'adaptation du champ acoustique aux conditions de surface et deux niveaux peuvent être distingués suivant que l'écoulement stationnaire est décrit de façon plus ou moins simplifiée. Le terme de couche limite acoustique sera utilisé mais prête quelque peu à confusion : la prise en compte de la viscosité laminaire est indispensable à l'analyse mais dans certains cas, les résultats finaux sont indépendants de la viscosité.

3.1.1.1.1. Théories de la couche limite acoustique

La couche limite représente en aérodynamique classique la zone mince adjacente à la paroi où sont concentrés les effets visqueux de l'écoulement. Si l'écoulement est oscillatoire à faible amplitude, une couche limite acoustique peut être mise en évidence sur une paroi inerte, sa description est aisée en laminaire. Le problème peut être réexaminée pour une paroi débitante. Les premiers travaux ont été conduits par G.A. Flandro (réf. 42) qui a en particulier démontré que, vue de l'intérieur de la cavité, la surface de combustion présente une admittance qui n'est pas l'admittance liée au couplage pression mais cette dernière corrigée d'un terme traduisant la présence de la couche acoustique. Les hypothèses utilisées ainsi que la démarche suivie sont rappelées, en suivant les notations de la référence 43 :

- l'écoulement stationnaire est uniforme et normal à la paroi, ce qui lui confère un caractère irrotationnel.
- le rapport de l'épaisseur δ_c de la couche limite acoustique sans injection à la longueur d'onde est de l'ordre du nombre de Mach d'injection, soit

$$F = \frac{\sqrt{\varepsilon}\,\bar{M}_x a}{\sqrt{\omega\nu}} = O(1) \qquad (3.1)$$

- le problème est bidimensionnel en x et y, l'axe des x étant parallèle à la surface et l'axe des y perpendiculaire (figure 14).

- les équations aux dérivées partielles linéaires sont écrites pour les perturbations des composantes de vitesse, de pression et de température ; les conditions limites sur la surface se traduisent par $u' = 0$ et v'/p' proportionnel à l'admittance A_p ; les conditions limites à l'infini suivant y correspondant au raccordement avec le champ acoustique.

- les solutions analytiques sont recherchées sous la forme :

$$p' = C e^{i\omega t} e^{kx} \ldots\ldots \quad (3.2)$$

- l'intégration donne directement les solutions u', v', p'

Les conséquences principales de cette analyse sont les suivantes :

- extension de la couche limite acoustique : une expression approchée peut être obtenue (réf. 43, 44 et 45) sous la forme :

$$\delta = \delta_0 \left[\sqrt{\frac{F^2 + \sqrt{F^4 + 64}}{8}} - \frac{F}{2} \right]^{-1} \quad (3.3)$$

L'épaisseur de la couche limite acoustique en présence d'un soufflage de paroi est toujours supérieure à celle sur paroi inerte, l'amplification étant liée au paramètre F qui combine le nombre de Mach de soufflage, la viscosité laminaire et la fréquence.

- la composante longitudinale de vitesse présente, comme indiqué sur la figure 14, un comportement oscillatoire qui s'amortit au fur et à mesure de l'éloignement de la surface. Un maximum d'amplitude près de la surface ainsi qu'un déphasage vis-à-vis de la vitesse acoustique sont mis en évidence ; cet effet peut être essentiel pour la compréhension du couplage-vitesse. Le champ de pression est quant à lui insensible à la couche limite acoustique.

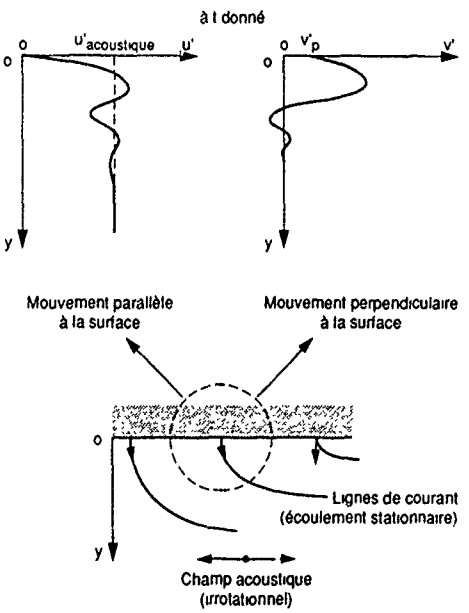

Figure 14 - Raccordement du champ instationnaire au champ acoustique

- la correction d'admittance, ou la correction de réponse équivalente, peut être calculée ; elle s'exprime en fonction du Mach d'injection M_x et du nombre de Reynolds acoustique :

$$Re_a = \left(\frac{\rho a}{\omega \delta_0} \right)^2 \quad (3.4)$$

Remarque sur le comportement limite des solutions

Les résultats se simplifient lorsque F >> 1, ce qui correspond bien à la plupart des applications mais contredit l'hypothèse de départ F = 0(1).

Le premier résultat concerne l'épaisseur de la couche limite acoustique :

$$\delta \simeq \frac{\delta_0 F^2}{4} = \frac{M_x^2 a^2}{\gamma \omega^2} \quad (3.5)$$

Pour des moteurs homothétiques sujets à des modes d'instabilités semblables, ω sera inversement proportionnel à l'échelle et il en va de même du rapport de δ à une dimension caractéristique de la cavité. La théorie de la couche limite acoustique, qui ne présente d'intérêt que si l'épaisseur de cette dernière est négligeable vis-à-vis des dimensions de la cavité, semble mieux adaptée aux petits moteurs qu'aux gros moteurs. Pour ces derniers, la couche limite acoustique des modes de basse fréquence peut occuper une fraction notable de la cavité.

La correction d'admittance tend, dans les mêmes conditions vers une valeur indépendante de la viscosité :

$$\Delta A_{pc}^{(r)} \simeq - M_x \quad (3.6)$$

Le bilan acoustique peut être alors facilement corrigé soit dans l'expression du terme de couplage-pression, soit en introduisant un terme correctif proportionnel à l'intégrale $\int_{\sigma_0} \tilde{p}_0^2 \, d\sigma_0$.

Il est intéressant de remarquer que pour un canal cylindrique, le terme correctif issu de la couche limite acoustique est strictement équivalent au terme de "Flow Turning" : l'approche globale du "Flow Turning" et l'approche plus détaillée de la couche limite acoustique se rejoignent dans ce cas particulier et confirment l'intuition de F.E.C. Culick. Toutefois cet accord n'existe plus pour des géométries complexes. L'objet du travail présenté dans la référence 43 était justement de comparer les deux approches, sur la base de la cohérence des résultats expérimentaux obtenus sur le petit moteur de la figure 8. Différentes géométries de chargement conduisent, aux mêmes pression stationnaire et fréquence, à des termes différents de "Flow Turning" et de correction d'admittance. Les réponses déduites des amortissements mesurés, sur un même propergol, doivent être identiques pour l'analyse la plus réaliste. La figure 15 donne un exemple des résultats obtenus ; les deux tracés récapitulatifs dans l'espace (F, $\bar{p}$, $R_{pc}^{(r)}$) dégagent les conditions pour lesquelles les comparaisons peuvent être faites et les différences entre les résultats. Les diverses comparaisons effectuées inclinent à penser que l'approche par correction d'admittance est meilleure. Cette conclusion suppose qu'il n'existe pas de phénomène dépendant de la géométrie qui aurait été omis dans le bilan acoustique, comme par exemple l'émission tourbillonnaire (géométrie A).

L'approche qui vient d'être rappelée est celle de la couche limite acoustique classique, elle a permis un premier pas dans la compréhension des phénomènes aérodynamiques d'adaptation près de la surface de combustion. Elle limite la portée de la simplification traduite par la relation (2.14) mais ne tient compte que du terme $(\vec{\nabla} \wedge \vec{\Pi}) \wedge \vec{\Pi}$. Par contre, il subsiste le problème du terme $((\vec{\nabla} \wedge \vec{\Pi}) \wedge \vec{\Pi}) \cdot \vec{\nabla} \bar{p}_0$ qui fait intervenir le rotationnel de l'écoulement stationnaire. La théorie de la couche

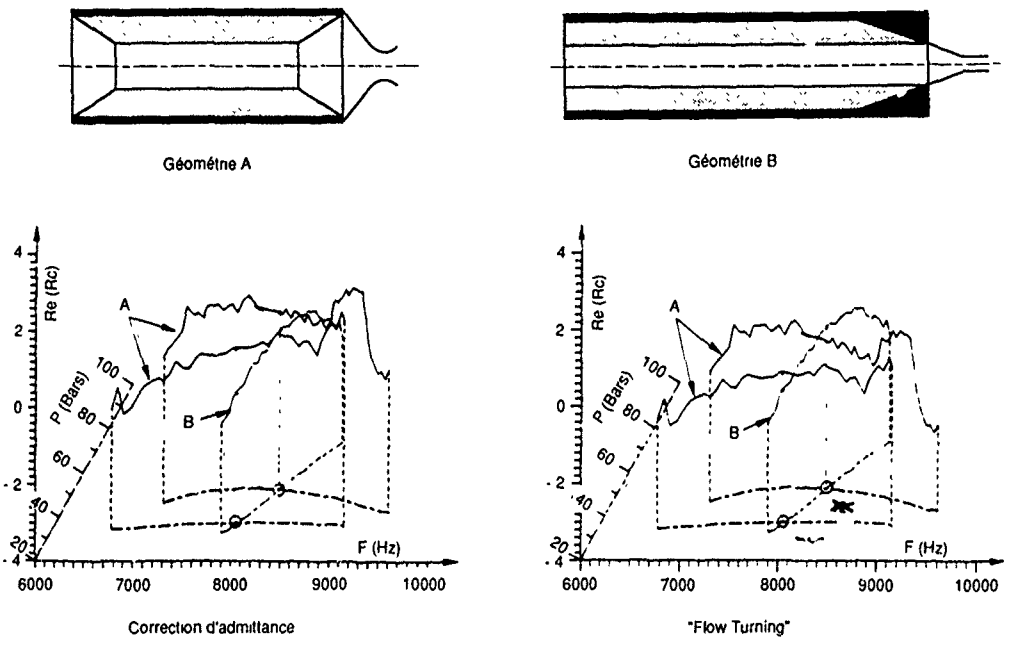

Figure 15 - Coherence des réponses déterminées à partir des approches "low Turning" et correction d'admittance (réf 43)

limite acoustique a été reprise par plusieurs chercheurs pour tenir compte plus précisément du champ stationnaire près de la surface et expliquer les observations en simulation gazeuse instationnaire (réf. 44 à 47). Travaillant sur une cavité cylindrique, U.G. Hegde, F. Chen et B.T. Zinn introduisent l'expression du champ stationnaire dans toute la cavité et limitent les développements au premier ordre (réf. 44). Les calculs ne seront pas reproduits ici. L'influence de la vitesse d'injection et de la fréquence, déjà établie, est bien retrouvée mais des résultats nouveaux sont également démontrés. Le principal est que les phénomènes de couche limite acoustique varient de façon sensible avec la position axiale sur la surface de combustion. C'est le cas pour la répartition des composantes longitudinales et radiales de vitesse ainsi que de la correction d'admittance. La correction d'admittance comprend le terme classique et un terme supplémentaire lié au champ stationnaire et proportionnel à

$$\vec{u}_s \frac{d\vec{p}_s}{dz},$$

$\vec{u}_s$ étant la vitesse stationnaire sur l'axe et $\frac{d\vec{p}_s}{dz}$ le gradient de pression acoustique. Ce terme supplémentaire induit un comportement singulier au voisinage du minimum de pression acoustique.

Les conséquences sur le bilan acoustique de l'extension de la théorie de la couche limite acoustique sont importantes :

- la limitation reste liée à l'épaisseur de la couche limite acoustique, c'est-à-dire à la possibilité de traduire l'effet de cette couche par un terme de surface.

- le bilan acoustique n'est plus indépendant du champ stationnaire, qui doit avoir fait l'objet d'un calcul préalable, ce qui complique notablement la démarche.

Il semble possible d'étendre l'approche de U.G. Hegde et al. à des géométries complexes. Il paraît naturel de caractériser dans ce cas chaque point de la surface par le rotationnel local $\mathcal{R}_p$ et de reprendre les calculs avec le champ stationnaire local :

$$\vec{\omega} = \gamma \mathcal{R}_p \ , \ \vec{v} = \vec{v}_s \qquad (2D) \qquad (3.7)$$

Un nouveau paramètre apparaît par l'adimensionnement des grandeurs :

$$\frac{\mathcal{R}_p \delta_s}{a} \ , \qquad (3.8)$$

il doit être comparé en ordre de grandeur aux autres paramètres.

3.1.1.1.2. Généralisation du bilan acoustique

L'idée générale qui sous-tend cette généralisation est de limiter les simplifications telles que (2.14), lorsqu'ont été combinés les problèmes linéaires décrivant respectivement l'instabilité et l'acoustique ; elle est illustrée par les travaux de T.J. Chung (réf. 48 et 49). Le problème peut être résolu sur le plan formel et conduit à des intégrales où apparaissent $\vec{p}$, $\vec{\Omega}$ et $\vec{\nabla}\wedge\vec{\Omega}$, en combinaison avec les caractéristiques du champ stationnaire de vitesse ; $\vec{\Omega}$ peut être décomposé en une composante irrotationnelle $\vec{\Omega}^{(a)}$ et une composante rotationnelle $\vec{\Omega}^{(v)}$. $\vec{p}$ et $\vec{\Omega}^{(v)}$ sont assimilables à $\vec{p}_M$ et $\vec{\Omega}_M$ mais il reste évidemment une difficulté avec $\vec{\Omega}^{(a)}$.

Cette approche est uniquement intéressante du point de vue théorique. Elle permet d'identifier les sources potentielles d'instabilité au travers des termes des équations et de proposer leur interprétation physique, elle sépare les sources dépendant de la viscosité des autres. Par contre, il n'est pas possible de donner une traduction de la théorie pour la plupart des applications sauf à admettre un calcul séparé du champ $\vec{\Omega}^{(v)}$, ce qui ramène à la théorie de la couche limite acoustique.

3.1.1.2. Calcul numérique

Un travail très approfondi a été mené par J.D. Baum sur une cavité cylindrique (réf. 32). Les équations de l'écoulement visqueux turbulent (modèle k-ε) sont intégrées à l'aide d'une méthode de différences finies pour trois situations de complexité croissante :

- une paroi inerte en l'absence d'écoulement moyen,
- une paroi inerte en présence d'un écoulement moyen,
- une paroi débitante.

Des ondes propagatives et stationnaires sont successivement considérées.

Le calcul numérique retrouve et précise ce qui a été mis en évidence par les méthodes analytiques :

- le phénomène dépend de la fréquence et de la vitesse d'injection mais aussi de la direction de propagation de l'onde, il varie avec la position axiale.

- la dissipation de l'énergie acoustique est principalement concentrée dans la couche limite acoustique, elle est accrue avec la fréquence et la vitesse d'injection et plus importante pour les ondes se propageant vers l'amont que pour celles se propageant vers l'aval.

- l'écoulement stationnaire joue un rôle important et le couplage devient rapidement non-linéaire.

Le rôle de la turbulence n'est pas facile à apprécier puisque il y a, même en stationnaire, transition du laminaire au turbulent suivant l'abscisse. R.A. Beddini, utilisant une technique de linéarisation des équations turbulentes, conclut que le champ instationnaire peut favoriser la transition à la turbulence même pour de faibles amplitudes et induire un couplage-vitesse (réf. 33). Il faut remarquer que la turbulence en moteur reste imparfaitement connue et qu'il n'est pas assuré que les modèles standards de turbulence développée en fournissent une bonne représentation.

Les travaux de F. Vuillot et G. Avalon (réf. 50 et 51) portent sur des situations pour lesquelles la couche limite acoustique occupe une grande partie de la cavité. Les équations de Navier-Stokes pour l'écoulement laminaire sont intégrées par une méthode de volumes finis utilisant un schéma explicite de Mc Cormack. Le travail préliminaire de la référence 50 considère une cavité parallélipipédique et un débit unitaire constant ; la condition limite aval porte sur la pression statique d'abord constante pour obtenir le fonctionnement stationnaire puis oscillatoire autour de sa valeur stationnaire pour l'étude du mode stationnaire forcé. La figure 16 illustre le champ instationnaire de vitesse vers le fond arrière de la cavité lorsque la fréquence d'excitation est 0,8 fois celle du premier mode longitudinal, et l'amplitude relative de la pression d'excitation de 5 %. On peut constater, d'une part le caractère très rotationnel de l'écoulement et, d'autre part, l'incidence de l'écoulement moyen qui rompt la symétrie du cycle. Le travail plus récent de la référence 51 intéresse un propulseur axisymétrique de grande taille représentatif du MPS d'Ariane 5. Le propulseur est complet et le calcul porte à la fois sur la chambre et sur la tuyère ; l'excitation est simulée par une source acoustique de pression pendant quelques périodes, l'analyse des signaux instationnaires étant conduite soit pendant la phase d'excitation soit après. L'amortissement calculé numériquement est comparé à celui prévu par un bilan acoustique utilisant la correction d'admittance, le débit injecté étant constant. Il apparaît que le développement de la couche limite acoustique dans la cavité limite l'amortissement qui est de ce fait fortement surestimé par le bilan acoustique ; des effets non-linéaires

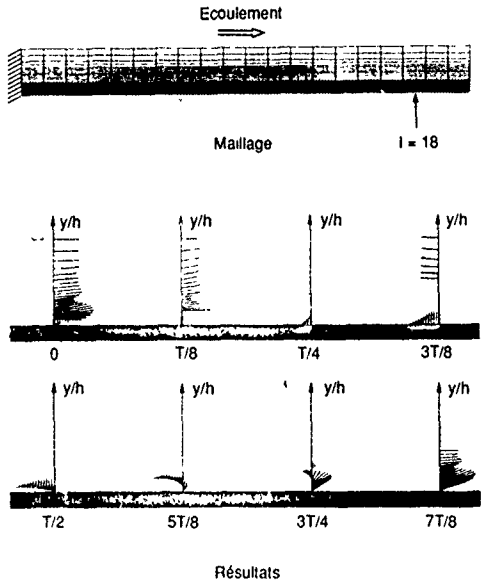

Figure 16 - Calcul du champ instationnaire au voisinage de la surface de combustion (réf 50)

sont également mis en évidence avec l'apparition de modes de haute fréquence après l'excitation.

3.1.1.3. Récapitulation

L'ensemble des recherches réalisées convergent vers l'idée que l'interaction entre champs stationnaire et oscillatoire en surface de combustion doit être prise en compte dans l'analyse de la stabilité ; il existe un accord au moins qualitatif entre les théories analytiques et les calculs numériques (réf. 46). Deux situations extrêmes peuvent être distinguées par l'examen de l'épaisseur de la couche limite acoustique. Si cette épaisseur est très faible devant les dimensions de la cavité, ce qui est le cas pour les petits moteurs, le bilan acoustique doit inclure un terme stabilisant de correction d'admittance dont l'expression dépend en toute rigueur de l'écoulement stationnaire en surface de combustion. Si l'épaisseur est au contraire comparable aux dimensions de la cavité, le couplage se fait dans tout le volume et seul le calcul numérique est utilisable. Dans les deux cas, le calcul numérique est nécessaire soit pour déterminer l'écoulement stationnaire seul, soit pour traiter l'écoulement complet, ce qui tend à orienter les efforts vers le traitement numérique des instabilités ; des limites existeront toutefois pour le calcul numérique en raison de l'extreme finesse du maillage indispensable en surface de combustion. La description du fluide pour le calcul numérique doit être au moins laminaire, l'influence de la turbulence et sa modélisation demandent à être précisées.

3.1.2. Instabilités hydrodynamiques de l'écoulement

3.1.2.1. Généralités

L'émission naturelle de tourbillons par un obstacle placé dans un écoulement est un phénomène commun résultant d'une instabilité hydrodynamique. L'analyse élémentaire des instabilités hydrodynamiques d'un écoulement peut être réalisée par linéarisation de l'équation du rotationnel et conduit, pour un écoulement stationnaire bidimensionnel, dans une seule direction mais possédant un profil de vitesse, à l'équation de Rayleigh (non

visqueux) ou d'Orr-Sommerfeld (laminaire). Un exemple particulièrement simple d'écoulement se résolvant en allée tourbillonnaire est celui de la couche de mélange. Les tourbillons se forment à une fréquence généralement caractérisée par un nombre de Strouhal, leur dynamique est complexe et très dépendante des conditions environnantes ; on assiste généralement à un développement de la taille du tourbillon puis à une saturation suivie d'un nouveau développement. Les tourbillons peuvent également s'apparier ou au contraire éclater et les effets tridimensionnels peuvent être prépondérants. Le caractère non-linéaire des phénomènes suivant la naissance des tourbillons est donc très net.

L'impact d'une couche de mélange sur une surface a également été longuement étudié, il induit une source sonore. Cette source peut entrer en interaction avec l'émission tourbillonnaire et donner lieu à une émission forcée. L'effet d'un champ acoustique sur l'émission tourbillonnaire a également été étudié par certains chercheurs ; R.D. Blevins est en particulier parvenu, dans le cas de l'émission d'un cylindre excitée transversalement, aux conclusions suivantes (réf. 52) :

- l'émission naturelle n'est pas un processus harmonique pur, la fréquence d'émission peut fluctuer de quelques pour cent.

- lorsque l'amplitude du champ acoustique est suffisante, la fluctuation de fréquence de l'émission disparaît. Si la fréquence acoustique est voisine de la fréquence naturelle d'émission, la fréquence d'émission s'accorde à la fréquence acoustique ; le décalage de fréquence de l'émission peut atteindre 8 % si l'amplitude de pression est de 0,03 b.

- le couplage se produit préférentiellement lorsque la fréquence acoustique est au-dessous de la fréquence naturelle d'émission, c'est plutôt la vitesse acoustique qui influence l'émission que la pression acoustique.

- la turbulence tend à supprimer l'influence du champ acoustique, la vitesse acoustique doit excéder la vitesse turbulente pour que le couplage se fasse.

Bien qu'obtenus dans des conditions particulières, ces résultats prouvent qu'un champ acoustique peut piloter l'émission des tourbillons, que le couplage est assez lâche et dépendant de l'amplitude de vitesse et qu'il existe certains seuils liés en particulier à la turbulence. Il s'agit donc d'un couplage de nature non-linéaire.

Les observations faites sur les moteurs segmentés des lanceurs américains ont conduit à rendre responsable des instabilités une émission tourbillonnaire prenant naissance dans l'interaction de l'écoulement avec les diaphragmes d'inhibiteur disposés sur la face amont des segments. Dans le prolongement des travaux de G.A. Flandro et H.R. Jacobs (réf. 53) un grand nombre de travaux, surtout expérimentaux ont été consacrés au problème (réf. 35, 54 à 59). La référence 35 est la plus détaillée pour le problème du Titan 34D :

- elle démontre que le "vortex shedding" est une source d'instabilité puisque le phénomène est reproduit et mesuré sur une maquette de simulation gazeuse à l'échelle 4,65 %.

- elle met en évidence la zone sensible où se réalise le couplage acoustique-émission tourbillonnaire, vers les bords amonts des segments 3 et 4, c'est-à-dire au voisinage du ventre de vitesse acoustique.

- elle propose une explication pour la décroissance de la fréquence d'instabilité en fonction du temps, à partir d'une conservation du nombre de Strouhal de l'émission ; l'effet de cascade serait dû à la transition vers un mode "supérieur" d'émission.

Le cas des moteurs à chargement axisymétrique usiné pose un problème différent puisqu'il n'existe pas d'obstacle dans l'écoulement. L'hypothèse la plus plausible repose sur l'émission de tourbillons par les angles vifs du chargement. L'équation linéarisée du rotationnel s'écrit :

$$\frac{\partial \vec{\Omega}'}{\partial t} + \vec{\nabla} \wedge (\vec{\Omega} \wedge \vec{u}') + \vec{\nabla} \wedge (\vec{\Omega}' \wedge \vec{u}) = 0 \qquad (3.9)$$

Les coins amonts des gorges sont caractérisés par une variation importante du rotationnel stationnaire (réf. 14) et constituent donc une source potentielle de couplage par le second terme de l'équation 3.9 ; on peut aussi noter que la marche descendante est une situation typique favorisant l'émission tourbillonnaire et incriminée en particulier sur certains statoréacteurs. la figure 17 propose un scénario pour cette situation :

- les tourbillons naissent sur l'angle vif du chargement.

- les tourbillons sont convectés par l'écoulement, se développent et s'organisent (ou de désorganisent...).

- les tourbillons impactent le fond arrière du moteur ou sont avalés par la tuyère ; dans les deux cas une onde progressive est produite et remonte l'écoulement stationnaire.

- l'onde est réfléchie par le fond avant, les ondes progressives descendant et remontant l'écoulement interagissent avec l'émission tourbillonnaire.

- le couplage se développe et, si les conditions favorables sont réunies, un phénomène oscillatoire s'entretient.

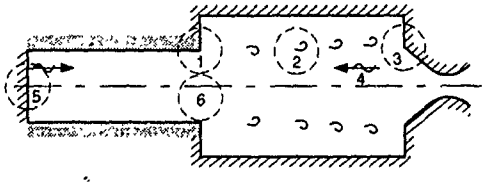

1 Naissance des tourbillons
2 Développement, organisation, convection des tourbillons
3 Impact des tourbillons
4 Onde progressive de retour
6 Réflexion de l'onde
6 Couplage acoustique - émission tourbillonnaire

Figure 17 - Mécanismes de l'émission tourbillonnaire

3.1.2.2. Approche linéaire de l'émission tourbillonnaire acoustiquement couplée

Le phénomène d'ensemble présente une juxtaposition d'événements convectifs et de propagations d'ondes ; les observations mettent par ailleurs en évidence des effets non-linéaires. Aussi peut-on légitimement s'interroger sur la possibilité d'une description linéaire de mode stationnaire qui permettrait de compléter le bilan acoustique. C'est toutefois une démarche qui a tenté plusieurs chercheurs et notamment G.A. Flandro (réf. 53 et 60), pour des raisons pratiques évidentes, et qui sous-entend quelques hypothèses simplificatrices : le couplage entre l'acoustique et l'émission tourbillonnaire n'est réalisé

qu'à la source, ce qui évite de prendre en compte toute modification par le champ oscillatoire de la phase de développement (réf. 61) ; le phénomène d'impact est assimilé à une source acoustique. Les résultats ne peuvent donc être qu'approchés et constituent plutôt un guide pour une recherche plus précise. Suivons la démarche théorique :

- le champ stationnaire de l'écoulement étant supposé préalablement calculé, un profil de vitesse longitudinal peut être établi au point suspecté d'émission des tourbillons ; l'épaisseur caractéristique de la couche cisaillée est un paramètre important puisqu'il conditionne le gradient transversal de la vitesse longitudinale qui intervient directement dans la prévision de l'instabilité hydrodynamique.

- la résolution de l'équation d'Orr-Sommerfeld, ou de l'équation de Rayleigh dans le cas de G.A. Flandro, conduit à la fréquence critique f_{cr} correspondant à l'onde la plus instable ainsi qu'aux caractéristiques principales de cette onde dont sont déduites la vitesse de convection des tourbillons et leur amplification spatiale. La solution n'est définie qu'à une constante multiplicative près.

- le couplage se réalise par l'intermédiaire de l'équation linéaire déduite de (3.19), pour laquelle on ne retient que le terme faisant intervenir le rotationnel de l'écoulement stationnaire, et permet de calculer la constante multiplicative. La composante instationnaire du rotationnel est alors exprimée, elle est proportionnelle à la pression acoustique et au rotationnel stationnaire au point d'émission.

- l'impact des tourbillons est traduit en terme de source d'un "pseudo-son" d'amplitude $\widetilde{P}_\Sigma$ à la fréquence critique puis le terme du bilan acoustique est déduit :

$$\alpha_{SN} = - \frac{\bar{\rho} a^2}{2 E_N} \int_{S_\Sigma} \widetilde{P}_\Sigma \widetilde{u}_N \, dS \,, \qquad (3.10)$$

où S_Σ est la surface d'impact.

L'émission tourbillonnaire n'est déstabilisante que si $\widetilde{P}_\Sigma$ et $\widetilde{u}_N$ sont en opposition de phase.

L'application de cette théorie a été récemment effectuée à l'ONERA pour le MPS d'Ariane 5 et montre une grande sensibilité du calcul aux données d'entrée : profil de vitesse, condition d'impact... L'amplification spatiale provenant du calcul est tout à fait énorme et certainement très surestimée ; les déphasages entre émission et impact demandent en outre à être précisément calculés. Quelles que soient ses limites prédictives, cette méthode présente toutefois l'intérêt de mettre en évidence les occurrences de couplage par l'examen des écarts entre fréquences de modes et fréquences d'émission et des déphasages entre $\widetilde{P}_\Sigma$ et $\widetilde{u}_N$.

3.1.2.3. Calcul numérique

La non-linéarité intrinsèque du couplage acoustique-émission tourbillonnaire rend attractive le recours au calcul numérique. Un premier travail a été réalisé par P.H. Shu et al (réf. 59) sur une géométrie représentative d'un moteur segmenté, par l'intégration des équations de Navier-Stokes bidimensionnelles incompressibles ; le modèle est soit laminaire soit turbulent à deux équations de transport. La fréquence d'émission observée expérimentalement est assez bien retrouvée ainsi que sa dépendance avec le nombre de Reynolds ; on peut toutefois penser que l'hypothèse incompressible rend hypothétique tout couplage. Un travail plus récent de l'ONERA, préliminaire à l'application MPS Ariane 5, est illustré par la figure 18 (réf. 62). Le moteur est axisymétrique, avec un profil de chargement présentant un angle vif situé à mi-longueur de chambre. Le calcul est effectué dans la chambre et la tuyère par intégration des équations de Navier-Stokes laminaires et en deux temps : un état stationnaire est d'abord recherché en utilisant une forte viscosité artificielle puis la viscosité artificielle est quasiment annulée. Un maillage fin (environ 10000 mailles) et resserré près de l'angle du profil a été utilisé. Des tourbillons apparaissent dans la seconde partie du calcul ; émis périodiquement de l'angle vif du profil, ils se déplacent vers la tuyère où ils sont avalés. La pression s'organise de façon oscillatoire. Les résultats préliminaires obtenus, dont l'analyse se poursuit, semblent prouver que le calcul numérique peut servir à la prévision d'un mode d'instabilité impliquant une émission tourbillonnaire.

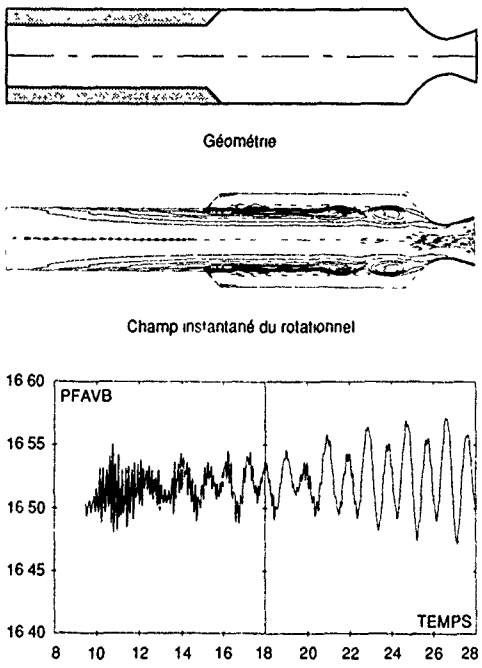

Figure 18 - Calcul du couplage acoustique-émission tourbillonnaire

3.1.3. Comportement instationnaire de la tuyère

La tuyère intervient de manière significative dans le bilan acoustique et constitue l'origine d'une perte acoustique pour les modes longitudinaux ; le rôle de la tuyère dans les modes tangentiels est par contre plus complexe. Le bilan acoustique fait apparaître une admittance d'entrée de tuyère qui doit être calculée indépendamment. Les bases de ce calcul ont été établies depuis longtemps et des codes sont universellement opérationnels. Cinq problèmes se posent cependant à l'utilisateur :

- choix du plan de fermeture de la cavité acoustique,
- rôle des oscillations d'entropie à l'entrée de la tuyère,
- incidence des caractéristiques détaillées de l'écoulement moyen sur l'admittance de tuyère,
- effets bidimensionnels de tuyère,
- non-linéarités pour des amplitudes importantes d'oscillations.

Le traitement des non-linéarités peut être résolu par le calcul numérique. Les effets bidimensionnels peuvent être partiellement pris en compte par un traitement pseudo mono-dimensionnel (réf. 63) de l'écoulement stationnaire. Les oscillations d'entropie peuvent être caractérisées par une coadmittance en description monodimensionnelle.

Nous détaillerons ici deux problèmes pratiques liés à l'application du bilan acoustique : le choix du plan de fermeture de la cavité et la possibilité de définir une admittance d'entrée uniforme dans le plan de fermeture. L'incidence du caractère rotationnel de l'écoulement stationnaire peut être quant à lui apprécié en réalisant un calcul couplé de la chambre et de la tuyère ; un tel calcul élimine de plus toute difficulté de raccordement (paragraphe 4.3.2.).

3.1.3.1. Choix du plan de fermeture de la cavité

Ce problème a été étudié par F. Vuillot à l'occasion de l'application du bilan acoustique au moteur de la figure 8, dont certaines variantes comportaient des convergents de tuyère d'une longueur assez forte par rapport à la longueur de la chambre (réf. 64). La fréquence et l'amortissement s'avèrent alors sensibles à la position du plan de fermeture, même si, conformément aux hypothèses de base, le nombre de Mach de l'écoulement moyen reste très inférieur à 1. Pour différentes positions, le champ acoustique change en effet et les intégrales du bilan acoustique en sont affectées . Une modification du calcul du champ acoustique est proposée en remplaçant l'hypothèse d'une admittance nulle dans le plan d'entrée de la tuyère par une relation linéaire entre $\tilde{p}_N$ et $d\tilde{p}_N/dz$ utilisant la partie imaginaire de l'admittance de tuyère. Le bilan acoustique ainsi modifié montre une insensibilité de la fréquence acoustique à la position du plan de fermeture et une sensibilité réduite de l'amortissement. La modification proposée ne devrait pas induire de difficulté majeure dans le calcul des modes acoustiques de géométries complexes.

3.1.3.2. Uniformité de l'admittance de tuyère dans le plan de fermeture

Cette question a été étudiée numériquement par G. Avalon et F. Vuillot (réf. 65). Les équations bidimensionnelles d'Euler sont résolues dans une tuyère ; l'écoulement stationnaire est tout d'abord recherché puis un mode acoustique stationnaire est établi grâce à une modification des conditions d'entrée. Les signaux instationnaires sont ensuite exploités par transformée de Fourier. La figure 19 donne quelques résultats pour l'admittance adimensionnée dans un plan d'entrée :

$$Y = \bar{\rho} c \frac{\tilde{u}}{\tilde{p}} = A_T \qquad (3.11)$$

Les résultats de l'analyse bidimensionnelle sont comparés à ceux de l'analyse monodimensionnelle qui se ramène classiquement à l'intégration d'une équation de Riccati. On constate que les écarts restent modérés mais que les effets bidimensionnels ne sont pas entièrement négligeables lorsque le divergent est très abrupt, l'écoulement stationnaire restant irrotationnel (voir aussi paragraphe 4.3.2).

3.1.4. Aspect biphasique de l'écoulement

Une onde acoustique est dispersée et atténuée par une suspension de particules et le problème élémentaire de la perte acoustique dû à la phase condensée des produits de combustion d'un propergol métallisé a reçu une réponse depuis plus de vingt ans (réf. 66). Le phénomène est intimement lié aux échanges irréversibles de quantité de mouvement et de chaleur entre phases.

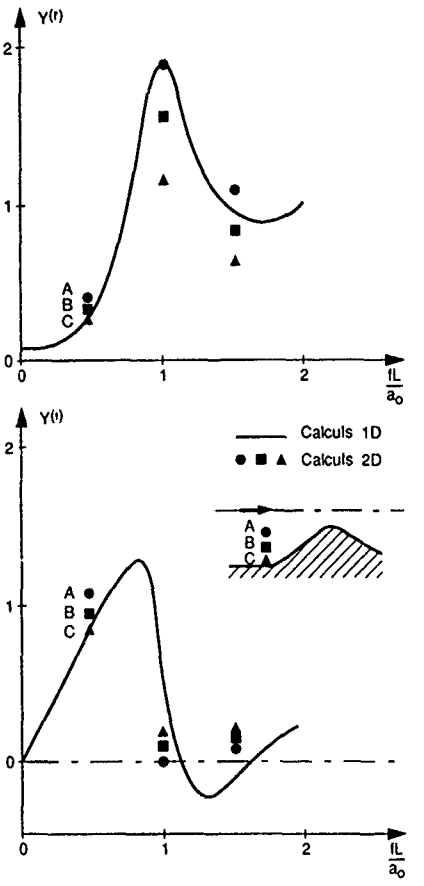

Figure 19 - Calculs bidimensionnels de l'admittance de tuyère

L'hypothèse est communément admise que les particules sont suffisamment fines pour que l'équilibre biphasique entre phases soit réalisé localement dans l'écoulement stationnaire ; les équations instationnaires du mouvement des particules peuvent être linéarisées et conduisent :

- pour la contribution de la traînée à un terme proportionnel à :

$$\frac{\int_V |\nabla \tilde{p}_N|^2 dv}{E_N^4} \qquad (3.12)$$

- pour la contribution du transfert thermique, souvent négligée, à une expression où, après simplification par E_N^2, le champ $\tilde{p}_N$ n'intervient plus.

L'amortissement biphasique est dépendant de la fréquence, de la taille des particules, de leur masse volumique et de la proportion de phase condensée dans les produits de combustion. Pour la contribution de la traînée et des particules de diamètre d_p uniforme, le maximum d'amortissement sera obtenu, selon la théorie élémentaire, pour :

$$\omega \frac{\rho_p d_p^2}{18\mu} = 1 \qquad (3.13)$$

La théorie du phénomène n'a pas connu de progrès récents mais on peut signaler quelques problèmes qui subsistent ou qui sont apparus à la suite des développements réalisés par ailleurs :

- distribution de la phase condensée : la phase condensée est supposée répartie uniformément dans le moteur. Cette approximation n'est valable que pour les gros propulseurs : les gouttelettes d'aluminium brûlent sur une certaine distance et forment les particules d'alumine. En conséquence, il existe près de la surface des gouttelettes dont le diamètre est de l'ordre 100 μm et au centre de la cavité une large distribution des particules, entre 0,1 et quelques dizaines de μm. L'hypothèse d'une répartition uniforme de la phase condensée tend, pour des modes élémentaires, à surestimer l'amortissement (réf. 67) ; les petits moteurs doivent logiquement être plus sensibles à cet effet.

- granulométrie de la phase condensée : la phase condensée est caractérisée par le carré d'un diamètre moyen des particules. Or il n'existe pas de données expérimentales sur moteur de la granulométrie de la phase condensée dans la chambre mais des données obtenues dans des conditions différentes de temps de séjour, par exemple par captation des particules issues de la combustion d'un échantillon. L'incertitude des calculs est donc forte. Un autre problème tient au fait que les particules d'alumine sont liquides à la température des produits de combustion et donc susceptibles de s'agglomérer au cours de leur évolution dans la chambre par le jeu des gradients de l'écoulement stationnaire et des fluctuations turbulentes ; l'agglomération pourrait être favorisée par une instabilité.

- lois de traînée et de transfert thermique des particules : l'adoption de la loi de Stokes et d'un nombre de Nusselt égal à 2 est cohérente avec l'approche linéaire ; les calculs numériques indiquent une assez forte sensibilité au choix de lois de traînée et de transfert thermique plus générales.

- calcul des intégrales : l'existence d'une couche limite acoustique induit un champ de vitesse instationnaire qui peut être notablement différent du champ de vitesse acoustique. L'influence de cet écart sur l'amortissement dû à la phase condensée doit être plus marqué pour les gros propulseurs (la couche limite se développe largement dans la cavité pour les modes longitudinaux) et pour le terme de traînée (l'intégrale porte sur $|\vec{U}_w|^2$). Des calculs numériques simples devraient permettre d'estimer cet effet.

On notera que le changement de granulométrie entre les gouttelettes ou agglomérats d'aluminium quittant la surface de combustion et les particules d'alumine formées a été déjà pris en compte, sous l'appellation de combustion distribuée, pour expliquer certains résultats sur propulseur en T (réf. 68 à 70). Pour les très basses fréquences caractéristiques des moteurs segmentés, on peut également s'interroger sur le rôle respectif, dans l'amortissement des instabilités, des gouttelettes d'aluminium et des particules d'alumine car la formule (3.13) privilégie les diamètres de quelques dizaines de μm.

3.2. Phénomènes de combustion

La combustion du propergol détermine les conditions limites du problème aérodynamique. L'oscillation locale des grandeurs aérodynamiques en surface de combustion induit une modification du débit unitaire des produits de combustion et de leur température d'arrêt ; on parle alors de réponse instationnaire du propergol. La combustion des gouttelettes d'aluminium produite en surface de combustion présente par contre une cinétique de volume et il est permis de s'interroger sur ses caractéristiques instationnaires.

3.2.1. Réponse du propergol aux oscillations de l'écoulement

Historiquement, les travaux sur la réponse du propergol ont suivi une démarche parallèle à ceux sur la combustion stationnaire. La réponse du propergol aux oscillations de la pression statique a d'abord été étudiée car il s'agit d'une propriété intrinsèque du propergol et qui peut être déterminée indépendamment du fonctionnement d'un moteur. La réponse aux oscillations des autres grandeurs de l'écoulement a été résumée dans le terme de couplage-vitesse et constitue l'équivalent instationnaire de la combustion érosive stationnaire ; le couplage-vitesse oblige par principe à traiter simultanément les mécanismes de combustion et le champ aérodynamique local, comme pour la combustion érosive, et il s'agit d'une propriété qui n'est plus intrinsèque du propergol mais qui doit associer le propergol et l'écoulement. Dans ces conditions, les recherches sur le couplage-vitesse ont été très dépendantes de la description de l'écoulement adoptée, monodimensionnelle ou multidimensionnelle, et ont donné lieu aux mêmes tâtonnements que la combustion érosive.

L'étude des réponses du propergol nécessite de traiter séquentiellement le comportement instationnaire de la phase condensée et celui de la phase gazeuse, siège des flammes. La phase condensée reçoit un flux thermique de la zone de flamme et ce sont les mécanismes de conduction couplés à ceux de la dégradation en phase condensée qui provoquent une modification instationnaire de la vitesse de combustion ; pour la phase condensée, toute modification du flux thermique est équivalente en première approximation, qu'elle soit due à un effet de pression ou à un effet de "vitesse". Il en va autrement pour la phase gazeuse où deux effets peuvent se superposer : la pression agit directement sur la cinétique chimique tandis que le champ aérodynamique doit être pris en compte à un autre niveau. Il semble raisonnable de supposer que le champ aérodynamique se manifeste, comme en combustion érosive stationnaire, dans l'interaction de la turbulence et des flammes, par l'intermédiaire d'une modification des paramètres de transfert.

Dans le cadre d'une analyse linéaire, il est légitime de postuler que les réponses au couplage-pression et au couplage-vitesse sont additives mais l'existence d'un couplage-vitesse linéaire reste contreversée.

Le couplage-pression a donné lieu à de nombreux travaux théoriques et expérimentaux et peut être considéré comme assez bien connu ; une faiblesse de certaines méthodes expérimentales est toutefois d'utiliser en mode inverse le bilan acoustique et donc de faire porter sur le couplage-pression toutes les incertitudes de la description théorique de départ. Le couplage-vitesse a souvent été étudié en liaison avec une description monodimensionnelle de l'écoulement et une tendance générale a été de lui faire porter le poids de ce qui, dans les expériences, ne pouvait être attribué au couplage-pression (réf. 71). Il apparaît que la description monodimensionnelle ne possède pas la cohérence interne suffisante pour donner une compréhension claire du couplage-vitesse (réf. 72) et qu'il faut passer à la description bidimensionnelle pour parvenir à une maîtrise satisfaisante de ce couplage mystérieux. Cette démarche est exactement celle qui a permis de dominer la combustion érosive stationnaire et, comme pour cette dernière, l'objectif prioritaire devrait être la mise au point d'un modèle de paroi évitant le recours à des maillages trop resserrés pour le traitement numérique complet de l'instabilité. Ce modèle de paroi ne peut être établi avant que la couche limite acoustique ait reçu une description générale couvrant toutes les applications pratiques.

3.2.2. Combustion instationnaire des gouttelettes d'aluminium

Le problème de la combustion distribuée de l'aluminium a déjà été évoqué (réf. 68 à 70) à l'occasion de l'examen de l'amortissement dû aux phases condensées. La combustion instationnaire en volume est connue pour entretenir les instabilités des systèmes à combustible ou propergol liquide (réf. 1). Aussi doit-on s'interroger sur la possibilité d'une participation de la combustion de l'aluminium aux instabilités. La visualisation de la combustion stationnaire d'un échantillon de propergol montre que les agglomérats d'aluminium brûlent de manière isolée, principalement par une flamme de diffusion ; la combustion se fait également en déséquilibre de vitesse avec la phase gazeuse, la flamme-enveloppe ne possède pas une symétrie sphérique et le mouvement des gouttelettes est assez irrégulier. Il faudrait établir un modèle de combustion des gouttelettes d'aluminium, recalé par rapport aux observations pour le stationnaire, puis étendu par le calcul pour l'instationnaire, comme cela est actuellement réalisé pour les gouttelettes d'ergols liquides. Ceci devrait permettre d'établir les relations entre les oscillations de débit et de dégagement de chaleur avec les oscillations de la pression et de la vitesse du gaz, puis de réintroduire sous forme de termes sources ces contributions dans le bilan acoustique. Cette démarche ne devrait pas poser de problème de principe au niveau formel mais se heurtera probablement à de grandes difficultés expérimentales de validation.

4. TRAVAUX RECENTS DE L'ONERA

Les trois exemples sélectionnés correspondent à des situations de complexité croissante et faisant appel à des moyens numériques de plus en plus sophistiqués. Le premier exemple s'intéresse à un aspect théorique des instabilités en volume. Le second exemple porte sur l'analyse linéaire de l'instabilité longitudinale d'un propulseur sans tuyère. Le troisième exemple illustre la simulation numérique bidimensionnelle d'un moteur axisymétrique.

4.1. Recherche théorique sur la frontière de stabilité pour l'instabilité de volume

4.1.1. Objectifs

L'instabilité en volume n'est observée qu'à basse pression et ne présente donc qu'un intérêt pratique limité pour les moteurs à propergol solide classiques ; on peut toutefois signaler que certains générateurs à semi-propergol de statofusée sont sensibles à ce type d'instabilité et que l'utilisation de la technique du moteur en L* permet d'accéder à la réponse du propergol à basse pression.

L'analyse théorique linéaire de l'instabilité en volume est relativement simple et débouche sur des relations analytiques, comme rappelé dans la référence 3. Dans sa forme la plus répandue, la relation de base s'écrit, en notation complexe :

$$R_c = 1 + \frac{\gamma - 1}{2\gamma} + i\,\frac{\omega \bar{\tau}_s}{\gamma} \quad , \qquad (4.1)$$

où R_c est la réponse en combustion du propergol au couplage-pression,
γ est l'exposant isentropique des produits de combustion,
ω est la pulsation complexe $2\pi f - i\alpha$,
$\bar{\tau}_s$ est le temps de séjour des produits de combustion dans la chambre.

La séparation des parties réelle et imaginaire conduit à :

$$R_c^{(r)} = 1 + \frac{\gamma - 1}{2\gamma} + \frac{\alpha \bar{\tau}_s}{\gamma} \quad , \qquad (4.2)$$

$$R_c^{(i)} = \frac{2\pi f \bar{\tau}_s}{\gamma} \qquad (4.3)$$

La frontière de stabilité est donc atteinte lorsque :

$$R_c^{(r)} = 1 + \frac{\gamma - 1}{2\gamma} \quad , \qquad (4.4)$$

ce qui définit la fréquence si la partie réelle de la réponse est connue en fonction de la fréquence, à pression donnée, et en tenant compte de $R_c^{(i)} > 0$.

Le temps de séjour $\bar{\tau}_s$ s'en déduit par :

$$\bar{\tau}_s = \frac{\gamma R_c^{(i)}}{2\pi f} \qquad (4.5)$$

Des expressions plus explicites de la frontière de stabilité peuvent être recherchées si la réponse en combustion du propergol peut s'exprimer analytiquement, par exemple par le modèle à deux paramètres A et B, et au prix de quelques simplifications supplémentaires comme par exemple le développement au second ordre de la réponse en fonction de la fréquence complexe. Le résultat le plus connu est que la frontière de stabilité dans le plan pression p-longueur caractéristique L* peut être représentée par :

$$L^* p^{2n} = \text{constante}, \qquad (4.6)$$

où n est l'exposant de pression du propergol.

Les observations réalisées sur différents propergols composites indiquent que la frontière de stabilité présente parfois une forme plus complexe que prévu, notamment pour des propergols fortement chargés en aluminium. Certains mécanismes échappant à la description théorique mise en oeuvre peuvent être incriminés et en particulier la combustion distribuée de l'aluminium dans la chambre.

Le travail a porté ici, sans remettre en cause le cadre théorique classique, sur l'influence d'une hypothèse implicitement admise et réfutée a posteriori par les résultats, à savoir que $|\omega \bar{\tau}_s| >> 1$ alors que les calculs indiquent plutôt $|\omega \bar{\tau}_s| = O(1)$.

4.1.2. Description mathématique du problème

La linéarisation des équations instationnaires pour les bilans de masse et d'énergie, compte tenu des conditions limites, conduit à :

$$(1 + i\omega\bar{\tau}_s) R_{MP} + (0{,}5 + i\omega\bar{\tau}_s) R_{TP} = 1 + \frac{3\gamma + 1}{2\gamma} i\omega\bar{\tau}_s + \frac{(i\omega\bar{\tau}_s)^2}{\gamma} \quad , \qquad (4.7)$$

où R_{MP} est la réponse en débit du propergol,
R_{TP} est la réponse en température de flamme du propergol (réf. 26).

Cette équation se réduit à (4.1) si $|\omega\bar{\tau}_s| >> 1$, avec $R_c = R_{MP} + R_{TP}$ et R_{TP} dépend de R_{MP} par :

$$R_{TP} = D(R_{MP} - n) \qquad (4.8)$$

La relation (4.7) ne permet pas de séparer comme précédemment le rôle respectif des parties réelle et imaginaire de la réponse en combustion, aussi convient-il de procéder autrement. Le modèle à deux paramètres A et B sera adopté pour décrire la réponse :

$$R_{MP} = \frac{nAB s}{s^2 + (AB - A - 1)s + A} \quad , \qquad (4.9)$$

où $s^2 - s = i\mathcal{R}$, $s^{(r)} > 0$ (4.10)

et $\mathcal{R} = \frac{\omega a}{V_c^2}$ (4.11)

Cette expression invite à poser :

$$\omega\bar{\tau}_s = \mathcal{R}K \quad , \qquad (4.12),$$

où K est le rapport du temps de séjour au temps thermique α/γ_c^2 caractéristique de la combustion stationnaire.

L'équation (4.7) peut donc être réécrite sous une forme adimensionnelle :

$$n\,AB\,\Omega\left[1+\frac{D}{2}+K(1+D)(\Omega^2+s)\right] \qquad (4.13)$$

$$-\left[\Omega^2+(AB-A-1)s+A\right]\left[1+\frac{nD}{2}+\left(\frac{3n^2+n-2}{2^3}+nD\right)K(\Omega^2+s)+K^2\frac{(\Omega^2+s)^2}{2^3}\right]=0$$

Il s'agit d'une équation algébrique du sixième degré en s où apparaissent 6 paramètres :

- n, exposant de pression de la vitesse de combustion,
- A, B et D, liés au modèle de combustion adopté,
- γ, exposant isentropique des produits de combustion,
- K, paramètre de Damkohler.

Les solutions de l'équation (4.13) ont fait l'objet d'une recherche systématique en deux étapes :

- calcul direct des racines, permettant par déduction la détermination de la pulsation complexe Ω pour tout jeu des paramètres,
- l'établissement d'un procédé autorisant l'accès direct à la frontière de stabilité, K étant alors déterminé en fonction des autres paramètres.

Les domaines de variation des paramètres ont été pris assez larges et représentatifs des applications :

- n : de 0,3 à 0,6.
- A : de 5 à 11.
- B : de 1,1 à 2,3 B_c, B_c étant défini par :

$$B_c = 1 + \frac{1-\sqrt{1+8A}}{2A}$$

Il a en effet été démontré que la partie réelle de la réponse ne pouvait présenter un maximum que pour les valeurs de B supérieures à B_c.

- D : de 0,05 à 0,15.
- γ : de 1,15 à 1,25.
- K : de 0 à 5, pour la première étape du calcul.

4.1.3. Calcul direct des racines

Les racines complexes d'une équation algébrique du sixième degré à coefficients réels sont réelles ou deux à deux conjuguées. Des considérations physiques permettent de réduire le nombre maximal de solutions admissibles à 3. Certaines solutions ne sont valables que dans un domaine borné de K, soit inférieurement soit supérieurement. Les résultats permettent d'identifier trois modes d'instabilité :

- un mode harmonique toujours stable,
- un mode stable transitant de l'harmonique à l'exponentiel,
- un mode passant par les phases successives suivantes, lorsque K croît : instable exponentiel, instable harmonique, stable harmonique, stable exponentiel. Ce dernier seul correspond à une frontière de stabilité.

4.1.4. Frontière de stabilité

La frontière de stabilité est caractérisée par $\alpha = 0$ ou Ω réel. La variable auxiliaire s reste cependant complexe ; il est donc intéressant de faire un changement de variable : $S = s + \Omega^2$, où S est réel et Ω s'exprime par :

$$\Omega = \frac{1}{2}\sqrt{S(S-1)^2(S-2)} \quad , \quad S \geq 2$$

La séparation des parties réelle et imaginaire de l'équation (4.13) conduit à deux équations algébriques du 5ième degré en S et du second degré en K, équations qui doivent posséder une solution commune. Ces équations peuvent être réécrites sous la forme de deux équations du second degré pour H = K(S-1)/2, à coefficients dépendant de S. La relation de compatibilité des deux équations du second degré conduit à une équation du huitième degré en S qui ne peut être résolue que numériquement ; on déduit pour chaque racine H puis K. La sélection des racines est aisée, puisque S doit être supérieur à 2 et K positif, et conduit sans ambiguité à une solution unique pour tout jeu des paramètres ou à l'absence de solution. Toute solution permet le calcul de $K\Omega = \omega\bar{\tau}_s$ et des réponses.

- influence de γ : pour A = 11, B/B_c = 1,1 et D = 0,10, les augmentations de Ω, K et $K\Omega$ restent modérées lorsque γ varie entre 1,15 et 1,25. Les variations de Ω sont faibles et amplifiées par les fortes valeurs de n tandis que celles de K sont plus fortes et peu sensibles à n ; $K\Omega$ est par suite peu sensible à n. La partie réelle de R_c reste toujours très voisine de 1, à quelques pour cent près.
- influence de D : pour A = 11, B/B_c = 1,1 et γ = 1,20, on note tout d'abord peu d'influence de n. Ω tend à diminuer légèrement, K et $K\Omega$ à augmenter de façon modérée lorsque D passe de 0,05 à 1,15. La partie réelle de R_c reste toujours voisine de 1, à quelques pour cent près.
- influence de A et B : pour γ = 1,20 et D = 0,10, les paramètres A, B/B_c et n ont été balayés systématiquement car les résultats en dépendent sensiblement. La synthèse met en évidence qu'à B/B_c fixé, $K\Omega$ est peu sensible à A et n ; au-delà d'une valeur limite de B/B_c, il n'existe pas de solution. Cette valeur limite dépend principalement de n, elle varie de 1,45 pour n = 0,3 à 2,59 pour n = 0,6 et correspond au fait que la partie réelle de la réponse n'atteint plus des valeurs suffisamment élevées. La partie réelle de R_c reste toujours voisine de 1, à quelques pour cent près, lorsque la frontière de stabilité existe.

Quelques résultats sont présentés sous forme synthétique sur les figures 20 et 21. La figure 20 donne la partie réelle de R_c en fonction de B/B_c pour γ = 1,20, D = 0,10 et n variant entre 0,3 et 0,6 ; les résultats se regroupent particulièrement bien sur une courbe légèrement évolutive au dessus de 1. Sur la figure 21 est reportée $\omega\bar{\tau}_s$ en fonction de la partie imaginaire de R_c dans les mêmes conditions ; à nouveau les résultats se regroupent sur une courbe unique qui fait apparaître deux faits. Le premier est que la courbe ne correspond pas à la relation linéaire (4.5) de la théorie simplifiée. Le second fait tient à ce que $\omega\bar{\tau}_s$ ne dépasse pas 1,5 pour l'ensemble des paramètres considérés et donc que l'interrogation de départ sur la possibilité de simplifier l'équation (4.7) est justifiée.

A posteriori, les calculs présentés ont été repris par la même procédure pour la théorie simplifiée correspondant à l'équation (4.1). Des écarts très importants des résultats obtenus respectivement par les théories complètes et simplifiées sont mis en évidence lorsque B/B_c tend vers la valeur limite au-delà de laquelle la frontière de stabilité disparaît.

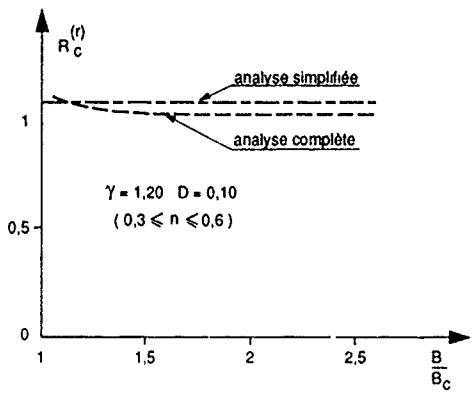

Figure 20 - Partie réelle de la réponse en combustion sur la frontière de stabilité en volume

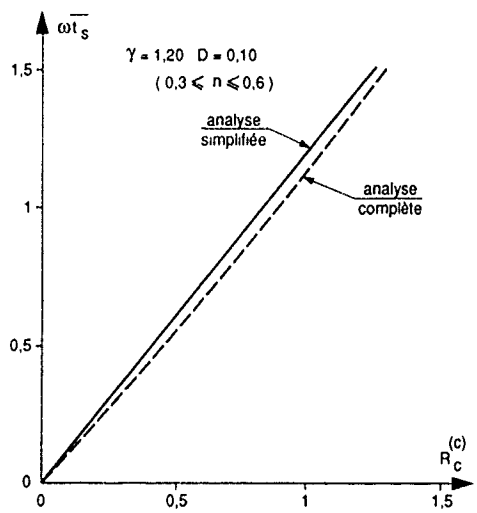

Figure 21 - Corrélation entre $\omega\bar{t}_s$ et la partie imaginaire de la réponse en combustion sur la frontière de stabilité en volume

4.1.5. Récapitulation

La théorie présentée ne remet pas en cause les conclusions qualitatives de l'approche classique :

- la frontière de stabilité correspond à une valeur de la partie réelle de R_c de la réponse en combustion proche de 1. Elle ne peut donc exister pour toute courbe de réponse ; si la courbe s'y prête c'est la condition $R_c^{(r)} \simeq 1$ qui détermine, à une pression donnée, la fréquence sur la frontière de stabilité.

- elle correspond également à une valeur positive de la partie imaginaire de R_c de la réponse en combustion, valeur qui permet de calculer le temps de séjour ou la longueur caractéristique à une pression donnée.

Cette théorie précise la sensibilité de la frontière de stabilité aux paramètres du calcul et démontre que sa disparition pour les faibles valeurs de temps de séjour ne peut être exactement prédite qu'en l'absence de toute simplification.

4.2. Instabilité longitudinale d'un moteur sans tuyère

Le moteur sans tuyère est un type de moteur particulièrement simple et de performances modestes qui trouve l'une de ses applications privilégiées dans l'accélération de missiles à statoréacteur. C'est également un moteur dont l'étude est particulièrement délicate puisque son fonctionnement est complètement dépendant des mécanismes de combustion ; il constitue par conséquent un excellent banc d'essai des connaissances. Le fonctionnement stationnaire est caractérisé par un champ de pression statique et de vitesse très hétérogène et une décroissance des pressions en fonction du temps. En fin de fonctionnement, les pressions peuvent être de l'ordre de quelques bars et il est fréquent que le fonctionnement devienne oscillatoire et conduise à une extinction suivie ou non de réallumage (fig. 22). Ce type d'instabilité est intéressant d'un point de vue théorique mais n'a fait l'objet que de rares travaux (réf. 6 et 75). Il présente des caractéristiques qui le rapprochent d'un mode d'instabilité en volume : il se produit à basse pression et à basse fréquence, les oscillations de pression sont homogènes dans le canal, mais dans la mesure seulement où il s'agit des amplitudes de pression réduites c'est-à-dire rapportées à la pression stationnaire. D'un autre côté, ce type d'instabilité échappe par principe à la description classique des instabilités en volume puisque le nombre de Mach de l'écoulement stationnaire n'obéit pas à l'hypothèse $\bar{M} << 1$ mais est au contraire compris dans le domaine [0,1]. Il s'agissait donc de reposer rationnellement le problème et de trouver une méthode pour le résoudre.

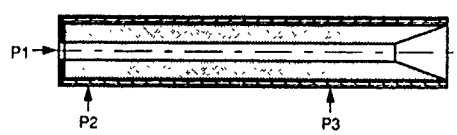

P1, P2, P3 capteurs de pression

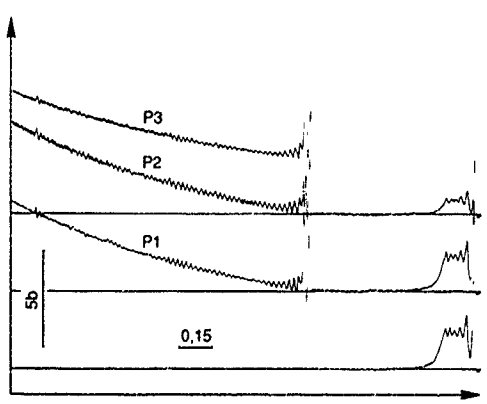

Figure 22 - Extinction naturelle d'un moteur sans tuyère par instabilité

4.2.1. Description du problème

Le problème est décrit par les équations monodimensionnelles, en s'inspirant de la technique utilisée pour le calcul d'admittance d'entrée d'une tuyère. La linéarisation porte uniquement sur l'hypothèse d'une faible amplitude des oscillations vis-à-vis des valeurs stationnaires ; par contre le champ stationnaire n'est pas simplifié. Les amplitudes sont rapportées à leur valeurs stationnaires pour la pression et la vitesse, l'entropie est également adimensionnée :

$$\tilde{\varphi} = \frac{\tilde{p}}{\bar{p}} \quad , \quad \tilde{v} = \frac{\tilde{u}}{\bar{u}} \quad , \quad \tilde{s} = \frac{\tilde{s}}{r} \qquad (4.14)$$

Comme rappelé dans la référence 6, la linéarisation conduit à 3 équations différentielles homogènes pour $\tilde{\varphi}$, $\tilde{v}$ et $\tilde{S}$:

$$\begin{aligned} (\bar{a}^2 - \bar{u}^2)\frac{d\tilde{\varphi}}{d\xi} &= A_{\varphi\varphi}\tilde{\varphi} + A_{\varphi v}\tilde{v} + A_{\varphi s}\tilde{S} \\ \gamma\bar{u}(\bar{a}^2 - \bar{u}^2)\frac{d\tilde{v}}{d\xi} &= A_{v\varphi}\tilde{\varphi} + A_{vv}\tilde{v} + A_{vs}\tilde{S} \\ \bar{u}\frac{d\tilde{S}}{d\xi} &= A_{s\varphi}\tilde{\varphi} + A_{sv}\tilde{v} + A_{ss}\tilde{S} \end{aligned} \qquad (4.15)$$

Les différents coefficients $A_{\varphi\varphi}$ ... A_{ss} apparaissant au second membre sont des fonctions des grandeurs stationnaires, de la fréquence complexe ω_c et des réponses en débit et en température au couplage-pression (on néglige le couplage-vitesse). La résolution de ce système nécessite trois conditions limites :

- le système étant homogène, on peut choisir $\tilde{\varphi} = 1$ en $\xi = 0$,
- les équations font apparaître deux singularités algébriques pour $\xi = 0$ ($\bar{M} = 0$, fond avant) et $\xi = L$ ($\bar{M} = 1$, fin du canal).

Un développement analytique autour de chaque singularité donne les valeurs des inconnues et de leurs dérivées en ces points :

. $\bar{M} = 0$: $\tilde{v}_0$ et $\tilde{S}_0$; $\tilde{v}'_0 = \tilde{S}'_0$; $\tilde{\varphi}''_0$, $\tilde{v}''_0$, $\tilde{S}''_0$.

. $\bar{M} = 1$: $\tilde{S}'_1 = 0$; $\tilde{v}_1$ et $\tilde{v}'_1$.

$$\tilde{\varphi}_1 - \frac{\rho\sigma}{\sigma - 1}\tilde{v}_1 + \tilde{S}_1 = 0 \qquad (4.16)$$

Ces valeurs permettent, d'une part de calculer les inconnues à proximité de $\bar{M} = 0$ et de commencer l'intégration numérique et, d'autre part, de reporter la condition (4.16) un peu avant $\bar{M} = 1$. L'intégration numérique est réalisée en nombre complexe. La fréquence complexe ω_c est valeur propre du problème puisqu'elle doit prendre certaines valeurs pour que les conditions limites en $\bar{M} = 0$ et $\bar{M} = 1$ soient simultanément satisfaites. Pratiquement, on forme le système adjoint d'équations différentielles linéaires homogènes pour les sensibilités :

$$\tilde{g}_\varphi = \frac{\partial\tilde{\varphi}}{\partial\omega_c} \quad , \quad \tilde{g}_v = \frac{\partial\tilde{v}}{\partial\omega_c} \quad , \quad \tilde{g}_s = \frac{\partial\tilde{S}}{\partial\omega_c} \qquad (4.17)$$

Ce système possède les mêmes singularités algébriques que le système (4.14) et on peut déterminer les valeurs des nouvelles inconnues et de leurs dérivées en $\bar{M} = 0$.

L'intégration numérique porte simultanément sur le système (4.14) et sur le système adjoint, en partant du voisinage de $\bar{M} = 0$ jusqu'à une valeur de $\bar{M}$ proche de 1 où l'écart à 0 de la condition déduite de (4.16) est calculé. Partant d'une valeur estimée de ω_c, une méthode de Newton utilisant ce dernier écart permet de converger rapidement vers la valeur propre recherchée.

4.2.2. Résultats

Le calcul dépend des grandeurs stationnaires et de la réponse du propergol. Pour les grandeurs stationnaires, la solution est grandement simplifiée si le canal est cylindrique et la vitesse de combustion uniforme : toutes les grandeurs peuvent s'exprimer analytiquement en fonction de l'abscisse réduite et l'intégration peut être réalisée suivant $\bar{M}$ (réf.6). Si le canal n'est pas cylindrique, un calcul séparé, également monodimensionnel doit être réalisé pour exprimer les grandeurs en fonction de ξ, on peut à nouveau choisir $\bar{M}$ comme variable d'intégration en combinant les équations stationnaires et instationnaires. La réponse du propergol peut être prise constante et égale à celle correspondant à la pression fond avant ou au contraire varier avec la pression stationnaire locale par l'intermédiaire des paramètres A et B. Pour l'application considérée, la réponse du propergol a été déduite d'essais sur moteur en L*, comme indiqué au paragraphe 4.1. et avec les réserves inhérentes à cette méthode expérimentale pour les propergols métallisés.

La synthèse des résultats est illustrée par la figure 23 pour laquelle la fréquence et l'amplification pour le mode de plus basse fréquence sont tracées en fonction de la pression au fond avant. On constate que la fréquence à la limite de stabilité est bien prédite par le calcul, tandis que la pression est un peu sous-estimée. L'influence des différentes hypothèses touchant la forme du canal ou l'uniformité de la réponse du propergol reste assez modérée.

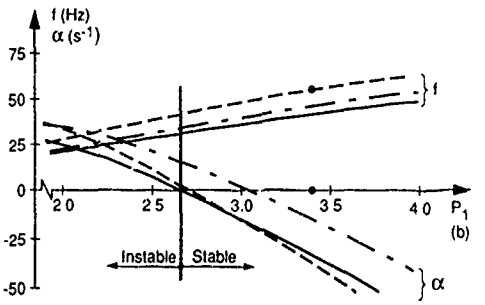

Canal cylindrique et réponse calculée au fond avant
Canal cylindrique et réponse calculée localement
Canal réel et réponse calculée localement
• Essai

Figure 23 - Prévision de la stabilité d'un moteur sans tuyère sur son premier mode longitudinal

Par ailleurs, il est démontré :

- que $\tilde{\varphi}$ est quasiment constant en fonction de ξ, conformément aux observations.
- que $\tilde{S}$ est quasiment constant, en fonction de ξ.
- que $\tilde{v}$ varie très peu en module mais assez largement en phase, en fonction de ξ.

Les modes longitudinaux d'ordre élevé peuvent également être calculés par le même programme. Les fréquences sont approximativement en progression arithmétique, comme en acoustique classique ; par contre les répartitions d'amplitude et de phase sont extrêmement différentes en raison de l'influence de l'écoulement stationnaire.

4.2.3. Récapitulation

Une théorie linéaire des instabilités longitudinales d'un propulseur sans tuyère a été élaborée et mise en pratique. L'essentiel des observations expérimentales peut être retrouvé par le calcul, les faibles écarts constatés pouvant provenir soit de l'approximation liée à la description monodimensionnelle de l'écoulement, soit de l'incertitude sur la réponse du propergol ou la forme du canal. Pour les applications, cette théorie ne donne pas des résultats très différents de ceux résultant de l'application directe de l'analyse de la stabilité du moteur en L*, si la précaution est prise de calculer le temps de séjour réel pour le propulseur sans tuyère. L'intérêt de l'analyse théorique menée est plutôt fondamental ; cette analyse confirme en effet qu'instabilité en volume et instabilité acoustique procèdent exactement des mêmes phénomènes et qu'un traitement unifié permet de la décrire : un mode en volume peut, dans ces conditions, être considéré comme un mode acoustique d'ordre 0.

4.3. Simulation numérique de modes longitudinaux-radiaux

La simulation numérique des instabilités au moyen d'une description bidimensionnelle sera illustrée par deux exemples. Le premier exemple intéresse le chargement axisymétrique usiné de la figure 10 et constitue une extension de la simulation monodimensionnelle signalée dans la référence 6 ; la simulation utilise les équations d'Euler et un modèle de combustion instationnaire, la méthode est du type volumes finis explicite. Le second exemple traite d'une géométrie également axisymétrique mais un peu plus simple, la géométrie A de la figure 15 ; l'accent est mis sur le raffinement du maillage et la comparaison entre l'amortissement déterminé numériquement et celui déduit du bilan acoustique.

4.3.1. Géométrie axisymétrique usinée (réf. 76)

Le maillage utilisé est donné sur la figure 24 ; il s'agit d'un maillage assez grossier (moins de 1000 mailles) et simplifié puisqu'il ne suit pas exactement les parois du chargement réel bien que reproduisant exactement le volume ; ces caractéristiques sont dictées d'une part par le souci de limiter les temps de calcul en exploitation et d'autre part par le choix d'un maillage orthogonal dans la chambre. Les calculs ont été conduits à trois instants de fonctionnement de la maquette à l'échelle 1/6 : t = 0, 0,5 et 1s. Le calcul procède en trois étapes :

- recherche de l'état stationnaire, la vitesse de combustion étant décrite par la loi stationnaire.
- déstabilisation numérique par injection d'un débit réparti au fond avant et présentant trois périodes d'oscillation à une fréquence voisine de la fréquence de cavité attendue ; le modèle de combustion instationnaire est activé.
- étude du mode d'instabilité naturel, de son amortissement ou de son amplification.

Les principaux résultats ont été les suivants :

- la fréquence d'instabilité est très voisine de celle prévue par le calcul acoustique, elle évolue très peu avec le temps de fonctionnement.
- l'instabilité est très amortie comme le montre la figure 24, ce qui a été une vive déception par comparaison avec les observations mais ce qui est cohérent avec la prévision du bilan acoustique. Un contrôle précis des calculs n'a pas permis de déceler une quelconque anomalie, ce qui laisse supposer qu'un mécanisme essentiel d'entretien des instabilités n'a pas été reproduit par le calcul ; l'émission tourbillonnaire pourrait être ce mécanisme et il était exclu de pouvoir la décrire avec un maillage aussi grossier.

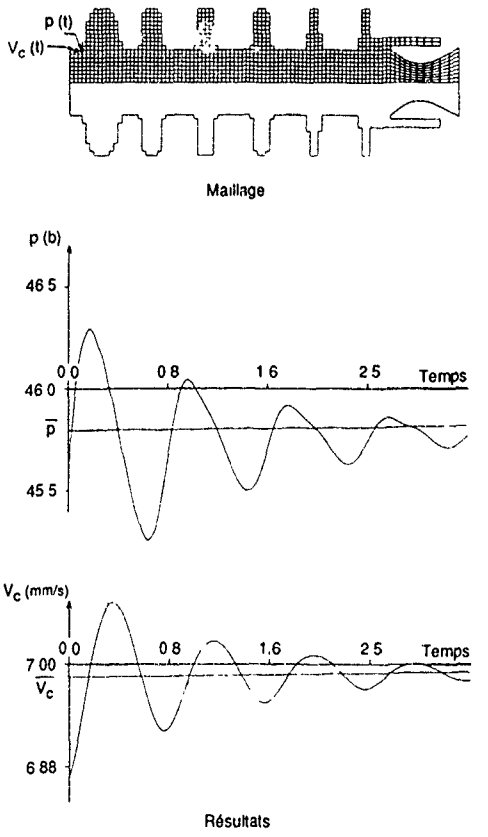

Figure 24 - Calcul bidimensionnel Euler (chargement axisymétrique)

Au vu des premiers résultats, la réponse du propergol a été artificiellement augmentée en jouant sur l'exposant de la loi de vitesse stationnaire ou les paramètres du modèle de combustion, ou encore en modifiant l'échelle pour que la fréquence corresponde à un maximum de réponse du propergol. Il est ainsi possible d'arriver à des amplifications de la perturbation initiale et à un comportement naturellement instable du moteur. La figure 25 correspond au cas d'une géométrie cylindrique décrite monodimensionnellement ; un amortissement préalable de l'oscillation déclenchée est observée suivie de la naissance, de l'amplification puis de la stabilisation d'un mode supérieur. Ce cycle limite a pu être retrouvé pour diverses amplitudes et fréquences de déstabilisation, il peut être atteint soit par amortissement d'une forte perturbation initiale (stabilité dynamique) soit à partir d'une faible perturbation (stabilité statique) ; l'amplitude limite paraît assez peu affectée par le traitement monodimensionnel ou bidimensionnel de l'écoulement.

La simulation numérique des instabilités des chargements axisymétriques usinés n'a donc pas permis d'expliquer les instabilités naturelles observées. Cette tentative a cependant été fructueuse puisqu'elle a mis en évidence la possibilité de prévoir, lorsque les circonstances le permettent, le niveau d'instabilité. Il semble qu'un progrès supplémentaire doive encore être fait dans la

physique des écoulements ou des mécanismes de combustion pour parvenir à une prévision correcte de la stabilité sur ce type de chargement.

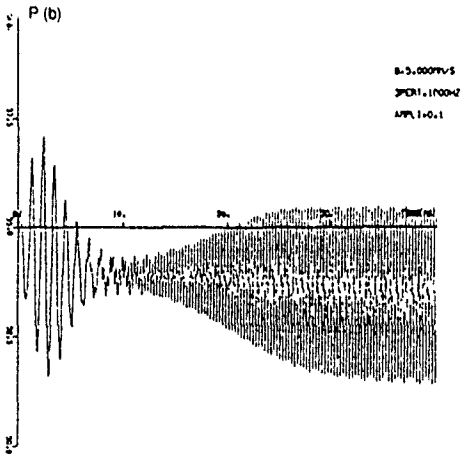

Figure 25 - Calcul monodimensionnel (cycle limite)

4.3.2. Géométrie axisymétrique standard (réf. 77 et 78)

Le maillage utilisé est donné sur la figure 26 : il s'agit d'un maillage fin (près de 20000 mailles) qui suit exactement le profil du chargement. Les calculs ont été conduits à deux instants de fonctionnement correspondant respectivement à la géométrie initiale et à la géométrie à mi-épaisseur brûlées. La réponse du propergol au couplage-pression n'est pas prise en compte autrement que par la loi de combustion stationnaire $\overline{v_b} = a\overline{P}^n$. Le calcul procède en trois étapes :

- recherche de l'état stationnaire après une initialisation monodimensionnelle.
- déstabilisation numérique sur une période, à la fréquence estimée du premier mode acoustique, par simulation d'une source acoustique.
- étude du mode d'instabilité naturel et de son amortissement.

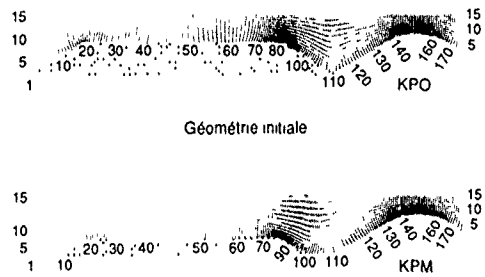

Figure 26 - Calcul bidimensionnel Euler maillage (réf 77)

Un soin particulier a été apporté à la sensibilité des résultats stationnaires au maillage. Le maillage fin apparaît indispensable pour capter, pour la géométrie initiale, la couche de mélange entre l'écoulement provenant du canal et celui issu du cône arrière du chargement, ce mélange provoquant en outre une alimentation très hétérogène de la tuyère (figure 27). Le maillage fin permet également de mettre en évidence le tourbillon stable au fond avant, pour la seconde géométrie.

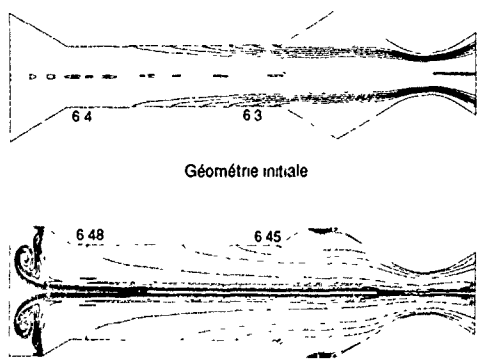

Figure 27 - Calcul bidimensionnel Euler : écoulement stationnaire

Les résultats instationnaires mettent en évidence de gros écarts entre l'amortissement calculé numériquement et celui prédit par le bilan acoustique. La figure 28 rassemble, d'une part les signaux de pression instationnaire au fond avant, pour les deux géométries, et, d'autre part les amortissements numériques et du bilan acoustique 1D ; l'exposant de la loi de pression station-

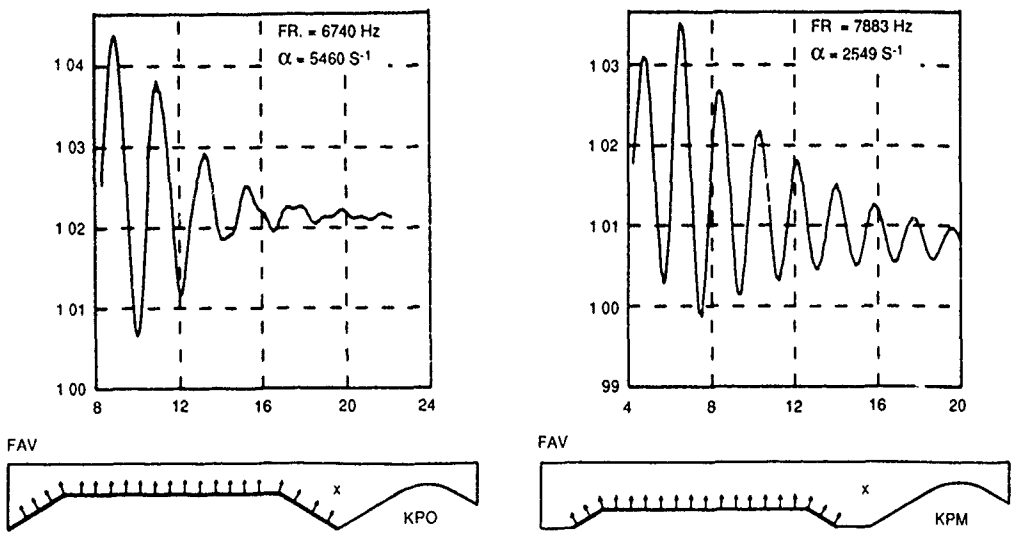

	1D	2D
F (Hz)	6362	6730
α (S^{-1})	- 2567	- 5200
α_N (S^{-1})	- 1942	
α_{PC} (S^{-1})	+ 1082	
α_{CA}^{*} (S^{-1})	- 1707	

* correction d'admittance

	1D	2D
F (Hz)	7900	7880
α (S^{-1})	- 1860	- 2520
α_N (S^{-1})	- 1610	
α_{PC} (S^{-1})	+ 432	
α_{CA}^{*} (S^{-1})	- 682	

* correction d'admittance

Figure 28 - Calcul bidimensionnel Euler amortissement du premier mode longitudinal

naire vaut 0,7. L'analyse des écarts fait apparaître au moins une explication : l'hétérogénéité de l'écoulement à l'entrée de la tuyère induit une admittance d'entrée de tuyère non uniforme si bien que le bilan acoustique 1D sous-estime assez largement la perte de tuyère, notamment dans le cas de la géométrie initiale pour laquelle la surface du cône arrière représente plus de 50 % de la surface du canal cylindrique. Le bilan acoustique tient d'autre part compte de l'amortissement de la couche limite acoustique qui n'est pas résolue par le calcul effectué, ce qui complique la comparaison.

Ces résultats sont encourageants dans la mesure où ils laissent espérer la possibilité de parvenir à la prévision numérique de la stabilité d'un moteur et sans doute à une exploitation plus précise des essais en terme de réponse du propergol par la prise en compte d'une meilleure description de l'écoulement. Une prochaine étape devrait porter sur le traitement laminaire de l'écoulement et des problèmes de couche limite acoustique associés, ce qui nécessitera probablement la mise au point d'un modèle de paroi.

5. CONCLUSION

L'étude des instabilités de combustion des moteurs à propergol solide reste d'actualité et passe nécessairement par une analyse détaillée des phénomènes d'écoulement et de combustion. Le succès mais aussi les limites des méthodes d'analyse linéaire et du bilan acoustique tiennent autant à leur relative simplicité de mise en oeuvre qu'à leur apparente facilité d'interprétation : il n'est pas indispensable de connaître dans le détail l'écoulement stationnaire dans la chambre du moteur et il est possible d'attribuer un gain et une perte à chaque phénomène élémentaire retenu. Cette démarche se heurte à des difficultés conceptuelles qui malheureusement réintroduisent les caractéristiques fines de l'écoulement stationnaire, que ce soit au niveau de la surface de combustion (zone d'adaptation traduite par les termes de de l'écoulement (instabilités hydrodynamiques ou émission tourbillonnaire). L'introduction d'un terme de couche limite acoustique dans le bilan acoustique paraît possible si cette couche limite est suffisamment peu épaisse pour que son effet soit ramené en surface de combustion ; la prise en compte de l'émission tourbillonnaire semble par contre plus délicate mais l'analyse théorique fournit un guide permettant d'apprécier si ce phénomène peut être déstabilisant.

Le calcul numérique de l'écoulement connaît une montée en puissance qui n'est pas seulement justifiée par la disponibilité de supercalculateurs ou le goût prononcé qu'éprouvent les jeunes ingénieurs pour l'informatique. Il s'agit au contraire d'une approche obligatoire pour le stationnaire, indispensable pour la stabilité non-linéaire et utile pour mieux comprendre certains effets encore mystérieux tels que le couplage-vitesse. Les premiers résultats obtenus numériquement dans les activités de recherche sur les instabilités de combustion sont spectaculaires mais doivent encore être passés au crible des connaissances disponibles et de la comparaison avec l'expérience. Beaucoup d'efforts restent donc encore à faire avant que les progrès puissent bénéficier aux applications ; il faut compléter la compréhension physique des instabilités de combustion, affiner les simulations numériques et les données d'entrée, valider les codes de calcul.

Remarque finale et remerciements

Le souci d'intéresser simultanément spécialistes et non-spécialistes, expérimentateurs et théoriciens, et le parti pris d'une lecture moderne des instabilités de combustion, ont conduit à une sélection des références. Comme toute sélection, elle peut être contestée ; elle doit cependant pouvoir être utilisée comme point de départ d'un travail bibliographique d'approfondissement.

L'auteur tient à remercier ses collègues de l'ONERA qui l'ont aidé à préparer ce texte et exprime sa particulière gratitude à F. Vuillot. Il est également reconnaissant aux organismes et sociétés : DRET/DGA, DME/DGA, CNES, SNPE, SEP et BPD, de leur soutien passé et présent aux études de l'ONERA sur les instabilités de combustion des moteurs à propergol solide.

BIBLIOGRAPHIE

1. Culick, F.E.C., "Combustion Instabilities in Liquid-Fueled Propulsion Systems, an Overview", in "Combustion Instabilities in Liquid-Fuelled Propulsion Systems", AGARD CP450, April 1989, paper 1.

2. Williams, F.A., Barrère, M. et Huang, N.C., "Fundamental Aspects of Solid Propellant Rockets", AGARDograph 116, October 1969, chapitres 9 et 10.

3. Price, E.W., "Experimental Observations of Combustion Instability", in "Fundamentals of Solid-Propellant Combustion", Progress in Astronautics and Aeronautics, Vol. 90, AIAA, 1984, chapitre 13.

4. T'ien, J.S., "Theoretical Analysis of Combustion Instability", in "Fundamentals of Solid-Propellant Combustion", Progress in Astronautics and Aeronautics, Vol. 90, AIAA, 1984, chapitre 14.

5. "A Detailed Technology Roadmap for Rocket Propulsion", Aerospace Industries Association of America, Inc, October 1988, pp. 41-65.

6. Kuentzmann, P., "Etudes récentes à l'ONERA sur les instabilités de combustion dans les moteurs-fusées à propergol solide", in "Solid Rocket Motor Technology", AGARD CP-259, July 1979, paper 22.

7. Gossant, B., "Combustion des propergols solides et balistique intérieure des propulseurs", in "Technologie des propergols solides", Masson, 1989, pp. 119-198.

8. Swithenbank, J., "Combustion Instability in Solid Propellant Rocket Motors", report NO.H.I.C. 100, University of Sheffield, October 1969.

9. Hughes, P.M., et Smith, D.L., "Nonlinear Combustion Instability in Solid Propellant Rocket Motors - Influence of Geometry and Propellant Formulation", in "Solid Rocket Motor Technology", AGARD CP-259, July 1979, paper 26.

10. De Luca, L., "Extinction Theories and Experiments", in "Fundamentals of Solid-Propellant Combustion", Progress in Astronautics and Aeronautics, Volume 90, AIAA, 1984, chapitre 12.

11. Schöyer, H.F.R., "Low Frequency Oscillatory Combustion - Experiments and Results, in "Solid Rocket Motor Technology", AGARD CP-259, July 1979, paper 25.

12. Brown, R.S., Blackner, A.M., Willoughby, P.G., et Dunlap, R., "Coupling between Velocity Oscillations and Solid Propellant Combustion", AIAA 24th Aerospace Meeting, January 6-9, 1986, Reno, Nevada, AIAA Paper 86-0531.

13. Avalon, G., et Comas, P., "Simulative Study of the Unsteady Flow inside a Solid Propellant Rocket Motor" AIAA/SAE/ASME/ASEE 27th Joint Propulsion Conference and Exhibit, June 24-17, 1991, Sacramento, California.

14. Chaumette, J., "Etude aérodynamique de l'écoulement dans des cavités avec injection pariétale", Thèse de docteur-ingénieur, Université de Paris VI, 1977.

15. Culick, F.E.C., "The Stability of One-Dimensional Motions in a Rocket Motor", Combustion Science and Technology, 1973, Vol.7, pp 165-175.

16. Culick, F.E.C., "Stability of Three-Dimensional Motions in a Rocket Motor", Combustion Science and Technology, 1974, Vol. 10, pp. 109-124.

17. Van Moorhem, W.K., "Flow Turning in Solid Propellant Rocket Combustion Stability Analyses", AIAA Journal, Vol. 20, n° 10, October 1982, pp. 1420-1425.

18. Micheli, P.L., "The Effect of Mode Coupling on Combustion Stability", CPIA, Vol. 20, October 1981, pp. 81-91.

19. Culick, F.E.C., "Nonlinear Behavior of Acoustic Waves in Combustion Chambers, I", Astronautica Acta, Vol. 3, 1976, pp. 715-734.

20. Culick, F.E.C., "Nonlinear Behavior of Acoustics Waves in Combustion Chambers, II", Astronautica Acta, Vol. 3, 1976, pp. 735-757.

21. Yang, V., Kim, S.I. et Culick, F.E.C., "Third-Order Nonlinear Acoustic Waves and Triggering of Pressure Oscillations in Combustion Chambers, Part I : Longitudinal Modes", AIAA/SAE/ASME/ASEE 23rd Joint Propulsion Conference, June 29, July 2, 1987, San Diego, AIAA paper 87-1773.

22. Yang, V., Kim, S.I. et Culick, F.E.C., "Triggering of Longitudinal Pressure Oscillations in Combustion Chambers, I : Nonlinear Gas Dynamics", Combustion Science and Technology, August 1990, pp. 183-214.

23. Yang, V. et Culick, F.E.C., "On the Existence and Stability of Limit Cycles for Transverse Acoustic Oscillations in a Cylindrical Combustion Chamber, I : Standing Modes", Combustion Science and Technology, July 1990, pp. 37-65.

24. Gadiot, G.M.H.J.L., et Gany, A., "Nonlinear Propellant Response as a Possible Cause for Triggered Nonlinear Acoustic Instabilities in Low Smoke Solid Propellant Rocket Motors", 37th Congress of the International Astronautical Federation, October 4-11, 1986, Innsbruck, IAF paper 86-194.

25. Gadiot, G.M.H.J.L., et Gany, A., "Instability Modeling with Nonlinear Pressure Coupling", La Recherche Aérospatiale, n° 1988-5, pp. 23-37.

26. Kuentzmann, P., "Modèles de combustion instationnaire des propergols solides composites", La Recherche Aérospatiale, n° 1978-2, pp. 77-93.

27. Levine, J.N., et Baum, J.D., "A Numerical Study of Nonlinear Instability Phenomena in Solid Rocket Motors", AIAA Journal, Vol. 21, n° 4, April 1983, pp. 557-564.

28. Baum, J.D., Lovine, R.L., et Levine, J.N., "Pulsing Techniques for Solid-Propellant Rocket Motors : Modeling and Cold Flow Testing", Journal of Spacecraft and Rockets, Vol. 20, n° 2, March-April 1983, pp. 150-157.

29. Baum, J.D., et Levine, J.N., "A Critical Study of Numerical Methods for the Solution of Nonlinear Hyperbolic Equations for Resonance Systems", Journal of Computational Physics, Vol. 58, n° 1, March 1985, pp. 1-28.

30. Baum, J.D., Levine, J.N., et Levine. R.L., "Pulse-Triggered Instability in Solid Rocket Motors" ; AIAA Journal, Vol. 22, n° 10, October 1984, pp. 1413-1419.

31. Baum, J.D., et Levine, J.N., "Modeling of Nonlinear Longitudinal Instability in Solid Rocket Motors", Astronautica Acta, Vol. 13, n° 6/7, 1986, pp. 339-348.

32. Baum, J.D., Consultation AGARD à l'ONERA, 22-26 juin 1989.

33. Beddini, R.A., Consultation AGARD à l'ONERA, 23-27 Avril 1990.

34. Kuentzmann, P., et Laverdant, A. "Détermination expérimentale de la réponse d'un propergol solide aux oscillations de pression de haute fréquence", La Recherche Aérospatiale, 1984-1, pp. 39-55.

35. Brown, R.S., Dunlap, R., Young, S.W., et Vaugh, R.C. "Vortex Shedding as a Source of Acoustic Energy in Segmented Solid Rockets", Journal of Spacecraft and Rockets, Vol. 18, n° 4, pp. 312-319.

36. Mason, D.R., Folkman, S.L., et Behring, M.A., "Thrust Oscillations of the Space Shuttle Solid Rocket Booster Motor During Static Tests", AIAA 15th Joint Propulsion Conference, June 18-20, 1979, Las Vegas, Nevada, AIAA paper 79-1138.

37. Mathes, H.B., "Assessment of Chamber Pressure Oscillation in the Shuttle Solid Rocket Booster Motor", AIAA/SAE/ASME 16th Joint Propulsion Conference June 30, July 2, 1980, Hartford, Connecticut, AIAA paper 80-1091.

38. Philippe, A., et Tchepidjian, P., "Prediction of Longitudinal Combustion Instabilities in Axisymmetrical Propellant Grains", AIAA/SAE/ASME 20th Joint Propulsion Conference, June 11-13, 1984, Cincinnati, Ohio, AIAA paper 84-1358.

39. Pendleton, L.R., "Sinusoidal Vibration of Poseidon Solid Propellant Motors", The Shock and Vibration Bulletin, Bulletin 42, part 3, January 1972, pp. 89-95.

40. Flandro, G.A., Consultation AGARD à l'ONERA, 16-19 Septembre 1986.

41. Glick, R.L., et Kirschner Jr, T.J., "Combustion Stability of Low L/D Space Motors", AIAA/SAE/ASME 17th Joint Propulsion Conference, July 27-29, 1981, Colorado Springs, Colorado, AIAA paper 81-1558.

42. Flandro G.A., "Solid Propellant Acoustic Admittance in a Combustion Chamber", Journal of Sound and Vibration, Vol. 36, n° 3, 1974, pp. 297-312.

43. Vuillot, F., et Kuentzmann, P. "Flow Turning and Admittance Correction : an Experimental Comparison", Journal of Propulsion and Power, Vol. 2, n° 4, July-August 1986, pp. 345-353.

44. Hegde, U.G., Chen, F., et Zinn, B.T., "Investigations of the Acoustic Boundary Layer in Porous Walled Ducts with Flow", AIAA 23rd Aerospace Sciences Meeting, January 14-17, 1985, Reno, Nevada, AIAA paper 85-0078.

45. Hegde, U.G., et Zinn, B.T., "Rocket Motor Flow-Turning Losses", AIAA Journal, Vol. 24, n° 8, August 1986, pp. 1394-1395.

46. Flandro, G.A., "Effects of Vorticity Transport on Axial Acoustical Waves in Solid Propellant Rocket Chamber", ASME Winter Meeting, December 1989, San Francisco, California.

47. Ben-Reuven, M., "Nonlinear Combustion Instability in Solid Propellant Motors : Visco-Acoustic Coupling", AIAA 22nd Aerospace Sciences Meeting, January 9-12, 1984, Reno, Nevada, AIAA paper 84-0289.

48. Chung, T.J., "Recent Advances in Combustion Instability Analysis for Solid Propellant Rocket Motors", Technical report RK-CR-82-11, US Army Missile Command, May 1982.

49. Chung, T.J., et Sohn, J.L., "Interaction Coupled Acoustic and Vortical Instability", AIAA Journal, Vol. 24, n° 10, October 1986, p. 1582-1596.

50. Vuillot, F., et Avalon, G., "Acoustic-Mean Flow Interaction in Solid Rocket Motors Using Navier-Stokes Equations", AIAA/ASEE/ASME/SAE 24th Joint Propulsion Conference and Exhibit, July 11-14, 1988, Boston, Massachusetts, AIAA Paper, 88-2940.

51. Vuillot, F., "Numerical Computation of Acoustic Boundary Layers in Large Solid Propellant Space Booster, "AIAA 29th Aersopace Science Meeting, January 7-10, 1991, Reno, Nevada, AIAA paper 91-0206.

52. Blevins, R.D., "The Effect of Sound on Vortex Shedding from Cylinders", Journal of Fluid Mechanics, Vol. 161, 1985, pp. 217-237.

53. Flandro, G.A., et Jacobs, H.R., "Vortex Generated Sound in Cavities", AIAA Aero-Acoustics Conference, October 15-17, 1973, Seattle, Washington, AIAA Paper 73-1014.

54. Magiawala, K., et Culick, F.E.C., "Excitation of Acoustic Modes in a Chamber by a Vortex Shedding", Journal of Sound and Vibration, Vol. 64, n° 3, 1979, pp. 455-457.

55. Nomoto, H., et Culick, F.E.C., "An Experimental Investigation of Pure Tone Generation by Vortex Shedding in a Duct", Journal of Sound and Vibration, Vol. 84, n° 2, 1982, pp. 247-252.

56. Dunlap R., et Brown, R.S., "Exploratory Experiments on Acoustic Oscillations Driven by Periodic Vortex Shedding", AIAA Journal, Vol. 19, n° 3, March 1981, pp. 408-409.

57. Isaacson, L.K., et Marshall, A.G., "Acoustic Oscillations in Internal Cavity Flows : Nonlinear Resonant Interactions", AIAA Journal, Vol. 20, n° 1, January 1982, pp. 152-154.

58. Isaacson, L.K., et Marshall, A.G., "Nonlinear Interactions in Internal Cavity Flows", AIAA Journal, Vol. 21, n° 5, May 1983, pp. 785-786.

59. Shu, P.H., Sforzini, R.H., et Foster Jr, W.A., "Vortex Shedding from Solid Rocket Propellant Inhibitors", AIAA/ASME/SAE/ASEE 22nd Joint Propulsion Conference, June 16-18, 1986, Huntoville, Alabama, AIAA Paper 86-1410.

60. Flandro, G.A., "Vortex Driving Mechanism in Oscillatory Rocket Flows", Journal of Propulsion and Power, Vol. 2, n° 3, May-June 1986, pp. 206-217.

61. Shaw, J.H., Yang, V., et Koshigoe, S., : "Generation of Acoustic Waves in a Two Dimensional Forced Shear Layer", AIAA/SAE/ASME/ASEE 23rd Joint Propulsion Conference, June 29-July 2, 1987, San Diego, California, AIAA 87-1877.

62. Lupoglazoff, N., "Simulation numérique du phénomène de détachement périodique de tourbillon (vortex shedding), TN1 : approche de faisabilité", rapport technique interne ONERA, à paraître, 1991.

63. Crocco, L., et Sirignano, B.T., "Behavior of Supercritical Nozzles under Three-Dimensional Oscillatory Conditions", AGARDograph 117, London, 1977.

64. Vuillot, F., "Acoustic Mode Determination in Solid Rocket Motor Stability Analysis", Journal of Propulsion and Power, Vol. 3, n° 4, July-August 1987, pp. 381-384.

65. Avalon, G., et Vuillot, F., "Prévision du comportement instationnaire d'une tuyère amorcée", 25ième Colloque d'Aérodynamique Appliquée, 12-14 Octobre, 1988, Talence, conférence 28.

66. Temkin, S. et Dobbins, R.A., et "Attenuation and Dispersion of Sound by Particulate-Relaxation Process", Journal of the Acoustical Society of America, Vol. 40, n° 2, May 1966, pp. 317-324.

67. Yang, J.Y S., "Particulate Damping in Solid Propellant Rockets", AIAA Journal, March 1972, pp. 337-339.

68. Beckstead, M.W., Richards, R.S., et Brewster, B.S., "Distributed Combustion Effects on Particle Damping", AIAA Journal, Vol. 22, n° 3, March 1984, pp. 383-387.

69. Beckstead, M.W., "Evidences for Distributed Combustion", 24th JANNAF Combustion Meeting, October 1987, CPIA n° 476, Vol. I.

70. Beckstead, M.W., Consultation AGARD à l'ONERA, 22 Juin 1990.

71. Pascal, J., "Vitesse de combustion d'un propergol solide composite en présence d'oscillations de la vitesse de l'écoulement", Thèse de doctorat, Université de Paris XI, 1987.

72. Price, E.W., "Velocity Coupling in Oscillatory Combustion of Solid Propellants", AIAA Journal, Vol. 17, n° 7, July 1979, pp. 799-800.

73. Thrasher, D.I., "Bulk Mode Instabiliy in Nozzleless Rocket Motor", 9th JANNAF Combustion Meeting, 1972.

74. Kuentzmann, P., "Fonctionnement des propulseurs à propergol solide sans tuyère", rapport interne ONERA 1/3435 EY, Novembre 1979.

75. Traineau, J.C., "Fonctionnement des propulseurs à propergol solide sans tuyère", rapport interne ONERA 3/3435 EY, Août 1980.

76. Guillement, G., "Simulation numérique des instabilités de combustion d'un propulseur à propergol solide à chargement usiné", La Recherche Aérospatiale, à paraître.

77. Lupoglazoff, N., et Vuillot, F., "Two-Dimensional Numerical Simulation of the Stabiliy of a Solid Propellant Rocket Motor", AIAA 29th Aerospace Science Meeting, January 7-10, 1991, Reno, Nevada, AIAA paper 91-0205.

78. Lupoglazoff, N., et Vuillot, F., "Simulation numérique bidimensionnelle des écoulements instationnaires dans les propulseurs à propergol solide", La Recherche Aérospatiale, à paraître.

Ignition and Unsteady Combustion of Solid Propellants

by

Kenneth K. Kuo, Ph.D.
Director of the High Pressure Combustion Laboratory
Dept. of Mechanical Engineering
312 Mechanical Engineering Building
University Park
Pennsylvania 16802
United States

ABSTRACT

The second lecture will be based upon the book chapter entitled "Solid Propellant Ignition Theories and Experiments", by Prof. C.E. Hermance and the *AIAA Journal* paper on "Review of Solid-Propellant Ignition Studies", by Profs. A.K. Kulkarni, M. Kumar, and K.K. Kuo. The experimental and theoretical literature pertaining to the ignition of solid propellants over the past 25 years will be reviewed. The purpose is to present a cohesive description and evaluation of the research in solid-propellant ignition to date. The effects of important parameters on ignition processes will also be discussed. Major technological gaps in this area will be presented and future research study topics will be recommended.

The portion concerning transient burning of solid propellants will be based upon the book chapter by K.K. Kuo, J. Gore, and M. Summerfield. Transient burning behavior of solid propellants often occurs under a rapid pressure excursion and is caused by the finite relaxation times required for the solid and/or gas phases to adjust their temperature profiles. The instantaneous burning rate under transient conditions may, therefore, differ significantly from the steady-state value corresponding to the instantaneous pressure.

All the presentation materials are available in the open literature.

COMBUSTION AND SAFETY OF SOLID PROPELLANT ROCKET MOTORS

T. L. Boggs
Research Department
Naval Weapons Center
China Lake, CA 93555-6001, USA

INTRODUCTION

The subject of munition safety is one of continuing importance, with recent emphasis in various insensitive munition requirements, because of the potential damage that can be caused by any device highly loaded with energetic materials. It is a difficult task to prevent inadvertent initiation and to mitigate the effects of reactions once initiation has occurred. This difficulty is compounded by several considerations such as:

(1) The initiation can occur via many mechanisms. It can be due to bullet or fragment impact; through electrostatic discharge; accidental dropping of ordnance; or through exposure to fire, hot gases, steam leaks, etc. There are mixed sensitivities in many instances; for example, nitramine containing propellants are hard to ignite by thermal stimuli; however, they are more sensitive to mechanical shock that can cause detonation.

(2) Solid propellants have evolved to meet increased performance requirements. The need for high burn rates have led to some propellants that are extremely easy to ignite, especially as they age. Similarly, the need for increased range and decreased signature has led to propellants having high specific impulse with little or no metal ingredients. Some propellant formulations, in an attempt to meet low signature, high performance requirements, are almost identical to high energy plastic bonded explosives.

This topic area has been widely discussed in the past. For example, the recent AGARDograph No. 316 "Hazard Studies for Solid Propellant Rocket Motors (Ref. 1) devotes over 150 pages of text and over 200 references to this subject. Obviously the present paper cannot discuss the subject to the depth of the AGARDograph. Instead, because of space limitations, this paper will be devoted to the combustion aspects, and will only briefly discuss these topics. The intent is to provide an overview of the subject (and the material contained in the AGARDograph), and refer the reader to Reference 1 for more detail. In many instances passages from Ref. 1 are repeated here.

The authors of Reference 1 felt that a program leading to mechanistic understanding of reactions and the ability to predict hazard response was required. It was felt that the traditional, standard go/no-go tests did not provide this understanding nor the predictive capability. A hazard assessment method that considered classes of output (detonation, explosion, burning, and no reaction) in terms of input stimulus and target (includes sample and environment) was developed after many discussions. Key to this effort was the hazard assessment protocol. By working through a hazard protocol, the user could develop hazard assessment/response plots that described his munition subject to many stimuli of a given type (for example those combinations of fragment mass, fragment velocity, and fragment shape leading to detonation, those combinations leading to explosion, and those combinations leading to no reaction). The hazard assessment/response plots can then be compared to the fragment masses, velocities, and shapes for a given threat (e.g., warhead) to determine the likely response of a given munition for a given threat.

It was said that one of the key elements of this approach is the hazard assessment protocol. What is a hazard assessment protocol? It is an orderly procedure that results in a flow-chart that directs the user through consideration of a hazard area. This consideration will be of his sample (whether it be an all-up munition, a component, or a test article) in its environment subject to the threat stimuli likely to be encountered. The hazard assessment protocol helps tell the designer and test personnel, (1) what paths are most likely to be encountered, and hence must be considered, and (2) what information must be obtained in order to perform the assessment. Because the assessment is based on logic and directly associated with the ordnance item in a real environment and subject to real threats, it has more value than the results of a few go/no-go hazard tests. The protocol approach is intended to be (1) a design tool used early in the design cycle to anticipate potential hazard problems, and (2) an aid to program personnel to mitigate existing munition hazard problems. The protocol approach is more extensively described and used in Reference 1.

Perhaps it is easier to understand the protocol approach by working through a simplified example: impact of a fragment on an idealized munition consisting of a case wall-energetic fill-case wall. There are several possible reactions as illustrated in Fig. 1. The first consideration is the prompt shock to detonation. In this situation the fragment impacts the munition, sending a shock wave into the cased energetic material that this shock wave transitions into a detonation. If the fragment does not impart sufficient energy to cause a detonation, we may still have a significant problem resulting from the fragment penetrating the case. If the fragment penetrates several possibilities are likely to occur. The worst is that the fragment ignites the energetic material and the combustion rapidly produces gases that can't be vented quickly. In this instance the munition may violently explode sending large to modest fragments at high velocities. Another situation that often occurs, generally with less severe consequences, is that the fragment because of its high velocity and/or large mass, either penetrates directly through the munition and doesn't ignite the energetic material and/or provides an extremely large vent and/or breaks open the case. In these instances, a fire may ensue but at least there was no detonation or explosion. The last instance, and the most desired, is that the fragment simply hits the case and bounces/ricochets off causing no reaction.

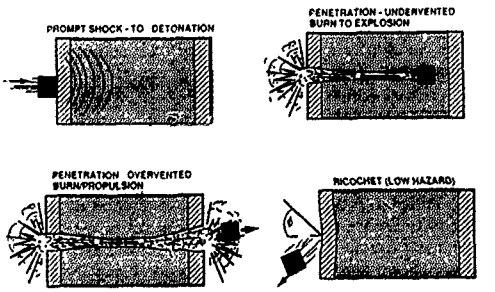

Fig. 1. Possible Reactions When a Fragment Impacts a Cased Energetic Material.

Which reaction is likely to occur? This is where the protocol comes in. Let's take a simplified look at this problem. Our first concern was: "Do we get a prompt shock to detonation?" (SDT) The protocol path of Fig. 2 addresses this concern. We first start with the fragment having mass, velocity, size/shape, and orientation; and let's say that this is the first fragment impacting the munition. The first question to ask is how does the diameter of the fragment compare to the critical diameter of the energetic propellant (or explosive). The critical diameter is the smallest diameter that will sustain a detonation. If the fragment diameter is much less that the critical diameter of the energetic material then a prompt shock to detonation transition is unlikely (however other mechanisms such as deflagration to detonation transition may be possible) and one should proceed to penetration considerations.

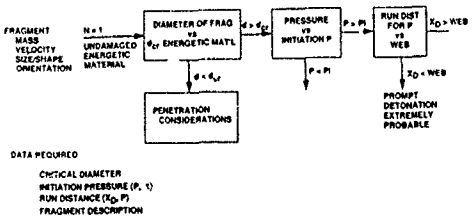

Fig. 2. Simplified Hazard Assessment Protocol for Prompt Shock Induced Detonation of a Cased Energetic Material Subject to Fragment Impact.

If however the fragment diameter is approximately equal to or bigger than the critical diameter, a prompt shock to detonation may ensue; and one must compare the shock pressure imparted to the energetic material by the impact to the initiation pressure required to cause detonation. If the imparted pressure is below the threshold, prompt shock to detonation is unlikely (but again other detonation mechanisms may occur - DDT, XDT).

If however the imparted pressure is above the threshold, a detonation is very likely and we must compare the web thickness to the run distance. Do we have enough energetic material to allow the shock wave to build to a detonation? Unfortunately usually if we have a small enough critical diameter and a low enough threshold, we also have a small enough run distance that a detonation is extremely probable, and it's back to the drawing board or time to consider mitigation devices or start thinking up clever arguments why a waiver should be granted.

Even if you come through this path relatively unscathed, you may have to go through it again, this time considering damaged energetic fill. The damage can come from many sources: handling, age, hit by previous fragment, etc. Now you must go through the path, but this time with the values for damaged material. The damaged materials are usually more sensitive than their undamaged counterpart. For example, 1% voids can cause the initiation pressure to drop from 40 kbars to 20 kbars (Ref. 1-3).

Before leaving this path, let's think about what data are required for the assessment. We need the critical diameter, the initiation pressure threshold (as a function of time), the run distance (as a function of pressure) of the undamaged and damaged energetic material, as well as the description of the fragment. References 1 and 2 discuss techniques for obtaining these data.

If there is no prompt shock to detonation, we still must be concerned with the penetration effects [Note: We consider SDT first because (1) it is usually the worst reaction, and (2) if it's going to occur it will be the first (and last) occurrence, taking place in microseconds, for that munition.] In the penetration path, Fig. 3, we are first concerned with whether the fragment can penetrate the case, that is, is there sufficient mass and velocity of the projectile to exceed the ballistic limit of the case. If not, we have the desired bounce-off/ricochet. However if the mass and velocity exceed the ballistic limit, we must ascertain by how much. If the mass and velocity greatly exceed the ballistic limit, the fragment may pass through the munition without igniting the energetic material and/or overventing the case.

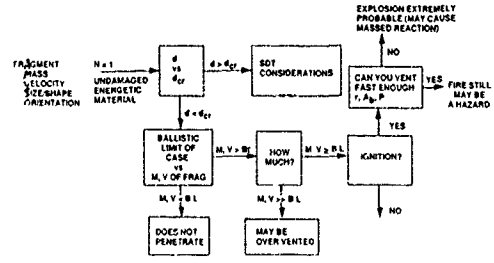

Fig. 3. Simplified Hazard Assessment Protocol for Fragment Impact/Penetration of a Cased Energetic Material.

If the mass and velocity don't greatly exceed the ballistic limit, e.g., the fragment lodges within the grain, we must then ask if ignition occurs. If no, that's desirable. If yes, then we need to know the burn rate, burn area, pressure and vent size (not independent parameters) in order to determine if we can vent the products fast enough or whether an explosion is probable. If we can vent, we still have a fire problem to contend with. If the products are not vented fast enough an explosion can occur and the explosion can lead to other sympathetic reaction of adjacent stores - up to and including sympathetic detonation.

To predict likely reactions in this path, we must know the ballistic limit of the case, the high rate mechanical properties of the energetic material, deformation of the fragment, ignitability of the energetic material, burn rate, and burn area of the energetic material, as well as case confinement and venting.

The protocol discussed above and depicted in Figs. 2 and 3 is a simplified example. The current bullet/fragment impact protocol is on a 2 foot by 3 foot chart and is described in several pages of text. Before dismissing this as being unwieldy, the reader must be cautioned that (1) while the protocol considers all the paths, the user doesn't "go down" all the paths, (2) the responses that the user gives direct him through the path appropriate to his situation, and (3) the protocol is being put into user-friendly, personal computer compatible software. At present it is easy to use and when the software is complete it will be even easier to use.

Once you have the data required by the protocol, what do you do with them? The data can be used to construct a hazard assessment plot shown in Fig. 4. Starting at the right hand of this figure, we first determine what combinations of projectile mass-velocity will cause prompt

detonation. This region is ameliorated at the lower values of mass (smaller diameters) by critical diameter considerations (for a more complete discussion of critical diameter effects, please consult pg. 140 of Reference 1). Also shown on Fig. 4 are the ballistic limit lines for the case (B.L. is the single ballistic limit line, while 2 B.L. is the ballistic limit for penetrating one side and emerging through the second side.). Somewhere between/near these lines is the explosion phenomena (sometimes referred to as burn to violent reaction, or BVR for short). The region to the left of the ballistic limit line is the bounce-off/ricochet zone, while the region to the right of the explosion region and to the left of the detonation region is the zone of over-vented reactions.

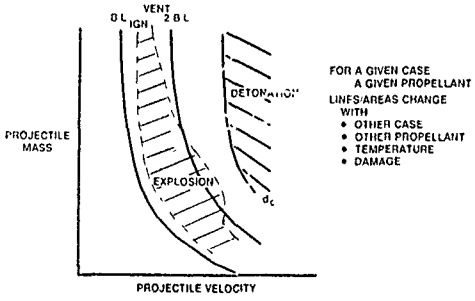

Fig. 4. Hazard Assessment Plot for Fragment Impact of a Cased Energetic Material.

The actual locations of such lines on a hazard assessment plot are going to be dependent on the various munition designs, the environment, and the threat stimuli, and will change as you change the design, the environment, and the stimuli. The point to be made here is that one of our goals has been met: you can predict the hazard response, based on laboratory and small-scale field tests, early in the design cycle, and then if you experience an unwanted response, see the effects of design changes. This will be more clear below.

While the cartoon of Fig. 4 shows the over-vented zone, in reality at present we have difficulty predicting the exact location of this zone. We know it exists and have specific examples of when it exists for given munitions and given threats, it's just that we have difficulty in a priori prediction. So instead of the hazard plot of Fig. 4, we use the semi-logarithmic plot of Fig. 5. [This is an actual plot for a given ordnance item.] Here the three areas (prompt detonation, burn to violent reaction, and ricochet) are shown and one can see the general vulnerabilities of this particular munition.

While knowledge of a munition's vulnerability is very desirable, it can be extended to determine the vulnerability of the munition to a specific threat such as detonation of an enemy warhead or detonation of one of our own warheads (sympathetic detonation). To do this we need a mapping of the threat fragments.

Figure 6 presents such a threat spectrum overlaid on the hazard map of Fig. 5. The circles show the various fragments in terms of their mass and velocity. The size of the circle is indicative of the approximate number of fragments having that mass and velocity (1, 10, 100, 1000).

This overlay plot is obviously very valuable in showing the vulnerability of one munition to another. In the example given in Fig. 6, there are many fragments over 1000 grains with a velocity of approximately 6800 ft/sec. [Note: There are 7000 grains/lb. A 1/2 x 1/2 x 1/2 inch cube of steel is approximately 250 grains.] Similarly there are several fragments of 6600 grains (almost a pound each) with a velocity of 4200 ft/sec. These are obviously in the prompt shock to detonation region and represent a serious problem that must be designed away or mitigated.

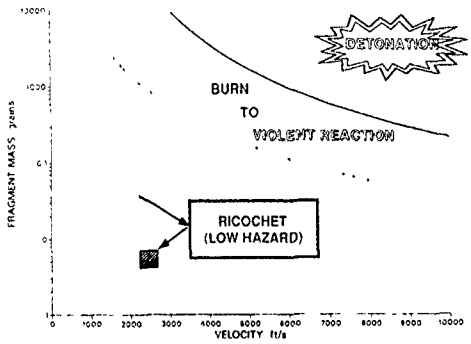

Fig. 5. Hazard Assessment/Response Plot of Fragment Impact of an Actual Munition Component.

Also shown on Fig. 6 by the square symbol is the standard U.S. insensitive munition fragment test fragment (250 grains and 8300 ft/sec). Obviously in this example this test would say that there was not a prompt shock to detonation problem, although the munition would fail the test due to explosion.

Once you know that you're in trouble, plots can be used to help get you out of trouble. Figure 7 shows the effect of using various steel barriers in mitigating the impact of the two fragments discussed previously. These calculations were done using the Thor description of fragment/barrier interaction. Other descriptions are also available. In the Thor description 1/4 inch thick steel barriers will move the 1140 grain fragments out of the detonation region and approximately 3/4 inch thick steel barriers will move the effects of these fragments, not only out of the detonation region, but out of the burn to violent reaction region.

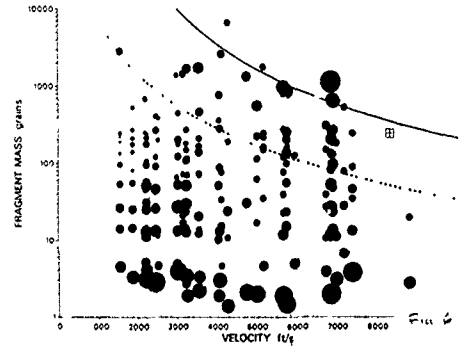

Fig. 6. Overlay of Actual Fragment Distribution (the Size of Circle Denotes Approximate Number of Fragments: 1, 10, 100, 1000) From Threat Warhead Overlaid on Hazard Assessment/Response Plot of Fig. 5.

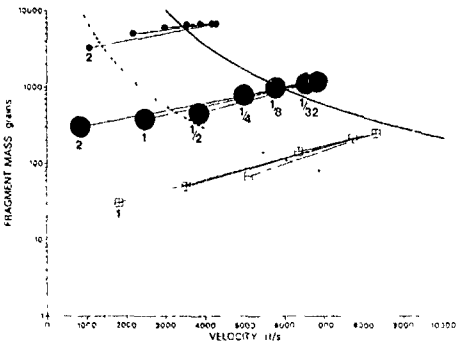

Fig. 7. Effect of Placing Different Thicknesses (in inches) of Steel Barrier Between Threat and Acceptor Munitions.

The above is an illustration of one hazard assessment protocol. Protocols exist for all of the hazard areas. From these protocols for bullet and fragment impact, sensitivity to electrostatic discharge, cook-off, shaped charge jet impingement, and sympathetic detonation; many ignition, combustion, explosion, and deflagration to detonation considerations are called for. It is suggested that the reader review Reference 1 for an appreciation of what must be considered in the various protocols. In the ensuing sections the ignition, combustion, explosion, and detonation phenomena will be presented in a general form, irrespective of what protocol, or what path within a protocol, the phenomena might find application.

IGNITION

The transition of a combustible system from a nonreactive or very slowly reactive state to the state of self-sustained combustion can either be effected by an external source of ignition or may originate in the combustible system on its own, if the boundary conditions are in an appropriate range. This latter process is called autoignition or thermal explosion and has been dealt with in Section 5.1 of the AGARDograph (Ref. 1) and will not be discussed in this paper. Ignition is the beginning of every combustion process. Hence it must be handled effectively when a controlled combustion process is to be initiated, and it must be prevented reliably if accidental fires and explosions are to be avoided. This process is also important in laboratory type investigations either to look into the ignition process itself, or else to classify the sensitivity of propellants with respect to planned or accidental ignition stimuli, to classify additives, or to assess the influence of external parameters.

Solid propellant ignition is both a process and the successful completion of that process. As a propellant sample is externally heated, there is an increase in the surface temperature and a build up of a thermal profile. When gasification of the sample begins, the gaseous products begin to react exothermically. This heat release increases the gas temperature, and thus, the reaction rates. With additional heating and accumulation of gas phase species the flame will "snap back" toward the propellant surface. At this point, the flame provides sufficient energy for propellant pyrolysis, the external heat source is no longer necessary, and ignition is complete. These processes are graphically illustrated in the general log flux-log time, ignition plot shown in Fig. 8.

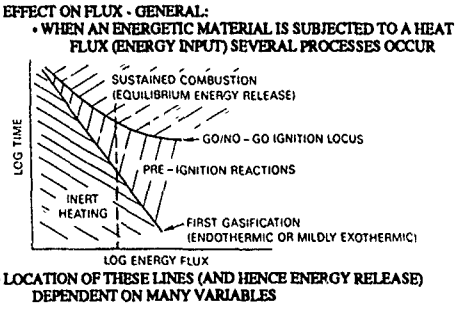

Fig. 8. General Depiction of Ignition Process.

For a given energy level (the dotted line in Fig. 8) a series of events are shown at various times over which the sample is subject to the flux. For some initial time, nothing appears to be happening. If the energy flux is terminated during this time and the sample examined, no significant decomposition of the exposed surface is seen. Figure 9a shows a sample of a high energy propellant containing nitramine which was subjected to 200 cal/cm^{2}sec for a time just prior to first gasification (evidenced by "first light" detected by a photodiode). No significant reaction has occurred but a thermal profile is being established within the solid. It is not until the "first gasification" time is achieved that the sample starts to significantly decompose. The flux has established and deepened the thermal profile in the solid until a surface temperature is reached that causes significant ablation/decomposition at the surface. For exposures slightly longer than the time necessary for this initial gasification, the sample continues to gasify but does not ignite in the classic sense of ignition. That is, if the external energy flux is removed, the sample will cease gasifying, the temperature profile in the solid will collapse, and the sample will not combust. Figure 9b is a sample subjected to 200 cal/cm^{2}sec at a time just after first gasification (as evidenced by "first light") and shows some decomposition of the surface, while Fig. 9c shows another sample at 200 cal/cm^{2}sec and a time just less than that required for "go/no-go" ignition. This sample shows significant decomposition. Ignition is not achieved until the conditions of flux-time associated with the line indicated as "go/no-go ignition" on Fig. 8 have been achieved. At this time, and for longer exposure times, the sample is ignited in the sense that if the external energy flux is removed, the sample will continue to burn by itself without the external stimulus (Ref. 4). There is another region of "overdriven" combustion--higher fluxes and steeper thermal profiles, where removal of the flux will also cause the sample to extinguish (Ref. 5).

Figure 8 is a generalized depiction of the ignition process. It defines three regions separated by two lines:

Inert heating region
First gasification line
Pre-ignition region
Go/no-go ignition curve
Self-sustained combustion region

The location of these lines and their relationship to the described regions is dependent on many variables. Propellant formulation, external energy level, and test pressure all contribute to the time relationship between the establishment of the thermal profile and self-sustained combustion.

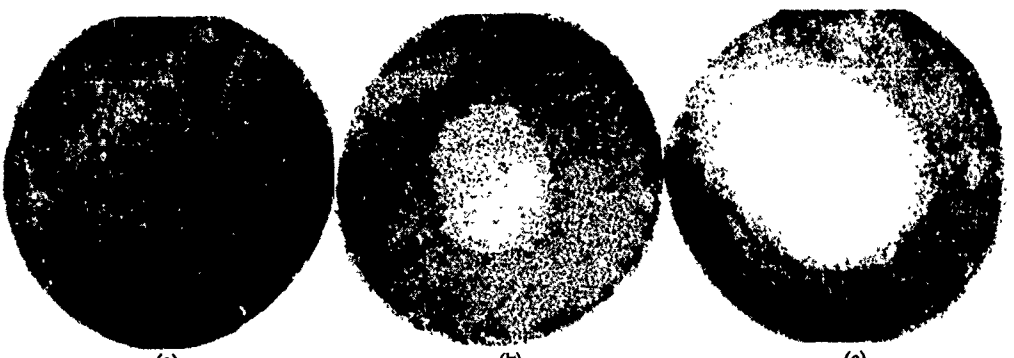

Fig. 9. Nitramine Containing Propellant Exposed to 200 cal/cm^{2}sec at (a) Prior to First Light/Gasification, (b) Just After First Light/Gasification, and (c) At a Time Preceding Go/No-Go or Complete Ignition.

Exposing a solid propellant to high energy levels may not be sufficient to initiate combustion. The pre-ignition region is important in that it is in this region that the solid has gasified into reactive intermediate species (pyrolysis products), but these intermediate species have not reacted to final products; thus self-sustained combustion has not been attained. Unfortunately, many investigators view propellant ignition as simply a switch based on a critical surface temperature of the solid. When satisfied, an instantaneous change is made from a non-reacting inert solid to burning at steady-state with fully reacted gases. While this criteria may be useful in some cases of ammonium perchlorate-rubber propellants where the samples ignite almost immediately after first gasification, it does not match reality for all solid propellants and test conditions (Ref. 2). Concepts such as minimum ignition energy or ignition temperatures have been introduced in this manner, notions which have certain merits in spite of the fact that their meaning is equivocal and that boundary conditions are important, which usually is ignored when applying the data to other situations. In general, AP-based propellants tested at low flux levels and high ambient pressures show little or no detectable difference between go/no-go and first light/first gasification. Nitramine based propellants under similar conditions, display significant pre-ignition behavior (Ref. 6). Pre-ignition behavior can be demonstrated in the AP-based propellants by increasing the flux level and decreasing the test pressure (Ref. 7).

Typical Results

The effects of flux and of pressure are shown in Fig. 10 for a predominantly ammonium perchlorate-HTPB binder propellant. The effect of flux is clearly seen for the first gasification line and the various go/no-go lines. The effect of pressure is also clearly shown. Since the first gasification is essentially the ablation of the solid and primarily dependent on surface temperature, pressure should have little or no effect on this line. However, the rate of conversion of pyrolysis products to final reaction products is very pressure dependent and the go/no-go ignition locus reflects that pressure dependence. The region of pre-ignition reactions discussed earlier (the difference between first gasification and go/no-go lines) is clearly evident for the 50 psia case, as is the diminishment of the pre-ignition region with pressure increase to 100 and 200 psia.

Similar behavior, but with even more pronounced pre-ignition behavior, is shown in Fig. 11, the ignition map for a cast modified double base. Propellants incorporating high nitramine loading also display this pronounced pre-ignition behavior.

The implications of the pre-ignition region on deflagration to detonation transition and other transient combustion related hazards has been discussed in Refs. 6, 8, and 9.

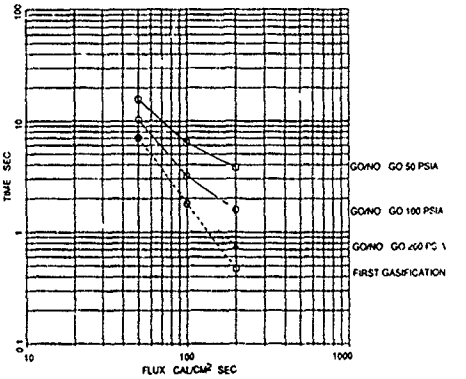

Fig. 10. Effect of Flux and Pressure on Ignition of Ammonium Perchlorate-HTPB Propellant.

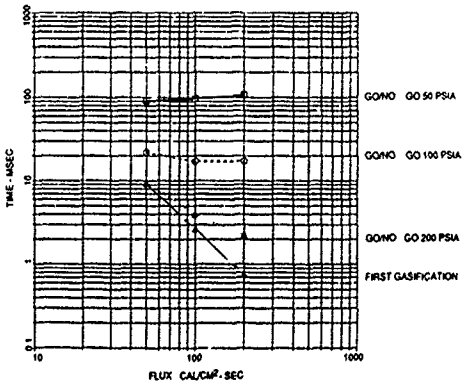

Fig. 11. Effect of Flux and Pressure on Ignition of Cast Modified Double Base Propellant.

This is a general overview of ignition due to thermal flux delivered to the surface (the examples given were for radiant flux). A more detailed description of ignition is

given in Reference 1, and is part of this course (Professor Kuo's discussion of ignition). Reference 1 also discusses ignition due to impact, friction, fracture, and electrostatic discharge.

In addition to a basic understanding of ignition, there exist several "rules of thumb" that people sometimes use. Two such "rules" that are sometimes helpful are:

(1) Propellants based on ammonium perchlorate often ignite as soon as the stimulus causes rapid gasification of the propellant. Remember AP propellants usually have less of a pre-ignition region than do double-base or nitramine based propellants.

(2) Within a family of propellants, the faster the burning rate the easier it is to ignite the propellant.

As with all "rules of thumb," the above rules should not be blindly used.

What are some of the implications for hazards based on the above discussion? Obviously propellants that don't ignite at low pressures (i.e., don't sustain) have some advantages in several hazard areas. We also know that high burn rate propellants, especially those incorporating ammonium perchlorate and catocene, ignite easily; in some cases during routine storage and handling. As will be briefly shown later, and in more detail in Reference 1, propellants with significant pre-ignition behavior, friability, and shock sensitivity are extremely susceptible to deflagration to detonation transition (DDT) and other forms of delayed detonation.

COMBUSTION

The pressure-time history due to burning propellant in a closed (or semi-closed) container is a function of several considerations and can result in propulsion, explosion and even transition to detonation. As shown earlier in the simplified fragment impact protocol, the balance between gas generation vs gas venting determines whether an explosion can occur. Similarly a deflagration to detonation transition can occur if several conditions, some related to ignition and combustion, are met.

The pressure-time history is a function of the mass burning rate which in turn is a function of the propellant density, burning surface area, and surface regression rate (often called the linear burn rate or simply burn rate)

$$p, t = f(\dot{m}, \ldots)$$
$$\dot{m} = \rho r A_b$$

However, the surface regression rate is a function of pressure, often given as $r = Cp^n$.

From the above brief discussion, we can see that there are several factors involved with the combustion of a confined energetic material, and how that combustion can lead to hazardous situations. The pressure-time produced from the combustion of the energetic material must be compared to the dynamic mechanical behavior of the case, with proper consideration of the venting, to determine the overall response. The gas production rate produced by the propellant is a function of: (1) the surface regression rate of the propellant, which in turn is a function of the pressure, and (2) the burn surface area of the propellant which is in turn a function of the surface regression history.

The following sections briefly discuss burn rate and burn area considerations, as well as providing references to more detailed discussions.

Burn Rates of Energetic Materials

The rate at which a solid is converted to gas during combustion is commonly called the burn rate and is a function of pressure, as discussed above, initial sample temperature, and boundary considerations such as flow past the surface (often called erosive burning). (This topic is discussed in another section of this lecture series.) The effects of pressure and initial sample temperature are shown in Fig. 12a.

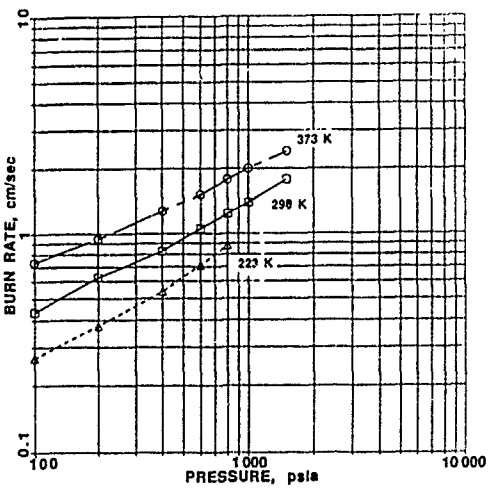

Fig. 12a. Burn Rate as a Function of Pressure and Initial Sample Temperature.

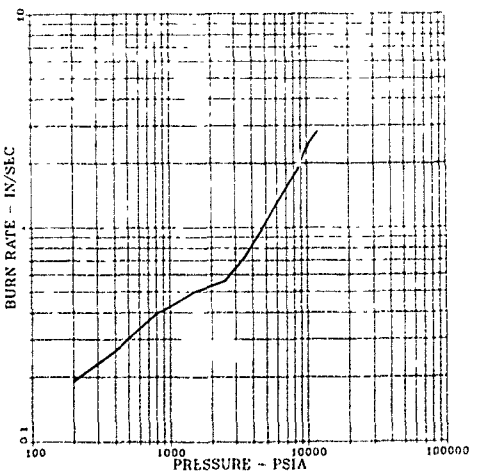

Fig. 12b. Burn Rate as a Function of Pressure, Showing a Slope Break at High Pressure.

Burn rates have been measured using various devices. These devices and the data that they produce have been reviewed in Ref. 10. As discussed in Ref. 10, there are basically two types of combustion bombs: low loading density (less than 0.01 gram of sample per cubic centimeter of bomb volume) combustion bombs (LLDCB), such as

strand burners or window bombs, and high-loading density (greater than 0.01 gram per cubic centimeter) combustion bombs (HLDCB), such as the closed bomb. The LLDCB are essentially constant-pressure, constant-volume devices which give the burn rate at a given pressure. To get a burn rate versus pressure curve, multiple runs have to be made.

The HLDCB is essentially a constant-volume device. As the sample burns, the pressure within the closed vessel increases. By measuring the pressure-time record of the process and applying suitable thermochemistry, the mass burning rate-time can be calculated. By assuming a form function (a burn area-surface regression relationship), the surface regression rate (burn rate)-pressure relationship can be calculated. Thus in one run, a burn rate-pressure curve can be calculated.

Burn rate data are required for protocol considerations as discussed earlier, and in other protocols presented in Ref. 1. The data are used in other not so obvious ways: (1) the slope of the burn rate-pressure curve, when plotted logarithm burn rate-logarithm pressure is the burn rate exponent (n in the equation $r = Cp^n$) and can give some indication of potential hazards, and (2) the temperature and pressure sensitivity of burn rate, coupled with ignition data, can be used to evaluate kinetic parameters, that are, in turn, "frozen" input variables to be used in transient combustion codes to predict convective combustion and deflagration-to-detonation transition.

Burn rate exponents very near unity and above are to be avoided since a small increase in pressure has a corresponding larger effect on burn rate, which increases the pressure, and increases the burn rate and so on until a case failure or explosion results. In rocket propellants slope breaks as illustrated in Fig. 12b often occur at high pressures. Many times the high pressure portion of the burn rate curve has a burn rate exponent very near or slightly greater than one. [NOTE: Before leaving this subject of burn rate exponent, it should be mentioned that one must be cautious of data showing slope breaks in burn rate curves. In some instances, combustion within the sample, as will be discussed later, occurs and as a result the burning surface area is increased. If the tests were run in a HLDCB, and if the pressure-time curve were treated using a laminar regression of the sample form factor description, then a higher surface regression rate than actually occurring would be predicted. Thus a slope break may be predicted in the burn rate where none occurred - the increase was in the burn area.]

The sensitivity of burn rate to pressure and initial sample temperature, coupled with flux-time ignition data can be used to determine kinetic parameters to be used in a transient combustion analysis. These transient combustion analyses are used to model high rate combustion phenomena such as deflagration to detonation. In fact, transient combustion analyses must be used, as opposed to combustion descriptions such as $r = Cp^n$, if one is to fully predict the various aspects of DDT (a later section will discuss this subject). This is because the plots of Fig. 12 are essentially the "steady state" values of burn rate-pressure, and may be altered in very rapidly changing environments such as present in DDT experiments. A mistake often made by analysts is to try to apply steady state data to a highly transient situation - almost implying that the transient is a special case of steady state, when in reality steady state is the special case of fully transient.

If one keeps the above consideration in mind, one can use the burn rate data and ignition data as special cases to evaluate kinetic data.

Discussion of such a model is beyond the scope of this paper but can be found in Ref. 12. Briefly, these models are based on two competing solid to pyrolysis product reactions, followed in each path by sequential pyrolysis product to final product second order gas phase reactions. The kinetic parameters of Arrhenius pre-factor and activation energy (four pre-factors and four activation energies) together with corresponding energy release are determined by evaluating what values give the best fit to actual burn rate [$r = r(p,T_0)$] data and flux-time-pressure ignition data. These parameters are then "frozen" and used in other experiments to predict laser augmented burn rate, convective combustion, and DDT.

Burn Area

Burn area is an extremely important determinant of the hazard severity given inadvertent ignition of the propellant. Damage is involved in many hazard scenarios such as bullet/fragment impact, ESD, and some slow cook-off areas. The damage can be pre-existing before ignition/combustion, or it may accompany the ignition/combustion. The burning of pre-strained (hence, in some cases, pre-damaged propellant) is described below.

The Effect of Strain on the Burning Rates of High Energy Solid Propellants

High energy propellants usually have a high solids loading (the portion of solid ingredients such as ammonium perchlorate (AP), cyclotetramethylenetetranitramine (HMX), aluminum and other ingredients such as solid catalysts) as compared to the polymeric binder. An obvious condition accompanying high solids loading is that there is less polymeric binder "glue" to hold the solid particles together to form propellants having acceptable mechanical properties. Given these highly loaded propellants, one would like to know such things as how far can a propellant be strained before ballistic anomalies (such as burn rate augmentation) become significant.

The burning rate of a high energy propellant as a function of strain is presented in Fig.13. [NOTE: The propellant was strained prior to burning. Thus any damage was pre-existing and held open.] The data show that no significant augmentation of burning rate occurs for pressure below 500 psi regardless of strain (the samples fail at approximately 25% strain). At higher pressures ($p \geq 750$ psi) burn rate augmentation appears for strains above approximately 8%. At 1500 psi and strains above approximately 12%, the sample burns in a vigorous and nonplanar fashion precluding meaningful measurement of a linear surface regression.

Data for several types of propellants show burn rate increase at pressures and strains greater than some threshold values. (The magnitude of the threshold values depends on the propellant.) It should be emphasized that both threshold values have to be exceeded, exceeding just one is not sufficient. For example high strain but low pressure will not cause augmentation nor will high pressure but low strain.

The mechanical response of the propellants to strain was studied using a binocular microscope. These studies showed, using the propellant of Fig. 13a as an example, that at 4% strain, debonds (separation, on a micro-scale,

of the solid particle from the polymeric binder) between ingredients occurs. Between 9-11% strain, these debonds are often fully developed cracks, with the walls of the crack in close proximity. At approximately 16% these cracks are open voids; that is, the walls of the crack are no longer in contact with one another. At approximately 24% the sample is often riddled with large cracks and the sample fails.

The above, coupled with our knowledge of flame stand-off distance decrease with pressure increase, provides a mechanistic understanding for the burn rate augmentation due to strain and pressure. The mechanism is shown in Fig. 13b. At low strain values the propellant is not significantly damaged and so regardless of the flame stand-off (Fig. 13b (top)) augmentation will not occur. When the propellant is highly strained and fissured, augmentation occurs if the flames can penetrate into these fissures. At low pressures the flame stands too far from the surface to allow penetration, but at high pressures the flame is close enough to the surface to penetrate the fissures and cause burn rate augmentation.

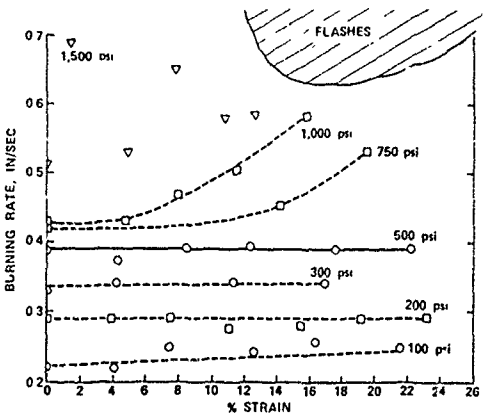

Fig. 13a. Burning Rate of a High Energy Propellant as a Function of Pressure and Strain.

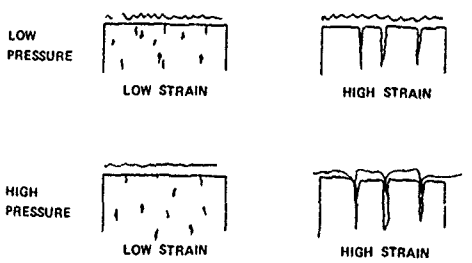

Fig. 13b. A Mechanism for the Augmentation of Burning Rate Due to Pressure and Strain.

Since flame penetration into the defects seems to be required for burn rate enhancement a study was done using propellants that had been strained almost to failure and then the tension removed. The voids closed and when these samples with the closed voids were burned, the burn rate was identical to the undamaged propellant burned at that pressure.

These data indicate that under certain conditions strain can cause damage, and if that damage is sufficient and open, and if the pressure is high enough to allow flame penetration into the defects, then burn rate enhancement can occur.

In addition, Professor Kuo and co-workers at Pennsylvania State University have studied the combustion of propellants with various cracks and other defects, observing crack growth during combustion.

In addition to the growth of cracks during combustion there are other dynamic effects. As burn rate increases the thermal zone gets thinner and the thermal gradient gets steeper. Under these conditions many samples, and ingredients within samples, crack, allowing combustion into these fissures. Under some conditions the cracking is so severe that the sample actually comes apart. Robert Fifer and his colleagues at the Ballistic Research Laboratory have extensively studied this deconsolidation, and the reader is referred to their works.

If the propellant undergoes significant break-up then DDT or other burn to violent reactions may occur. Ensuing sections of this paper briefly discuss these possibilities.

Before leaving this section, two other items need to be discussed. While most insensitive munition programs treat detonation as the most serious event, this is sometimes not the case, especially for ships at sea. Fire has been and will continue to be one of the sailor's worst fears. Often a ship can withstand the detonation of a warhead and the resultant fragments, and yet experience great difficulty with fires caused by the unburned propellant remaining in the motor. The missile attack on the U.S.S. Stark is a good example. The ship survived the detonation of the Exocet warhead; however, the unspent propellant caused fires that probably would have sunk the Stark had not several fortunate instances occurred (e.g., the Stark was not in a high sea condition, and a salvage tug with fire fighting capability happened to be relatively close to the Stark when the Stark started to burn). Similarly, many ships of the United Kingdom were lost to fire in the Falkland's campaign.

The other point to be made is that combustion instability may cause missile motors to explode. Fortunately, these explosions occur after launch, usually with a good distance between the launch platform and the missile.

COOK-OFF

Although cook-off has been widely studied, there are still many questions unanswered and much controversy surrounding cook-off.

When cook-off is discussed it usually is in terms of fast or slow cook-off. Fast cook-off is usually associated with ordnance in a fuel fire, or subjected to hot exhaust gases from adjacent aircraft or starter motors. Slow cook-off is characterized by very low heating rates (a few degrees per hour to a few degrees per minute). While there is much controversy surrounding the relevance of the heating rates used in slow cook-off tests, slow cook-off is a viable consideration. The slow heating rates occur primarily in storage or handling mishaps. (For example, munitions in a rail car heated by the burning of adjacent rail cars, or munitions in storehouse adjacent to a burning storehouse, or weapons in the hold of a ship with fire in adjacent compartments.)

A detailed discussion of thermal explosion, the slowest cook-off - the temperature is uniform throughout the sample, is contained in Reference 1. Reference 1 also discusses and presents a hazard assessment protocol for

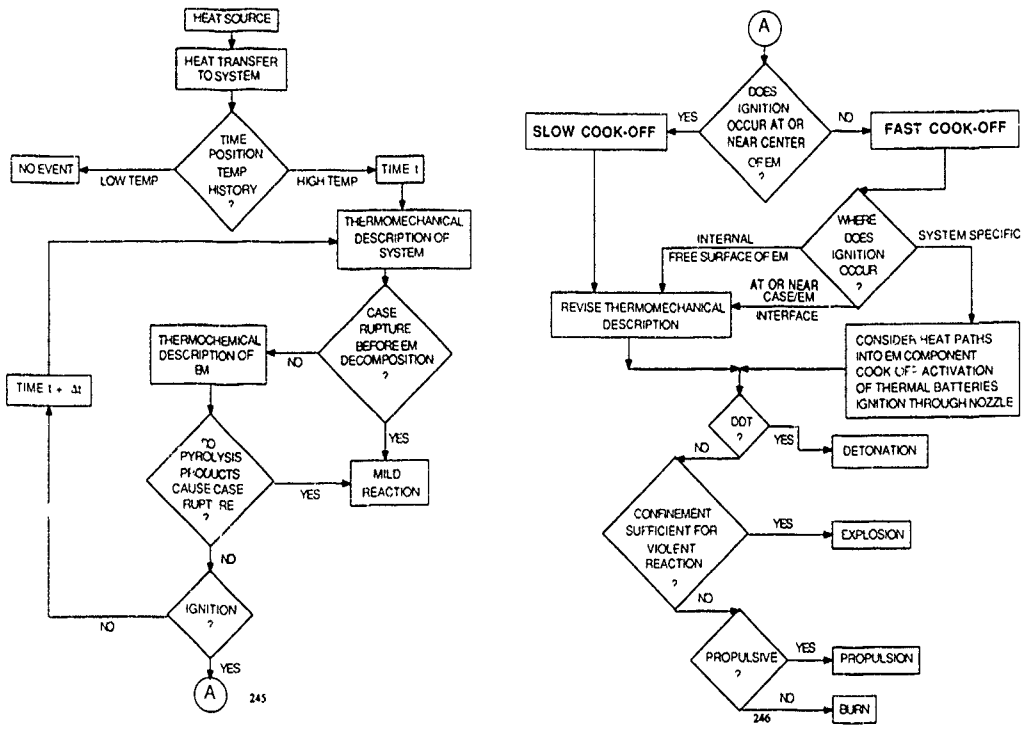

Fig. 14. Hazard Assessment Protocol for Cook-Off Phenomena.

fast and slow cook-off and since that time others have also attempted protocols for cook-off. The following is from a joint Australia, Canada, United Kingdom, and United States effort.

There are several requirements to be considered in the cook-off area. We often refer to cook-off in terms of slow cook-off and fast cook-off; fuel fire, bonfire versus bulk heating, and/or thermal explosion. Figure 14, while it includes these phenomena, attempts to treat cook-off or thermal phenomena in a more systematic way. That is, rather than define requirements of cook-off based on some test criterion, e.g., slow cook-off is equivalent to a 6°F/hr (3.3°C/hr) heating rate, we choose instead to take a more general approach, from which fast or slow cook-off routes emerge naturally. The protocol is shown in flow-chart form in Fig. 14.

Heat Source

The first step is a description of the heat source. This must include:

- The energy source
  - Is it a fire?
    - What is the fuel and its extent? What are the air sources? Are there other combustibles?
  - Is it indirect heating caused by
    - An adjacent fire?
    - Fire in an adjacent compartment separated from the target system?
  - Is it caused by a steam leak?
  - Is it a result of impingement of exhaust from a "huffer" (aircraft starter blower) or from an adjacent aircraft exhaust?
  - Is it a result of impingement of the exhaust from a rocket motor or torching from a damaged rocket motor or warhead?
- The environment
  - Is the target in a confined or unconfined space?
  - If it is unconfined, is there air flow across it, either due to wind or motion of the fire?
- Situational aspects
  - Is the fire separated from the stores by
    - Distance?
    - Intervening structures?
  - Are the munitions in shipping containers or bare?
  - Is there venting of the compartment so that heat can escape and oxygen can be replenished?

The description of the heat source is obviously the necessary first step, since it is the definition of the stimulus. We are trying to predict the response the munition is going to give to this stimulus, both in terms of initiation (when does a reaction occur and where, in the energetic material does it start) and output (how violent is the reaction).

Heat Transfer to the Target System

The next step, once we have characterized the heat source, is to describe how the energy is transferred from the source to the munition, through conduction, convection, or radiation. This is a necessary, but difficult, task usually done by analysis. The analysis is complicated by many unknown properties and the need to make assumptions. These assumptions often determine the answer and hence it is vital that they are clearly stated.

The result of the heat transfer analysis is a description of the energy flow to the munition and a description of the thermal response of the munition . This thermal response is usually described in terms of temperature-time-position profiles in the munition .

Temperature-Time-Position Profiles

If the temperature gradient is very low, not much heat is being transferred into the munition; and, if the time is not excessively long, the energetic material remains at some low or modest temperature and, usually, no event occurs. This is the desired result, but unfortunately many situations do not yield this result.

Fast heating rates, associated with a munition in a fuel-fire, or subject to hot exhaust gases, or the effects of torching, usually produce steep temperature gradients within the munition causing rapid heat transfer into it, resulting in the outer portions attaining very high temperatures. This is the so-called fast cook-off regime. On the other hand, heating which produces low temperature gradients in the weapon, but is applied for long periods of time can bring the bulk of the item to a relatively uniform high temperature, as opposed to the steep gradients characteristic of fast cook-off situations. This slow-cook-off regime often produces violent events, because ignition tends to occur at or near the center of the energetic material, and chemical decomposition is accelerated by self-confinement. Fast cook-off regimes, by contrast tend to lead to lower intensity events, because ignition occurs near the case-energetic material interface and the case may fail early. Some motor cases are intentionally designed to fail at high temperatures to relieve confinement and prevent catastrophic response.

The process for evaluating the response of a munition to cook-off is iterative, requiring several separate reviews of the thermomechanical environment during the evolution of the thermal environment until a reaction occurs, or it is clear that it cannot.

Time Increments

The selection of time intervals, appropriate to the munition under review, will require an appreciation of the mechanical and thermomechanical characteristics of the munition .

Uniform step increases in time are not essential, as experience and knowledge of the munition may enable a more efficient "phase to phase" progression to be adopted.

Thermomechanical Description of the System

On the initial pass through the protocol, the thermomechanical description may be confined to a simple appraisal of the design and its relationship to its surroundings. This should be sufficient to indicate whether the case will be ruptured before there has been any appreciable heat transfer to the interior of the store. For example, is the case fitted with any thermally initiated mitigation devices? What is the case material? Is it fabricated from homogeneous metal, composite metal/ nonmetal, or composite nonmetal/ nonmetal? Are there any stress raisers, etc.? On subsequent passes through the protocol, the effects of temperature on thermomechanical properties will need to be taken into account for all energetic and nonenergetic materials affected by heat. The description is also required to assist the determination of $T = T(x,t)$ and identify effects of phase changes and chemical reactions, e.g., pyrolysis. These will give system pressurization rates, changes of thermal insulation effects, etc. In some cases chemical reactions produce significant changes in materials properties, e.g., intumescence as a result of charring. Basic data required for such evaluations will include the heat transfer characteristics of the case and chemical descriptions of all materials used, such as adhesives, insulants, energetics, etc.

Pyrolysis Products

It has been established that pyrolysis products can influence the failure mechanism of munitions in fuel fires. If pyrolysis products are generated between the case and energetic material, say from the decomposition of an insulator, and these products are unable to escape, a localized increase in pressure will be generated. This pressure may cause the energetic material to be damaged, or it may lead to rupture of the case.

However, if the pyrolysis products are able to escape and eventually attain their flash point, this can lead to ignition of the free surface of the energetic material.

It may be that the pressurization is the result of effects in other than the energetic material and a pressure burst of the case can occur without significant energetic material reaction. The latter may ignite later in an unconfined state.

Other Ignition Mechanisms

The energetic material may reach its ignition temperature by internal decomposition reactions, or as a result of impinging flame(s) after some damage to the case or its closures.

System Specific Considerations

The munition or its storage container or conditions may impose specific preferential heat flow paths into the energetic material, so that local intense heating, sufficient to cause rapid decomposition can result. Alternatively, thermal batteries, boosters, igniters, etc., may preferentially ignite. Ignition of a rocket propellant or a thermal battery may occur through the nozzle of a rocket motor.

No protocol can legislate for all possible combinations and permutations of munition assemblies. It is therefore incumbent upon the assessor to consider if there are any others which could affect the response of the store.

Location of Ignition Point

Evidence exists from many experimental/theoretical sources that the location of the point of ignition is a direct outcome of the rate of heating. Slow heating results in central initiation, fast heating in surface initiation. In general, all those ignitions occurring within the body of the energetic material have at least some tendency towards self acceleration due to self confinement. The point at which the self-confinement effect is sufficient to change the process from burning to explosion is a function of the latest thermomechanical description of the system. This analysis enables a clear distinction to be made between slow and fast cook-off regimes.

The slow cook-off regime requires a reevaluation of the thermomechanical environment, since substantial material properties changes may have occurred due to the slow temperature rise. These effects may or may not lead to DDT, explosion, propulsion, etc., dependent upon the nature of the confinement and/or the chemical reactions

generated in the energetic material and/or materials in contact with it. It is important in the fast cook-off scenario to know where the ignition occurs, so that the likely effect of self-confinement of the energetic material in conjunction with the case can be assessed. If ignition occurs at an internal free surface (e.g., interior of a rocket motor grain), or at the case/energetic material interface, there is a need to re-evaluate the thermomechanical environment before assessing whether DDT, explosion, propulsion,burn, etc., can occur.

In each case the same questions need to be asked and, dependent upon the chemical kinetics and the effect of the thermal environment to date on the structure of the system, the same four possibilities of event emerge: detonation, explosion, propulsion, or burn.

Reference 1 discusses various cook-off tests and provides data from the various tests.

DELAYED DETONATION REACTIONS

There are several delayed detonation reactions. These include the widely studied deflagration to detonation (DDT), the reactions labeled XDT, and burn to violent reactions (BVR) up to and including detonation.

DEFLAGRATION-TO-DETONATION TRANSITION (DDT)

This technical area considers whether or not a propellant reaction can transition from a burning reaction to a detonation. The considerations are shown in the flow chart (Fig. 15). The key requirement for this transition to occur is a sufficient surface to volume ratio and porosity of the energetic sample either through manufacture and loading, in the case of some gun propellants, or through large scale damage in the case of missile propellants. For missile propellants the first consideration then is the likelihood of the propellant being damaged either before or during the burn. This is a critical consideration because, with rare exceptions, it is impossible for a consolidated propellant at near theoretical maximum density (TMD) to undergo a DDT reaction.

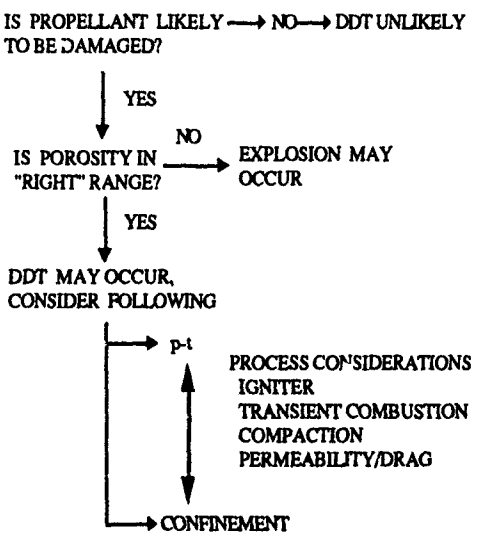

Fig. 15. Hazard Analysis Protocol for Deflagration to Detonation Transition.

The next consideration is whether or not sufficient surface-to-volume and porosity exist. Figure 16 presents the limits of DDT for granulated propellant samples of a given type (Ref. 11). This plot shows that you must have sufficient TMD - for this propellant formulation and confinement about 49% TMD; any less will not sustain and accelerate the reaction. If the sample is too dense, the DDT reaction will not occur. Similarly there is a range of surface to volume required (100-700 inches^{-1}) if DDT is to occur. If these conditions, or similar conditions for other samples, are not met then a DDT reaction is extremely improbable. Although transition to detonation may not be probable, an explosion may still occur. In order to determine whether an explosion may occur, the pressure and the rate of pressurization caused by gasification must be determined and compared to the rupture characteristics of the motor case.

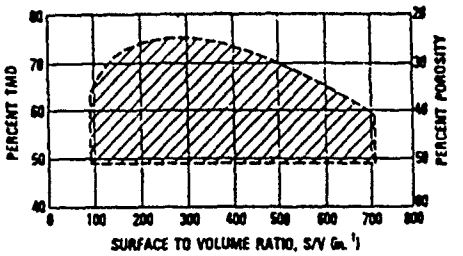

Fig 16. Limits of DDT for Granulated Propellant Samples (Ref. 11).

If the propellant is damaged and if the resulting %TMD and surface-to-volume ratio are in the "right" range then DDT is extremely likely. Whether or not the DDT occurs is determined by the pressure and pressurization rate within the vessel and the rupture characteristics of the vessel (motor case). If the motor case ruptures "too soon," then confinement is lost and the DDT reaction becomes unlikely. (The rupture may be a violent explosion.) The rupture characteristics of the vessel need to be determined experimentally and/or analytically but will not be discussed further in this paper.

The distance-time history of a DDT reaction of 1080 μm HMX powder, originally loaded in a heavy walled tube to 61% TMD is shown in Fig. 17. The figure shows the build up to detonation that occurs 104 mm down the tube and after approximately 400 μseconds. [Note: In this experiment, time = 0 was taken to be first detection of luminosity at the igniter interface, not necessarily first reaction of the igniter.] After this transition the detonation wave moves through the rest of the sample at 5.9 mm/μsec. The location of the lines in the x-t plane are strongly influenced by several considerations. These include the degree of confinement, the strength or "brisance" of the ignition stimulus, the sample thermochemical and physical characteristics, the charge dimensions (diameter and column length), and the intrinsic detonability of the material. The physical characteristics of the sample include the size and shape of the damaged pieces, the porosity and gas permeability, and the compressibility. The thermochemical considerations include the chemical composition of propellant, pyrolysis products, and final products; the kinetics and energetics associated with the pyrolysis (solid propellant going to reactive intermediate species) process, and the kinetics and energetics associated with the conversion of the reactive intermediate gases to final products.

It must be stressed that the above items are listed separately but in fact the DDT process is a highly coupled interaction of these various considerations.

From the above discussion it can be seen that the following types of data are necessary in order to predict whether DDT is likely to occur:

- Strength and brisance of ignition stimulus
- Confinement and rupture characteristics of the case
- Compaction behavior of the sample - how the %TMD changes with pressure
- The compaction/drag/permeability - the compaction is caused by an imbalance of forces between the drag of the gases flowing over the particles and the particles ability to resist compression. As the sample is compacted, the permeability (the ability of gas to flow through the sample) is changed
- The kinetics and energetics associated with the pyrolysis and conversion to final products
- The compressive ignition characteristics of the compacted material
- The detonability of the propellant

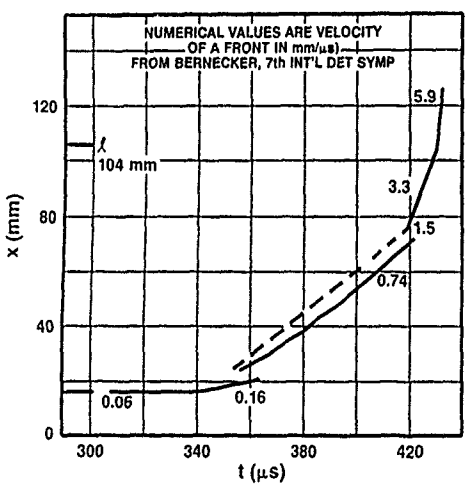

Fig. 17. Wave Front Velocities for a DDT Reaction (From Bernecker, Ref. 14).

Reference 1 discusses the various test techniques used in conjunction with DDT studies, as well as providing references to detailed analytical studies.

Previous sections mentioned that the ignition flux-pressure-time data, together with burn rate-pressure-initial sample temperature data, are used to determine kinetic parameters in a transient combustion code. This transient combustion code is then used in a larger DDT code to predict aspects of: (a) gas pressure in the tube as a function of location and time, (b) compaction profiles in distance and time, (c) amount of solid pyrolyzed, and amount of pyrolysis products reacted to final products, and data for thermally and mechanically (piston) stimulated DDT. These results have been reported in Refs. 8 and 12, and a few examples are shown here in Figs. 18-20.

Figure 18a presents the predicted gas pressure-distance profiles at 120, 200, 280, 360, and 440 μseconds, showing a relatively slow build-up in pressure, for 1080 μm HMX burning in a heavy walled tube (essentially the same conditions of the actual experiments shown in Fig. 17.

Figure 18b shows the corresponding compaction profiles. At t = 0, the tube is uniformly filled at 61% TMD. As the first material reacts, some of the material is gasified, and starts pushing adjacent material down the tube. As the reactions continue, more and more of the powder is compacted by, and ahead of, the pressure wave, and a plug of approximately 85% TMD is formed.

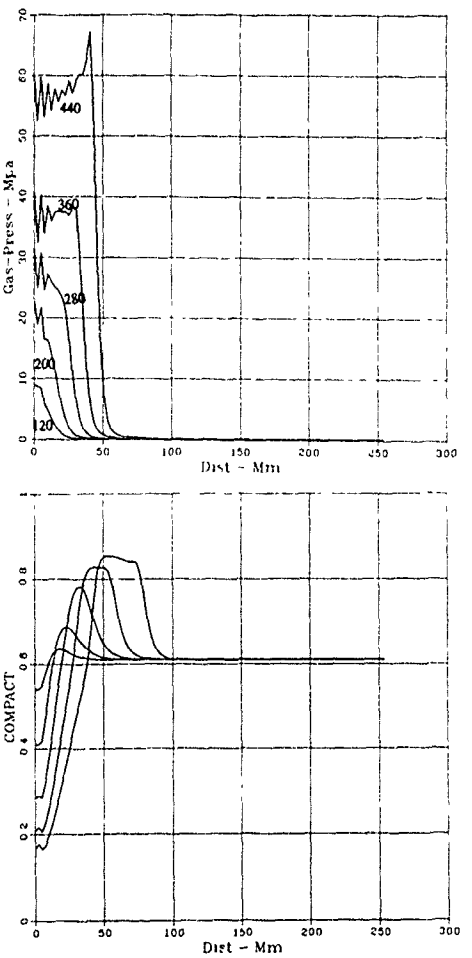

Fig. 18. Pressure (a) and Compaction (b) Profiles at Beginning of DDT Process.

Figure 19a presents the gas pressures at the transition at 595, 605, 615, and 624 μseconds. When this plot is compared with 18a two observations are made: in 18a the pressure slowly builds (the time steps were 80 μs) to a modest pressure (60-70 MPa) while in 19a the gas pressure goes from less than 1 GPa to over 12 GPa in 10 μseconds - a tremendous acceleration. Figure 19b presents the corresponding compaction plots. At 595 μs, the reactions have caused an almost impermeable plug of approximately 95% TMD. As the reactions continue that plug is rapidly consumed with the TMD going to zero in the area of reaction.

Figure 20 is a plot of the location of the leading edge of the compaction profile as a function of time. The solid curve is for the calculations presented in Figs. 18 and 19, and shows transition to detonation at approximately

125 mm and 600 μseconds. These values can be compared to the experimental values of 104 mm and approximately 430 μseconds from first luminosity presented in Fig. 17. [Note: The time differences are not unexpected. The calculations use t = 0 to be when the igniter is initiated, while t = 0 for the experiment was when first illumination out of the igniter was observed.] The dashed curve is for the case where the prefactors for the gas phase reactions were increased by 3 orders of magnitude (from 10^8 to 10^{11}, for one reaction path, and from 10^{11} to 10^{14} in the other gas phase reaction path). As can be seen this change to faster kinetic produces significant change. The transition to detonation occurs too quickly, but more importantly it occurs in the wrong place. Predictions for other cases has borne out the tremendous importance of the gas phase kinetics if experiments are to be properly modeled. As mentioned earlier these kinetic parameters are independently determined from the burn rate as a function of pressure and initial sample temperature coupled with the ignition flux-time-pressure data.

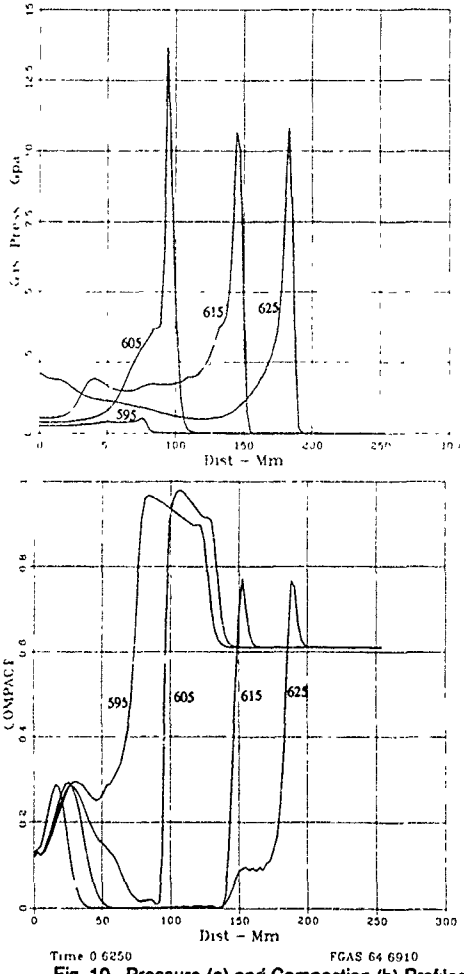

Fig. 19. Pressure (a) and Compaction (b) Profiles at Onset of Transition to Detonation.

The XDT reactions are also presented in Reference 1 and will not be presented here except to say that XDT reactions are usually associated with lower shock levels than for SDT, and in practical instances involve propellant impact upon hard objects. The process involves fragmentation of the sample, rapidly followed by recompression of the fragmented material, initiation of combustion and subsequent build up to detonation (similar to DDT).

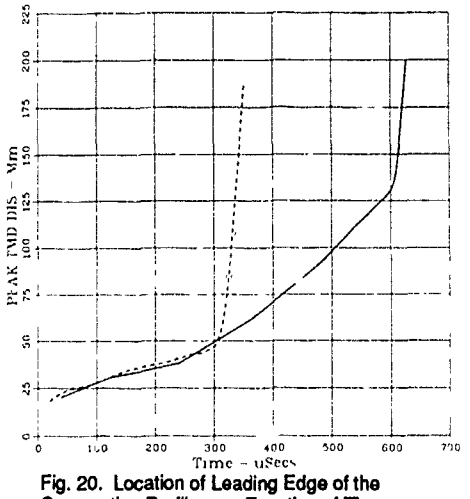

Fig. 20. Location of Leading Edge of the Compaction Profile as a Function of Time.

Another class of reactions is the burn to violent reactions. Included in this class is the already discussed fragment penetration reactions where the fragment ignites the propellant but does not supply sufficient venting and causes an explosion. There is another BVR reaction; however, that can lead to detonation. These reactions are particularly of concern to rocket motors having some form of a center perforation. As observed by Nougues and co-workers at SNPE (Ref. 15), a bullet when fired through the propellant web caused no detonation, while a similar bullet, at the same velocity, when fired so that it went through the bore caused detonation. Finnegan and co-workers investigated this phenomena in an idealized one dimension geometry: they fired fragments at a target consisting of metal cover to simulate the motor case, slab of propellant, air gap, propellant, and metal. What they found was that the projectile penetrated the metal cover and first slab of propellant. As the projectile penetrated the first slab of propellant it damaged the propellant and a debris cloud moved across the air gap. When this debris cloud impacted the second propellant slab, it ignited and depending on the gap and the propellant material would either burn vigorously or detonate. This test is of interest because so far it mimics responses to ordnance items to bullet and fragment impact. Those items that detonate in the large-scale test, also detonate in Finnegan's test, while those that violently burn in the large-scale tests also do so in Finnegan's test.

These phenomena have been incorporated into the bullet/fragment impact hazard assessment protocol.

NATO INSENSITIVE MUNITIONS INFORMATION CENTER (NIMIC)

Hazard protocols and data necessary in using the protocols for hazard evaluation, will be available through NIMIC.

In 1979 NATO formed AC/310, "Group on the Safety and Suitability for Service of Munitions and Explosives." In turn, AC/310 proposed in 1986 that a NIMIC be created.

In 1988 a Pilot NIMIC was formed and located at the Applied Physics Laboratory/Johns Hopkins University, Laurel, Maryland, USA. In 1990 the Pilot NIMIC became NIMIC and in 1991 this function will be transferred to NATO headquarters, Brussels. This group receives, analyzes, generates, stores, and disseminates technical information on:

- Technical requirements for insensitive munitions.
- Methods and systems for assessing and improving munitions to meet these requirements. - The hazard assessment protocols, hazard response maps, and threat evaluation programs are part of this effort, together with documents such as Reference 1.
- Databases of sensitivity tests using explosives and munitions.
- Insensitive munition technology deficiencies that prevent requirements from being achieved and proposals for remedial actions.
- Recommendations for possible solutions or design approaches to meet insensitive munitions development requirements. Again the hazard assessment protocols are part of this effort.
- Techniques for facilitating interaction among designers.

SUMMARY

Much of this paper is already a summary of work presented in more detail in Ref. 1, and in the references cited in Ref. 1. The attempt here has been to provide a brief introduction and overview and hope that the reader will turn to Reference 1 for more detail.

REFERENCES

1. T. L. Boggs and R. L. Derr, editors. "Hazard Studies for Solid Propellant Rocket Motors," NATO Advisory Group for Aerospace Research and Development, AGARDograph No. 316, Sept. 1990, 202 pp.

2. T. L. Boggs, A. I. Atwood, K. J. Graham, A. H. Lepie, C. F. Price, H. P. Richter, and D. E. Zurn. "Hazards of Solid Rocket Propellants," Proceedings of the Eastern States Combustion Institute - Physical and Chemical Processes in Combustion, Philadelphia, PA, November 1985, pp. B1-12.

3. T. L. Boggs, C. F. Price, H. P. Richter, A. I. Atwood, A. H. Lepie, N. G. Zwierzchowski, and L. R. Boyer. "Detonation of Undamaged and Damaged Energetic Materials," 19th International Annual Conference of ICT, 1988, Combustion and Detonation Phenomena, Fraunhofer-Institute fur Chemische Technologie, Karlsruhe, Federal Republic of Germany, pp. 30-1 to 30-13.

4. T. L. Boggs, C. F. Price, and R. L. Derr. "Transient Combustion: An Important Consideration in Deflagration to Detonation Transition," Propulsion and Energetics Panel 63(A)th Meeting, Lisse, Netherlands, AGARD Conference Proceedings, AGARD CP-367, May 1984, pp. 12-1 thru 12-2.

5. T. J. Ohlemiller, L. H. Caveny, L. DeLuca, and M. Summerfield. "Dynamic Effects on Ignitability Limits of Solid Propellants Subjected to Radiative Heating," in Proc., 14th Symposium (International) on Combustion, The Combustion Institute, Aug. 1972.

6. T. L. Boggs, C. F. Price, A. I. Atwood, D. E. Zurn, and R. L. Derr. "Role of Gas Phase Reactions in Deflagration-to-Detonation Transition," Seventh Symposium (International) on Detonation, Naval Surface Weapons Center, NSWC MP-82 834, pp. 216-224.

7. Naval Weapons Center. "Combustion Instability and Ignition Testing of NOS/IH Extruded Composite Propellant (Hycar Formulation, Mix 8514)," by J. E. Crump, A. I. Atwood, and D. E. Zurn. NWC TP 5427, China Lake, CA, December 1984.

8. C. F. Price and T. L. Boggs. "Modeling the Deflagration to Detonation Transition in Porous Beds of Propellant," The Eighth Symposium (International) on Detonation, Preprint 850706, Vol. 2, 1983.

9. M. J. Isler. "Contribution Du Mode De Combustion Des Explosifs Compacts Au Processus De Transition Combustion-Deflagration-Detonation," Combustion and Detonation Phenomena, 1988, pp. 18-1 to 18-13.

10. Naval Weapons Center. "Combustion Bombs: A Review and Recommendation for Use in High-Energy Propellant Safety Program, by T. L. Boggs, H. H. Bradley, Jr., T. S. Eitzen, and D. E. Zurn. China Lake, CA, NWC TM 2922, August 1976.

11. A. G. Butcher, B. D. Hopkins, and N. J. Robinson, as presented in R. R. Bernecker "The DDT Process in High Energy Propellants," in Hazard Studies for Solid Propellant Rocket Motors, NATO AGARD Conference Proceedings, AGARD-CP-367, Sept. 1984, pp. 14-1 to 14-16.

12. C. F. Price, A. I. Atwood, and T. L. Boggs. "An Improved Model of the Deflagration-to-Detonation Transition in Porous Beds," The Ninth Symposium (International) on Detonation, Preprint Vol. I, August/September 1989, pp. 162-168.

13. C. F. Price and T. L. Boggs. "Transient Combustion: An Important Aspect of Deflagration-to-Detonation Transition," accepted for publication in AIAA Progress Series on Transient Combustion, 1991.

14. R. R. Bernecker, H. W. Sandusky, and A. J. Clairmont, Jr. "Deflagration-to-Detonation Transition Studies of Porous Explosive Charges in Plastic Tubes," Seventh Symposium (International) on Detonation, NSWC MP 82-334, pp. 119-138.

15. B. Nouguez, H. Berger, B. Gondouin, and J. Brunet. "An Odd Bore Effect on Bullet Induced Detonation of High Energy Propellant Grains," American Defense Preparedness Association Symposium on Compatibility of Plastics and Other Materials with Explosives, Propellants and Pyrotechnics, 23-25 October 1989.

Bibliography

The bibliography that follows was prepared by CEDOCAR (the French Defence Documentation Centre) and has been approved by the Lecture Series Director, Dr B.ZELLER of SNPE, France.

1/72 - (C) C.NTIS
NUMERO SIGNALEMENT AD-A224 074/5/XAD
TITRE ANGLAIS Experimental Investigation of Strand Burning Metallized **Solid** **Propellants**
AUTEUR(S) ARNOLD K. J
AUTEUR COLLECTIF Naval Postgraduate School, Monterey, CA
CLASSIFICATION INT 019895000, 251450
TYPE DE DOCUMENT Thesis
CODE LANGUE ENG
CODE PAYS D'ORIGINE US
SOURCE Master's thesis, NP 73, DP Dec 89
CODE JOURNAL NTIS U9022
CODE TARIF NTIS NTIS Prices PC A04/MF A01
RESUME Characteristics of the products of combustion of metallized **solid** **propellant** strands at pressures between 250 and 750 psi were investigated using holography and light scattering measurements In addition, scanning electron microscope and light scattering measurements were used to examine quenched residue A reduced smoke ZrC **propellant** and three **propellants** of varying aluminum loading (2%, 4 8%, and 16%) were examined The objective of the experiments was to provide to determine if any correlation of results from this method of analysis could be made with results from other more complex **solid** **propellant** motor measurements, such as plume probe and signature measurements.The results of these efforts reflected the inability of any single technique of analysis to completely describe particle size distributions These results also suggest the need for modification of current experimental apparatus and procedures (JES).
CODE CLASSIFICATION 79 01; 79 05; 81 01
DESCRIPTEUR(S) Metallizing*;Solid propellants*,Aluminum;Combustion,Correlation, Distribution;Electron microscopes,Electronic scanners,Holography, Light scattering,Measurement,Particle size,Plumes;Probes; Propellants,Reduction,Signatures;Smoke,Strands
IDENTIFICATEUR(S) Combustion products*,NTISDODXA

2/72 - (C) C.NTIS
NUMERO SIGNALEMENT AD-A224 068/7/XAD
TITRE ANGLAIS Spectroscopy of **Propellant**-Related Flames.
AUTEUR(S) EDWARDS T
AUTEUR COLLECTIF Astronautics Lab (AFSC), Edwards AFB, CA.
CLASSIFICATION INT 095218000, 420405
TYPE DE DOCUMENT Report
CODE LANGUE ENG
CODE PAYS D'ORIGINE US
NUMERO DE RAPPORT AL-TR-90-033
SOURCE Final rept. Jan 89-May 90, NP 130, DP Jun 90.
CODE JOURNAL NTIS U9022
CODE TARIF NTIS NTIS Prices. PC A07/MF A01
NUMERO PROJET 2308
NUMERO ACTIVITE M1
RESUME This report summarizes the progress made in **solid** **propellant** flame chemistry studies.This work involves LIF studies of OH, CN, NO, and C2.Success was achieved in laboratory flame studies, but was rare in **solid** **propellant** applications.Preliminary studies in a hydrazine/methane/nitrogen dioxide diffusion flame yielded emission spectra from OH, NH, CN,

	CH, and C2.The vibrational temperatures of the NH and CN were consistent with published mechanisms for chemiluminescent excitation.Chemical kinetic studies of high pressure **propellant** flame yielded inconclusive results because of gaps in the knowledge of the combustion mechanisms of important species such as CN and NO2 Keywords: Hydroxyl radicals;Amide radicals;Cyanide radicals,Laser induced fluorescence;Combustion spectroscopy,Chemical kinetics,**Solid** **propellant** combustion (jhd)
CODE CLASSIFICATION	79 05; 81 01; 99 06
DESCRIPTEUR(S)	Chemical reactions*,Flames*,Solid propellants*;Spectroscopy*; Amides,Chemical radicals,Chemiluminescence;Chemistry;Combustion, Cyanides,Emission spectra,Excitation;High pressure;Hydroxyl radicals,Laboratory tests,Laser induced fluorescence;Propellants; Reaction kinetics,Temperature,Vibration
IDENTIFICATEUR(S)	NTISDODXA

3/72 - (C) C.NTIS

NUMERO SIGNALEMENT	AD-A222 591/0/XAD
TITRE ANGLAIS	Temperature and OH Concentrations in a **Solid** **Propellant** Flame Using Absorption Techniques
AUTEUR(S)	VANDERHOFF J A , KOTLAR A J
AUTEUR COLLECTIF	Army Ballistic Research Lab , Aberdeen Proving Ground, MD.
CLASSIFICATION INT	082505000, 050750
TYPE DE DOCUMENT	Report
CODE LANGUE	ENG
CODE PAYS D'ORIGINE	US
NUMERO DE RAPPORT	BRL-TR-3098
SOURCE	Technical rept, NP 30, DP Apr 90
CODE JOURNAL NTIS	U9020
CODE TARIF NTIS	NTIS Prices PC A03/MF A01
NUMERO PROJET	1L161102AH43
RESUME	Rotationally resolved absorption spectroscopy in the A-X (0,0) vibrational band system of OH around 306.4 nm has been performed to determine the temperature and OH concentration in **solid** **propellant** flames.OH is sufficiently well characterized that the spectra can be least squares fitted under a variety of conditions These conditions include the peculiarities of the experimental setup, instrument response parameters and absorption baseline, as well as the temperature and OH concentration The multi-parameter least squares fit of the spectra gives values and statistical uncertainties for temperature, OH concentration, and other experimental design parameters This technique has been applied to a nitramine **propellant** flame burning in a windowed combustion vessel pressurized with 1.5 MPa nitrogen.A **propellant** feed mechanism coupled to the combustion vessel extended the data taking time such that good quality OH absorption spectra could be obtained for this transient event.Here the light source was an arc lamp and the detector a spectrometer with an intensified photodiode array Keywords: Absorption, **Solid** **propellant**, Combustion, Temperature, Pressure, Flame, OH Concentration, HMX1 (JES).
CODE CLASSIFICATION	79 01, 81 02, 99 06
DESCRIPTEUR(S)	Absorption spectra*;Nitrogen*;Propellants*;Solid propellants*, Absorption,Arc lamps,Arrays;Band spectra;Base lines;Combustion, Experimental design;Feeding;Flames;Instrumentation;Least squares method,Light sources;Mechanical components;Nitramines,Parameters, Photodiodes;Response;Spectrometers,Spectroscopy,Vibrational spectra
IDENTIFICATEUR(S)	Hydroxyl radicals*,NTISDODXA

4/72 - (C) C NTIS

NUMERO SIGNALEMENT	AD-A220 198/6/XAD
TITRE ANGLAIS	Nitramine Composite **Solid** **Propellant** Modelling.
AUTEUR(S)	BLOMSHIELD F. S.
AUTEUR COLLECTIF	Naval Weapons Center, China Lake CA.
ORGAN FINANCEMENT	Shared Bibliographic Input.
CLASSIFICATION INT	020165000; 403019
TYPE DE DOCUMENT	Report
CODE LANGUE	ENG
CODE PAYS D'ORIGINE	US

NUMERO DE RAPPORT NWC-TP-6992
SOURCE Final rept Dec 84-Dec 88; NP. 184, DP. Jul 89
CODE JOURNAL NTIS U9015
CODE TARIF NTIS NTIS Prices: PC A09/MF A01
NUMERO(S) AGENCE SBI-AD-E900-942
RESUME This report summarizes work performed at the Naval Weapons Center to develop a theoretical model for the combustion of nitramine composite **solid** **propellants**.
CODE CLASSIFICATION 79 01; 81 08
DESCRIPTEUR(S) Solid rocket propellants*;Composite propellants*,Combustion*, Nitramines;HMX;Ammonium perchlorate;Mathematical models, Polybutadiene
IDENTIFICATEUR(S) HTPB;NTISDODXA

6/72 - (C) C.NTIS
NUMERO SIGNALEMENT AD-A219 644/2/XAD
TITRE ANGLAIS Implementation of Image Action Plus Software for Image Analysis of **Solid** **Propellant** Combustion Holograms.
AUTEUR(S) HOCKGRAVER V. R
AUTEUR COLLECTIF Naval Postgraduate School, Monterey, CA.
CLASSIFICATION INT 019895000, 251450
TYPE DE DOCUMENT Thesis
CODE LANGUE ENG
CODE PAYS D'ORIGINE US
SOURCE Master's thesis, NP. 91, DP Sep 89
CODE JOURNAL NTIS U9014
CODE TARIF NTIS NTIS Prices: PC A05/MF A01
RESUME This thesis supports computer-aided data analysis of holograms produced from **rocket** **motor** firings.The work reported in this thesis modified existing software code to make it compatible with installed upgrades in the microcomputer imaging system In particular this involved converting the format of C language function calls to ITEX/PC image processing software to that dictated by ITEX/PCplus software Additional modifications were performed to enhance code portability and optimization Results indicate that all efforts to incorporate the new system software have been successful (AW)
CODE CLASSIFICATION 81 07, 81 08, 82 01
DESCRIPTEUR(S) Combustion*,Holograms*,Solid propellant rocket engines*,Solid rocket propellants*;Coding;Computer programs,Captive tests, Functions;Image processing;Images,Microcomputers;Optimization, Programming languages;Theses
IDENTIFICATEUR(S) Computer applications*;NTISDODXA

7/72 - (C) C NTIS
NUMERO SIGNALEMENT AD-A219 566/7/XAD
TITRE ANGLAIS CARS Diagnostics of **Solid** **Propellant** Combustion at Elevated Pressure.
AUTEUR(S) STUFFLEBEAM J. H., ECKBRETH A C.
AUTEUR COLLECTIF United Technologies Research Center, East Hartford, CT.
ORGAN FINANCEMENT Army Research Office, Research Triangle Park, NC.
CLASSIFICATION INT 100940000; 409252
TYPE DE DOCUMENT Report
CODE LANGUE ENG
CODE PAYS D'ORIGINE US
SOURCE Pub. in Combstustion Science and Technology, v66 p163-179 1989; NP 18; DP. 1989.
CODE JOURNAL NTIS U9014
CODE TARIF NTIS NTIS Prices: PC A03/MF A01
NUMERO DE CONTRAT DAAL03-87-C-0005
NUMERO(S) AGENCE ARO-24413.2-CH
RESUME The first Coherent Anti-Stokes Raman Spectroscopy measurements of temperature and species concentrations in the exhaust of **solid** **propellants** burning at elevated pressure (<35 atmospheres) are reported.Multiple species data are acquired at high temporal and spatial resolution from both a homogeneous, double-base and a composite nitramine **propellant** CARS spectra have been obtained from three spectral regions that encompass the signatures of the major combustion products, Carbon dioxide, Carbon monoxide-hydrogen and water The CARS data are analyzed by

comparison with computer synthesized spectra generated at various temperatures and species concentrations Results in the postflame zone from nitramine combustion at 23 atmospheres indicate temperatures as high as 2600 K with species concentrations of Nitrogen approx.23%, Carbon monoxide approx.36%, and hydrogen approx.23%.These results compare favorably with predictions of temperature and concentration from a chemical equilibrium code that simulates the combustion parameters.Utilization of dual broadband approaches will allow the simultaneous acquisition of data from the three spectral regions with each laser pulse.CARS, High pressure combustion diagnostics, **Propellants**, Nitramines, Double-base, Temperature measurement, Concentration measurement, Nonintrusive combustion diagnostics, Reprints, Coherent anti-stokes spectroscopy, **Solid** **propellant**.(jg)

CODE CLASSIFICATION 81 01, 81 08

DESCRIPTEUR(S) Combustion*,Solid propellants*;Acquisition,Broadband;Carbon dioxide;Carbon monoxide,Chemical equilibrium;Coding;Combustion products;Composite propellants;Computers;Concentration Chemistry, High pressure;High resolution;Hydrogen;Measurement;Nitramines, Nitrogen,Parameters;Predictions;Pulsed lasers,Reprints;Spatial distribution,Spectra,Spectroscopy,Synchronism,Synthesis; Temperature,Water

IDENTIFICATEUR(S) Coherent Anti Stokes Spectroscopy CARS,NTISDODXR,NTISDODA

8/72 - (C) C NTIS

NUMERO SIGNALEMENT PB90-201526/XAD

TITRE ANGLAIS Composite **Propellants** with High Burning Rates.

AUTRE TITRE Kompositkrut med Hoeg Foerbraenningshastighet

AUTEUR(S) LILJEGREN T.

AUTEUR COLLECTIF Foersvarets Forskningsanstalt, Stockholm (Sweden) Dept of Weapons Technology.

CLASSIFICATION INT 063330005

TYPE DE DOCUMENT Report

CODE LANGUE SWE

CODE PAYS D'ORIGINE SE

NUMERO DE RAPPORT FOA-C-20781-2 1

SOURCE Text in Swedish, summary in English; NP 29; DP Feb 90.

CODE JOURNAL NTIS U9013

CODE TARIF NTIS NTIS Prices: PC A03/MF A01

RESUME Composite **propellants** with high burning rates, up to 75 mm/s at 10 MPa, have been manufactured by using ultra-fine ammonium perchlorate, UFAP The grinding process and the manufacture of the **propellants** are described and discussed.Results concerning burning rate, mechanical properties and migration of a liquid burning catalyst, catocene, are reported

CODE CLASSIFICATION 79 01; 81 01

DESCRIPTEUR(S) Burning rate*;Solid propellants*;Catalysts;Test facilities; Mechanical properties;Particle size,Combustion;Experimental data, Composite materials

IDENTIFICATEUR(S) Foreign technology*,NTISTFSEAB;NTISFNSW;NTISLNSWE

9/72 - (C) C.NTIS

NUMERO SIGNALEMENT AD-A218 642/7/XAD

TITRE ANGLAIS Temperature Measurements through a **Solid**-**Propellant** Combustion Wave Using Imbedded Fine Wire Thermocouples.

AUTEUR(S) ALSPACH D. A.

AUTEUR COLLECTIF Astronautics Lab.(AFSC), Edwards AFB, CA.

CLASSIFICATION INT 095218000; 420405

TYPE DE DOCUMENT Report

CODE LANGUE ENG

CODE PAYS D'ORIGINE US

NUMERO DE RAPPORT AL-TR-89-085

SOURCE Final rept. Aug-Dec 89; NP. 29; DP. Jan 90.

CODE JOURNAL NTIS U9013

CODE TARIF NTIS NTIS Prices: PC A03/MF A01

NUMERO PROJET 5730

NUMERO ACTIVITE 00

RESUME Temperature profile measurements have been measured through the combustion wave of burning **solid** **propellant** strands using imbedded fine-wire (75-micron diameter) thermocouples.The

	techniques necessary to construct, imbed, and measure temperature with this size and type of thermocouple were demonstrated The experiments were performed at pressures ranging from 100 to 450 psi inside a high-pressure test cell designed for this type of operation Surface temperature measurements have been estimated from the measured profiles for HMX, AN, and Double-Base **propellants** Combustion temperature measurement,Embedding thermocouples,**Solid** rocket **propellants**,Ammonium nitrate.(edc)
CODE CLASSIFICATION	81 01,. 81 08; 94 11
DESCRIPTEUR(S)	Combustion*,Solid rocket propellants*,Ammonium nitrate,Double base propellants,Embedding;High pressure;Hmx,Measurement,Profiles,Solid propellants;Strands;Surface temperature,Temperature,Test equipme t, Thermocouples,Waves,Wire
IDENTIFICATEUR(S)	Temperature measurement*,Combustion waves;NTISDODXA
11/72 - (C) C NTIS	
NUMERO SIGNALEMENT	AD-A217 578/4/XAD
TITRE ANGLAIS	Structure of Model Gas Flames in Nitramines.
AUTEUR(S)	BRANCH M. C.
AUTEUR COLLECTIF	Colorado State Univ , Fort Collins Dept of Mechanical Engineering.
ORGAN FINANCEMENT	Air Force Office of Scientific Research, Bolling AFB, DC.
CLASSIFICATION INT	006665016; 405570
TYPE DE DOCUMENT	Report
CODE LANGUE	ENG
CODE PAYS D'ORIGINE	US
SOURCE	Final technical rept 1 Oct 88-30 Nov 89; NP 14, DP Dec 89
CODE JOURNAL NTIS	U9010
CODE TARIF NTIS	NTIS Prices PC A03/MF A01
NUMERO ALLOCATION	AFOSR-88-0331
NUMERO PROJET	2308
NUMERO ACTIVITE	A1
NUMERO(S) AGENCE	AFOSR-TR-90-0116
RESUME	The purpose of this paper is to summarize the current status of studies we have undertaken of model gas phase flames associated with the combustion of nitramine based **solid** rocket **propellants** These studies consist of measurements of the structure of stable and unstable species concentration profiles and temperature in laminar, premixed, flat flames of fuel Nitrogen Oxide mixtures at low pressure.The experimental measurements are then compared to calculations of the concentration profiles using a one dimensional flame code which models the transport processes and chemistry of the flame The transport processes include species diffusion and thermal conduction through the flame and the chemistry is modeled by a detailed chemical kinetic reaction mechanism The flames which have been studied thus far are supplied with Methane, CH2O or CO as fuel and NO2, N2O or O2 as oxidizer.The overall characteristics of the flames are presented in the paper and the preliminary conclusions of the flame modeling are discussed.Keywords Formaldihyde;Carbon monoxide,Nitrogen dioxide;Nitrous oxide;Oxygen;Diagnosis general.(aw)
CODE CLASSIFICATION	81 08, 81 01
DESCRIPTEUR(S)	Combustion*,Flames*,Nitramines*.Solid rocket propellants*;Carbon monoxide,Chemical reactions,Coding;Diagnosis General,Diffusion, Experimental data,Fuels;Gases,Laminar flow;Low pressure; Measurement,Methane,Mixing,Mixtures,Mathematical models,Nitrogen dioxide,Nitrogen oxides;Nitrous oxide,One dimensional,Oxidizers, Oxygen,Reaction kinetics,Thermal conductivity;Transport properties, Vapor phases
IDENTIFICATEUR(S)	NTISDODXA,NTISDODAF
12/72 - (C) C NTIS	
NUMERO SIGNALEMENT	AD-A216 740/1/XAD
TITRE ANGLAIS	Combustion Instability in **Solid** **Propellant** **Rockets**.
AUTEUR(S)	PRICE E. W., FLANDRO G. A.
AUTEUR COLLECTIF	Georgia Inst.of Tech., Atlanta School of Aerospace Engineering.
ORGAN FINANCEMENT	Air Force Office of Scientific Research, Bolling AFB, DC.
CLASSIFICATION INT	010263051; 403914
TYPE DE DOCUMENT	Report
CODE LANGUE	ENG

CODE PAYS D'ORIGINE US
SOURCE Final rept. Oct 85-Mar 89; NP. 291; DP 21 Mar 89
CODE JOURNAL NTIS U9009
CODE TARIF NTIS NTIS Prices: PC A13/MF A02
NUMERO DE CONTRAT F49620-86-C-0005
NUMERO PROJET 2308
NUMERO ACTIVITE A1
RESUME This report constitutes the principal of a book on combustion stability in **solid** **propellant** **rockets**.The present report contains nine chapters that are each substantially complete except for some editorial, bibliographical and art work in some chapters Chapters 1 thru 9 include: Introduction to Combustion Instability,Combustion Chamber Processes,Guidance in Missile System and **Motor** Design;Fundamentals of **Propellant** Combustion;Analytical Modeling of Combustor Flow;Modeling of Combustion Dynamics,Bulk Mode Oscillations and L* Instability,and Combustor Stability Analysis.(aw)
CODE CLASSIFICATION 81 07, 81 08; 81 01
DESCRIPTEUR(S) Combustion stability*;Solid propellant rocket engines*,Solid propellants*,Books;Combustion;Combustion chambers,Combustors, Dynamics,Flow;Guided missiles,Mathematical models,Models;Motors, Oscillation,Propellants,Rockets,Stability
IDENTIFICATEUR(S) Combustion Instability*,NTISDODXA;NTISDODAF

13/72 - (C) C NTIS
NUMERO SIGNALEMENT AD-A216 605/6/XAD
TITRE ANGLAIS Improved Approach for the Measurement of Acoustic Admittance of **Solid** **Propellants**
AUTEUR(S) SUN W.; HU J ; SUI Y ; FANG J.; ZHANG X
AUTEUR COLLECTIF Foreign Technology Div , Wright-Patterson AFB, OH
CLASSIFICATION INT 000550000, 141600
TYPE DE DOCUMENT Report
CODE LANGUE ENG
CODE PAYS D'ORIGINE US
NUMERO DE RAPPORT FTD-ID(RS)T-0973-89
SOURCE Trans of Ginggong Xuebao (China) n4(38) p14-19 1988; NP. 14, DP. 7 Dec 89.
CODE JOURNAL NTIS U9009
CODE TARIF NTIS NTIS Prices. PC A03/MF A01
RESUME The paper proposes a method of experimental research in which the controlled pressure burner and two samples furnishing different burning surfaces are used.After ignition, the growth constants are measured with the different burning surfaces, while the average pressure is maintained as a constant.Obviously this method is distinct from the conventional growth/decay method, which has two deficiencies: The constant, of growth and decay are measured under variables pressure, and the required damping during burning period is replaced by damping after burning.This method undoubtedly will increase accuracy of measurement for the acoustic admittance of **solid** **propellants**.Russian translations (AW).Improved Approach for the Measurement of Acoustic Admittance of **Solid** **Propellants**-Translation.
CODE CLASSIFICATION 81 08, 46 01
DESCRIPTEUR(S) Admittance*;Combustion*;Solid propellants*,Acoustic absorption*, Accuracy;Acoustic properties,Burners,Constants;Control,Damping; Decay;Deficiencies;Growth General,Ignition;Measurement,Pressure; Russian language;Sampling,Surfaces;Translations;Ussr;Variables
IDENTIFICATEUR(S) Foreign technology*;NTISDODXA

14/72 - (C) C.NTIS
NUMERO SIGNALEMENT AD-A216 445/7/XAD
TITRE ANGLAIS Contractors Meeting on Combustion Rocket Propulsion Diagnostics of Reacting Flow.Held in Monrovia, California on June 13-17, 1988.
AUTEUR(S) TISHKOFF J. M.; BIRKAN M. A.; ROY G. S.; LEKOUDIS S. G.
AUTEUR COLLECTIF California Inst.of Tech., Pasadena.Div.of Engineering and Applied Science.
ORGAN FINANCEMENT Air Force Office of Scientific Research, Bolling AFB, DC
CLASSIFICATION INT 005100008; 071585
TYPE DE DOCUMENT Report
CODE LANGUE ENG

CODE PAYS D'ORIGINE US
SOURCE Technical rept. NP 349, DP 13 Jun 88
CODE JOURNAL NTIS U9009
CODE TARIF NTIS NTIS Prices PC A15/MF A02
NUMERO ALLOCATION AFOSR-86-0337
NUMERO PROJET 2308
NUMERO(S) AGENCE AFOSR TR-89-1710
RESUME Abstracts are given for research efforts on airbreathing combustion, rocket propulsion, and diagnostics of reacting flows Keywords: Shear layers, Turbulence, Instability, Electromagnetic propulsion, Plasma propulsion, Erosion, Magnetoplasmadynamic thrusters, Fluid dynamics, Arcjet thrust chambers, Electrothermal propulsion, Laser thermal propulsion, Electric discharges, Chemical kinetics, Nitramines, Nitroform compounds, **Solid** **propellants**, Acoustic flow fields, **Solid** rocket combustion chambers, Acoustic waves (aw).
CODE CLASSIFICATION 81 07, 81 01
DESCRIPTEUR(S) Air breathing engines*;Combustion*,Rocket propulsion*,Thermal propulsion systems*,Acoustic fields,Acoustic waves,Combustion chambers,Diagnosis General;Electric discharges,Electromagnetic drives;Erosion,Flow,Fluid dynamics,Lasers,Layers,Nitramines, Nitromethane,Plasmas Physics;Propulsion systems;Reaction kinetics, Rockets,Shear properties;Solid propellants;Solids, Thermoelectricity;Turbulence,Electric propulsion,Rocket engines
IDENTIFICATEUR(S) Magnetoplasmadynamic Thrusters,Electrothermal Propulsion,Laser Thermal Propulsion;Nitroform Compounds,NTISDODXA,NTISDODAF

15/72 - (C) C.NTIS
NUMERO SIGNALEMENT PB90-133521/XAD
TITRE FRANCAIS Modelisation de la Combustion des Propergols Solides Rapport Final de Stage aux Etats-Unis au Brigham Young University (Provo, Utah)
TITRE ANGLAIS Modeling the Combustion of **Solid** **Propellants** Final Report on a Course Taken at the Brigham Young University (Provo, Utah)
AUTEUR(S) BIZOT A
AUTEUR COLLECTIF Office National d'Etudes et de Recherches Aerospatiales, Chatillon (France).
CLASSIFICATION INT 021377000
TYPE DE DOCUMENT Report
CODE LANGUE FRE
CODE PAYS D'ORIGINE FR
NUMERO DE RAPPORT ONERA-RTF-23/7128-EY
SOURCE Technical rept (Final), Text in French, summary in English; NP 42; DP 25 Apr 89
CODE JOURNAL NTIS U9006
CODE TARIF NTIS NTIS Prices, PC E04/MF E04
RESUME A numeric single-dimensional model was developed to achieve a better understanding of the combustion mechanisms of homogeneous **solid** **propellants**.Applied to the study of double-base and HMX **propellants**, the model appears to represent a good tradeoff between overly simplified models yielding many results but sometimes of little use in understanding the mechanisms involved, and elaborate numeric models which yield few results because of the length and cost of computations The model proposed has been simplified as required to reduce computing time,it also involves a few parameter adjustments.It will compute temperature and species profiles for the condensed and gaseous phases of a **propellant** during combustion.
CODE CLASSIFICATION 79 01, 81 01
DESCRIPTEUR(S) Solid propellants*;Combustion*;Mathematical models;Pressure, Numerical analysis,Temperature;Reaction kinetics,Combustion products;Burning rate
IDENTIFICATEUR(S) Foreign technology*;NTISTFCDA;NTISFNFR;NTISLNFRE

16/72 - (C) C.NTIS
NUMERO SIGNALEMENT AD-A213 857/6/XAD
TITRE ANGLAIS Spectral Studies of **Solid** **Propellant** Combustion 2 Emission and Absorption Results for M-30 and HMX1 **Propellants**.
AUTEUR(S) VANDERHOFF J. A.
AUTEUR COLLECTIF Army Ballistic Research Lab., Aberdeen Proving Ground, MD.
CLASSIFICATION INT 082505000; 050750

TYPE DE DOCUMENT Report
CODE LANGUE ENG
CODE PAYS D'ORIGINE US
NUMERO DE RAPPORT BRL-TR-3035
SOURCE Final rept. Jun 88-Jun 89; NP. 58; DP 1989.
CODE JOURNAL NTIS U9004
CODE TARIF NTIS NTIS Prices: PC A04/MF A01
RESUME A windowed strand burner with a **propellant** feed mechanism has been used to characterize the steady-state burning of two composites **propellants**, M-30 and HMX1, at moderate pressure Both emission and absorption spectroscopy have yielded profile data on three important combustion species: OH, NH, and CN Relative appearance of these three species are inferred from emission intensity profiles, and absolute concentration profiles are calculated from the absorption data This is the first absolute determination of these combustion intermediates in a **propellant** flame.These concentration measurements for OH indicate that the **propellant** flame temperatures are about 200 K below adiabatic A maximum value of 40 ppm NH is found for the M-30 **propellant** flame.Fluctuations in the flame front of HMX1 compromised the determination of maximum concentrations for NH and CN.Keywords: Combustion;**Solid** **propellant**;Spectroscopy,Absorption,Emission,Concentration,Profiles;**Solid** **propellants** (JES).
CODE CLASSIFICATION 79 01; 81 01; 99 01
DESCRIPTEUR(S) Absorption spectra*;Combustion*,Combustion products*,Flames*;Solid propellants*,Spectroscopy*,Absorption;Burners;Composite materials, Determination,Emission;Feeding;Intensity;Mechanical components; Profiles;Propellants;Spectra,Strands,Temperature
IDENTIFICATEUR(S) M 30 Propellant;HMX 1 Propellant;NTISDODXA

17/72 - (C) C NTIS
NUMERO SIGNALEMENT AD-A213 330/4/XAD
TITRE ANGLAIS Workshop Summary of 'Model Predictions of the Piston-Driven-Compaction Experiment'.
AUTEUR(S) KOOKER D E
AUTEUR COLLECTIF Army Ballistic Research Lab , Aberdeen Proving Ground, MD.
CLASSIFICATION INT 082505000, 050750
TYPE DE DOCUMENT Report
CODE LANGUE ENG
CODE PAYS D'ORIGINE US
NUMERO DE RAPPORT BRL-TR-3029
SOURCE Technical rept. Jun 88-Mar 89; NP 50; DP. Aug 89.
CODE JOURNAL NTIS U9003
CODE TARIF NTIS NTIS Prices: PC A03/MF A01
RESUME A JANNAF Propulsion Systems Hazards Subcommittee Workshop was held on 25-26 october 1988 in conjunction with the 25th JANNAF Combustion Meeting in Huntsville, AL.The area of interest is the transition to detonation in confined granular energetic material.This workshop focused on the acceleration of a strong compaction wave, before the onset of detonation.The objective was to compare model predictions to four Piston-Driven-Compaction experiments involving two different ball **propellants** These were true predictions, since the experimental data were not released until the second day of the workshop Several of the models came close to the compaction wave locus.However, it was more difficult to predict wall stress time-history seen by two transducers at fixed locations along the tube.The timing of a runaway is extremely sensitive to the intense competition among sources of reaction and heat loss.Keywords: Stress waves;Elastic waves;Granular explosives;**Solid** **propellants**,Impact;Compaction Waves,Modeling;Combustion;Deflagration,Transition to detonation.(KT).
CODE CLASSIFICATION 81 01; 79 01; 46 05
DESCRIPTEUR(S) Combustion*;Compacting*;Ball powder propellants*;Blast waves*; Detonations*;Models*;Predictions*;Acceleration;Confinement General; Day;Deflagration;Elastic waves;Energetic properties;Experimental data;Granules;Hazards;Heat loss;History;Locus;Position Location; Propulsion systems;Response;Solid propellants;Sources;Stress waves;

	Stresses,Time,Transducers;Transitions,Walls;Waves
IDENTIFICATEUR(S)	NTISDODXA
20/72 - (C) C NTIS	
NUMERO SIGNALEMENT	N89-26109/3/XAD
TITRE ANGLAIS	Metal Combustion in **Solid**-**Propellants**
AUTEUR(S)	IZUMIKAWA M , TAKAHASHI M , MITANI T , NIIOKA T., CHIBA M
AUTEUR COLLECTIF	National Aerospace Lab , Tokyo (Japan)
ORGAN FINANCEMENT	National Aeronautics and Space Administration, Washington, DC.
CLASSIFICATION INT	022054000; NE789421
TYPE DE DOCUMENT	Report
CODE LANGUE	JAP
CODE PAYS D'ORIGINE	JP
NUMERO DE RAPPORT	NAL-TR-998
SOURCE	In Japanese, English Summary, NP 35, DP Sep 88
CODE JOURNAL NTIS	S2720
CODE TARIF NTIS	NTIS Prices PC A03/MF A01
RESUME	A technique using a strand burner was developed to investigate the combustion efficiency of metals in **solid** **propellants** A strand of **propellants** was burned under a given pressure and all reactants and products were trapped in the closed vessel.Condensed and gaseous species were analyzed quantitatively using various titration methods and gas-chromatography.The results derived from the strand burner were compared with the eta(c)* evaluated from firing tests of subscale motors The combustion efficiency of Al and B in various **propellants** was measured A combustion model for metal powders including agglomeration, ignition and steady burning of particles was investigated.Effects of B/Al ratios and particle size of B on the combustion efficiency of **propellants** containing Al and B were discussed based on the combustion model
CODE CLASSIFICATION	81 08
DESCRIPTEUR(S)	Combustion efficiency*;Metal propellants*,Powder metallurgy*; Propellant combustion*;Gas chromatography;Particle size distribution,Titration
IDENTIFICATEUR(S)	Foreign technology*,NTISNASAE,NTISLNJAP,NTISFNJA
21/72 - (C) C NTIS	
NUMERO SIGNALEMENT	AD-A210 221/8/XAD
TITRE ANGLAIS	Kinetic and Related Aspects of **Propellant** Combustion Chemistry JANNAF (Joint Army-Navy-NASA-Air Force) Combustion Subcommittee Workshop Held in Laurel, Maryland on May 2-4, 1988.
AUTEUR(S)	BECKER D L
AUTEUR COLLECTIF	Johns Hopkins Univ., Laurel, MD.Chemical Propulsion Information Agency.
CLASSIFICATION INT	054839001; 081100
TYPE DE DOCUMENT	Report
CODE LANGUE	ENG
CODE PAYS D'ORIGINE	US
NUMERO DE RAPPORT	CPIA-PUB-503
SOURCE	Availability: National Technical Information Service, Springfield, Va 22161 PC $42 00 MF $42 00 No copies furnished by DTIC, NP. 386; DP. May 88
CODE JOURNAL NTIS	U8922
CODE TARIF NTIS	NTIS Prices. PC $42 00/MF $42 00
NUMERO DE CONTRAT	N00039-87-C-5301
RESUME	This workshop was sponsored by the Joint Army-Navy-NASA-Air Force (JANNAF) Combustion Subcommittee The workshop was held 2-4 May 1988 at The Johns Hopkins University/Applied Physics Laboratory, Laurel, Maryland.This workshop was the first meeting of the' Kinetic and Related Aspects of **Propellant** Combustion Chemistry' panel.This report reflects the efforts made in recent years by both individuals and agencies in this research area.Keywords: Deflagration, Liquid **propellants**, Combustion products, Gun **propellants**, Ignition, Kinetics, **Solid** **propellants**, Nitramines.(AW).
CODE CLASSIFICATION	81 01, 79 01
DESCRIPTEUR(S)	Combustion*;Propellants*;Chemistry;Combustion products; Deflagration,Gun propellants;Ignition;Joint military activities; Liquid propellants;Panel Committee;Workshops;Solid propellants;

	Nitramines;Reaction kinetics
IDENTIFICATEUR(S)	Meetings*;NTISDODXA
22/72 - (C) C.NTIS	
NUMERO SIGNALEMENT	PB89-210157/XAD
TITRE ANGLAIS	N-Hexyl Carborane as Combustion Catalyst in Composite **Propellants**.
AUTRE TITRE	N-Hexylkarboran som Foerbraenningskatalysator i Kompositkrut
AUTEUR(S)	ROSENQUIST T., SANDEN R
AUTEUR COLLECTIF	Foersvarets Forskningsanstalt, Stockholm (Sweden) Huvudavdelning 2.
CLASSIFICATION INT	063330004
TYPE DE DOCUMENT	Report
CODE LANGUE	SWE
CODE PAYS D'ORIGINE	SE
NUMERO DE RAPPORT	FOA-C-20755-2.1
SOURCE	Text in Swedish, summary in English; NP 27, DP. 1989
CODE JOURNAL NTIS	U8921
CODE TARIF NTIS	NTIS Prices: PC E03/MF A01
RESUME	The feasibility of using n-hexyl carborane (NHC) as a combustion catalyst in composite **propellants** has been investigated.The results indicate that NHC is an efficient combustion catalyst at high concentrations In other respects it seems to act mainly as a plasticizer Good bonding for NHC-containing hydroxyl-terminated polybutadiene (HTPB) **propellants** to liners and inhibitors has been obtained.NHC migrates as easy as dioctyl seabacate or n-butyl ferrocene in the polymer.Despite a high boiling point NHC evaporates noticeably at ambient temperatures.Differently from n-butyl ferrocene, NHC does not seem to catalyze the thermal aging or the curing of HTPB Thermal analyses show no indication that NHC should considerably enhance the sensitivity of ignition of the **propellant**.A great disadvantage with NHC is the very high price.Before larger batches of **propellants** containing NHC are manufactured, more sensitivity tests should be carried out
CODE CLASSIFICATION	81 08; 99 06, 99 03, 71 08
DESCRIPTEUR(S)	Composite rocket propellants*,Catalysts*;Carboranes*,Combustion, Solid rocket plasticizers;Heat measurement,Polybutadiene;Tables Data;Graphs Charts,Polymers
IDENTIFICATEUR(S)	Foreign technology*;NTISTFSEAB;NTISFNSW,NTISLNSWE
23/72 - (C) C NTIS	
NUMERO SIGNALEMENT	AD-A210 026/1/XAD
TITRE ANGLAIS	JANNAF (Joint Army-Navy-NASA-Air Force) Combustion Meeting (25th) Held in Huntsville, Alabama, 24-28 October 1988.Volume 1
AUTEUR(S)	BECKER D. L.
AUTEUR COLLECTIF	Johns Hopkins Univ., Laurel, MD.Chemical Propulsion Information Agency.
CLASSIFICATION INT	054839001, 081100
TYPE DE DOCUMENT	Report
CODE LANGUE	ENG
CODE PAYS D'ORIGINE	US
NUMERO DE RAPPORT	CPIA-PUB-498-VOL-1
SOURCE	See also Volume 2, AD-A210 027; Availability: National Technical Information Service, Springfield, Va 22161. PC $70 00 MF $70 00 No copies furnished by DTIC; NP. 468; DP. Oct 88
CODE JOURNAL NTIS	U8921
CODE TARIF NTIS	NTIS Prices: PC $70 00/MF $70 00
NUMERO DE CONTRAT	N00039-87-C-5301
RESUME	This volume, the first of five volumes, is a collection of 36 unclassified/unlimited papers which were presented at the 25th Joint Army-Navy-NASA-Air Force (JANNAF) Combustion Meeting, October 24-28, 1988, at the NASA Marshall Space Flight Center, Huntsville, Alabama.Specific subjects discussed include combustion instability, ignition, burn rate, flame structure, and particle size measurement of **solid** rocket **propellants** and supersonic mixing and combustion, combustion instability and boron-based fuels for airbreathing systems.Keywords: **Solid** **propellant**;Rocket Engines;**Solid** rocket **propellants**;Combustion stability;Flames;Ignition;Ramjet engines;Rocket fuels.(AW).
CODE CLASSIFICATION	81 04; 81 08

DESCRIPTEUR(S) Air breathing engines*;Combustion*;Ramjet engines*;Solid rocket propellants*;Symposia*;Alabama;Burning rate,Combustion stability, Flames;Ignition;Jet mixing flow;Joint military activities, Measurement;Particle size;Rocket engines;Solid propellants, Supersonic flow
IDENTIFICATEUR(S) NTISDODXA

24/72 - (C) C NTIS
NUMERO SIGNALEMENT AD-A206 510/0/XAD
TITRE ANGLAIS Experimental Investigation in the Behavior of Metallized **Solid** **Propellants**
AUTEUR(S) SMITH M J
AUTEUR COLLECTIF Naval Postgraduate School, Monterey, CA
CLASSIFICATION INT 019895000; 251450
TYPE DE DOCUMENT Thesis
CODE LANGUE ENG
CODE PAYS D'ORIGINE US
SOURCE Master's thesis; NP 76; DP Dec 88
CODE JOURNAL NTIS U8915
CODE TARIF NTIS NTIS Prices. PC A05/MF A01
RESUME The combustion behavior of metallized **solid** **propellants** at pressures between 100 and 750 psi was investigated using high speed motion pictures together with scanning electron microscope and light diffraction examinations of collected residue A reduced smoke ZrC **propellant** and two **propellants** with low aluminum loadings were utilized.ZrC was observed to agglomerate and ignite on the **propellant** surface before being ejected The aluminum did not agglomerate but did ignite on the **propellant** surface ZrC was found to burn in part with a detached flame and the flame moved closer to the particle surface as pressure increased Aluminum particles were observed to burn with similar behavior, but with flames more detached from the particle surface Increased aluminum loading resulted in smaller particles above the **propellant** surface, but the flames were further from particle surfaces.Keywords **Solid** **rocket** **propellants**,**Solid** **propellants**;High speed motion pictures,Combustion bomb,Malvern,SEM,Flame envelope sizes;Particle sizes;Two-dimensional **rocket** **motor**.(kt).
CODE CLASSIFICATION 81 08
DESCRIPTEUR(S) Solid propellants*;Solid rocket propellants*;Aluminum,Bombs, Combustion,Electron microscopes;Electronic scanners;Envelope Space; Flames;High speed photography,Metallizing,Motion pictures;Particle size;Particles,Propellants,Reduction,Rocket engines;Sizes Dimensions;Smoke;Surfaces,Two dimensional
IDENTIFICATEUR(S) Theses;NTISDODXA

25/72 - (C) C.NTIS
NUMERO SIGNALEMENT N89-18526/8/XAD
TITRE ANGLAIS SRB (**Solid** Rocket Booster) Combustion Dynamics Analysis Computer Program (CDA-2).
AUTEUR(S) CHUNG T. J., PARK O Y
AUTEUR COLLECTIF Alabama Univ.in Huntsville.
ORGAN FINANCEMENT National Aeronautics and Space Administration, Washington, DC
CLASSIFICATION INT 053562000, AM584056
TYPE DE DOCUMENT Report
CODE LANGUE ENG
CODE PAYS D'ORIGINE US
NUMERO DE RAPPORT NAS 1.26:184663
SOURCE Final Report; NP. 156; DP. Jan 89.
CODE JOURNAL NTIS S2711
CODE TARIF NTIS NTIS Prices: PC A08/MF A01
NUMERO DE CONTRAT NAG8-627
NUMERO(S) AGENCE NASA-CR-184663
RESUME Two-dimensional combustion dynamics of **solid** **propellants** numerically modeled by finite element calculations and applied to a one-dimensional cast for comparison is examined.A multi-dimensional numerical model was developed for the unsteady state oscillatory combustion of **solid** **propellants** subject to acoustic pressure disturbances.Including the gas-phase effects, the assumption of uniform pressure across the flame zone, which

was conventionally used, is relaxed such that a higher frequency response in the long flame of a double-base **propellant** can be calculated.The formulation is based on a premixed, laminar flame with a one-step overall chemical reaction and the Arrhenius law of decomposition with no condensed phase reaction.In a given geometry, the Galerkin finite element solution shows the strong resonance and damping effect at the lower frequencies Extended studies deal with the higher frequency region where the pressure varies in the flame thickness The nonlinear system behavior is investigated by carrying out the second order expansion in wave amplitude when the acoustic pressure oscillations are finite in amplitude Offset in the burning rate shows a negative sign in the whole frequency region considered, as confirmed by existing experimental results.Finally, the velocity coupling in the two-dimensional model is discussed in terms of higher order perturbations

CODE CLASSIFICATION 81 08
DESCRIPTEUR(S) Computer programs*,Propellant combustion*,Solid rocket propellants*,Finite element method,Mathematical models,Burning rate;Galerkin method;Heat transfer,Laminar flow;Premixed flames; Pressure oscillations
IDENTIFICATEUR(S) NTISNASA

26/72 - (C) C.NTIS
NUMERO SIGNALEMENT AD-A204 576/3/XAD
TITRE ANGLAIS Chemical Kinetics of Nitramine **Propellant** Combustion
AUTEUR(S) BRANCH M. C
AUTEUR COLLECTIF Colorado Univ at Boulder.Dept.of Mechanical Engineering.
ORGAN FINANCEMENT Air Force Office of Scientific Research, Bolling AFB, DC
CLASSIFICATION INT 068646004, 407675
TYPE DE DOCUMENT Report
CODE LANGUE ENG
CODE PAYS D'ORIGINE US
SOURCE Final technical rept 1 Oct 87-30 Sep 88; NP. 24; DP. Oct 88
CODE JOURNAL NTIS U8912
CODE TARIF NTIS NTIS Prices. PC A03/MF A01
NUMERO ALLOCATION AFOSR-84-0006
NUMERO PROJET 2308
NUMERO ACTIVITE A1
NUMERO(S) AGENCE AFOSR-TR-89-0073
RESUME Many **solid** rocket **propellants** and other energetic materials consist of complex chemical compounds of carbon, hydrogen, oxygen and nitrogen The decomposition of these **solid** reactants leads to the formation of gaseous hydrocarbons and oxides of nitrogen which can react to support a flame above the surface of the **solid**.These flames can provide heat which is fed back to the **propellant** surface and thereby influence the burning rate of the **solid** In the case of nitramine based **solid** rocket **propellants**, the gas phase decomposition products include significant amounts of Ethyloxide, Hydrogen cyanide, Nitrogen dioxide, Nitric oxide, Nitrous oxide and Oxygen This study is intended to provide experimental data on the structure of hydrocarbon flames supported by oxides of nitrogen in order to establish the reaction mechanism for such flames.Laminar, premixed, flat flames of Methane/N02/02 and CH20/N02/02 have been investigated and a reaction mechanism is suggested which accounts for all of the major observations in the data.(aw).
CODE CLASSIFICATION 81 01; 81 08
DESCRIPTEUR(S) Combustion*;Flames*,Nitramines*;Reaction kinetics*;Solid rocket propellants*;Burning rate;Carbon;Chemical compounds,Complex compounds;Decomposition;Dioxides;Energetic properties;Experimental data Gases;Hydrocarbons;Hydrogen;Hydrogen cyanide;Laminar flow; Materials,Mixing;Nitrogen;Nitrogen oxides;Nitrous oxide;Oxides; Oxygen;Response;Solids;Surfaces,Vapor phases
IDENTIFICATEUR(S) NTISDODXA;NTISDODAF

27/72 - (C) C.NTIS
NUMERO SIGNALEMENT AD-A204 136/6/XAD
TITRE ANGLAIS Nitramine **Propellant** Ignition and Combustion Research: New Tools and New Directions.

AUTEUR(S) ALEXANDER M H , DAGDIGIAN P J , JACOX M E ; KOLB G. E ; MELIUS G F
AUTEUR COLLECTIF Army Research Office, Research Triangle Park, NC
CLASSIFICATION INT 054824000; 040900
TYPE DE DOCUMENT Report
CODE LANGUE ENG
CODE PAYS D'ORIGINE US
SOURCE Technical rept ; NP 79, DP Feb 89
CODE JOURNAL NTIS U8912
CODE TARIF NTIS NTIS Prices. PC A05/MF A01
RESUME The efficient and successful design of new generations of highly energetic **propellants** based on evolving nitramine chemistry will require a thorough knowledge of the chemical and physical parameters controlling their ignition and combustion The necessary level of insight can be attained and successfully embodied in the predictive computer models necessary for effective **propellant** design, development and testing activities if a coordinated, hierarchical program of theoretical modeling and confirming and supporting experiments is designed and properly executed This paper reviews the current state of our understanding of the chemistry and physics of nitramine **propellant** ignition and combustion and develops and motivates the basic research program necessary to put advanced nitramine **propellant** development on a firm and effective scientific basis Confronting and solving problems involving complex physicochemical phenomena which intertwine complex heat, mass and radiative transfer processes with chemical kinetics is a challenge which physical and engineering scientists are becoming much more adept at meeting Modern theoretical and experimental tools are now available which allow the design and utilization of much more comprehensive analytical models as well as their concomitant supporting and confirming experimental measurements Gun **propellants**, Rocket **propellants**, LOVA **propellants**, **Solid** **propellants**, RDX, HMX.(aw).
CODE CLASSIFICATION 79 01, 81 08, 81 01
DESCRIPTEUR(S) Combustion*,Gun propellants*,Ignition*;Solid rocket propellants*; Chemicals,Chemistry;Computerized simulation,Energetic properties; Experimental data,Heat,Hierarchies,HMX,Mathematical models; Measurement,Nitramines;Orientation Direction;Physical properties, Physicochemical properties;Physics,Predictions,Problem solving, Propellants,Radiative transfer;Rdx,Reaction kinetics,Solid propellants;Theory
IDENTIFICATEUR(S) NTISDODXA

28/72 - (C) C.NTIS
NUMERO SIGNALEMENT AD-A203 988/1/XAD
TITRE ANGLAIS Magnetic Flowmeter Measurement of **Solid** **Propellant** Pressure-Coupled and Velocity-Coupled Responses
AUTEUR(S) MICCI M M , TAYLOR R. D., CHUNG I.; COLOZZA A.
AUTEUR COLLECTIF Pennsylvania State Univ , University Park Dept of Aerospace Engineering
ORGAN FINANCEMENT Air Force Avionics Lab., Wright-Patterson AFB, OH
CLASSIFICATION INT 009222027; 401750
TYPE DE DOCUMENT Report
CODE LANGUE ENG
CODE PAYS D'ORIGINE US
SOURCE Final rept. 20 Sep 82-31 May 88; NP 87; DP. Nov 88.
CODE JOURNAL NTIS U8911
CODE TARIF NTIS NTIS Prices: PC A05/MF A01
NUMERO DE CONTRAT F04611-82-X-006
NUMERO PROJET 5730
NUMERO ACTIVITE 00
NUMERO(S) AGENCE AFAL-TR-88-075
RESUME This report documents a continuation of previous work with the pressure-coupled magnetic flowmeter burner to extend its measurements capacity to include a wider frequency spectrum and variety of **propellants**.The results obtained in this experimental program extend the operable frequency range of a magnetic flowmeter burner to a lower limit of 200 Hz, well into the range where intermediate frequency instabilities occur.Six

formulations of AP-HTPB composite **propellant** (including one moderately aluminized composition) were successfully tested, and their pressure-coupled response functions measured over the burner's operating frequency range.This research also attempted to directly measure a high-frequency **solid** **propellant** velocity-coupled admittance The velocity-coupled admittance was defined in this research as the complex ratio of the oscillatory mass-flow velocity generated from the surface of a burning **propellant** to the oscillatory cross-flow velocity above the surface.These oscillatory velocities were measured simultaneously inside a rectangular slab-burning combustion chamber with a magnetic flowmeter.The high-frequency cross flows were created by spinning a spur gear over the sonic nozzle exhaust of the combustion chamber, thus exciting acoustic modes inside the chamber.The admittance results show similar trends under the same burning conditions, and approximate values could be estimated.Keywords **Solid** rocket **propellants**, Combustion stability, Acoustic admittance

CODE CLASSIFICATION 81 08; 94 11

DESCRIPTEUR(S) Combustion*,Solid rocket propellants*;Acoustic properties, Acoustics;Admittance,Burners;Combustion chambers,Combustion stability;Cross flow,Flowmeters,Frequency;Gears,Limitations, Magnetic devices,Magnetometry,Mass flow,Oscillation,Propellants, Ratios;Spectra,Spinning Motion,Value,Velocity;Ammonium perchlorate; Polybutadiene,Hydroxyl radicals

IDENTIFICATEUR(S) Magnetic flowmeters*,HTPB Hydroxyl Terminated Polybutadiene, Polybutadiene hydroxyl terminated;NTISDODXA;NTISDODAF

29/72 - (C) C NTIS

NUMERO SIGNALEMENT AD-A203 928/7/XAD

TITRE ANGLAIS Holographic Investigation of **Solid** **Propellant** Combustion

AUTEUR(S) BUTLER A G

AUTEUR COLLECTIF Naval Postgraduate School, Monterey, CA.

CLASSIFICATION INT 019895000; 251450

TYPE DE DOCUMENT Thesis

CODE LANGUE ENG

CODE PAYS D'ORIGINE US

SOURCE Master's thesis, NP. 56, DP. Dec 88

CODE JOURNAL NTIS U8911

CODE TARIF NTIS NTIS Prices PC A04/MF A01

RESUME An investigation into the behavior of aluminized **solid** **propellant** combustion in a two-dimensional windowed **rocket** **motor** was conducted using holographic techniques.Holograms were recorded in the **motor** port, aft of the **propellant** grain and at the entrance to the exhaust nozzle for two different **propellant** compositions at varying operating pressures Quantitative particle size data for particles larger than 20 microns were obtained from the holograms.From these data, the mean diameters (D32) of the larger particles were calculated and utilized to compare what effects pressure, location in the **motor** and aluminum content had on the behavior of the aluminum/aluminum oxide particles.D32 was found to decrease with increasing pressure, but was unaffected by variations in low values of **propellant** aluminum loading.D32 at the grain exit was found to be significantly less than within the grain port Keywords: **Solid** **propellant** **rocket** engines, **Solid** **rocket** **propellants**, Theses.(aw)

CODE CLASSIFICATION 81 08; 82 01

DESCRIPTEUR(S) Aluminized propellants*;Combustion*;Holography*;Solid rocket propellants*,Aluminum;Aluminum oxides;Chemical composition; Diameters,Exhaust nozzles,Holograms;Mean;Particle size;Particles, Propellant grains;Solid propellant rocket engines;Solid propellants;Theses

IDENTIFICATEUR(S) NTISDODXA

30/72 - (C) C.NTIS

NUMERO SIGNALEMENT AD-A203 732/3/XAD

TITRE ANGLAIS Characterization of Particle Combustion in a Rijke Burner.

AUTEUR(S) BECKSTEAD M. W.

AUTEUR COLLECTIF Brigham Young Univ., Provo, UT.Dept.of Chemical Engineering.

ORGAN FINANCEMENT Air Force Office of Scientific Research, Boiling AFB, DC
CLASSIFICATION INT 004414004, 403273
TYPE DE DOCUMENT Report
CODE LANGUE ENG
CODE PAYS D'ORIGINE US
SOURCE Final rept. Mar 83-Sep 88,; NP 69; DP Nov 88.
CODE JOURNAL NTIS U8911
CODE TARIF NTIS NTIS Prices PC A04/MF A01
NUMERO ALLOCATION AFOSR-83-0157
NUMERO PROJET 2308
NUMERO ACTIVITE A1
NUMERO(S) AGENCE AFOSR-TR-89-0054
RESUME This report summarizes a research program to study the acoustic interaction of particle additives used in **solid** **propellants** Various examples of combustion instability found in the literature are discussed that give evidence to the existence and nature of distributed combustion A modified Rijke burner was constructed as the basic experimental tool and was characterized extensively.Stability boundaries were determined, and growth rates were observed to increase with increasing oxygen content and overall mass flow rate The data indicate that the overall acoustic driving forces in a Rijke burner are dependent upon the acoustic mode shape relative to the flame location and the distribution of energy through the burner, (i e the gas flow rates and heat losses).A mathematical model for the Rijke burner has been developed which accounts for the effects of heat loss, variable gas temperature and particle interactions on acoustic oscillations The model has been verified by comparing predicted frequency and growth rates for several simple test cases with the corresponding analytical solutions.The model was also compared directly with the experimental data.Unstable combustion, Distributed combustion, Acoustic instability (MJM)
CODE CLASSIFICATION 81 08,; 81 01
DESCRIPTEUR(S) Combustion*,Combustion stability*;Particles*;Solid propellants*, Acoustic waves,Acoustics,Additives,Boundaries;Burners;Distribution; Energy,Experimental data,Flames;Flow rate,Gas flow;Gases;Growth General,Heat loss,Interactions,Mass flow,Mathematical models; Oscillation,Particle collisions,Rates;Shape,Solutions General, Stability,Temperature,Tools;Variables
IDENTIFICATEUR(S) NTISDODXA,NTISDODAF

32/72 - (C) C NTIS
NUMERO SIGNALEMENT AD-A202 293/7/XAD
TITRE ANGLAIS High-Speed Laser Photography.
AUTEUR(S) BECKER R J.
AUTEUR COLLECTIF Dayton Univ , OH Research Inst.
ORGAN FINANCEMENT Air Force Avionics Lab , Wright-Patterson AFB, OH
CLASSIFICATION INT 007431003; 105400
TYPE DE DOCUMENT Report
CODE LANGUE ENG
CODE PAYS D'ORIGINE US
NUMERO DE RAPPORT UDRI-TR-88-45
SOURCE Final rept 1 May 83-30 Sep 87,; NP. 84; DP Aug 88.
CODE JOURNAL NTIS U8909
CODE TARIF NTIS NTIS Prices · PC A05/MF A01
NUMERO DE CONTRAT F04611-83-K-0023,; F04611-83-K-0018
NUMERO PROJET 5730
NUMERO ACTIVITE 00
NUMERO(S) AGENCE AFAL-TR-88-050
RESUME High-speed movies of **solid** **propellant** deflagration have long provided useful qualitative information on **propellant** behavior.Consequently, an extension of performance to include quantitative behavior of the surface, particularly the spacial relationship of particles across the surface, the temporal behavior of particle through extended periods of time, and accurate measurements of particle sizes, is highly desirable.Such measurements require the ability to take detailed movies across an extensive surface through the **propellant** flame for longer periods than the residence time of a given particle.The modulation

transfer function (MTF) of the camera optics and film will greatly affect performance.The MTF of the optics can be improved by a factor of two or more at practical spatial frequencies by the use of monochromatic light, such as the reflected light from a laser The use of an intense, short-pulsed laser has the additional advantage of suppressing flame brightness and motion blur.High resolution at unity magnification is achieved by the use of 2 mJ of illumination energy per pulse in conjunction with a fine-grain film.The surfaces of the wide-distribution **propellants** were found to be molten.Keywords: **Solid** **propellant** rocket engines, **Solid** rocket **propellants**, Combustion chambers, **Propellant** grains, Combustion, Cinephotography (aw).

CODE CLASSIFICATION 81 08, 81 01; 82 02
DESCRIPTEUR(S) Combustion*;Deflagration*,High speed photography*;Solid rocket propellants*,Accuracy;Brightness;Cameras;Combustion chambers, Energy;Films;Fine grained materials;Flames,Frequency,High resolution,Illumination,Lasers,Light,Magnification,Measurement; Modulation;Monochromatic light,Motion pictures,Optics;Particle size;Particles,Propellant grains;Reflection;Short pulses,Solid propellant rocket engines,Spatial distribution,Time intervals, Transfer functions;Laser applications;Surfaces
IDENTIFICATEUR(S) NTISDODXA,NTISDODAF

33/72 - (C) C.NTIS
NUMERO SIGNALEMENT AD-A201 634/3/XAD
TITRE ANGLAIS Spectral Studies of **Propellant** Combustion. Experimental Details and Emission Results for M-30 **Propellant**
AUTEUR(S) VANDERHOFF J. A
AUTEUR COLLECTIF Army Ballistic Research Lab , Aberdeen Proving Ground, MD
CLASSIFICATION INT 082505000, 050750
TYPE DE DOCUMENT Report
CODE LANGUE ENG
CODE PAYS D'ORIGINE US
NUMERO DE RAPPORT BRL-TR-3714
SOURCE Final rept. Jun 87-Jun 88; NP 29, DP Dec 88
CODE JOURNAL NTIS U8908
CODE TARIF NTIS NTIS Prices: PC A03/MF A01
RESUME A windowed strand burner has been constructed and used to characterize the steady state burning of **propellants** at moderate pressure using uv - visible spectroscopic techniques.Emission spectroscopy has been performed on a triple base **propellant** (M-30) and three reactive transient combustion species (CN, NH and OH) have been profiled over a pressure range from 0.66 to 1.5 MPa.Reaction zone lengths on the order of 1 mm were determined from the CN and NH profiles.The strand burner is expected to be useful for future planned absorption and laser induced fluorescence studies on a variety of **propellants** Keywords: Emission,Spectroscopy;**Solid** **propellant**;Combustion;Steady state burning,Hydroxides;Nitrogen compounds;Cyanides (mgm)
CODE CLASSIFICATION 81 01; 81 08
DESCRIPTEUR(S) Combustion*,Cyanides*,Hydroxides*;Multibase propellants*;Nitrogen compounds*;Absorption;Burners,Emission;Emission spectroscopy;Laser induced fluorescence;Length;Pressure;Propellants;Solid propellants, Spectra;Spectroscopy;Steady state;Strands;Visible spectra
IDENTIFICATEUR(S) M 30 propellant*;NTISDODXA

34/72 - (C) C.NTIS
NUMERO SIGNALEMENT N89-11163/7/XAD
TITRE ANGLAIS Modeling of Combustion Processes of Stick **Propellants** Via Combined Eulerian-Lagrangian Approach.
AUTEUR(S) KUO K. K , HSIEH K. C.; ATHAVALE M M.
AUTEUR COLLECTIF Pennsylvania State Univ., University Park.Dept of Mechanical Engineering.
ORGAN FINANCEMENT National Aeronautics and Space Administration, Washington, DC.
CLASSIFICATION INT 009222071, PJ304292
TYPE DE DOCUMENT Report
CODE LANGUE ENG
CODE PAYS D'ORIGINE US
SOURCE In NASA, Marshall Space Flight Center, Mixing and Demixing

Processes in Multiphase Flows with Application to Propulsion Systems p 181-193; NP 13; DP. Jul 88.
CODE JOURNAL NTIS S2702
CODE TARIF NTIS NTIS Prices (Order as N89-11153/8, PC A09/MF A01)
NUMERO DE CONTRAT DAAG29-83-K-0081
RESUME This research is motivated by the improved ballistic performance of large-caliber guns using stick **propellant** charges A comprehensive theoretical model for predicting the flame spreading, combustion, and grain deformation phenomena of long, unslotted stick **propellants** is presented.The formulation is based upon a combined Eulerian-Lagrangian approach to simulate special characteristics of the two phase combustion process in a cartridge loaded with a bundle of sticks The model considers five separate regions consisting of the internal perforation, the **solid** phase, the external interstitial gas phase, and two lumped parameter regions at either end of the stick bundle.For the external gas phase region, a set of transient one-dimensional fluid-dynamic equations using the Eulerian approach is obtained,governing equations for the stick **propellants** are formulated using the Lagrangian approach.The motion of a representative stick is derived by considering the forces acting on the entire **propellant** stick.The instantaneous temperature and stress fields in the stick **propellant** are modeled by considering the transient axisymmetric heat conduction equation and dynamic structural analysis
CODE CLASSIFICATION 81 01, 79 01
DESCRIPTEUR(S) Combustion physics*;Euler lagrange equation*,Flames*,Gun propellants*,Interior ballistics*,Propellant combustion*, Propellant grains*;Solid propellants*;Coordinates;Deformation; Fluid dynamics,Heat transfer;Mathematical models,Simulation, Spreading;Stresses;Temperature gradients,Vapor phases
IDENTIFICATEUR(S) NTISNASA

35/72 - (C) C.NTIS
NUMERO SIGNALEMENT AD-A199 761/8/XAD
TITRE ANGLAIS Combustion Mechanisms of Wide Distribution **Propellants**
AUTEUR(S) FREDRICK R A.
AUTEUR COLLECTIF Purdue Research Foundation, Lafayette, IN.
ORGAN FINANCEMENT Air Force Avionics Lab , Wright-Patterson AFB, OH.
CLASSIFICATION INT 010962000; 291600
TYPE DE DOCUMENT Report
CODE LANGUE ENG
CODE PAYS D'ORIGINE US
SOURCE Final rept May 84-May 88, NP. 281 DP Jun 88
CODE JOURNAL NTIS U8904
CODE TARIF NTIS NTIS Prices PC A13/MF A01
NUMERO DE CONTRAT F04611-84-K-0019
NUMERO PROJET 2308
NUMERO ACTIVITE M1
NUMERO(S) AGENCE AFAL-TR-88-008
RESUME The objective of this research is to describe the effects of oxidizer particle size distribution on the burning rate of **solid** **propellants** used in **rocket** **motors** Current models over predict the burning rate of wide distribution (wide distribution denotes two oxidizer modes that have extreme differences in mean diameter) formulations by 40 to 200 percent indicating combustion mechanisms unique to this type of **propellant** Four sets of AP/HTPB **propellants** were formulated to control the physical and chemical heterogenities characteristic of the **propellant** surface using 400 and 20 microns oxidizer particles The **propellants** were tested at pressure levels from 0 to 2000 psig An optical, distance measurement technique was developed and used to measure the local, non-steady surface deflagration of the **propellant** burning surface.The method uses a laser beam, synchronous detection, and closed-loop tracking to locate the surface in the hostile combustion environment.An acoustic emission technique determined average burning rates.Combustion phenomena were also accessed using high-speed photography and scanning electron microscopy Keywords: Particle size distribution, Burning rate,

	Solid **propellants**, **Rocket** **motors**, Combustion mechanisms, AP/HTPB **propellants**, Laser diagnostics, Acoustic emissions, Scanning electron.(MJM)
CODE CLASSIFICATION	81 08, 81 01
DESCRIPTEUR(S)	Combustion*;Particle size*;Solid rocket oxidizers*,Ammonium perchlorate*;Acoustic emissions,Burning rate;Closed loop systems; Deflagration;Diagnosis General;Diameters;Distribution,Electron microscopy;Electronic scanners;Enemy;Environments;High speed photography;Indicators;Laser applications;Laser beams;Mean, Measurement;Models,Oxidizers;Pressure;Propellants,Range Distance; Rocket engines;Solid propellants;Steady state,Surfaces,Tracking
IDENTIFICATEUR(S)	NTISDODXA;NTISDODAF

38/72 - (C) C.NTIS

NUMERO SIGNALEMENT	AD-A199 334/4/XAD
TITRE ANGLAIS	**Solid** **Propellant** Flame Spectroscopy.
AUTEUR(S)	EDWARDS J. T.
AUTEUR COLLECTIF	Air Force Astronautics Lab., Edwards AFB, CA.
CLASSIFICATION INT	088843000; 417458
TYPE DE DOCUMENT	Report
CODE LANGUE	ENG
CODE PAYS D'ORIGINE	US
NUMERO DE RAPPORT	AFAL-TR-88-076
SOURCE	Interim rept. Jan 84-Jan 88; NP. 229; DP. Aug 88
CODE JOURNAL NTIS	U8903
CODE TARIF NTIS	NTIS Prices. PC A11/MF A01
NUMERO PROJET	2308
NUMERO ACTIVITE	M1
RESUME	This report summarizes the progress made in **solid** **propellant** flame chemistry studies.These chemistry studies involved the spectroscopic determination of species concentration and temperature profiles in **solid** **propellant** flames at pressures from atmospheric to 7 MPa (1000 psi).The **propellants** involved contained AP and HMX, as well as several other formulations.The molecules studied were OH, CH, NH, and NO, primarily, although other atomic and molecular species were seen in the **propellant** flames in emission The primary diagnostic employed was laser-induced fluorescence (LIF), although the chemiluminescence (emission) from the **propellant** flames was also studied.These experiments are continuing.
CODE CLASSIFICATION	79 01; 99 06, 81 01
DESCRIPTEUR(S)	Flames*;Solid propellants*;Spectroscopy*;Carbon;Chemical radicals; Chemiluminescence;Chemistry;Combustion;Determination;Diagnosis General;HMX,Hydrogen;Laser induced fluorescence,Molecules,Nitrogen, Oxygen,Profiles,Propellants;Temperature
IDENTIFICATEUR(S)	NTISDODXA

39/72 - (C) C NTIS

NUMERO SIGNALEMENT	DE88011286/XAD
TITRE ANGLAIS	Combustion of Energetic Materials. Semi Annual Progress Report, April-September 1987.
AUTEUR COLLECTIF	Sandia National Labs., Livermore, CA.
ORGAN FINANCEMENT	Department of Energy, Washington, DC.
CLASSIFICATION INT	070378000; 9511238
TYPE DE DOCUMENT	Report
CODE LANGUE	ENG
CODE PAYS D'ORIGINE	US
NUMERO DE RAPPORT	SAND-88-8001
SOURCE	Portions of this document are illegible in microfiche products; NP. 45; DP. 1988.
CODE JOURNAL NTIS	U8902
CODE TARIF NTIS	NTIS Prices: PC A03/MF A01
NUMERO DE CONTRAT	AC04-76DP00789
RESUME	Our program emphasizes fundamental research and is directed towards understanding the combustion, chemistry and physics of energetic solids and liquids.Experimental effort consists of the following: (1) **solid** **propellant** thermal decomposition and deflagration studies and (2) liquid monopropellant ignition and combustion studies.A gas-flame experiment designed to model the two-stage flame characteristics of **solid** **propellant**

	deflagration has been established and both conventional and laser diagnostics have been incorporated into it.Thermal decomposition (using laser heating) of **solid** **propellants** is being studied using a modulated molecular beam mass spectrometer that will be complemented by laser-induced fluorescence diagnostics Gas-phase flame models used previously for hydrocarbon flame analysis are being extended to study gas-phase reactions in nitramine **propellants**.Quantum chemistry calculations are being performed to investigate the molecular decomposition mechanisms of energetic materials.**Solid** **propellant** deflagration is being modeled analytically and through the use of two-dimensional thermochemical codes developed earlier for related research programs.Droplet combustion models developed for hydrocarbon fuels are being extended for liquid monopropellant applications.43 refs , 40 figs , 2 tabs.(ERA citation 13 041129).
CODE CLASSIFICATION	81 01; 79 01
DESCRIPTEUR(S)	Chemical Explosives*,Combustion*,Nitro Compounds*;Propellants*, Chemical Composition,Chemical Reaction Kinetics;Chemical Reaction Yield;Chemical Reactions;Ignition,Progress Report,Pyrolysis Products,Research Programs;Solids,Thermal Degradation
IDENTIFICATEUR(S)	ERDA 450100,ERDA 400800;NTISDE

40/72 - (C) C NTIS

NUMERO SIGNALEMENT	AD-A197 854/3/XAD
TITRE ANGLAIS	Report on JANNAF Workshop 'Influence of Gas-Phase Chemical Kinetics on Low-Pressure Ignition and Flamespreading in **Solid** **Propellant**'
AUTEUR(S)	KELLER G K
AUTEUR COLLECTIF	Army Ballistic Research Lab., Aberdeen Proving Ground, MD
CLASSIFICATION INT	082505000; 050750
TYPE DE DOCUMENT	Report
CODE LANGUE	ENG
CODE PAYS D'ORIGINE	US
NUMERO DE RAPPORT	BRL-TR-2918
SOURCE	Technical rept for period ending Oct 86; NP. 22; DP. Jul 88.
CODE JOURNAL NTIS	U8824
CODE TARIF NTIS	NTIS Prices: PC A03/MF A01
NUMERO PROJET	1L161102AH43
NUMERO ACTIVITE	00
RESUME	A workshop on the subject influence of Gas-Phase Chemical Kinetics on the Low-Pressure Ignition and Flamespreading in **Solid** **Propellants** was held at Hampton, VA, on 23 and 24 October 1986 in conjunction with the 23rd JANNAF Combustion Meeting The objectives of the workshop were to a) force a synergisitc interaction between those whose measurements have provided evidence for the participation of chemical kinetics in low-pressure **solid** **propellant** burning and those who are striving to simulate these events with interior ballistic models and b) address problems of anomalous ignition behavior in gun propelling charges.The workshop participants a) reviewed the evidence for the participation of chemical kinetics in the low-pressure burning of **solid** **propellants**, b) reviewed model simulations which include finite-rate kinetics, and c) determined which model simulations and further experimental characterizations would be most fruitful.This report documents the workshop.(AW).
CODE CLASSIFICATION	81 01; 79 01
DESCRIPTEUR(S)	Ignition*;Solid propellants*;Flame propagation*;Gun propellants*; Anomalies;Combustion;Interior ballistics;Low pressure;Models; Propelling charges;Reaction kinetics;Simulation;Workshops;Vapor phases
IDENTIFICATEUR(S)	NTISDODXA

42/72 - (C) C NTIS

NUMERO SIGNALEMENT	AD-A196 689/4/XAD
TITRE ANGLAIS	Method for Obtaining Empirical Correlations for Predicting Crack Propagation in a Burning **Solid** **Propellant** Grain.
AUTEUR(S)	NIMIS J A.
AUTEUR COLLECTIF	Air Force Inst.of Tech , Wright-Patterson AFB, OH.
CLASSIFICATION INT	000805000; 012200

TYPE DE DOCUMENT Thesis
CODE LANGUE ENG
CODE PAYS D'ORIGINE US
NUMERO DE RAPPORT AFIT/CI/NR-88-85
SOURCE Master's thesis; NP. 70; DP. 1988.
CODE JOURNAL NTIS U8823
CODE TARIF NTIS NTIS Prices. PC A04/MF A01
RESUME The importance of crack propagation in **solid** **rocket** **motors** is widely recognized.However, the processes of crack propagation and branching in burning **solid** **propellants** are not as yet well understood.These processes could be instrumental in creating large specific surface areas for burning causing **rocket** **motor** failure.Key factors influencing the crack combustion, propagation and branching process considered in the dimensional analysis include chamber pressurization rate, initial crack length, initial temperature, sample geometry, and mechanical and thermal properties of the **solid** **propellant** (jes).
CODE CLASSIFICATION 81 08
DESCRIPTEUR(S) Propellant grains*;Solid propellant rocket engines*,Combustion, Crack propagation;Cracks;Failure;Mechanical properties, Pressurization;Rates;Rocket engines;Solid propellants;Thermal properties
IDENTIFICATEUR(S) Combustion chambers,NTISDODXA

44/72 - (C) C.NTIS
NUMERO SIGNALEMENT AD-A194 944/5/XAD
TITRE ANGLAIS Combustion Diagnostics of **Propellant** with New Grain Geometries
AUTEUR(S) TOMPKINS R. E ; WHITE K J , JUHASZ A. A
AUTEUR COLLECTIF Army Ballistic Research Lab , Aberdeen Proving Ground, MD.
CLASSIFICATION INT 082505000; 050750
TYPE DE DOCUMENT Report
CODE LANGUE ENG
CODE PAYS D'ORIGINE US
NUMERO DE RAPPORT BRL-TR-2899
SOURCE Technical rept.; NP. 37, DP. Mar 88.
CODE JOURNAL NTIS U8821
CODE TARIF NTIS NTIS Prices· PC A03/MF A01
RESUME High progressivity/density (HPD) **propellants** are under consideration at the Ballistic Research Laboratory (BRL) for a variety of enhanced ballistic applications The HPD concept involves the tailoring of the mass generation rate to match the increasing chamber volume as the projectile moves down the gun tube This can be accomplished physically by designing a grain which will increase in surface area at a designated point in the ballistic cycle.It can also be done chemically by formulating grains with compositions that vary throughout the grain.As these layers burn through, the burn rate can be tailored to change at specific points in the ballistic cycle
CODE CLASSIFICATION 79 05; 79 01; 81 08; 81 01
DESCRIPTEUR(S) Burning rate*;Combustion*;Diagnosis General*;Propellants*; Propellant grains*;Ballistics;Gun barrels;Mass;Rates,Solid rocket propellants;Propelling charges
IDENTIFICATEUR(S) High Progressivity Density Propellants;Fastcare propellants; NTISDODXA

47/72 - (C) C.NTIS
NUMERO SIGNALEMENT AD-A191 556/0/XAD
TITRE ANGLAIS Chemical Kinetics of Nitramine **Propellant** Combustion.
AUTEUR(S) BRANCH M. C.
AUTEUR COLLECTIF Colorado Univ.at Boulder.Dept of Mechanical Engineering
ORGAN FINANCEMENT Air Force Office of Scientific Research, Bolling AFB, DC.
CLASSIFICATION INT 068646004; 407675
TYPE DE DOCUMENT Report
CODE LANGUE ENG
CODE PAYS D'ORIGINE US
SOURCE Interim technical rept. 1, Oct 86-30 Sep 87; NP. 14; DP. Nov 87.
CODE JOURNAL NTIS U8815
CODE TARIF NTIS NTIS Prices: PC A03/MF A01
NUMERO ALLOCATION AFOSR-84-0006
NUMERO PROJET 2308

NUMERO ACTIVITE A1
NUMERO(S) AGENCE AFOSR-TR-88-0044
RESUME The decomposition of many **solid** reactants during combustion leads to the formation of gaseous hydrocarbons and oxides of nitrogen which can react to support a flame above the surface of the **solid** These flames can provide heat which is fed back to the **propellant** surface and thereby influence the burning rate of the **solid** In the case of nitramine based **solid** rocket **propellants**, the gas phase decomposition products include significant amounts of Formaldehyde.Nitrogen dioxide, Hydrogen Cyanide, Nitric oxide, Nitrous oxide, oxygen.This study is intended to provide experimental data on the structure of hydrocarbon flames supported by oxides of nitrogen in order to establish the reaction mechanism for such flames Laminar, premixed, flat flames of methane/NO2/O2 and CH2O/NO2/O2 have been investigated and a reaction mechanism is suggested which accounts for all of the major observations in the data.
CODE CLASSIFICATION 79 01; 81 01
DESCRIPTEUR(S) Combustion*,Nitramines*,Propellants*;Solid rocket propellants*; Combustion products*;Decomposition,Experimental data,Flames; Formaldehyde,Hydrocarbons;Hydrogen cyanide,Laminar flow;Nitrogen oxides;Oxygen;Reaction kinetics;Vapor phases;Laser induced fluorescence
IDENTIFICATEUR(S) Chemical kinetics*;NTISDODXA,NTISDODAF

48/72 - (C) C NTIS
NUMERO SIGNALEMENT AD-A190 752/6/XAD
TITRE ANGLAIS Advanced B and Al Iota Combustion Kinetics over Wide Temperature Ranges.
AUTEUR(S) FONTIJN A
AUTEUR COLLECTIF Rensselaer Polytechnic Inst , Troy, NY.
ORGAN FINANCEMENT Air Force Office of Scientific Research, Bolling AFB, DC
CLASSIFICATION INT 024503000; 302100
TYPE DE DOCUMENT Report
CODE LANGUE ENG
CODE PAYS D'ORIGINE US
SOURCE Annual rept. 1 Dec 86-31 Nov 87; NP 13, DP. 17 Dec 87
CODE JOURNAL NTIS U8814
CODE TARIF NTIS NTIS Prices: PC A03/MF A01
NUMERO ALLOCATION AFOSR-86-0019
NUMERO PROJET 2308
NUMERO ACTIVITE A1
NUMERO(S) AGENCE AFOSR-TR-88-0170
RESUME Current ability to improve the combustion efficiency of B and Al **solid** **propellants** and slurries is hampered by a lack of understanding and knowledge of the kinetics of the individual reactions involved and the ways and manner by which temperature affects the rate coefficients and product channels While the simple Arrhenius-type equation k(T) = AT(to the 1/2 power) exp(-E(A)/RT) has over limited temperature ranges been of great value, when applied to wide temperature ranges it is often not obeyed Particularly for exothermic and slightly endothermic reactions, order of magnitude errors can be made by extrapolations based on the Arrhenius equation.It is the goal of this program to provide an insight in the kinetic behavior of B and Al radical oxidation reactions as influenced by temperature.To this end measurements are made in high-temperature fast-flow reactors (HTFFR).These unique tools provide measurements on isolated elementary reactions in a heat bath.
CODE CLASSIFICATION 81 01, 81 08
DESCRIPTEUR(S) Combustion*;Solid propellants*;Arrhenius equation;Baths;Channels; Coefficients;Efficiency;Endothermic reactions;Errors;Extrapolation; Fast reactors;Heat;High temperature;Isolation;Reaction kinetics; Measurement;Oxidation reduction reactions;Range Extremes;Rates; Temperature;Solid rocket propellants,Aluminized propellants;Boron compounds,Aluminum compounds
IDENTIFICATEUR(S) Boron chloride;Aluminum chloride;Radiative lifetimes;NTISDODXA; NTISDODAF

49/72 - (C) C.NTIS
NUMERO SIGNALEMENT AD-A190 163/6/XAD
TITRE ANGLAIS JANNAF (Joint Army-Navy-NASA-Air Force) Combustion Meeting (24th) Held in Monterey, California, 5-9 October 1987 Volume 1
AUTEUR(S) BECKER D. L.
AUTEUR COLLECTIF Johns Hopkins Univ., Laurel, MD.Chemical Propulsion Information Agency
CLASSIFICATION INT 054839001; 081100
TYPE DE DOCUMENT Report
CODE LANGUE ENG
CODE PAYS D'ORIGINE US
NUMERO DE RAPPORT CPIA-PUB-476-VOL-1
SOURCE Meeting proceedings; See also Volume 2, AD-A190 164; Availability: National Technical Information Service, Springfield, Va. 22161 PC $70 MF $70 (No copies furnished by DTIC.); NP. 441; DP. Oct 87
CODE JOURNAL NTIS U8814
CODE TARIF NTIS NTIS Prices PC$70 00/MF$70.00
NUMERO DE CONTRAT N00039-87-C-5301
RESUME This volume, the first of four volumes, is a collection of 35 unclassified/unlimited papers which were presented at the 25th Joint Army-Navy-NASA-Air Force (JANNAF) Combustion Meeting, October 5-9, 1987, the Naval Postgraduate School, Monterey, California.Specific subjects discussed include combustion instability, ignition, burn rate, flame structure, and particle size measurement of **solid** rocket **propellants** and the ignition, chemistry and thermal degradation of nitramine **propellants**.Subject, author and source indexes for all four volumes are included, as is the list of meeting attendees.
CODE CLASSIFICATION 81 01; 81 08
DESCRIPTEUR(S) Flames*;Propellants*;Rocket propellants*,Burning rate;Combustion; Combustion stability;Ignition;Indexes,Joint military activities, Measurement;Nitramines;Particle size,Solid rocket propellants, Sources,Thermal degradation
IDENTIFICATEUR(S) Meetings*,NTISDODXA

50/72 - (C) C NTIS
NUMERO SIGNALEMENT PB88-182324/XAD
TITRE ANGLAIS Soviet Combustion Research.
AUTEUR(S) MCLEAN W J , AMANN C. A.; BOWMAN C. T., LIBBY P A.; PALMER R. E.
AUTEUR COLLECTIF Foreign Applied Sciences Assessment Center, La Jolla, CA.
CLASSIFICATION INT 089612000
TYPE DE DOCUMENT Report
CODE LANGUE ENG
CODE PAYS D'ORIGINE US
NUMERO DE RAPPORT FASAC-TAR-3120
SOURCE Technical assessment rept., See also PB88-182316; NP 299, DP Mar 87
CODE JOURNAL NTIS U8813
CODE TARIF NTIS NTIS Prices: PC E11/MF A01
RESUME The report is an assessment of Soviet basic and applied combustion research, prepared by a panel of seven US combustion scientists and engineers who evaluated a large body of published Soviet scientific literature.The panel examined a broad selection of topics in Soviet combustion research, spanning the range from very applied to very fundamental Soviet research related to combustion of energetic materials (e.g . **propellants** and explosives) was intentionally omitted from the assessment.Chapter headings include the following. Assessments,**Solid** fuels combustion;Heat-engine combustion,Practical combustion of gaseous and liquid fuels--Combustion and explosion safety;Theory of laminar and turbulent reacting flows,Combustion chemistry;Advanced combustion diagnostics and instrumentation.
CODE CLASSIFICATION 81 01; 99 06
DESCRIPTEUR(S) Combustion*;USSR*;Fuels;Safety;Research,Reviews
IDENTIFICATEUR(S) Foreign technology*;NTISNTIS

51/72 - (C) C.NTIS
NUMERO SIGNALEMENT N88-17733/2/XAD
TITRE ANGLAIS Shuttle Rocket Booster Computational Fluid Dynamics.
AUTEUR(S) CHUNG T. J.; PARK O. Y.

AUTEUR COLLECTIF	Alabama Univ in Huntsville.
ORGAN FINANCEMENT	National Aeronautics and Space Administration, Washington, DC
CLASSIFICATION INT	053562000; AM584056
TYPE DE DOCUMENT	Report
CODE LANGUE	ENG
CODE PAYS D'ORIGINE	US
NUMERO DE RAPPORT	NAS 1.26.182518
SOURCE	Final Report; NP. 108; DP. 1988
CODE JOURNAL NTIS	S2610
CODE TARIF NTIS	NTIS Prices: PC A06/MF A01
NUMERO DE CONTRAT	NAG8-629
NUMERO(S) AGENCE	NASA-CR-182518
RESUME	Additional results and a revised and improved computer program listing from the shuttle rocket booster computational fluid dynamics formulations are presented.Numerical calculations for the flame zone of **solid** **propellants** are carried out using the Galerkin finite elements, with perturbations expanded to the zeroth, first, and second orders The results indicate that amplification of oscillatory motions does indeed prevail in high frequency regions.For the second order system, the trend is similar to the first order system for low frequencies, but instabilities may appear at frequencies lower than those of the first order system.The most significant effect of the second order system is that the admittance is extremely oscillatory between moderately high frequency ranges.
CODE CLASSIFICATION	81 07; 84 03
DESCRIPTEUR(S)	Computational fluid dynamics*;Propellant combustion*,Space shuttle boosters*,Computer programs,Galerkin method,Combustion physics; Finite element method,Flame propagation;Perturbation theory;Solid rocket propellants
IDENTIFICATEUR(S)	NTISNASA

53/72 - (C) C NTIS

NUMERO SIGNALEMENT	AD-A189 260/3/XAD
TITRE ANGLAIS	Laser Ignition of Nitramine Composite **Propellants** and Crack Propagation and Branching in Burning **Solid** **Propellants**
AUTEUR(S)	KUO K. K., KIM J. U , NIMIS J , SMEDLEY J., CHAR J. M
AUTEUR COLLECTIF	Pennsylvania State Univ., University Park Dept.of Mechanical Engineering.
CLASSIFICATION INT	009222071; 401929
TYPE DE DOCUMENT	Report
CODE LANGUE	ENG
CODE PAYS D'ORIGINE	US
SOURCE	Final rept 1 Jan 86-31 Aug 87; NP 196, DP. Oct 87
CODE JOURNAL NTIS	U8812
CODE TARIF NTIS	NTIS Prices PC A09/MF A01
NUMERO DE CONTRAT	N00014-79-C-0762
RESUME	Two major tasks performed during the report period of investigation were: (i) laser ignition of nitramine-based composite **propellants** using a high-powered CO2 laser in (ii) crack propagation and branching in burning **solid** **propellants**.The laser ignition of a series of RDX-based composite **propellants** was studied theoretically and experimentally.A comprehensive model for the radiative ignition of the nitramine composite **propellants** was formulated.The theoretical model was solved numerically.A radiative ignition test setup employing a high-powered CO2 laser was designed and constructed to study ignition characteristics of a series of RDX-based nitramine composite **propellants** Interactions between the infrared laser beam and nitramine composite **propellants** revealed a number of interesting processes.The laser ignition of composite **propellants** involves many complex thermophysiochemical processes including gasification, initiation of a luminous flame, propagation of the flame, and chemical reactions near the sample surface as well as heat conduction in **solid** phases In general, the delay time based upon the onset of light emission decreases monotonically with the increase of incident laser energy flux
CODE CLASSIFICATION	79 01
DESCRIPTEUR(S)	Combustion*;Composite propellants*;Crack propagation*;Ignition

lag*,Solid propellants*;Thermal conductivity*,Carbon dioxide lasers,Chemical reactions;Delay;Emission;Energy;Extinguishing; Flames;Flux Rate;Formulations;Ignition;Infrared lasers,Laser beams; Lasers,Light,Luminosity;Models;Nitramines;Propagation;Pyrolysis; Radiation,Rdx,Response;Solid phases,Theory;Time
IDENTIFICATEUR(S) NTISDODXA

54/72 - (C) C.NTIS
NUMERO SIGNALEMENT AD-A189 160/5/XAD
TITRE ANGLAIS Combustion Theory and Related Questions.
AUTEUR(S) BUCKMASTER J. D.
AUTEUR COLLECTIF Cornell Univ., Ithaca, NY.
ORGAN FINANCEMENT Army Research Office, Research Triangle Park, NC.
CLASSIFICATION INT 000607000; 098550
TYPE DE DOCUMENT Report
CODE LANGUE ENG
CODE PAYS D'ORIGINE US
SOURCE Final rept. 1 Dec 84-31 Aug 87; NP 9, DP Oct 87.
CODE JOURNAL NTIS U8812
CODE TARIF NTIS NTIS Prices: PC A02/MF A01
NUMERO DE CONTRAT DAAG29-85-K-0022
NUMERO(S) AGENCE ARO-21306.14-MA
RESUME Modern asymptotic methods have been applied to a wide range of problems in combustion science and mechanics.Details are contained in the 22 Technical Reports and 5 Ph D.thesis listed A list of participating scientists is also given.
CODE CLASSIFICATION 81 01, 99 06
DESCRIPTEUR(S) Combustion*,Explosives,Flames,Flammability;Shear properties,Theory, Strain rate;Solid propellants;Detonation waves;Chemical reactions; Theses;Reports;Test and evaluation
IDENTIFICATEUR(S) Stephen problems,NTISDODXA,NTISDODA

55/72 - (C) C NTIS
NUMERO SIGNALEMENT AD-A187 979/0/XAD
TITRE ANGLAIS Combustion Mechanisms.
AUTEUR(S) EDWARDS T
AUTEUR COLLECTIF Air Force Astronautics Lab., Edwards AFB, CA
CLASSIFICATION INT 088843000, 417458
TYPE DE DOCUMENT Report
CODE LANGUE ENG
CODE PAYS D'ORIGINE US
NUMERO DE RAPPORT AFAL-TR-87-077
SOURCE Final rept. Jan 81-Sep 87, NP. 7, DP. Sep 87
CODE JOURNAL NTIS U8810
CODE TARIF NTIS NTIS Prices PC A02/MF A01
NUMERO PROJET 2303
NUMERO ACTIVITE M1
RESUME The Combustion Mechanism project covered a 6.5 year time period.Its general goal was to use the recently developed laser-based combustion diagnostic probes to learn more about the chemistry and physics occuring in high pressure **solid** **propellant** flames References to published results are included
CODE CLASSIFICATION 81 01
DESCRIPTEUR(S) Combustion*;Probes*;Chemistry;Diagnosis General;Laser applications, Laser induced fluorescence;Physics;Solid propellants
IDENTIFICATEUR(S) NTISDODXA

57/72 - (C) C.NTIS
NUMERO SIGNALEMENT AD-A187 119/3/XAD
TITRE ANGLAIS Correlation of HMX (Cyclotetramethylenetetranitramine) Particle Characterization Techniques to **Propellant** Burn Rate.
AUTEUR(S) CHANDLER K. G.
AUTEUR COLLECTIF Air Force Astronautics Lab., Edwards AFB, CA.
CLASSIFICATION INT 088843000; 417458
TYPE DE DOCUMENT Report
CODE LANGUE ENG
CODE PAYS D'ORIGINE US
NUMERO DE RAPPORT AFAL-TR-87-039
SOURCE Interim rept. Mar 86-Mar 87; NP. 20; DP Sep 87.
CODE JOURNAL NTIS U8807

CODE TARIF NTIS NTIS Prices PC A03/MF A01
NUMERO PROJET 5730
NUMERO ACTIVITE 00
RESUME Present methods of correlating **solid** **propellant** burn rate to oxidizer particle parameters solely depend upon the weight median diameters of the particle distribution.With the broad and variable distribution of the oxidizer particle, vastly different particle surface areas may results in variations in **propellant** burn rates.This study compares the burn rate of **solid** **propellant** to weight median diameters, calculated surface areas from size measurements, measured surface areas, and a new surface area distribution dependent solvolysis method.Comparison of the characterization techniques is performed to determine the role of surface area in the burning process, and the best parameter for **propellant** burn rate correlations.
CODE CLASSIFICATION 79 01, 81 08
DESCRIPTEUR(S) Burning rate*;Hmx*;Particles*;Combustion,Correlation;Distribution, Oxidizers,Propellant burn out;Rates;Solid propellants,Solvolysis, Surfaces,Variables
IDENTIFICATEUR(S) NTISDODXA

58/72 - (C) C.NTIS
NUMERO SIGNALEMENT AD-A187 000/5/XAD
TITRE ANGLAIS Holographic Investigation of Metallized **Solid** **Propellant** Combustion in Two-Dimensional and Three-Dimensional **Rocket** **Motors**
AUTEUR(S) WALKER J D
AUTEUR COLLECTIF Naval Postgraduate School, Monterey, CA.
CLASSIFICATION INT 019895000; 251450
TYPE DE DOCUMENT Thesis
CODE LANGUE ENG
CODE PAYS D'ORIGINE US
SOURCE Master's thesis; NP. 46; DP Sep 87
CODE JOURNAL NTIS U8807
CODE TARIF NTIS NTIS Prices: PC A03/MF A01
RESUME This experimental investigation included the design and construction of a new, two-dimensional, **rocket** **motor** that could be used to obtain better holographic data than obtained in previous investigations using a small three-dimensional **motor**.The **solid** **propellant** used during this investigation was AP, HTPB, with 2%, 40 micron aluminum particles and 0.25% iron oxide.Good quality holograms were obtained using the three dimensional **motor** at operating pressures of 93 and 94 psia.Successful holographic recordings were also acquired using the new, two dimensional **motor** at pressures of 45 and 183 psia.System limitations and suggested improvements to the apparatus are discussed
CODE CLASSIFICATION 81 07; 81 01; 81 07
DESCRIPTEUR(S) Holography*,Rocket engines*,Solid propellants*;Combustion; Holograms,Limitations,Metallizing;Motors,Quality;Recording systems; Three dimensional;Two dimensional
IDENTIFICATEUR(S) NTISDODXA

61/72 - (C) C.NTIS
NUMERO SIGNALEMENT AD-A186 215/0/XAD
TITRE ANGLAIS Effects of Turbulence on Stationary and Non-Stationary Processes in C-Systems
AUTEUR(S) ROBERTS T. A.; BEDDINI R. A
AUTEUR COLLECTIF Illinois Univ at Urbana-Champaign.Dept.of Aeronautical and Astronautical Engineering.
ORGAN FINANCEMENT Air Force Office of Scientific Research, Bolling AFB, DC
CLASSIFICATION INT 034597070; 176005
TYPE DE DOCUMENT Report
CODE LANGUE ENG
CODE PAYS D'ORIGINE US
NUMERO DE RAPPORT AAE-87-1; UILU-ENG-87-0501
SOURCE Technical rept. (Final) 1 Sep 85-30 Nov 86; NP. 36; DP. 1 Jun 87.
CODE JOURNAL NTIS U8806
CODE TARIF NTIS NTIS Prices: PC A03/MF A01
NUMERO ALLOCATION AFOSR-85-0348

NUMERO PROJET 2308
NUMERO ACTIVITE A1
NUMERO(S) AGENCE AFOSR-TR-87-0980
RESUME Turbularization of an acoustic boundary layer (Stokes Layer) on impermeable and permeable surfaces is analytically considered The theoretical approach uses a second-order closure model of turbulence Both an approximate, closed-form solution and a more comprehensive finite difference solution of the time dependent, parabolic, one-dimensional governing equations are obtained.For simple acoustic boundary-layers on impermeable surfaces, both the approximate solution and the numerical results for the critical acoustic Mach number required for turbulent transition are qualitatively confirmed by experiment.Calculations for acoustic boundary-layers with transpiration (injection) indicate a substantial reduction of the acoustic Mach number required for transition, up to a limiting injection velocity that is frequency dependent.The results may provide a mechanism for flow-related combustion instability in practical systems, particularly **solid** propellent rockets, since turbularization of the near-surface combustion zone could result at relatively low acoustic Mach numbers.This report documents a completed phase of work which is concerned with the analysis of turbulent flow and heat transfer behavior in rocket chamber flows (C-systems).Keywords: Acoustic instability,Aeroacoustics,**Solid** propellent rocket engines;Transpiration,Turbulent boundary layer;Acoustic boundary layer;Combustion instability,Laminar boundary layer.
CODE CLASSIFICATION 81 01; 46 02
DESCRIPTEUR(S) Combustion stability*,Turbulent boundary layer*;Acoustics; Aerodynamics,Boundary layer;Time dependence,Combustion chambers, Chambers,Combustion,Equations;Finite difference theory;Flow,Heat transfer;Injection,Laminar boundary layer;Layers;Limitations;Mach number,Methodology,Numerical analysis,Permeability,Rockets;Solid propellant rocket engines;Solutions General,Stability,Surfaces, Theory,Transitions,Transpiration,Turbulence,Turbulent flow,Velocity
IDENTIFICATEUR(S) Rocket chamberflow;Stokes layer,Turbularization;Instability, Aeroacoustics;Acoustic instability,NTISDODXA;NTISDODAF

62/72 - (C) C.NTIS
NUMERO SIGNALEMENT AD-A184 770/6/XAD
TITRE ANGLAIS Erosive Burning Study of Stick **Propellants**.
CONFERENCE GENERALE Presented at the AIAA/SAE/ASME/ASEE Joint Propulsion Conference (23rd), San Diego, CA, 29 Jun-2 Jul 87.
AUTEUR(S) HSIEH W. H., CHAR J M ; ZANOTTI C., KUO K K
AUTEUR COLLECTIF Pennsylvania State Univ., University Park.Dept of Mechanical Engineering.
ORGAN FINANCEMENT Army Research Office, Research Triangle Park, NC.
CLASSIFICATION INT 009222071, 401929
TYPE DE DOCUMENT Conference
CODE LANGUE ENG
CODE PAYS D'ORIGINE US
NUMERO DE RAPPORT PSU-ME-P-86/87-0041
SOURCE Interim rept.; NP. 11, DP. 6 Aug 87.
CODE JOURNAL NTIS U8801
CODE TARIF NTIS NTIS Prices: PC A03/MF A01
NUMERO DE CONTRAT DAAG29-83-K-0081
NUMERO(S) AGENCE ARO-20007.8-EG
RESUME A theoretical model was solved numerically for simulating erosive-burning processes occurring inside the center perforation of an unslotted NOSOL-363 stick **propellant** Results show that the erosive-burning phenomenon is caused by the enhanced heat feedback from the gas phase to **solid** phase resulting from the combined effect of increased turbulent mixing and reduction in flame stand-off distance from the burning surface The real-time X-ray radiography system was demonstrated to be a powerful and reliable tool for nonintrusive measurements of instantaneous burning rates.A model was validated by experimental data in terms of time variation of internal diameter distributions.Thermal wave structures of NOSOL-363 stick **propellants** under erosive- and strand-burning conditions were measured by fine-wire thermocouples.

. F CLASSIFICATION 79 01
D ?IPTEUR(S) Gun propellants*;Erosive burning*,Propellant grains,Burning rate, Turbulence;Radiography,Combustors
IDENTIFICATEUR(S) Stick propellants*;NTISDODXA;NTISDODA

67/72 - (C) C.NTIS
NUMERO SIGNALEMENT N87-27059/1/XAD
TITRE ANGLAIS Studies of **Solid** **Propellant** Combustion with Pulsed Radiography
AUTEUR(S) GODAI T.; TANEMURA T , FUJIWARA T , SHIMIZU M.
AUTEUR COLLECTIF National Aeronautics and Space Administration, Washington, DC
CLASSIFICATION INT 011249000; NC452981
TYPE DE DOCUMENT Report
CODE LANGUE ENG
CODE PAYS D'ORIGINE JP
NUMERO DE RAPPORT NAS 1 77:20081
SOURCE Trans into Engl:sh of Parusu Xsen Kanketsu Syashinho Niyoru Kotai Puroperanto No Nensyou Nikansuru Kenkya, Tokyo, Japan, National Aerospace Lab , Sep 78 Original langua document was announced as N79-77192. Trans by Kanner (Leo) Associates, Redwood City, CA. Original document prepared by Aerospace Research Group; NP. 31, DP Aug 87.
CODE JOURNAL NTIS S2521
CODE TARIF NTIS NTIS Prices· PC A03/MF A01
NUMERO DE CONTRAT NASW-4005
NUMERO(S) AGENCE NASA-TT-20081
RESUME Pulsed radiography was applied to observe **solid** **propellant** surface regression during **rocket** **motor** operation Using a 150 KV flash X-ray system manufactured by the Field Emission Corporation and two kinds of film suppliers, images of the **oropellant** surface of a 5 cm diameter end burning **rocket** **motor** were recorded on film The repetition frame rate of 8 pulses per second and the pulse train length of 10 pulses are limited by the capability of the power supply and the heat build up within the X-ray tube, respectively The experiment demonstrated the effectiveness of pulsed radiography for observing **solid** **propellant** surface regression Measuring the position of burning surface images on film with a microdensitometer, quasi-instantaneous burning rate as a function of pressure and the variation of characteristic velocity with pressure and gas stay time were obtained Other research items to which pulsed radiography can be applied are also suggested
CODE CLASSIFICATION 81 08, 81 01
DESCRIPTEUR(S) Propellant combustion*,Radiography*;Solid rocket propellants*; Surface reactions*,Burning rate;Photographic measurement,Pressure, Pulse repetition rate
IDENTIFICATEUR(S) Foreign technology,Translations,NTISNASA,NTISFNJA

69/72 - (C) C NTIS
NUMERO SIGNALEMENT NTN87-0395
TITRE ANGLAIS Measuring Combustion Advance in **Solid** **Propellants**. The **propellant** forms a dynamic part of capacitors
AUTEUR COLLECTIF National Aeronautics and Space Administration, Washington, DC
CLASSIFICATION INT 011249000
TYPE DE DOCUMENT Report
CODE LANGUE ENG
CODE PAYS D'ORIGINE US
SOURCE NTIS Tech Note, FOR ADDITIONAL INFORMATION: Contact: NASA Technology Transfer Div., PO Box 8757 BWI Airport, MD 21240, (301) 621-0100 ext 241 Refer to NPO-16585/TN; NP 1, DP. Apr 87
CODE JOURNAL NTIS D8716
CODE TARIF NTIS NTIS Prices. Not available NTIS
RESUME This citation summarizes a one-page announcement of technology available for utilization A set of gauges on a **solid**-**propellant** **rocket** **motor** with an electrically insulating case measures the advance of the combustion front and the local erosion rates of the **propellant** and insulation.The data furnished by the gauges aid in **motor** design, failure analysis, and performance prediction.The technique is also useful in determining **propellant** uni[illegible]city and electrical properties

	of the exhaust plume The gauges can be used both in flight and on the ground The foil-gauge technique may also be useful in basic research on pulsed plasmas or the combustion of solids Each gauge consists of a small metal foil on the outside of the **rocket** **motor** case Each gauge constitutes one electrode of a capacitor, while the combustion products constitute the other electrode Since the flame in the **motor** cavity is extremely hot - 2,000 to 3,000 K - the gaseous combustion products are ionized and, therefore, electrically conductive Because the components are located outside the combustion chamber, they do not affect the combustion process
CODE CLASSIFICATION	81 01, 81 08, 81 07
DESCRIPTEUR(S)	Propellants*,Combustion*
IDENTIFICATEUR(S)	NTISNTND

71/72 - (C) C NTIS

NUMERO SIGNALEMENT	AD-A179 701/8/XAD
TITRE ANGLAIS	Combustion Instability in **Solid** **Propellant** **Rockets**
AUTEUR(S)	PRICE E W , FLANDRO G A
AUTEUR COLLECTIF	Georgia Inst of Tech , Atlanta School of Aerospace Engineering
ORGAN FINANCEMENT	Air Force Office of Scientific Research, Bolling AFB, DC
CLASSIFICATION INT	010263051, 403914
TYPE DE DOCUMENT	Report
CODE LANGUE	ENG
CODE PAYS D'ORIGINE	US
SOURCE	Technical rept (Annual) 1 May 86-24 Feb 87, NP 112, DP 24 Feb 87
CODE JOURNAL NTIS	U8716
CODE TARIF NTIS	NTIS Prices PC A06/MF A01
NUMERO DE CONTRAT	F49620-86-C-0005
NUMERO PROJET	2308
NUMERO ACTIVITE	A1
NUMERO(S) AGENCE	AFOSR-TR-87-0459
RESUME	This project concerns assembly, synthesis and comprehensive presentation of information on combustion instability in **solid** **rockets**, in the form of a reference book The format is chosen to make the book suitable for a wide audience of readers including propulsion program managers, **motor** designers, **propellant** chemists, test engineers, and combustion specialists The diversity of audience is accommodated by opening with general introductory chapters for nonspecialist, with progression into more applied issues, such as experimental methods and remedial measures All chapters open with Introductions that give a relatively non-technical statement of the problem and content, and end with a qualitative summary of what was done in the chapter An extensive bibliography is included, and supplemented by a m complete, computer-based bibliography with search-retrieva capability
CODE CLASSIFICATION	81 01, 81 07, 81 08
DESCRIPTEUR(S)	Combustion*,Combustion stability*,Solid propellant rocket engines*, Solid rocket propellants*,Computer applications,Books,Handbooks, Information retrieval,Synthesis Chemistry
IDENTIFICATEUR(S)	Combustion instability,NTISDODXA,NTISDODAF

72/72 - (C) C NTIS

NUMERO SIGNALEMENT	AD-A179 690/3/XAD
TITRE ANGLAIS	Journal of Chinese Society of Astronautics (Selected Articles)
AUTEUR(S)	CHANG X., XU W A , YANG S X
AUTEUR COLLECTIF	Foreign Technology Div , Wright-Patterson AFB, OH
CLASSIFICATION INT	000550000; 141600
TYPE DE DOCUMENT	Report
CODE LANGUE	ENG
CODE PAYS D'ORIGINE	CN
NUMERO DE RAPPORT	FTD-ID(RS)T-0432-86
SOURCE	Edited trans. of Yuhang Xuebao (China) n1 p11-23 Jan 87, Availability Microfiche copies only, NP. 87, DP 6 Apr 87
CODE JOURNAL NTIS	U8715
CODE TARIF NTIS	NTIS Prices: MF A01
RESUME	In this paper, a numerical solution of basic equation for one dimensional two-phase nonequilibrium flow in a combustion chamber of **solid** **propellant** **rocket** **motors** is discussed in detail, the effect of particle size on flow field in combustion

chamber and pressure-time curves is analyzed, and some useful conclusions are obtained in comparison with results of one dimensional two-phase constant lag flow in combustion chamber It is useful for predicting pressure-time curves accurately and providing accurate boundary conditions for the calculation of two-phase flow through the nozzle (China, Chinese language, Translations).Journal of Chinese Society of Astronautics (Selected Articles)--Translation

CODE CLASSIFICATION 81 07, 81 01

DESCRIPTEUR(S) Combustion chambers*,Solid propellant rocket engines*,Astronautics, Boundaries,Numerical analysis,Solutions General,Particle size, Translations,Equations,Flow fields,One dimensional,Two phase flow; One dimensional flow,Solid rocket propellants,Movable nozzles, Nozzle gas flow,Combustion,Pressure distribution,Jet flow

IDENTIFICATEUR(S) Negative pressure,NTISDODXA;NTISFNCH

REPORT DOCUMENTATION PAGE

1. Recipient's Reference	2. Originator's Reference	3. Further Reference	4. Security Classification of Document
	AGARD-LS-180	ISBN 92-835-0630-8	UNCLASSIFIED

5. Originator Advisory Group for Aerospace Research and Development
North Atlantic Treaty Organization
7 rue Ancelle, 92200 Neuilly sur Seine, France

6. Title COMBUSTION OF SOLID PROPELLANTS

7. Presented on 4th—5th September 1991 in Quebec City, Canada, 16th—17th September 1991 in Saint-Médard-en-Jalles (near Bordeaux), France and 19th—20th September 1991 in Ankara, Turkey.

8. Author(s)/Editor(s)	9. Date
Various	July 1991
10. Author's/Editor's Address	**11. Pages**
Various	178

12. Distribution Statement This document is distributed in accordance with AGARD policies and regulations, which are outlined on the back covers of all AGARD publications.

13. Keywords/Descriptors

Solid propellant rocket engines
Solid rocket propellants
Erosive burning
Burning rate
Combustion efficiency
Safety
Ignition

14. Abstract

The history of solid propellants has dramatically changed since the end of the 19th century when Paul Vieille and Nobel discovered the phenomenon of gelatinization of nitrocellulose (either by solvent or by nitroglycerin). The products thus obtained exhibited a new combustion behaviour, combustion in parallel layers. This is the basis of modern gun and rocket solid propulsion.

Extruded double base propellant grains were used for propulsion of rockets before world war II. Composite propellants (a binder, a fuel and an oxidizer) were discovered during the 1940s. They also burn in parallel layers, although microscopically the process is more complex. Since that time, these families of propellants have been improved and are now widely used for the propulsion of tactical rockets, strategic missiles, as well as space launchers. During the operation of rocket motors, many complex combustion phenomena occur. It is the object of Lecture Series 180 to present, and analyse all these combustion phenomena, both theoretically and experimentally:

—Overview on solid propellant combustion within a rocket motor ;
—Solid propellant steady combustion ;
—Erosive burning ;
—Special effects in solid propellant combustion ;
—Combustion instabilities ;
—Ignition and unsteady combustion ;
—Combustion and safety of solid propellant rocket motors.

This Lecture Series, sponsored by the Propulsion and Energetics Panel of AGARD, has been implemented by the Consultant and Exchange Programme.

AGARD Lecture Series 180 Advisory Group for Aerospace Research and Development, NATO COMBUSTION OF SOLID PROPELLANTS Published July 1991 178 pages The history of solid propellants has dramatically changed since the end of the 19th century when Paul Vieille and Nobel discovered the phenomenon of gelatinization of nitrocellulose (either by solvent or by nitroglycerin). The products thus obtained exhibited a new combustion behaviour: combustion in parallel layers. This is the basis of modern gun and rocket solid propulsion. Extruded double base propellant grains were used for propulsion of rockets before world war II. Composite P.T.O.	AGARD-LS-180 Solid propellant rocket engines Solid rocket propellants Erosive burning Burning rate Combustion efficiency Safety Ignition	AGARD Lecture Series 180 Advisory Group for Aerospace Research and Development, NATO COMBUSTION OF SOLID PROPELLANTS Published July 1991 178 pages The history of solid propellants has dramatically changed since the end of the 19th century when Paul Vieille and Nobel discovered the phenomenon of gelatinization of nitrocellulose (either by solvent or by nitroglycerin). The products thus obtained exhibited a new combustion behaviour: combustion in parallel layers. This is the basis of modern gun and rocket solid propulsion. Extruded double base propellant grains were used for propulsion of rockets before world war II. Composite P.T.O.	AGARD-LS-180 Solid propellant rocket engines Solid rocket propellants Erosive burning Burning rate Combustion efficiency Safety Ignition
AGARD Lecture Series 180 Advisory Group for Aerospace Research and Development, NATO COMBUSTION OF SOLID PROPELLANTS Published July 1991 178 pages The history of solid propellants has dramatically changed since the end of the 19th century when Paul Vieille and Nobel discovered the phenomenon of gelatinization of nitrocellulose (either by solvent or by nitroglycerin). The products thus obtained exhibited a new combustion behaviour: combustion in parallel layers. This is the basis of modern gun and rocket solid propulsion. Extruded double base propellant grains were used for propulsion of rockets before world war II. Composite P.T.O	AGARD-LS-180 Solid propellant rocket engines Solid rocket propellants Erosive burning Burning rate Combustion efficiency Safety Ignition	AGARD Lecture Series 180 Advisory Group for Aerospace Research and Development, NATO COMBUSTION OF SOLID PROPELLANTS Published July 1991 178 pages The history of solid propellants has dramatically changed since the end of the 19th century when Paul Vieille and Nobel discovered the phenomenon of gelatinization of nitrocellulose (either by solvent or by nitroglycerin). The products thus obtained exhibited a new combustion behaviour: combustion in parallel layers This is the basis of modern gun and rocket solid propulsion. Extruded double base propellant grains were used for propulsion of rockets before world war II. Composite P.T.O.	AGARD-LS-180 Solid propellant rocket engines Solid rocket propellants Erosive burning Burning rate Combustion efficiency Safety Ignition

propellants (a binder, a fuel and an oxidizer) were discovered during the 1940s. They also burn in parallel layers, although microscopically the process is more complex. Since that time, these families of propellants have been improved and are now widely used for the propulsion of tactical rockets, strategic missiles, as well as space launchers. During the operation of rocket motors, many complex combustion phenomena occur. It is the object of Lecture Series 180 to present, and analyse all these combustion phenomena, both theoretically and experimentally:

- —Overview on solid propellant combustion within a rocket motor
- —Solid propellant steady combustion
- —Erosive burning
- —Special effects in solid propellant combustion
- —Combustion instabilities
- —Ignition and unsteady combustion
- —Combustion and safety of solid propellant rocket motors

This Lecture Series, sponsored by the Propulsion and Energetics Panel of AGARD, has been implemented by the Consultant and Exchange Programme

ISBN 92-835-0630-8

propellants (a binder, a fuel and an oxidizer) were discovered during the 1940s They also burn in parallel layers, although microscopically the process is more complex. Since that time, these families of propellants have been improved and are now widely used for the propulsion of tactical rockets, strategic missiles, as well as space launchers. During the operation of rocket motors, many complex combustion phenomena occur. It is the object of Lecture Series 180 to present, and analyse all these combustion phenomena, both theoretically and experimentally:

- —Overview on solid propellant combustion within a rocket motor
- —Solid propellant steady combustion
- —Erosive burning
- —Special effects in solid propellant combustion
- —Combustion instabilities
- —Ignition and unsteady combustion
- —Combustion and safety of solid propellant rocket motors.

This Lecture Series, sponsored by the Propulsion and Energetics Panel of AGARD, has been implemented by the Consultant and Exchange Programme.

ISBN 92-835-0630-8

propellants (a binder, a fuel and an oxidizer) were discovered during the 1940s. They also burn in parallel layers, although microscopically the process is more complex. Since that time, these families of propellants have been improved and are now widely used for the propulsion of tactical rockets, strategic missiles, as well as space launchers. During the operation of rocket motors, many complex combustion phenomena occur. It is the object of Lecture Series 180 to present, and analyse all these combustion phenomena, both theoretically and experimentally:

- —Overview on solid propellant combustion within a rocket motor
- —Solid propellant steady combustion
- —Erosive burning
- —Special effects in solid propellant combustion
- —Combustion instabilities
- —Ignition and unsteady combustion
- —Combustion and safety of solid propellant rocket motors.

This Lecture Series, sponsored by the Propulsion and Energetics Panel of AGARD, has been implemented by the Consultant and Exchange Programme.

ISBN 92-835-0630-8

propellants (a binder, a fuel and an oxidizer) were discovered during the 1940s. They also burn in parallel layers, although microscopically the process is more complex. Since that time, these families of propellants have been improved and are now widely used for the propulsion of tactical rockets, strategic missiles, as well as space launchers. During the operation of rocket motors, many complex combustion phenomena occur. It is the object of Lecture Series 180 to present, and analyse all these combustion phenomena, both theoretically and experimentally:

- —Overview on solid propellant combustion within a rocket motor
- —Solid propellant steady combustion
- —Erosive burning
- —Special effects in solid propellant combustion
- —Combustion instabilities
- —Ignition and unsteady combustion
- —Combustion and safety of solid propellant rocket motors.

This Lecture Series, sponsored by the Propulsion and Energetics Panel of AGARD, has been implemented by the Consultant and Exchange Programme.

ISBN 92-835-0630-8

AGARD

NATO OTAN

7 RUE ANCELLE · 92200 NEUILLY-SUR-SEINE

FRANCE

Télephone (1)47 38 57 00 · Télex 610 176
Télécopie (1)47 38 57 99

DIFFUSION DES PUBLICATIONS AGARD NON CLASSIFIEES

L AGARD ne détient pas de stocks de ses publications, dans un but de distribution generale a l'adresse ci-dessus L a diffusion initiale des publications de l'AGARD est effectuée aupres des pays membres de cette organisation par l intermediaire des Centres Nationaux de Distribution suivants A l'exception des Etats-Unis, ces centres disposent parfois d'exemplaires additionnels, dans les cas contraire, on peut se procurer ces exemplaires sous forme de microfiches ou de microcopies auprès des Agences de Vente dont la liste suite

CENTRES DE DIFFUSION NATIONAUX

ALLEMAGNE
Fachinformationszentrum
Karlsruhe
D-7514 Eggenstem-Leopoldshafen 2

BELGIQUE
Coordonnateur AGARD-VSL
Etat-Major de la Force Aerienne
Quartier Reine Elisabeth
Rue d'Evere, 1140 Bruxelles

CANADA
Directeur du Service des Renseignements Scientifiques
Ministère de la Défense Nationale
Ottawa, Ontario K1A 0K2

DANEMARK
Danish Defence Research Board
Ved Idraetsparken 4
2100 Copenhagen Ø

ESPAGNE
INTA (AGARD Publications)
Pintor Rosales 34
28008 Madrid

ETATS-UNIS
National Aeronautics and Space Administration
Langley Research Center
M/S 180
Hampton, Virginia 23665

FRANCE
O N E R A (Direction)
29, Avenue de la Division Leclerc
92320, Châtillon sous Bagneux

GRECE
Hellenic Air Force
Air War College
Scientific and Technical Library
Dekelia Air Force Base
Dekelia, Athens TGA 1010

ISLANDE
Director of Aviation
c/o Flugrad
Reykjavik

ITALIE
Aeronautica Militare
Ufficio del Delegato Nazionale all'AGARD
Aeroporto Pratica di Mare
00040 Pomezia (Roma)

LUXEMBOURG
Voir Belgique

NORVEGE
Norwegian Defence Research Establishment
Attn Biblioteket
P.O. Box 25
N-2007 Kjeller

PAYS-BAS
Netherlands Delegation to AGARD
National Aerospace Laboratory NLR
Kluyverweg 1
2629 HS Delft

PORTUGAL
Portuguese National Coordinator to AGARD
Gabinete de Estudos e Programas
CLAFA
Base de Alfragide
Alfragide
2700 Amadora

ROYAUME UNI
Defence Research Information Centre
Kentigern House
65 Brown Street
Glasgow G2 8EX

TURQUIE
Milli Savunma Başkanlığı (MSB)
ARGE Daire Başkanlığı (ARGE)
Ankara

LE CENTRE NATIONAL DE DISTRIBUTION DES ETATS-UNIS (NASA) NE DETIENT PAS DE STOCKS DES PUBLICATIONS AGARD ET LES DEMANDES D'EXEMPLAIRES DOIVENT ETRE ADRESSEES DIRECTEMENT AU SERVICE NATIONAL TECHNIQUE DE L'INFORMATION (NTIS) DONT L'ADRESSE SUIT

AGENCES DE VENTE

National Technical Information Service
(NTIS)
5285 Port Royal Road
Springfield, Virginia 22161
Etats-Unis

ESA/Information Retrieval Service
European Space Agency
10, rue Mario Nikis
75015 Paris
France

The British Library
Document Supply Division
Boston Spa, Wetherby
West Yorkshire LS23 7BQ
Royaume Uni

Les demandes de microfiches ou de photocopies de documents AGARD (y compris les demandes faites aupres du NTIS) doivent comporter la denomination AGARD, ainsi que le numéro de série de l'AGARD (par exemple AGARD-AG-315) Des informations analogues, telles que le titre et la date de publication sont souhaitables Veuiller noter qu'il y a lieu de specifier AGARD-R-nnn et AGARD-AR-nnn lors de la commande de rapports AGARD et des rapports consultatifs AGARD respectivement Des references bibliographiques completes ainsi que des résumés des publications AGARD figurent dans les journaux suivants·

Scientifique and Technical Aerospace Reports (STAR)
publié par la NASA Scientific and Technical
Information Division
NASA Headquarters (N I T)
Washington D C. 20546
Etats-Unis

Government Reports Announcements and Index (GRA&I)
publié par le National Technical Information Service
Springfield
Virginia 22161
Etats-Unis

(accessible egalement en mode interactif dans la base de données bibliographiques en ligne du NTIS, et sur CD-ROM)

Imprimé par Specialised Printing Services Limited
40 Chigwell Lane, Loughton, Essex IG10 3TZ